METALLOPHTHALOCYANINE DERIVATIVES AS CATALYSTS FOR THE DETECTION OF SULPHUR DIOXIDE, CYANIDE, NITRITE AND AMINO ACIDS

THESIS

Submitted to Rhodes University in fulfilment of the requirements for the degree of

DOCTOR OF PHILOSOPHY

By

MAMOTHIBE AMELIA THAMAE

March 2002

Department of Chemistry
Rhodes University
Grahamstown

TO MY FAMILY

ACKNOWLEDGEMENTS

I would like to express my sincere gratitude to my surpervisor, Prof. Nyokong for her greatest support, knowledge and guidance for the duration of this degree.

I would also like to thank the following:

* My fellow research group students in S22 and the whole Chemisty Department for providing a conducive learning environment and harmony over the years.
* Dr. Westbroek for his guidance and support.
* Mellon Foundation Scholarship for financial support.
* Lesotho gorvenment for financial assistance.
* Dr. Limson, Joshua Oni and Kenneth Ozoemena for proof reading the manuscript.
* David and Suzanne Maree for helping with NMR.
* Dr. Gary Watkins for helping with IR.
* My family for their continued support.

Abstract

Electrocatalytic reduction and oxidation of nitrite using cobalt phthalocyanine derivatives was studied. The detection limit of 1 x 10^{-10} mol dm^{-3} was achieved when these molecules were employed as catalysts for nitrite detection. The mechanisms for nitrite catalysis were proposed. The position of the peripheral substituents on cobalt porphyrazines (related to cobalt phthalocyanines) affected the catalytic activity of these complexes. The highest activity for nitrite reduction was observed on the cobalt(II) 2,3-tetramethyltetrapyridinoporphyrazine ($[CoTm\text{-}2,3\text{-}tppa]^{4+}$), with cobalt phthalocyanine showing the lowest activity, and the cobalt(II) 3,4-tetramethyltetrapyridinoporphyrazine ($[CoTm\text{-}3,4\text{-}tppa]^{4+}$), showing intermediate behaviour. A mixture of a negatively charged cobalt(II) tetrasulfophthalocyanine ($[Co^{II}TSPc]^{4-}$) and a positively charged $[CoTm\text{-}3,4\text{-}tppa]^{4+}$ showed better activity for nitrite reduction than did the individual components. Cobalt porphyrazines lowered the potentials for nitrite reduction in that peaking was observed, as opposed to cobalt phthalocyanine, where only the increase in currents was observed without peaking. Using the cobalt phthalocyanine derivatives, nitrite can be reduced to ammonia with high current efficiency.

A glassy carbon electrode modified with $[Co^{II}TSPc]^{4-}$ was employed for the determination of nitrite. Nitrate had an insignificant effect on nitrite oxidation on these modified electrodes.

Electrocatalytic determination of SO_2 was studied as a function of pH at a glassy carbon electrode modified with iron(II) tetrasulfophthalocaynine. It was found that depending on pH, $SO_2.xH_2O$, HSO_3^- and/or SO_3^{2-} are the main compounds in solution and that these compounds behave differently at the electrode surface. Detection limits ranging from 4.0 ± 0.1 x 10^{-5} to 7.5 ± 0.1 x 10^{-5} mol dm^{-3} depending on pH were

observed. Similar results were obtained when cobalt(II) tetrasulfophthalocaynine was employed for SO_2 catalysis under the same experimental conditions.

Cysteine and histidine determination using oxidation currents was performed on glassy carbon electrodes modified with $[CoTm\text{-}3,4\text{-}tppa]^{4+}$ (represented as $[CoTm\text{-}3,4\text{-}tppa]^{4+}$-GCE) in pH 7 Tris buffer. The detection limit of 1.0×10^{-5} mol dm^{-3} for cysteine and 2.24×10^{-7} mol dm^{-3} for histidine were obtained.

Cyanide can be detected down to 1×10^{-11} mol dm^{-3} using $[CoTm\text{-}3,4\text{-}tppa]^{4+}$-GCE in pH 10.8 buffer.

Cyanide and SO_2 coordinate to the $[CoTSPc]^{4-}$ species. The coordination is accompanied by oxidation of the central Co(II) metal, forming a $[Co^{III}CoTSPc]^{3-}$ species. The rate constants for cyanide coordination to the $[Co^{II}TSPc]^{4-}$ complex are larger than those reported for the coordination of cyanide to FePc and RuPc complexes in non-aqueous media.

Autoreduction of $[Co^{II}Tmtppa]^{4+}$ occurred in the presence of either histidine or cysteine, with the formation of metal reduced species, $[Co^{I}Tmtppa(-2)]^{3+}$. Nitric oxide and nitrite coordinate to the $[Co^{II}Tmtppa]^{4+}$ species, without auto-reduction of this species, which was observed for cysteine or histidine. The use of $[Co^{II}TSPc]^{4}$ resulted in improved rate of interaction with nitrite when compared to the $[Co^{II}Tmtppa]^{4+}$ species.

TABLE OF CONTENTS

LIST OF SYMBOLS

Γ	=	surface coverage
α	=	transfer coefficient
ΔE_P	=	separation between peak potential
ΔEs	=	square-wave step height in mV
A	=	electrode area
c	=	concentration
D	=	diffusion coefficient
$E_{½}$	=	half wave potential
$E^{o'}$	=	formal reduction potential
E_{pa}	=	anodic peak potential
E_{pc}	=	cathodic peak potential
F	=	Faraday's constant
f	=	square-wave frequency in Hertz
i_p	=	peak current
i_{pa}	=	anodic peak current
i_{pc}	=	cathodic peak current
k^o	=	standard rate constant
n	=	number of moles of electrons transferred
Q	=	charge
r	=	electrode radius
R	=	gas constant
t	=	electrolysis time
T	=	temperature in Kelvin
v	=	scan rate

LIST OF ABBREVIATIONS

$[MTSPc]^{4-}$	=	metallotetrasulfophthalocyanine
A_{ox}	=	oxidised form of analyte
A_{red}	=	reduced form of analyte
BDD	=	boron doped diamond
BE	=	bulk electrolysis
CCC matrix	=	conductive carbon cement matrix
CE	=	counter electrode
CRPc	=	crown phthalocyanine
CV	=	cyclic voltammetry
DDP	=	differential pulse polarography
DMA	=	dimethylamine
DMF	=	N,N-dimethylformamide
DMSO	=	dimethylsulphoxide
DPV	=	differential pulse voltammetry
ESR	=	electron spin resonance
FIA	=	flow injection analysis
FTIR	=	Fourier transform infra-red
GCE	=	glassy carbon electrode
HOMO	=	highest occupied molecular orbital
HOPG	=	highly oriented pyrolytic graphite
L	=	ligand
LMCT	=	metal to ligand charge transfer
LUMO	=	lowest occupied molecular orbital
MLCT	=	ligand to metal charge transfer

M_{ox}	=	oxidised form of mediator
MP	=	metalloporphyrin
MPc	=	metallophthalocyanine
M_{red}	=	reduced form of mediator
MTmtppa	=	metallotetramethyltetrapyridinoporphyrazine
Mtppa	=	metallotetrapyridinoporphyrazine
O	=	oxidised species
OBTPC	=	octabutylthiolphthalocyanine
OBuPc	=	octabutoxyphthalocyanine
OTE	=	optically transparent electrode
OTTLE cell	=	optically transparent thin layer cell
Pc	=	phthalocyaninato dianion
PDT	=	photodynamic therapy of cancer
ppb	=	parts per billion
ppm	=	parts per million
ppmv	=	parts per million by volume
R	=	reduced species
RE	=	reference electrode
S	=	solvent molecule
SAM	=	self-assembled monolayer
SCE	=	saturated calomel electrode
SPCE	=	screen-printed carbon electrode
SWV	=	square wave voltammetry
TAPc	=	tetraaminophthalocyanine
TMHPP	=	tetra(3-methoxy-4-hydroxyphenyl) porphyrin

TMPyP	=	meso-tetrakis(1-methylpyridinium-4-yl) porphyrin
Tmtppa	=	tetramethyltetrapyridinoporphyrazine
tppa	=	Tetrapyridinoporphyrazine
TPPS	=	meso-tetrakis(p-sulphonatophenyl) porphyrin
UV	=	ultra violet
V	=	volume
Vis	=	visible
WE	=	working electrode
WHO	=	world health organisation

LIST OF FIGURES

LIST OF SCHEMES

LIST OF TABLES

CHAPTER 1

INTRODUCTION

1.1. Metallophthalocyanines

1.1.1. History of metallophthalocyanines

During a large-scale preparation of phthalimide from phthalic anhydride at the Grangemouth plant of Scottish dyes in 1928,[1] a glass-lined vessel cracked, and the outer steel casing was exposed to the reaction. As a result, a blue impurity was formed in the phthalimide. The structural elucidation of the blue pigment resulted in the name phthalocyanine (phthalo from its precursor phthalic acid derivative, and cyanine from the Greek word for blue). The phthalocyanine (Pc) molecule is an 18 π-electron aromatic macrocycle, which is similar in structure to the naturally occurring porphyrins, Fig. 1.1. The Pc dianion (Pc(-2)) can be metallated. Metallation generally maintains the planarity of the molecule and increases the symmetry from D_{2h} of the non-metallated Pc (H_2Pc) to D_{4h} of metallophthalcyanine (MPc). For metals that do not fit into the inside of the ring, symmetry drops to C_{4v}. The complex discovered by Scottish dyes was an iron phthalocyanine (FePc) derivative.[1]

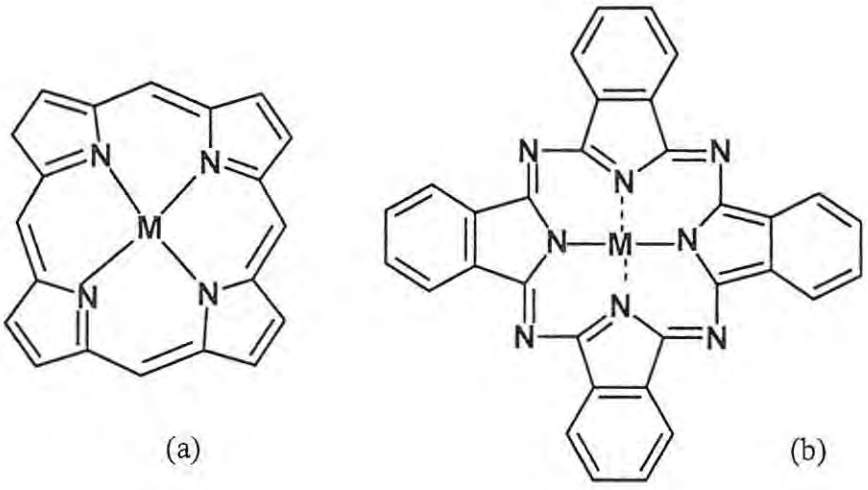

Fig. 1.1 Molecular structures of (a) metalloporphyrin and (b) metallophthalocyanine.

1.1.2. General synthesis of metallophthalocyanines

Heating a mixture of metal (or metal salt) and phthalonitrile (**1**), or phthalic anhydride (**2**) or 1,3-diiminoisoindoline (**3**) or *o*-cyanobenzamide (**4**) results in synthesis of MPc (**5**), Scheme 1.1.[2] In the case of **4** as the starting material anhydrous conditions should be employed. The cleanest complexes can be obtained by using **1** in the synthesis. In industry the more cost effective starting material **2** is employed.

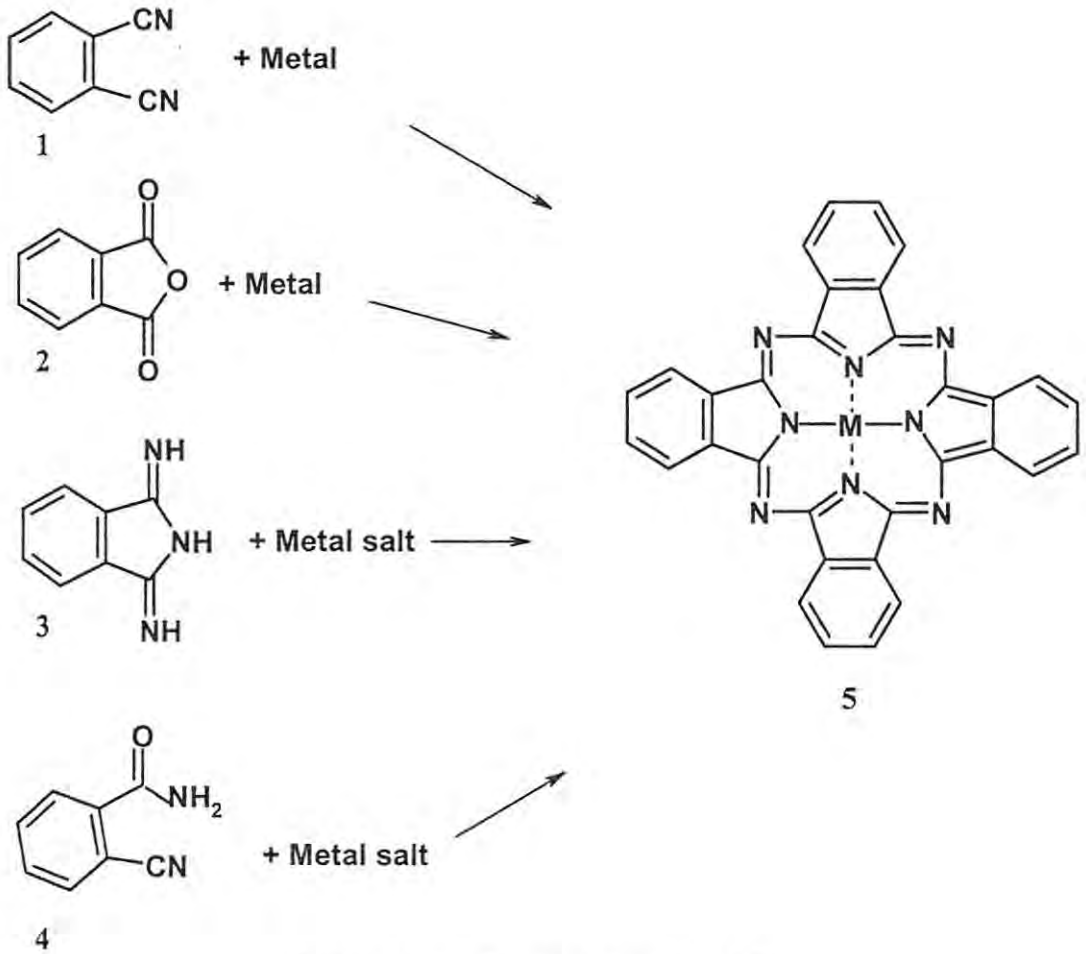

Scheme 1.1 Synthetic route for MPc.

Unsubstituted Pcs are highly insoluble in aqueous solutions. Substituents are introduced to the Pc ring to change their electrochemical properties and to improve solubility. Scheme 1.2 shows the introduction of sulfonic groups at the Pc ring,

forming metallotetrasulfophthalocyanine ([MTSPc]$^{4-}$) (**7**) which is water-soluble. Tetrasulfophthalocyanine may be produced from 4-sulfophthalic acid (**6**),[3] Scheme 1.2.

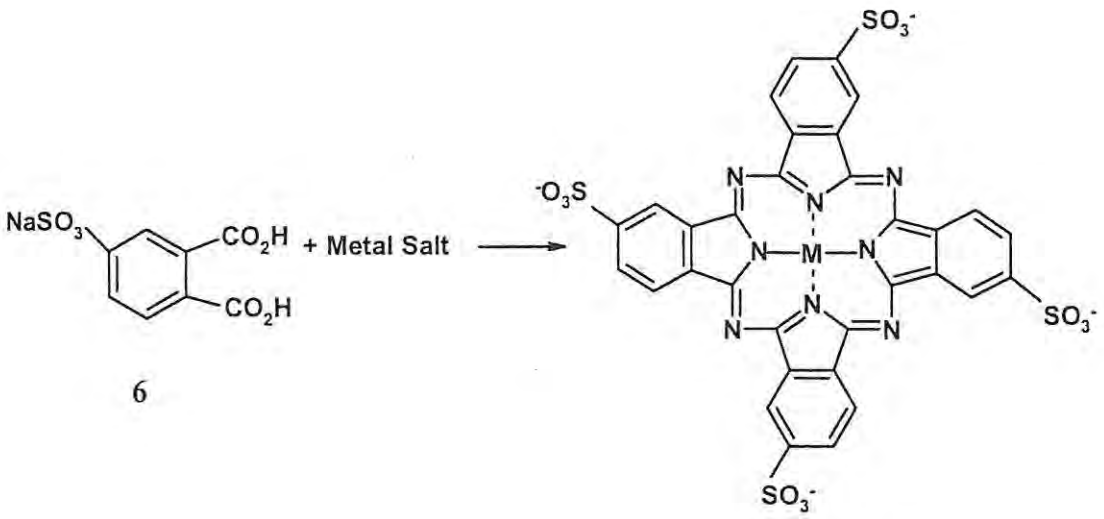

6 **7**

Scheme 1.2 Synthetic route for metallotetrasulfophthalocyanine, [MTSPc]$^{4-}$ from sulfophthalic acid.

1.1.3. General synthesis of porphyrazines

Benzene rings which are part of the Pc molecule can be replaced by pyridines forming pyridino compounds, referred to as pyridinoporphyrazines, Scheme 1.3.[2] Metallo-2,3-tetrapyridinoporphyrazine ([M-2,3-tppa]) (**9**) is prepared from 2,3-pyridinedicarboxylic acid (**8**) in the presence of urea, a metal salt and ammonium molybdate as catalyst, Scheme 1.3. The methyl groups are placed on the pyridine nitrogens, by refluxing **9** in N,N-dimethylformamide (DMF) and dimethyl sulphate to produce metal-2,3-tetramethyltetrapyridinoporphyrazine ([MTm-2,3-tppa]$^{4+}$) (**10**), Scheme 1.3.[2,4]

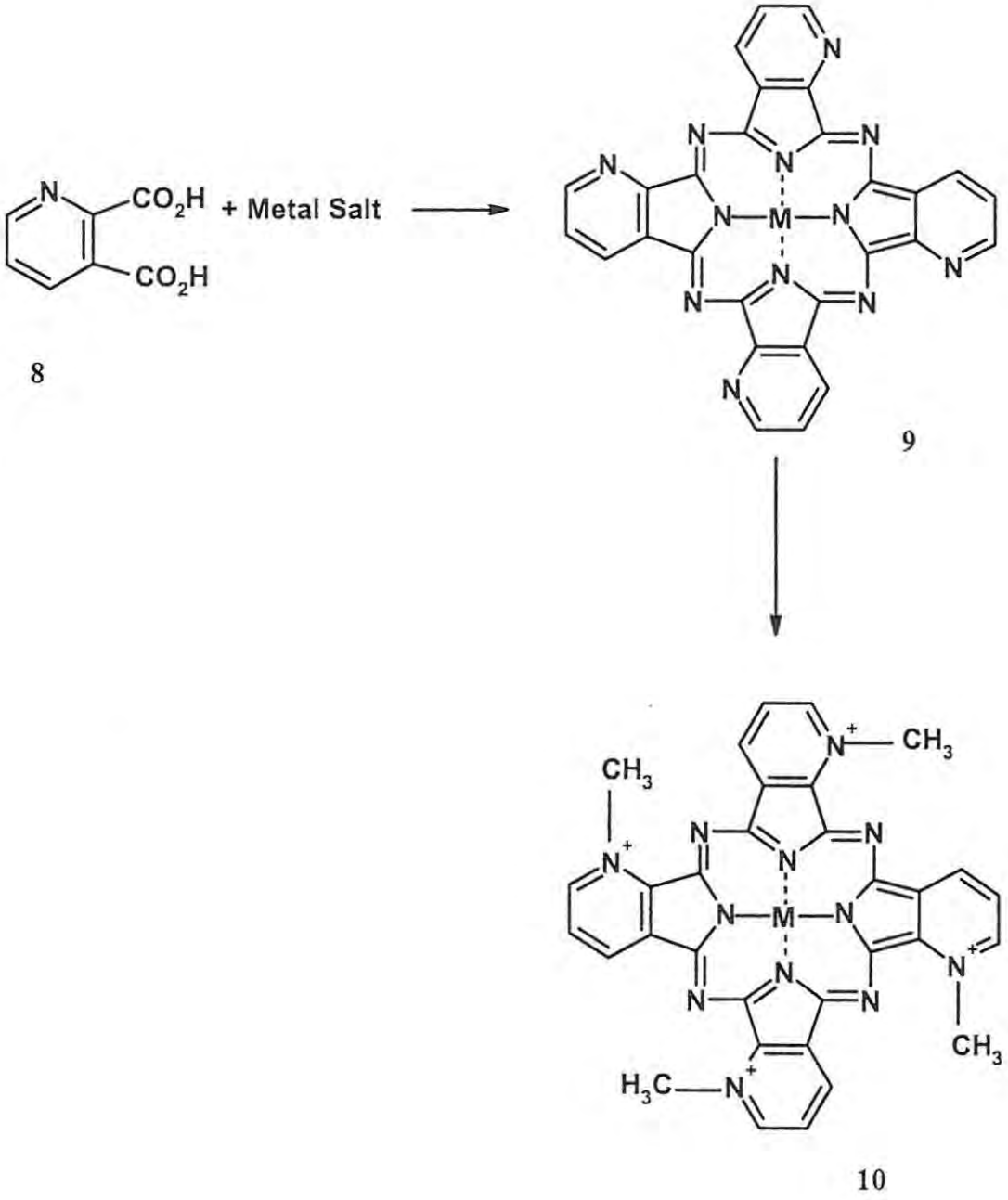

8 9 10

Scheme 1.3 Synthetic route for metallo-2,3-pyridinoporphyrazine, and its methylated derivative.

In addition, 3,4- substituted porphyrazine complexes can be prepared. 3,4-tetrapyridinoporphyrazine ([3,4-tppa]) is prepared from 3,4-pyridinedicarboxylic acid, and methylated to form metal-3,4-tetramethyltetrapyridinoporphyrazine (MTm-3,4-tppa]$^{4+}$). The procedure is similar to that followed in the synthesis of **10**.

In an alternative method, the tetrapyridinoporphyrazines can also be prepared from dicyanopyridine and metal acetates.[5]

1.1.4. Spectra of metallophthalocyanines, metalloporphyrazines and porphyrins

The ultra violet/visible (UV/Vis) absorption spectra of metallophthalocyanine or porphyrin show two bands that originate from the electronic transitions shown in Fig. 1.2. These bands are named Q and B bands, Fig. 1.3. The highest occupied molecular orbital (HOMO) of the MPc ring are the a_{1u} (π) and a_{2u} (π). The lowest unoccupied molecular orbital (LUMO) is the e_g (π^*), Fig. 1.2.

The Pc absorption spectrum shows a very intense Q band, Fig. 1.3 (a), while the porphyrin shows a weak Q band and a very intense B (or Soret) band, Fig. 1.3 (b). These may be explained as follows: The first two allowed transitions or bands, $\pi \rightarrow \pi^*$ (Q and B) arise from a_{1u} and a_{2u} to e_g. In MPcs a_{1u} lies well above a_{2u}, while in porphyrins a_{2u} lies above a_{1u}. These energy levels are close together in energy, resulting in extensive configuration interaction. Thus in porphyrins, the Q band is very weak compared to the B band, whereas in Pcs the Q band is very strong.[6]

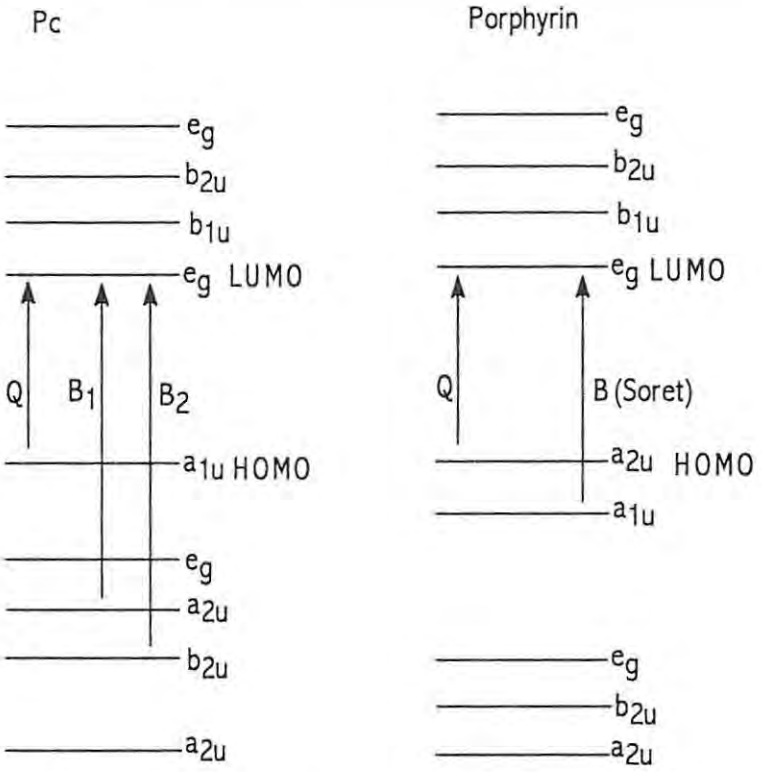

Fig. 1.2 Electronic transitions for Pcs and porphyrins showing the origin in the first two π - π^* transitions.[6]

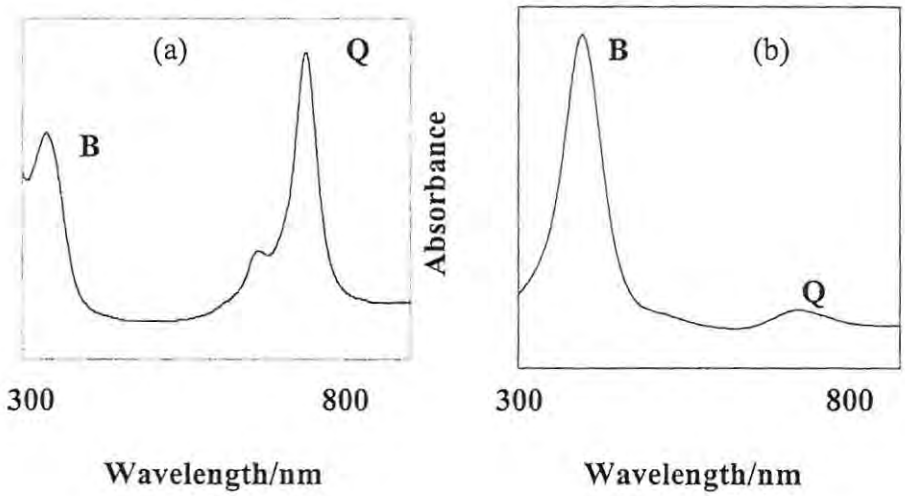

Fig. 1.3 A typical absorption spectrum of (a) Pc and (b) porphyrin in solution.

The distinction between spectra of different peripherally substituted Pcs is not as pronounced as for the porphyrins because Q-band in MPc complexes is an allowed

transition which does not depend on intensity-gaining mechanisms that are required by Q-band in porphyrins.[6]

MPc complexes dissolve in strongly coordinating solvents like pyridine, concentrated HCl and aromatic solvents. Coordination of solvent molecules to the central metal promotes Pc solubility. Solubility also differs greatly with coordinated central metal ion. Non-coordinating solvents, e.g. dichloromethane, provide a consistent environment to compare the spectra of various ligands and metals because the solvent itself does not affect the UV/Vis spectra.

If the metal in the MPc has d orbitals which lie in the HOMO-LUMO gap, there is a possibility of electron transfer from the occupied metal d orbital to the unfilled orbital of the ring, resulting in metal to ligand charge transfer (MLCT), Fig. 1.4. An electron transfer can also take place from the occupied ring orbital to the unfilled d orbital, resulting in ligand to metal charge transfer (LMCT), Fig. 1.4.

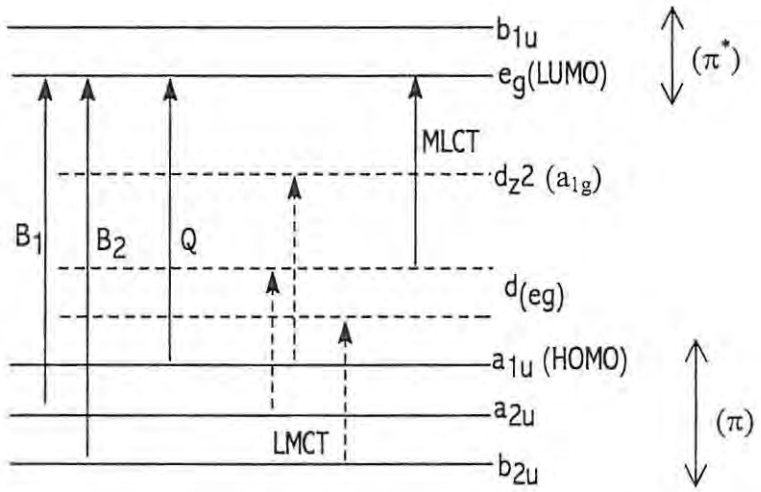

Fig. 1.4 Energy level diagram in a typical metallophthalocyanine, showing the origin of various LMCT, MLCT, Q and B-bands.[6]

—— = Ring energy levels and ---- = central metal ion energy levels

The sharp spectral Q bands in the visible region for the MPc complexes and strong Soret or B bands for the metalloporphyrin complexes, make them sensitive spectrophotometric reagents for the detection of analytes.

As explained above, tetrapyridinoporphyrazines are phthalocyanine derivatives in which the outer benzene ring has been replaced by pyridines. The NN'N''N'''tetramethylated quartenized forms of tetrapyridinoporphyrazines ($[Tmtppa]^{4+}$) are positively charged and are water-soluble.

Results from electron spin resonance (ESR) spectra indicate that the electronic environments within the phthalocyanine ring system and the tetrapyridinoporphyrazine macrocycle are comparable.[4] In solution, five and six coordinate cobalt(II) complexes do exist.

Unquartenised tetrapyridinoporphyrazine complexes are relatively insoluble in most organic solvents. Solubility may be enhanced by gently warming in pyridine under nitrogen.[3] The aqueous solution of $[Co^{II}Tmtppa]^{4+}$ is stable in acidic to neutral pH values but shows signs of decomposition in slightly alkaline solution.[4]

The quartenized tetrapyridinoporphyrazines exist as mixtures of four possible constitutional isomers.[5] The spectra of $[M^{II}Tmtppa]^{4+}$ ($M = Zn^{II}$ and Cu^{II}) complexes have been described in terms of their DMF insoluble (split Q band) and DMF soluble (single Q band) fractions due to the presence of mixtures of isomers.

1.1.5. Electrochemistry of metallophthalocyanines and metalloporphyrazines

1.1.5.1. Metallophthalocyanines

The redox potentials of MPc complexes depend on the following factors: the central metal ion, the nature of the supporting electrolyte, the solvent and axial ligands.[7,8] Organic solvents such as DMF or dimethylsulfoxide (DMSO) are often

employed for electrochemical studies, owing to the insolubility of unsubstituted MPcs in water.

A typical cyclic voltammogram of metallophthalocyanine in solution is characterised by multiple and often reversible redox processes located on the metal centre and/or the phthalocyanine ring. Ring reduction entails addition of electrons to the LUMO $e_g(\pi^*)$ of the ring where a maximum of four electrons can be added. Ring oxidation is the removal of electrons from the HOMO $a_{1u}(\pi)$. A maximum of two electrons can be removed, Fig. 1.5. The standard oxidation state of the ring is Pc(-2), and the ring can be oxidised singly or doubly as follows: (Pc(-2) → Pc(-) → Pc(0)). The ring can also be reduced four times in the following sequence: Pc(-2) → Pc(-3) → Pc(-4) → Pc(-5) → Pc(-6). Metallophthalocyanines containing electroactive central metal can be oxidised or reduced at the central metal, e.g. $Fe^{III}Pc(-2)$ → $Fe^{II}Pc(-2)$ → $Fe^{I}Pc(-2)$, with potentials located between the first ring oxidation and first ring reduction. The oxidation or reduction pathways can usually be characterised by spectroelectrochemical methods. The UV/Vis spectrum of the metal oxidised or reduced species is characterised by a shift in the Q band, without much change in intensity. The spectra of ring-oxidised species are characterised by loss in the intensity of the Q band, and the formation of weak bands near 700 and 800 nm, as well as a broad band near 500 nm.[9] For singly ring-reduced species, the loss in intensity of the Q band is accompanied by two weak bands between 500 and 600 nm.[9]

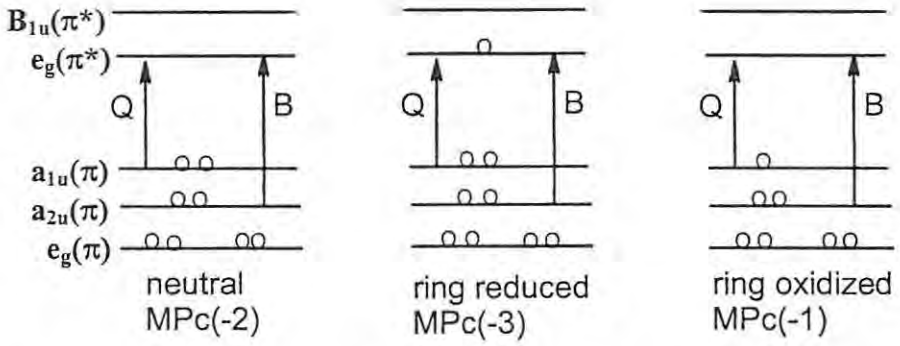

Fig. 1.5 A simplified energy level diagram for oxidised and reduced MPc species.

In this work, FePc and CoPc complexes are employed as catalysts, hence a brief discussion on their electrochemistry follows.

In FePc and CoPc, the central metal can exist in +1, +2 and +3 oxidation states. Ring oxidation may occur after the metal as M^{II} has been oxidised to M^{III}, and ring reductions after the metal has been reduced to M^{I}.

Iron(II) Phthalocyanine normally displays four reversible couples in the range + 1.00 to – 2.00 V.[10] Fe^{II} ligates to donor solvents to form six-coordinate species, $(S)_2Fe^{II}Pc(-2)$, where (S) is the solvent molecule. Oxidation of $Fe^{II}Pc(-2)$ to $[Fe^{III}Pc(-2)]^+$ occurs in the range – 0.15 to + 0.69 V depending on the solvent and counterion.[10] The $Fe^{III/II}$ potential shifts to more negative values with the type of the counter ion as follows: $ClO_4^- < Br^- < Cl^- < OH^-$.[10]

Through formation of $(Py)_2Fe^{II}Pc(-2)$, pyridine (Py) stabilises $Fe^{II}Pc(-2)$ to such a degree that the oxidation product $[Py)_2Fe^{III}Pc(-2)]^+$ is unstable in pyridine. The $Fe^{III/II}$ couple shifts positively with the nature of the solvent as follows: dimethylamine (DMA) = DMF < DMSO < Py.[10] Ring oxidation occurs following metal oxidation to form $[Fe^{III}Pc(-1)]^{2+}$.

The first reduction process in $Fe^{II}Pc$ is the formation of $[Fe^{I}Pc(-2)]^-$ species. The reduction for this couple also shows solvent dependence, shifting negatively with

potential as follows: DMA < DMSO < Py. The first reduction is however almost independent of the type of counter anion. Five coordinate $Fe^{I}Pc$ species are observed in pyridine.[10] In donor solvents such as DMA, both six and five coordinate Fe^{I} species do exist, with the six coordinate complex being oxidised at more negative potentials than the five coordinate complex.[13]

The second reduction process occurs at the Pc ring forming $[Fe^{I}Pc(-3)]^{2-}$ species, showing little dependence on solvent or anion. A further reduction occurs at $\approx$ 0.6 V more negative of the second reduction potential, to form $[(S)Fe^{I}Pc(-4)]^{3-}$.[10]

In strong coordinating solvents, metal oxidation in $Co^{II}Pc$ complexes occurs before ring oxidations. In dichloromethane, $Co^{III/II}$ couple is shifted to high potentials and is not observed. Studies on varying the donor capacity of the solvent on the Co^{III}/Co^{II} potential have shown that the potential shifts to more negative potentials from DMSO to pyridine. This is the reverse of the sequence observed for the oxidation of $Fe^{II}Pc$, as it is the higher oxidation state, Co^{III} that is stabilised by the strong donor solvents rather than the lower oxidation state in $Fe^{II}Pc$.[10]

1.1.5.2. Metalloporphyrazines

Aqueous solutions of Co^{II}, Cu^{II} or Ni^{II} complexes of $[Co^{II}Tm\text{-}2,3\text{-}tppa]^{4+}$ gave two polarographic waves. One wave with $E_{½}$ = - 0.55 V vs. saturated calomel electrode (SCE), and the larger wave at -1.20 V. The wave at - 0.55 V corresponds to a one-electron reduction process and the latter wave to a four-electron reduction.[4]

Solution electrochemistry of $[Co^{II}Tm\text{-}3,4\text{-}tppa]^{4+}$ in pH 4 phosphate buffer in the range + 0.5 to - 0.6 V vs. SCE showed two reduction couples, at + 0.25 and - 0.44 V vs. SCE respectively, assigned to metal and ring reductions, respectively.[11]

Cyclic voltammetry and spectroelectrochemistry of $[MTmtppa]^{4+}$ (with M = Pd and Pt) have been reported.[12] Two reduction peaks were observed. The first reduction peak was assigned to one electron transfer to the ring and formation of monoanion species. The second reduction with a number of electrons greater than 3, was assigned to reduction of methylpyridinium substituents.

1.1.5.3. Electrochemistry of Pcs and porphyrin ion pair dimer complexes

Phthalocyanines and porphyrins form ion pair dimers which have been reported to be face-to-face and held together by Coulomb interactions.[13] The ion pair dimers are formed when oppositely charged molecules associate. It is possible to have ion pairs between positively charged porphyrazines with negatively charged phthalocyanines and also between these ions with porphyrins. Spectroelectrochemistry has been used to characterize redox products of the ion pairs and to establish reversibility. Cyclic voltammetry (CV) of the meso heterodimers formed from (meso-tetrakis(1-methyl-4-pyridinium) porphyrinato) manganese(III) (Mn^{III}TMPyP) and (meso-tetrakis(4-sulfonatophenyl) porphyrinato) manganese(III) (Mn^{III}TPPS) showed two reversible two-electron redox waves which corresponded to the $Mn^{III/II}$ and $Mn^{IV/III}$ couples in each complex. The redox potentials were close to those of the individual Mn^{III}TMPyP.[13] UV/Vis monitoring of the titrations indicated quantitative trimerization at concentrations > 10^{-5} mol dm^{-3}.[14] Metallophthalocyanines bearing charged, peripheral substituents have been shown to associate with each other and with metalloporphyrins containing oppositely charged substituents.[13,14] From Job's plots, the analysis revealed that the aggregates may contain 1:1[14,15] or 1:2[14] ratio of phthalocyanine to phthalocyanine or phthalocyanine to porphyrin. The complexation is accompanied by significant spectral changes (in the near ultraviolet and visible region) of the individual components. The interaction can be explained as

an attraction between peripheral substituents of opposite charge and a hydrophobic interaction between the macrocycle cores. The aggregation may be disrupted by electrolytes.[15,16]

The $[MTSPc]^{4-}$:$[MTmtppa]^{4+}$ ion pairs are employed in this work as electrocatalysts.

1.1.6. Applications of metallophthalocyanines

Metallophthalocyanine complexes have found extensive applications due to their physical and chemical stability.[17] The compounds also serve as electrochromic materials.[17] The uses of MPcs include their commercial applications in photocopying, laser printing,[18,19] information storage,[19] odour removal,[20] and non-linear optical applications.[19] Metallophthalocyanines are readily available and are not expensive. The possibility of phthalocyanines finding use in artificial solar energy devices and as photosensitizers in photodynamic therapy of cancer (PDT)[17,21] has been discussed. Chlorinated aluminium disulfo phthalocyanine ($[ClAl^{III}Pc(SO_3)_2]^{2-}$) and the silicon phthalocyanine ([(L)SiPc]), where (L) is the ligand molecule, have been explored for use in PDT.

Many MPcs have been employed as catalysts[17,20,22] for analysis of a wide variety of molecules. In this work MPc and $[MTmtppa]^{4+}$ are employed as electrocatalysts for analysis of SO_2, CN^-, NO_2^- and amino acids.

1.2. Review of electrochemical methods

Cyclic voltammetry, square-wave voltammetry and bulk electrolysis were employed in this work.

1.2.1. Cyclic voltammetry (CV)

In CV the potential is scanned from an initial value, E_i, to another value, E_f and back to the initial value. A plot of current versus potential is shown in Fig. 1.6. Assuming that only an oxidised species (O), is initially present, scanning the potential from a region where no reduction occurs to more negative potentials results in the increase in cathodic current due to reduction of O (equation 1.1).

$$O + ne \rightleftharpoons R \qquad (1.1)$$

As a consequence, the concentration of O drops in the vicinity of the electrode surface. As the surface concentration of O approaches zero, the cathodic peak current (i_{pc}) corresponding to the cathodic peak potential (E_{pc}) is observed. The current then decays because of the increase in the thickness of the diffusion layer. The potential is switched to positive direction at E_f and oxidation of the reduced species (R) (back to O) occurs in the vicinity of the electrode. Oxidation is characterized by appearance of anodic current, which will increase until R is sufficiently depleted from the region near the electrode, the anodic current will result in a peak, (i_{pa}) at the anodic peak potential (E_{pa}), and then decrease. CV is thus able to generate species in the forward scan and monitor their reaction products in the reverse scan.[26]

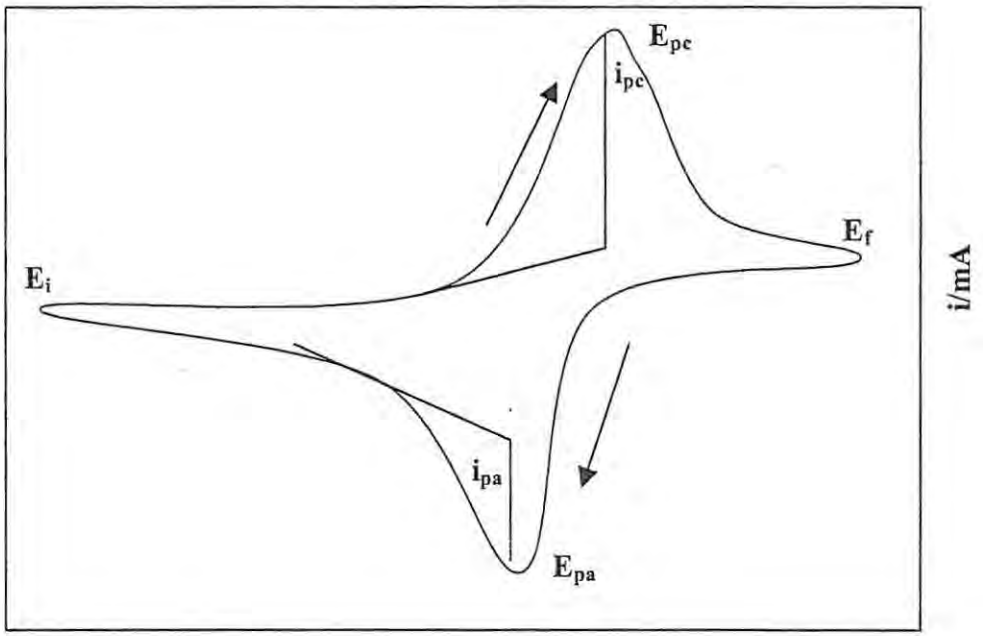

Fig. 1.6 A typical CV curve for a reversible couple.

There are three ways of mass transport of the species towards the electrode: migration, diffusion and convection. Diffusion is the spontaneous movement resulting from a concentration gradient. This gradient is induced by occurrence of the reaction in equation 1.1. In convection, transport to the electrode is by physical movement, for example, stirring. Migration involves movement due to difference in charge. An electrolyte is added to minimize migration, since migration disturbs the shapes of the voltammetric wave drastically. For electroanalytical purposes diffusion controlled reactions are favoured.[23] Electrochemical reactions are defined as reversible, irreversible or quasi-reversible.

Reversible systems

In an electrochemically reversible couple, Fig 1.6, both the oxidised and the reduced species easily exchange electrons with the working electrode. For cyclic voltammetry the peak current for a reversible reaction at 298 K is given by Randles-Sevcik equation, equation 1.2.

$$\mathbf{i_p = (2.69 \times 10^5) n^{3/2} A c D^{1/2} v^{1/2}} \qquad \mathbf{(1.2)}$$

where $\mathbf{i_p}$ is the peak current in mA

v is the scan rate in V sec^{-1}

A is the area of the electrode in cm^2

n is the number of electrons transferred

c is the concentration of the species to be oxidised or reduced in the bulk solution in mol dm^{-3}

D is the diffusion coefficient in cm^2 sec^{-1}.

As shown in equation 1.2, current is proportional to the concentration and to the square root of the scan rate. A plot of i_{pa} or i_{pc} versus $v^{1/2}$ is linear for diffusion controlled reactions and D can be determined from the slope (or from the plot of i_p vs. c if the concentration is known).[26] The values of the reverse-to-forward peak current, i_{pa} and i_{pc}, are similar in magnitude for reversible systems, and have no kinetic complications, equation 1.3.

$$\frac{i_{pa}}{i_{pc}} \approx 1 \qquad \mathbf{(1.3)}$$

Equation 1.3 is only true if the reverse current is corrected for the decay of the forward current. The formal potential ($E^{o'}$) corrected for the used reference electrode is centered between E_{pa} and E_{pc} and corresponds to the value where i = 0. For

reversible systems, the formal potential is equal to the half-wave potential ($E_{½}$), equation 1.4.

$$E^{o'} \sim E_{½} = \frac{E_{pa}+E_{pc}}{2} \qquad (1.4)$$

where $\mathbf{E_{pa}}$ is the anodic peak potential

$\mathbf{E_{pc}}$ is the cathodic peak potential.

The separation between the peak potentials (ΔE_p) is given by equation 1.5.[24,26]

$$\Delta E_p = E_{pa} - E_{pc} = \frac{2.3RT}{nF} \qquad (1.5)$$

At 298 K, equation 1.5 becomes equation 1.6.

$$\Delta E_p = E_{pa} - E_{pc} = \frac{0.059}{n} \qquad (1.6)$$

where n, $\mathbf{E_{pa}}$ and $\mathbf{E_{pc}}$ are defined above.

R is gas constant

T is temperature in Kelvin.

The $0.059/n$ separation depends slightly on switching potential and cycle number but does not depend on scan rate. The peak separation can be used to predict the number of electrons transferred, as well as the Nernstian or reversible behaviour. As an example, a one-electron process will exhibit ΔE_p of approximately 59 mV for a reversible system.

Irreversible and quasi-reversible systems

For irreversible systems, return peaks generally do not exist. When a return peak does exist, it is reduced in size and the cathodic and anodic peaks are widely

separated.[26] A system that is irreversible is characterized by a shift of the peak potential with scan rate, where the peak potential is determined as in equation 1.7.

$$E_p = E^{o'} - \frac{RT}{\alpha nF}[0.78 - \ln(k^o/D^{1/2}) + \ln(\alpha nFv/RT)^{1/2}] \quad (1.7)$$

where α is the transfer coefficient

k^o is the standard rate constant

All other symbols are described above.

E_p thus occurs at potentials higher than $E^{o'}$, with the overpotential being related to k^o and α.[26] For irreversible systems, at 298 K, the peak potential and half-wave potential differ by $(48/\alpha n)$ mV. The voltammogram becomes more drawn out as αn decreases. Often there is no return peak. The peak current is given by equation 1.8.

$$i_p = (2.99 \times 10^5) n(\alpha n)^{1/2} AcD^{1/2} v^{1/2} \quad (1.8)$$

All symbols are described above.

The current is still proportional to the concentration of the bulk solution, but generally lower in height.[26]

For a quasi-reversible system, with $10^{-1} > k^o > 10^{-5}$ cm s^{-1}, both charge transfer and mass transport control the current. Generally, the CV for a quasi-reversible system is more drawn out and accompanied by a larger peak separation in comparison with a reversible system. i_p is not proportional to square root of scan rate.[26]

1.2.2. Square-wave voltammetry (SWV)

This is a large-amplitude differential technique. Here a waveform that consists of a symmetrical square wave, which is superimposed on a base staircase potential, is applied to the working electrode. The square-wave is composed of two cycles, the forward and the reverse pulse; the current is sampled at the end of each cycle. The

difference between the two values is plotted against the base staircase potential. The charging current is discriminated by recording the difference resulting in high sensitivity in SWV. The resulting peak-shaped voltammogram is proportional to the concentration.[26] Effective scan rate is given by fΔEs. Where f is the square-wave frequency in Hz, and ΔEs is the step height in volts.[26]

1.2.3. Bulk electrolysis

Assuming that only the oxidised species is initially present in solution, the potential is set at a value sufficiently negative to cause rapid reduction, and is kept at this value until only the reduced species is present in solution. The total charge, Q, is related to the number of moles of oxidised species initially present in the solution by Faraday's law, equation 1.9.

$$\mathbf{Q = \mathit{n}FVc} \qquad (1.9)$$

where **V** is volume in dm^{-3}

F is Faraday constant

Constants are as described above, see also the list of symbols.

In bulk electrolysis (BE) the working electrode (WE) must have a large surface area to increase the rate of electrolysis (e.g. Pt gauze, reticulated vitreous carbon or mercury pool). Pt gauze may be employed as a counter electrode (CE). The solution is also stirred to enhance the rate of mass transport to and away from the working electrode. A two-compartment cell, Fig. 1.7, is normally employed, it separates the WE from the CE so that there is no interference between the CE electro-generated species and the WE reaction of interest.[23]

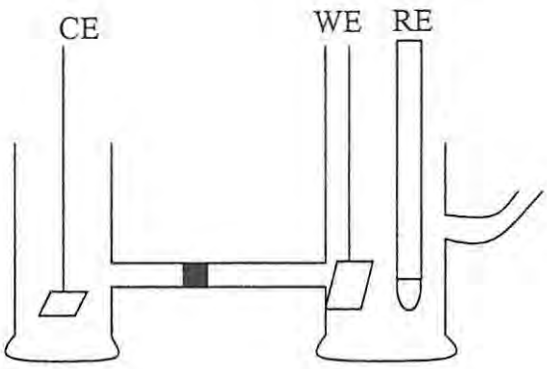

Fig. 1.7 A typical bulk electrolysis cell.

During BE experiment the current is integrated to obtain the charge. When the current has dropped to a residual level, 100% electrolysis is achieved. A 100% current efficiency implies that only one process is occurring at an electrode. Considering the result of electrolysis over a period of time, *t*, the fraction of the total number of coulombs involved in the process gives the overall current efficiency.[25]

1.2.4. Spectroelectrochemistry

Coupling of electrochemistry with spectroscopic techniques is termed spectroelectrochemistry. Optically transparent thin layer electrochemical (OTTLE) cells are usually employed for spectroelectrochemistry.

In spectroelectrochemistry a potential is applied to the optically transparent electrode, and the electrochemical consumption of species and/or formation of product is followed continuously by, for example, UV/Vis spectrophotometry.[26] The key factor in performing spectroelectrochemical experiments is the use of optically transparent electrodes (OTEs), which enable light to pass through their surface and the adjacent solution. An OTE consists of metal (e.g. silver) micromesh containing small holes (10 – 30 μm), which possess good optical transmission (over 50%) and good electrical conductivity. This minigrid is sandwiched between two transparent

disks or slides, forming a thin layer cell. The thickness of the thin layer of solution is less than 200 μm. In order to pass the optical beam through the transparent electrode, the OTE is placed in a spectrophotometer. Complete electrolysis takes place in a few seconds. Thin layer spectroelectrochemistry can be used to measure n (number of electrons involved) using equation 1.9 described above.

1.2.5. Electrochemical cell

1.2.5.1. Solvents and supporting electrolytes

Electrochemical experiments are carried out in a solvent containing a supporting electrolyte. The function of the supporting electrolyte is to decrease the resistance of the solution, to eliminate migration effects and to maintain a constant ionic strength. Electrolytes, which should not be easily oxidised or reduced, are prepared from highly purified reagents. Electrolyte concentration should be much higher than that of the electroactive species.

Nitrate, NaOH and buffers are often employed as electrolytes in aqueous media. The solvent of choice is the one in which the analyte of interest is soluble, does not react with the analyte and does not undergo an electrochemical reaction at the electrode surface over a wide range of potentials. Water has been used extensively as a solvent. Dried and purified acetonitrile,[26] DMSO[26] and DMF[26] are often employed in organic media.[26]

1.2.5.2. Macro- and micro-electrodes

Three electrodes are used in voltammetric cells. These consist of the working electrode, where the reaction of interest occurs, the reference electrode to establish the desired potential at the working electrode, and the counter electrode, an inert

conducting material (e.g. Pt or graphite rod) used to carry current and complete the circuit. A one-compartment cell is often used. Fig. 1.8 shows an example of a typical cell used for cyclic voltammetry and square wave voltammetry.

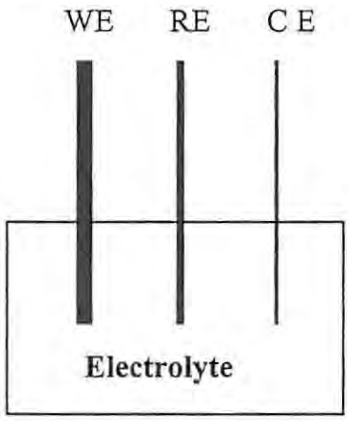

Fig.1.8 A typical voltammetry cell.

Popular working electrodes include mercury and solid electrodes such as carbon, platinum and gold. Electrodes with a large surface area (> 4.5 cm^2) may be referred to as macroelectrodes. The other types of electrodes are those with a smaller surface area, less than 4.5 cm^2, referred to as microelectrodes. Finally, electrodes with surfaces less than 3×10^{-6} cm^2 are termed ultra-microelectrodes.

Glassy carbon electrodes (GCE) employed in this work, are carefully prepared under a controlled-heating program of a premodeled polymeric (phenol-formaldehyde) resin body in an inert environment.[26] In order to ensure the removal of oxygen, nitrogen and hydrogen, the carbonized process proceed very slowly over the temperature range 573 – 1473 K. The structure of GCE consists of thin, tangled ribbons of cross-linked graphite sheets.[26] Surface pretreatment is very important and determines the electrochemical properties of GCE.[26] Electrochemical, chemical, heat and laser treatment are described in literature.[27] Removal of surface contaminants,

exposure of fresh carbon edges and an increase in the concentration of redox surface functionalities result in improved electron-transfer kinetics of GCE.[26] However, electron-transfer rates observed at GCE are slower than those observed at metal electrodes, hence electrode modification becomes necessary.[26]

1.2.5.3. Ultra microelectrodes

Their smaller dimensions result in analytical advantages such as exploration of microscopic domains, measurement of local concentration profiles, and detection in microflow systems and analysis of very small (microlitre) sample volumes. Some of the recent developments in ultra microelctrodes include time resolved probing of processes in single cells and in-vivo monitoring of neurochemical events.

Because of low capacitive current, it is possible to work in highly resistive solutions. The decrease in ohmic distortions allows electrochemical measurements to be made in unique environments, not possible with macro and micro dimensioned electrodes.[26] These media include frozen acetonitrile, low temperature glass, gas phase, supercritical carbon dioxide, ionically conductive polymers, oil based lubricants and electrolyte free organic solvents.

The total diffusion-limited current is composed of the planar flux and radial flux diffusion components,[26] equation 1.10.

$$i_{total} = i_{planar} + i_{radial} \qquad (1.10)$$

The general expression for the radial component in equation 1.10 is given by equation 1.11, for disc, spherical and hemispherical geometries.

$$i_{radial} = \mathbf{arnFDc} \qquad (1.11)$$

where **a** is a function of the electrode geometry,

(**a** = 4, 4π and 2π for discs, spherical and hemispheres respectively)

r is the electrode radius

Other symbols are defined above.

The extent to which the planar or radial component dominates depends on the relative dimensions of the electrode and the diffusion layer, given by Dt/r_o^2, where t is the electrolysis time, and r_o is the smallest dimension of the electrode.[26] Planar diffusion is dominant at small values of Dt/r_o^2 resulting in a peak-shaped behaviour. For large (> 1) values of Dt/r_o^2 (i.e. diffusion layer thickness larger than the electrode size), the current approaches steady state, and sigmoidal voltammograms are observed.[26] Hence, depending on the time scale of the experiment (i.e. the scan rate), the same electrode may exhibit peak-shaped or sigmoidal voltammogram.[26]

1.3. Electrocatalysis

1.3.1. General considerations

Electrocatalysis may be represented by equations 1.12 and 1.13.

$$\mathbf{O} + n\mathbf{e} \rightleftharpoons \mathbf{R} \qquad (1.12)$$

$$\mathbf{R} + \mathbf{A} \rightarrow \mathbf{P} + \mathbf{O} \qquad (1.13)$$

where **A** = analyte

P = product

O = oxidized species

R = reduced species.

Other symbols are described above.

The active form of the catalyst is generated by equation 1.12, and then reacts with the analyte as in equation 1.13. In cases where the chemical reaction is fast, and all R is converted to O by equation 1.13, there will be no return peak,[26] Fig. 1.9.

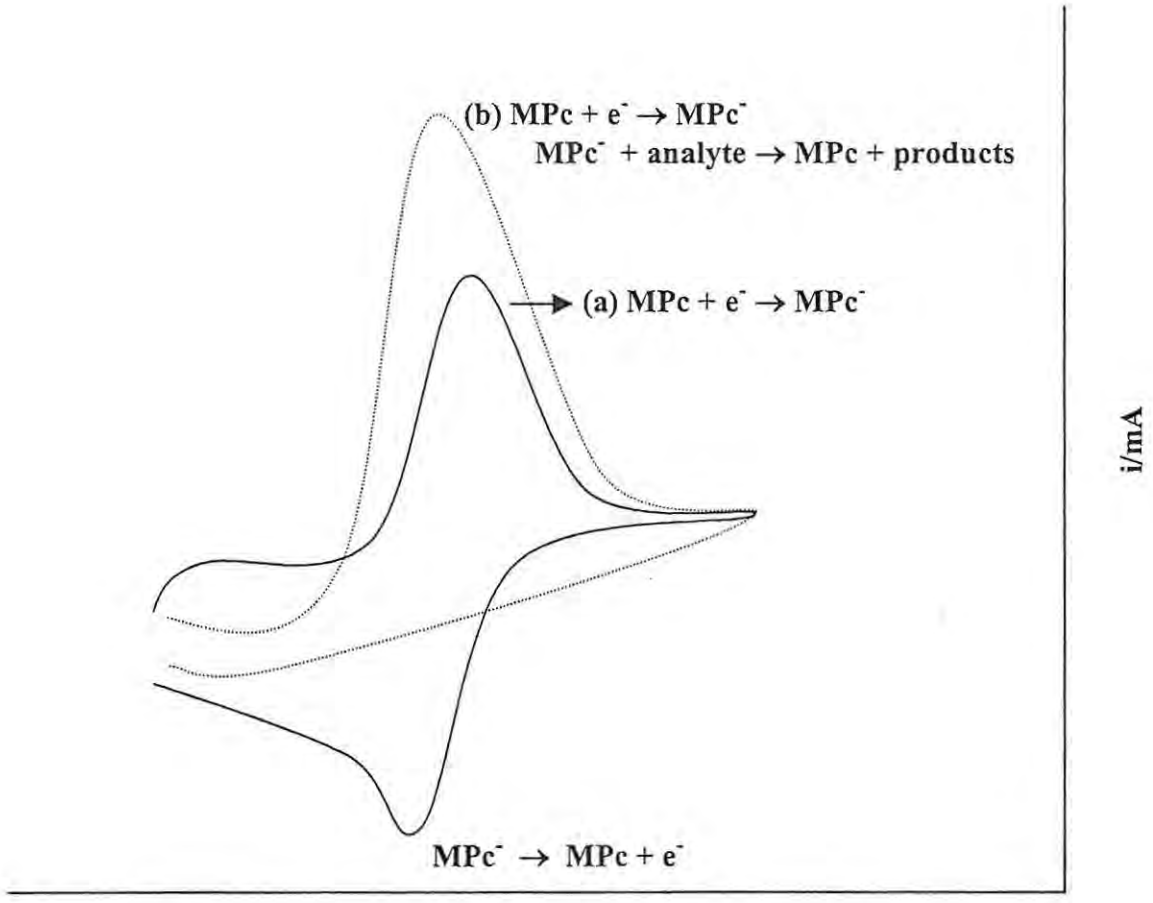

Fig. 1.9 A diagram showing a typical electrocatalytic behaviour on MPc modified electrode in (a) absence and (b) presence of analyte. In (b) the diffusion-shaped irrerversible wave would be observed if the catalysis is fast and the MPc is a thin layer on the electrode.

The amount of catalyst determines the extent of its catalytic activity.[28] When comparing the cyclic voltammogram of catalyst in electrolyte alone, Fig. 1.9 (a) and in the presence of analyte, Fig. 1.9 (b), the peak currents are increased in the presence of analyte, and the return peaks are absent or very small. Both the increased peak currents and absence of a return peak in the presence of the analyte indicate a catalytic process. A lowering in overpotential is also important in electrocatalysis.

An electron transfer process can also be investigated by coupling CV with coulometry, UV/Vis spectroscopy (spectroelectrochemistry) and infrared spectroscopy.

1.3.2. Phthalocyanines as electrocatalysts

MPc complexes are well known catalysts for many reactions.[11, 21,29,30,31,32,33,34,35,36,37,38,39,40,96] Table 1.1 shows some of the molecules whose oxidation and/or reduction has been electrocatalysed using MPc complexes. MPcs catalyse the oxidation and/or reduction of a variety of molecules ranging from pollutants such as chlorophenols[40] to neurotransmitters such as dopamine.[37] Some of the electrodes employed in these electrocatalytic reactions are highly oriented pyrolytic graphite (HOPG), conductive carbon cement (CCC) matrix and screen-printed carbon electrode (SPCE). The following phthalocyanines have also been employed as catalysts: tetraaminophthalocyanine (TAPc), octabutoxyphthalocyanine (ObuPc) and crown ether phthalocyanine (CRPc). The catalytic activity of MPc complexes can be described by definite parameters such as chemical structure, chemical and physical properties.

Table 1.1 Catalytic activity of MPc modified electrodes

MPc	Electrode	Analyte	Reference
Oxidation			
$[CoTSPc]^{4+}$	Graphite	2-Mercaptoethanol	22
$[CoTSPc]^{4+}$, CoPc	Graphite	Gluthathione	22
CoTAPc, CuTAPc	Glassy carbon	Glucose	31
CoTAPc	Glassy carbon, HOPG	Sulphide	32

Table 1.1 (cont.)

CoTAPc	Glassy carbon	2-Mercaptoethanol	32
$[CoTm\text{-}3,4\text{-}tppa]^{4+}$	Graphite	Hydrazine, Hydroxylamine	41
$[CoTm\text{-}3,4\text{-}tppa]^{4+}$	HOPG	Sulphide	11
$[CoTm\text{-}3,4\text{-}tppa]^{4+}$	Carbon fiber	Ascorbic acid	42
CoPc	CCC matrix	Penicillamine	33
CoPc	SPCE	HS, methanethiol	34
CoPc, CoOBuPc	Glassy carbon	Ortho-, meta-, para-cresol	38
$Fe^{II}Pc$, $[FeTSPc]^{4-}$	Carbon paste	Dopamine, serotonine	37
CoPc	Glass carbon	Phenol, chlorophenol, cresol	40
CoPc	Glassy carbon	NO*	36
$[CoTSPc]^{4-}$	Glassy carbon	NO*	39
Reduction			
CoPc	SPCE	Dimethyldisulphide	34
Zn^{II}, Co^{II} Fe^{I} - $[Cl_{16}Pc(-2)]$	HOPG	O_2	29
CuPc, FePc, NiPc, CoPc	GCE	Nitrite, nitrate	97
CoPc	Glassy carbon	NO	22
$[CoTSPc]^{4-}$, $[FeTSPc]^{4-}$, FePc	Polypyrrole matrix	O_2	22
CoPc	Carbon	CO_2	30
CoCRPc, FeCRPc	HOPG	O_2, H_2O_2	35
$[CoTm\text{-}3,4\text{-}tppa]^{4+}$	Graphite	CO_2	43

* = reactions in which both oxidation and reduction have been performed.

In eletrocatalysis the analyte is either oxidised or reduced, and the electrocatalytic current is detected. The mechanism that has been proposed[44] for CoPc electrocatalysed oxidation of species in acid media (e.g. cysteine) is given by equations 1.14 to 1.16.

$$Co^{II}Pc(-2) \rightarrow [Co^{III}Pc(-2)]^{+} + e^{-} \quad (1.14)$$

$$[Co^{III}Pc(-2)]^{+} + RSH \rightarrow Co^{II}Pc(-2) + RS^{\cdot} + H^{+} \quad (1.15)$$

$$2RS^{\cdot} \rightarrow RSSR \quad (1.16)$$

where RSH = cysteine and RSSR = cystine. In most cases the axial ligand coordination of the analyte to the metal centre occurs as an intermediate step.

The $Co^{III}Pc$ species generated during the first step catalyses the oxidation, and the catalyst is regenerated by the second step. A similar mechanism may be proposed by reactions catalysed by FePc species. The proposed mechanism for oxidations catalysed by ring-oxidised MPc species is shown by equations 1.17 to 1.19.[45]

$$MPc(-2) \rightarrow [MPc(-1)]^{+} + e^{-} \quad (1.17)$$

$$2[MPc(-1)]^{+} \rightarrow ([MPc(-1)]^{+})_2 \quad (1.18)$$

$$([MPc(-1)]^{+})_2 + 2RSH \rightarrow 2MPc(-2) + RSSR + 2H^{+} \quad (1.19)$$

1.3.3. Metalloporphyrazines as electrocatalysts

Electrochemically deposited $[Co^{II}Tm\text{-}3,4\text{-}tppa]^{4+}$ has been used in determination of sulphide ion, Table 1.1.[11] Graphite electrode modified with $[CoTm\text{-}3,4\text{-}tppa]^{4+}$ has been found to display electrocatalytic activity towards hydrazine and hydroxylamine oxidation through four-electron and two-electron reactions, respectively, Table 1.1.[41] A graphite disc electrode coated with $[Co^{II}Tm\text{-}3,4\text{-}tppa]^{4+}$ and protected by Nafion® film has also been used in electrocatalytic reduction of CO_2, Table 1.1.[43] $[Co^{II}Tm\text{-}3,4\text{-}tppa]^{4+}$-coated carbon fiber microelectrode has been

employed in ascorbic acid detection, Table 1.1.[42] Ascorbic acid chemically reduces $[Co^{II}Tm\text{-}3,4\text{-}tppa]^{4+}$ according to the equation 1.20.

$$2[Co^{II}Tmtppa]^{4+} + C_6H_8O_6 \rightarrow 2[Co^{I}Tmtppa]^{3+} + C_6H_6O_6 + 2H^+ \quad (1.20)$$

The resultant $[Co^{I}Tmtppa]^{3+}$ is oxidised back by means of the electrode reaction described by equation 1.21.[42]

$$[Co^{II}Tmtppa]^{4+} + e^- \leftrightarrow [Co^{I}Tmtppa]^{3+} \quad (1.21)$$

1.3.4. Modification of electrodes

1.3.4.1. General considerations

Electrocatalysis may either be homogeneous or heterogeneous. For homogeneous catalysis, both the catalyst and the analyte are in solution. For heterogeneous catalysis, the catalyst is in the solid form, either absorbed onto the electrode (forming a chemically modified electrode) or forming part of the constituents of the electrode (e.g. in carbon paste electrodes). Chemically modified electrodes are employed in this work and a discussion on electrode modification follows.

Redox reactions are often slow on unmodified electrodes. To catalyse such reactions a suitable electron mediator is attached on the electrode surface. The mediator, which can also be a catalyst, (e.g, a metalloporphyrin (MP) and its related compounds) functions by facilitating the charge transfer between the analyte and the electrode. The mediation process between the mediator (M) and the analyte (A) may be represented by equations 1.22 and 1.23.

$$M_{ox} + ne^- \rightarrow M_{red} \quad (1.22)$$

$$M_{red} + A_{ox} \rightarrow M_{ox} + A_{red} \quad (1.23)$$

where $\mathbf{M_{ox}}$ = oxidised form of mediator

$\mathbf{M_{red}}$ = reduced form of mediator

$\mathbf{A_{ox}}$ = oxidised form of analyte

$\mathbf{A_{red}}$ = reduced form of analyte.

The electron transfer occurs between the electrode and the mediator, not directly between the electrode and the analyte. The catalyst or the mediator is electrochemically regenerated. The potential is lowered to the formal potential of the mediator and there is an increase in current density. This can result in better sensitivity and selectivity.

In reversible and irreversible systems, the surface concentration of the adsorbed species, referred to as surface coverage (Γ), can be estimated from equation 1.24.

$$\mathbf{Q = nFA\,\Gamma} \qquad \textbf{(1.24)}$$

where **Q** is the charge under the voltammetric peak

Γ is the surface coverage

All the other symbols are described above.

These modified electrodes are used in electrocatalysis. In this thesis, carbon electrodes modified with MPcs and $[MTmtppa]^{4+}$ have been used for analysis of SO_2, CN^-, NO_2^-, histidine and cysteine.

1.3.4.2. Methods of electrode modification

Drop dry method

Here a drop of a solution containing the catalyst is placed on the electrode surface and left to dry. A layer of the species gets adsorbed onto the electrode surface, and acts as a mediator.

Electrochemical deposition

This refers to a repetitive scanning of potential in a particular direction to produce an active monolayer on the electrode surface, due to the oxidised or reduced species being less soluble than the starting species, and getting adsorbed onto the electrode surface.

Electrochemical polymerization

A solution containing the monomer is oxidised or reduced to the activated species that form a polymer film on the electrode surface. Normally the CV of the first scan is different from that of the subsequent scans, since a different MPc (polymer) is formed on the electrode.[46]

Chemisorption

This can be described as an adsorptive interaction between the catalyst and an electrode surface by sharing of electron density.[47] Porphyrins have been used to modify electrodes by this approach, and sharing of the π-electron density between the porphyrin and the electrode. During chemisorption, the catalyst and the electrode must be in direct contact. The highest achievable coverage is a monolayer. The shortcomings of chemisorption are: a coverage limitation, irreversibility and slow leaching of the catalyst or chemisorbed molecules into the analyte solution.[47]

"Self-assembled" monolayer (SAM)

This is a modification of chemisorption. Here thiols, sulfides and disulfides act as chemisorption agents for gold derivatisation. For example, equation 1.25 shows chemisorption reaction between gold and an alkyl thiol (R-SH).

$$\text{-Au} + \text{R-SH} \rightarrow \text{-Au-S-R} + \tfrac{1}{2}\text{H}_2 \qquad (1.25)$$

Au represents gold atoms at the electrode surface. R is the alkyl substituent. The reaction proceeds by immersing the electrode into a dilute solution of the thiol.[48] Interest in this approach is growing because the R groups can be varied and the resulting monolayer films on metal surfaces are densely packed and highly ordered.[47]

Drop dry method and electrochemical deposition have been employed to modify electrodes in this thesis.

1.4. Analytes studied in this work

The 1992 World Health Organisation (WHO) survey of air quality over 20 megacities (e.g. New York, Mexico City, Tokyo, etc) showed that urban air pollution is a major environmental health problem deserving high priority for action. Comparison of the concentrations of major air pollutants (SO_2, NO_2, O_3, CO, Pb and high-suspended particulate matter) was made with respect to existing WHO guidelines. The results showed that while several megacities still continued to have serious SO_2 and lead pollution problems, the levels of these pollutants have been decreasing in many of the megacities. SO_2 emissions have decreased over the last 30 years in industrialized countries of Europe and North America.[70]

In 1988 a directive was issued by the European Union and the USA requiring SO_2 reductions by 70% by the year 2003 (with reference to 1980 emissions). WHO air quality guidelines for maximum emissions of SO_2 stiputates 3.50×10^{-4} g m^{-3} in air. For cyanide containing effluents, the regulatory agencies have set point-source emission limits of the order of 1 parts per million (ppm), based on aquatic toxicity

tests. For the meat industry, regulations allow 200 ppm of nitrite in meat.[85] Allowable nitrite in potable water is 4×10^{-6} mol dm^{-3}.[49]

The pollutant analytes studied in this work are cyanide, sulphur dioxide and nitrite. A brief discussion on these analytes is given below. In addition, studies are performed on some amino acids (cysteine and histidine). These are also discussed.

1.4.1. Cyanide

1.4.1.1. Sources, general properties and applications

Cyanide is released into the environment by many processes and applications. The Andrussaw process in which ammonia, methane and air are reacted over platinum catalyst under high temperature to produce hydrogen cyanide, equation 1.26,[50] results in some of the product entering the environment.

$$NH_3 + CH_4 + {}^3/_2O_2 \xrightarrow{1100\ ^\circ C\ /\ Pt} HCN + 3H_2O \qquad (1.26)$$

This is the main process for HCN production used worldwide.

In an industrial application, alkaline solutions of cyanide have been employed in gold extraction in the process called leaching. Gold is electrochemically oxidised during leaching and dissolves to form the Au(I) cyanide complex, $Au(CN)_2^-$, in aqueous, alkaline cyanide solution. Although Au(III) cyanide complex is also formed, it is less stable than Au(I) complex. Cyanide is released from $Au(CN)_2^-$ as follows, equation 1.27.

$$Au(CN)_2^- + e \rightarrow Au + 2CN^- \qquad (1.27)$$

Cyanide is used in the leaching process because of its relatively low cost and great effectiveness for gold dissolution.[55] Cyanide from the effluents in the above process eventually finds its way into the environment.

Cyanide is used in electroplating[50] and case hardening. Case hardening refers to surface treatments applied to metals which result in production of hard, wear-resistant outer layers (case) around the core allowing the metal inside to retain its original properties. Cyanoethylates are important textile products.[50] Other cyanide compounds are used in pigments and photographic industries. For example, potassium ferricyanide ($K_3[Fe(CN)_6]$) is used in photography, blueprints and pigment manufacture.[50]

Cyanide containing molecules find use as precursors or reactants in the production of diverse items (e.g. paper bags and pharmaceuticals). The following materials may release cyanide when burnt: wool, silk, horsehair, tobacco, polyurethane, polyacrylonitrile and other N-containing synthetic materials.[50] Large quantities of hydrogen cyanide are used for the production of resin monomers. These include acrylates, methacrylates and hexamethylenediamine. For example, the synthesis of methacrylate is based on the reaction of acetone with HCN to form acetone cyanohydrin (as an intermediate which is then stabilised with H_2SO_4). The addition of methanol results in the formation of methacrylate, equation 1.28.

$$(CH_3)_2C{=}O + HCN \xrightarrow{(OH^-)} (CH_3)_2C(OH)CN$$

$$\xrightarrow{H_2SO_4} (CH_3C(=CH_2)C(=O)NH_3^+)(HSO_4^-)$$

$$\xrightarrow{CH_3OH} CH_3C(=CH_2)COOCH_3 + NH_4HSO_4 \qquad (1.28)$$

Some cyanide containing molecules find use as chelating agents, forming heterocyclic coordination compounds with metals.[50] Cyanato side chain is incorporated in synthetic analogues of pyrethrum alkaloids used as pesticides.[50] These pesticides have found utility in crop protection. The major synthetic amino acid, methionine, is made from carbon fragments based on propylene, methanol and cyanide.[50]

HCN is used in the production of lactic acid as shown in equation 1.29.[50]

$$CH_3CHO + HCN \longrightarrow CH_3CHOHCN$$

$$\xrightarrow{H^+ / H_2O} CH_3CHOHCOOH + NH_3 \quad (1.29)$$

Lactic acid is used as a food acidifier and dough emulsifier. It is also used in antiperspirants, leather tanning and floor polishes.

Cyanogenic glucosides found in plants release HCN following ingestion of these plants by humans. Sources of cyanogenic glycosides are bitter almonds, the pit of stone fruit such as cherry, peach and apricot, sorghum, vetch, lima beans, southern mock orange, apple seeds, cabbage and mustard. Particularly toxic are the young leaves of eastern wild cherry. Cyanogens are materials more complex than simple cyanides, they liberate free cyanides under appropriate chemical and/or physiological conditions. Cyanogenic glycosides in apricots have anti-cancer properties. Cassava, which is a tuberous plant and dietary staple in the tropics, contains cyanogenic glycoside.[50]

Mild cyanide poisoning may result in dizziness, nausea, vomiting and fainting. Long term toxic effects resulting from diet containing cyanide are goitre, ataxic neuropathy and cretinism.[51] Deaths from acute cyanide poisoning are compatible with blood cyanide concentrations of $1.0 - 2.0 \times 10^{-3}$ g dm^{-3} and above.[52]

An immediate measure following cyanide ingestion is administration of basic ferrous sulphate solution.[52] Antidotes of cyanide poisoning include: cystine, cysteine, gluthathione, histidine, pyruvates, cobalamins,[53] glucose, hydroxylamine and chlorpromazine.[54] Activated charcoal reduces absorption of swallowed cyanides.

Detoxification of cyanide containing waste can be achieved by oxidising cyanide with oxidants, such as chlorine or H_2O_2, to produce the less toxic cyanate (CNO^-).[55,56] Photocatalytic oxidation of free cyanide ions in aqueous TiO_2 suspensions irradiated by sunlight has also been reported.[57] Cyanide photo-oxidation

has been found to be affected by the presence of H_2O_2 showing no dependence on the initial amount of cyanide present nor the amount of the catalyst.

1.4.1.2. Detection methods

Spectroscopic methods

UV/Vis spectrophotometry has been used for cyanide determination.[58,59] The procedures utilise the reaction between cyanide and chloramine-T. Cyanide is converted to cyanogen chloride with chloramine-T solution. Cyanogen chloride is then reacted with a mixture of pyridine containing 0.1 % bis(pyrazolone) and 1-phenyl-3-methyl-5-pyrazolone, to form a dye which is stable for at least 30 minutes at 298 K. Many salts tested in the study[58,59] (e.g. borates, sulphates, etc) did not interfere with. The reaction between cyanide and chloramine-T does not depend on pH of the solution over the pH range 4.7 to 9.1. Cyanide concentration in the range 9.5 x 10^{-5} to 2.6 x 10^{-4} and 2.6 x 10^{-4} to 3.6 x 10^{-4} g dm^{-3} in alkaline and acidic media, respectively,[59] was obtained in these studies.

Electrochemical methods

Determination of cyanide by cathodic stripping voltammetry with both differential pulse voltammetry (DPV) and SWV modes at rotating silver electrode has been reported.[60] In these studies, sulphide facilitated deposition, with reproducible cyanide peaks observed at – 0.38 V vs. SCE. Detection limits of 0.35 x 10^{-6} and 1.2 x 10^{-6} mol dm^{-3} for cyanide were obtained for DPV and SWV, respectively. Electrooxidation of cyanide ions on cobalt oxide (deposited on Ti substrate by thermal decomposition) electrode has also been reported.[61] The oxidation product was found to be cyanate, equation 1.30.

$$CN^- + 2OH^- \rightarrow CNO^- + H_2O + 2e^- \qquad (1.30)$$

This electrochemical oxidation of cyanide shows slow kinetics. Highly corrosion resistant electrodes such as PbO_2 or cobalt oxide are generally employed.

There have been reports on the determination of cyanide using normal pulse voltammetry[62] and polarography.[63,64] For normal pulse voltammetry, the potential for cyanide oxidation was observed at 0.226 V vs. silver|silver chloride (Ag|AgCl), and the detection limit was 1.2×10^{-7} mol dm^{-3}.[62] Polarographic determinations of cyanide were performed in the presence of sulphide.[63,64] The polarographic wave of cyanide was observed at - 0.26 V vs. SCE.[63] The detection limit of cyanide ion was 1.25×10^{-3} g dm^{-3}.[63] Sulphide and thiosulphate concentrations higher than 5×10^{-4} mol dm^{-3} interfered with cyanide determination. Cyanide determinations were also performed in plant samples.[63] Basic media (e.g. pH 10.8) was employed, since hydroxide ion interferes with cyanide determination at pH values higher than 10.8. The detection limit of cyanide was 5×10^{-6} mol dm^{-3}.[64]

1.4.1.3. Interaction of MPcs with cyanide

The B band of zinc phthalocyanine in DMSO shows a single peak located at 345 nm. On addition of cyanide this band splits in two.[65] Addition of various ligands to iron(II) phthalocyanines have also shown a complex spectrum in the high energy region, with the bands being split and well separated when cyanide was the ligand. Splitting in high-energy bands was also observed on addition of CN^- to CoPc.[65]

The kinetics and equilibria for the reaction between cyanide and FePc[161] or iron(II) hexadecachlorophthalocyanine ($(Cl)_{16}PcFe$)[66] in DMSO have been reported. Kinetic studies on $Fe^{II}Pc$ and ruthenium phthalocyanine (RuPc) complexes have shown that the axial coordination of cyanide occurs in a stepwise manner, with the coordination of the first cyanide occurring much faster than that of the second.[66,67]

Low rate constants were observed. For example, the values of the rate for the forward reaction (k_f) for the coordination of cyanide to FePc were 17.5 dm^3 mol^{-1} s^{-1} and 0.2 dm^3 mol^{-1} s^{-1} for the ligation of first and second cyanide, respectively.[161] The equilibrium constants for cyanide coordination to $Fe^{II}Pc$ complex were 3.0 x 10^3 and 5.7 x 10^2 dm^3 mol^{-1} for the first and second cyanide, respectively.[161]

Interaction between porphyrins and cyanide has also been investigated. For example, the shift in the B and Q bands was observed on addition of cyanide to $Rh^{III}TPPS$.[68] The whole physiological pH range (5 – 9) was covered in order to determine the potential for this species as a cyanide-scavenging drug. The specific rate constant of 5.0 dm^3 mol^{-1} s^{-1} was obtained.[68]

1.4.1.4. Electrocatalysis of cyanide using MPc complexes

Co(III) tetra(3-methoxy-4-hydroxylphenyl) ($Co^{III}TMHP$) porphyrin[69] ($Co^{III}TMHPP$) porphyrin bound to the Pt electrode through a sol-gel network was used for cyanide detection. The peak for ($Co^{III}TMHPP$) on Pt electrode in pH 10 buffer was observed from – 0.05 to – 0.1 V vs. Ag|AgCl in the absence of cyanide.[69] Increased currents and more defined peaks were observed in the presence of oxygen (and absence of cyanide), indicating oxygen catalysis. However, when cyanide was added to the solution, the reductive peak of $Co^{III/II}$ disappeared, since the cyanide coordinated to the Co^{II} active centre. It was concluded that the catalytic sites were occupied and oxygen reduction was inhibited. In these studies,[69] when the electrochemical system had reached the steady state, cyanide was injected and the catalytic currents decreased rapidly. The percentage of inhibition was then calculated for different KCN concentrations. The response was linear for cyanide concentrations in the range of 10^{-8} mol dm^{-3}, the detection limit was within the range of 0.7 to 2.1 x

10^{-8} mol dm^{-3}. This poisoning effect can be used for highly sensitive cyanide detection.[69]

Aims of the project

No studies on the interaction between MPcs and cyanide in aqueous media have been reported. One of the aims of this thesis is to study the interactions of cyanide with MPcs in aqueous media, as a step towards the development of cyanide antidotes and spectroscopic methods of cyanide determination. Electrochemical methods based on the use of $[CoTmtppa]^{4+}$ as catalyst were employed in this thesis for analysis of CN^- with the aim of improving sensitivity.

1.4.2. Sulphur dioxide

1.4.2.1. Sources, properties and applications

The sources of SO_2 are classified as stationary, mobile and natural. Stationary sources of SO_2 are power stations, and other industries (e.g. sulphuric acid manufacturing plant and petroleum refineries). Mobile sources are emissions from motor vehicles, airplanes and ships. Natural sources include volcanoes. The sulphur that is present in coal (0.2 – 7%) and oil (0.3 – 4%) is oxidised to SO_2 during combustion. The simplified reaction is shown by equation 1.31.

$$\mathbf{S\ (fuel) + O_2 \rightarrow SO_2} \qquad \mathbf{(1.31)}$$

As a result of burning coal, SO_2 is released with the smoke. The combination of SO_2, smoke, and fog produces smog, often referred to as sulphurous smog. The typical SO_2 concentration found in flue gases of coal-fired power stations are 1500 parts per million by volume (ppmv). As a result of treatment, natural gas has negligible sulphur content. Wood also has a very small content of sulphur.[70]

The health effects of SO_2 include immediate coughing, eye irritation, throat irritation, reversible bronchial constriction as well as the decline in lung function of children, aggravated bronchitis and increased mortality.[70]

SO_2 is a contributor to acid rain. In the atmosphere, oxidation of SO_2 by hydroxyl radicals to sulphuric acid occurs, and the sulphuric acid is readily absorbed by rain. SO_2 may alternatively dissolve in cloud droplets to form dissolved $SO_2.H_2O$, bisulphite (HSO_3^-) and sulphite (SO_3^{2-}) ions according to equations 1.32 to 1.34.[70]

$$SO_2 + H_2O \rightleftharpoons SO_2.H_2O \qquad (1.32)$$

$$SO_2.H_2O \rightleftharpoons HSO_3^- + H^+ \qquad (1.33)$$

$$HSO_3^- \rightleftharpoons SO_3^{2-} + H^+ \qquad (1.34)$$

At pH values typical of rainwater (3 – 6), dissolved SO_2 exists predominantly as bisulphite ion,[70] which can be oxidised to sulphate (SO_4^{2-}) in cloud droplets by dissolved hydrogen peroxide and ozone. SO_2 oxidation by O_2 in cloud droplets may occur in polluted air, catalysed by trace metals such as iron and manganese, with the reaction rate increasing with pH.[70]

The harmful effects of acid rain include lake and river acidification, leading to the mobilization of soluble aluminium, which in association with low pH has initiated fish deaths. Acceleration of corrosion of limestone and iron is another consequence of acid rain. This leads to the damaging of important historical monuments and other building structures; adverse effect on plant growth, leading to forest decline and crop damage.[70]

1.4.2.2. Detection methods

In a routine SO_2 source emission control, SO_2 has been absorbed into a reagent solution, followed by subsequent chemical analysis. When the reagent solution is

hydrogen peroxide, SO_2 is oxidised to sulphate and the acidity (i.e. the amount of sulphate) can be determined by titration with a standard alkaline solution. The chemical analysis has a shortcoming in that alkaline substances such as NH_3 will neutralize acidity and give a negative response, while any atmospheric component, which dissolves to give a strong acid, will produce a positive response. In an alternative method, sulphate ion is analysed from the solution using ion chromatography, after SO_2 is absorbed into H_2O_2 solution. This method shows high selectivity.[70] Alternatively, following SO_2 adsorption into a reagent solution, (a) reaction with barium chloroanilate can be performed, with subsequent colorimetric analysis at 530 nm or (b) sulphate ion can be determined by flow injection analysis,[71] and sulphate ions in the range 0.08 to 10.00 x 10^{-3} g dm^{-3} may be analysed.

Spectroscopic methods

The technique mostly used for continuous analysis of SO_2 gas at air quality monitoring stations is UV fluorescence spectroscopy.[70] Measurements of sulphur dioxide and other sulphur compounds can be performed using flame photometric detection. In this technique, both inorganic and organic sulphur compounds may be detected. The reason being that these substances form S_2 species in the flame zone, which is responsible for the observed emission. The advantages of the flame photometric sensor include: low detection limit (0.005 ppm), linear response in ambient air concentration range, fast response and a gas flow system (no liquid reagents).[72]

SO_2 may also be dissolved into potassium tetrachloromercurate solution, followed by spectrophotometric analysis.[70]

Electrochemical methods

A sulphur dioxide analyser that consists of 2.0 mol dm^{-3} H_2SO_4 electrolyte, a gold sensing electrode and a lead dioxide counter-electrode has been reported.[72] The analyser is simple, compact, and cheap and can be employed in large monitoring networks for measurements in extended periods (e.g. 24 hours). A gold rod equipped with microporous Teflon membrane was used as an amperometric sensor for atmospheric SO_2.[73] Various electrolyte solutions were employed including H_2SO_4 and $HClO_4$ in DMSO. Sensitivity was 45 nA ppm^{-1}, and detection limit was 500 parts per billion (ppb) of SO_2. The electrochemical window for sensitive and selective SO_2 determination using this sensor is limited to potentials less positive than + 1.6 V, as above this potential oxygen evolution interferes with the analysis. The voltammograms for electrooxidation of SO_2 exhibit broad peaks corresponding to equation 1.35.[73]

$$\mathbf{SO_2 + 2H_2O \rightarrow SO_4^{2-} + 4H^+ + 2e^-} \qquad \mathbf{(1.35)}$$

These broad peaks are typical for SO_2 oxidation on gold and smooth platinum electrodes in aqueous sulphuric acid solutions.

Many electrochemical techniques for monitoring SO_2 have been described, such as polarography[74] and differential pulse polarography (DPP).[75]

The use of improved electrochemical sensor based on Au-solid polymer electrolyte sensing electrode in direct contact with the gases in the atmosphere has been reported.[76] SO_2 oxidation took place in the potential range + 0.15 to + 0.6 V vs. $Hg|Hg_2SO_4$. The latter potential corresponds to formation of gold oxide on the electrode surface. $SO_2.H_2O$ (aq) is the electroactive species in acidic media, equation 1.32. In basic media SO_3^{2-} is formed, equation 1.36.

$$\mathbf{SO_2\,(g) + H_2O \rightarrow SO_3^{2-}\,(aq) + 2H^+} \qquad \mathbf{(1.36)}$$

SO_3^{2-} (aq) ions are thus the predominant electroactive species under basic electrolyte conditions. SO_3^{2-} (aq) species undergo oxidation at potentials higher than for $SO_2.H_2O$ (aq). The oxidation is not a pure electron transfer process. On Au and Pt electrodes it is an enhancement of Au or Pt oxide peaks. Amperometric sensors therefore encounter a major problem in lack of sensitivity towards electroactive species. The presence of CO, NO and NO_2 were reported not to interfere with SO_2 measurements. The transport of O_2 was found to be the limiting stage in SO_2 oxidation. The detection limit of SO_2 was 1 ppb.[76]

1.4.2.3. Interaction of MPcs with sulphur dioxide

Photoassisted electron transfer between SO_2 and tin(IV) phthalocyanine (L_2)(SnPc) has been reported.[77] As the reaction proceeded, the Q band for (L_2)(SnPc) (located at 696 nm) decreased in intensity and two new weaker bands were formed at 585 and 616 nm.[77] The spectral changes were typical of ring reductions in MPc complexes.[78] The reaction that was first order in both SnPc and SO_2, was also found to involve a one-electron reduction of SnPc to anion radical species.[77]

Photochemically induced electron transfer between SO_2 and tin(IV) di-phthalocyanines has also been reported.[79] Photolysis of tin diphthalocyanine (Pc_2Sn^{IV}) in dichloromethane containing SO_2 resulted in one-electron oxidation of these species to $[Pc(-2)Sn^{IV}Pc(-1)]^+$.

The interaction of iron(II) tetraphenyl porphyrin ($Fe^{II}TPP$) with SO_2 resulted in three different sulfato complexes of (porphinato) iron(III) being isolated: binuclear species; $[Fe(TPP)]_2SO_4$, a mononuclear bisulfate complex; $[Fe(TPP)(OSO_3H)]$ and a mononuclear sulfate containing derivative.[80]

1.4.2.4. Electrocatalysis of sulphur dioxide using MPc complexes

The electrochemical oxidation of SO_2 on carbon gas diffusion electrodes modified with cobalt phthalocyanine has been reported.[81] The aim, which was to resolve the problem for the complete oxidation of SO_2 on gas diffusion electrodes when using SO_2 gas in mixtures, was achieved with mixtures of air containing up to 20% by volume SO_2. There have been some reports on the effect of pyrolysis temperature on the catalytic activity of cobalt phthalocyanine for the oxidation of SO_2 by O_2.[82] The catalytic oxidation of SO_2 to sulphuric acid was proposed.

SO_2 exists mainly as HSO_3^- in the pH range 3 - 6.[70] The reduction of HSO_3^- to H_2S on iron porphyrin modified electrodes has been reported.[83] The peak potential for HSO_3^- reduction was observed at – 0.64 V vs. SCE.[83]

Aims of the project

There is no literature on the kinetics and equilibria of the interactions of SO_2 with MPcs, hence, one of the aims of this thesis is to study the interactions of SO_2 with MPc complexes. This will be a step toward the development of spectroscopic methods of SO_2 detection. In this thesis, $[Fe^{II}TSPc]^{4+}$and $[Co^{II}TSPc]^{4+}$ are examined for their ability to lower the potential and improve sensitivity in the electrocatalytic determination of SO_2.

1.4.3. Nitrite

1.4.3.1. Sources, properties and applications

Nitrites find use as fertilizers in agriculture and as medicinal agents. For example, amyl nitrite is used to dilate coronary vessels and to reduce blood pressure.

Some meat products are treated with potassium and sodium nitrite. The importance of $NaNO_2$ and KNO_2 salt additives to the cured meat products are that the

cations provide the meat with salty and bitter tastes, anti-microbial action (important for long storage), colour fixation, preservation effect and indirect beneficial effect on flavour.[84] These industrial meat products include spiced ham, vienna sausages, frankfurters, bologna and smoked salmon.[85]

In addition, sodium nitrite, sodium nitrate and hydroxide are present in high concentrations in low-level nuclear waste, and contribute to environmental release hazards. The electrochemical reduction of these materials to gaseous products has been studied in a synthetic waste mixture.[86]

High concentrations of NO_2^- can have adverse effects such as respiratory disease. NO_2^- can also affect the immune system unfavourably. Nitrite produces carcinogenic nitrosamines. Nitrate reduction to nitrite by bacteria takes place under acidic conditions in human infant stomach (pH 5 – 7). Nitrite can oxidise haemoglobin iron(II) to iron(III) resulting in methaemoglobin, which has a lower affinity for oxygen than haemoglobin. The subsequent decrease of oxygen in an infant's body may cause diarrhoea, vomiting and possibly death. The condition is referred to as methaemoglobinaemia. Occasionally, a blue colour around affected infant's mouth has been observed, the condition thus also being referred to as blue baby syndrome.[87]

1.4.3.2. Detection methods

Spectroscopic and chromatographic methods

Ultra-trace analysis of nitrite in food samples by flow injection with spectrophotometry detection has been reported.[88] Analytical parameters such as acidity, reagent concentration, flow rate, sample size, time, temperature and interfering ions were studied. The flow injection analysis (FIA) method is based on

catalytic effect of nitrite on oxidation of gallocyanine (a dye) by bromate in sulphuric acid. A decrease in absorbance of gallocyanine at 530 nm is used in monitoring NO_2^- concentration.

Enzymic method for the determination of nitrite in meat and fish products has been reported.[89] In this spectrophotometric method, nitrite is measured enzymically through its reaction with nitrite reductase. The absorbance was monitored at 340 nm, and the calibration curves were linear in the range 0.1 to 10 x 10^{-6} g dm^{-3}.[89]

MacCarthy and co-workers have described many methods for nitrite analysis in natural water.[90] Nitrate can easily be reduced to nitrite and nitrite oxidised to nitrate. Therefore, simultaneous determination of the two becomes important. Simultaneous determination of NO_3^- and NO_2^- in seawater using UV detection ion chromatography has been reported.[90] The detection limit for nitrite was found to be 8 x 10^{-6} g dm^{-3}.[90] In another method, which determines NO_3^- and NO_2^- simultaneously, an azo dye has been added, with nitrite determined by spectrophotometry.[90] Chemiluminiscence has also been used to detect NO_3^- and NO_2^-, the analytes are reduced to NO in acidic medium with V^{III}.[90] UV/Vis absorption spectroscopy has been used for direct determination of NO_2^-, using the absorption band at 355 nm.[90] Spectroscopic determination of nitrate and nitrite in water and some fruit samples using column preconcentration has been reported.[91] In this method, nitrite is diazotised with sulphanilamide, sulphamethizole or sulphadimidine; using absorbance measurements, the detection limits were found to be 1.4 x 10^{-6} g dm^{-3}, 1.2 x 10^{-6} g dm^{-3} or 1.0 x 10^{-6} g dm^{-3} respectively. Interferences from various metal ions or alkali metal salts (e.g. Na_2CO_3, Co^{2+} etc) were observed, but no interference from nitrate was observed.[91]

Determination of nitrite in meat samples has been reported.[84,85] Nitrite is diazotised with N-(1-naphthyl)-ethylenediamine dichloride to form a highly coloured dye, the absorbance of which is employed in the analysis. Detection limit of 1.1×10^{-3} g dm^{-3} for sodium nitrite was obtained.[85] The strongest vibration band for nitrite is observed at 1271.5 cm^{-1} in infra-red spectrometry and can be used for its detection.

Ion chromatography has been used to detect NO_2^- in the presence of large amounts of Cl^-.[90]

Due to complex sample manipulation, slow analysis, toxicity of utilised products (carcinogenic intermediates such as nitrosamines) and difficulty of application to remote environmental determinations, the spectroscopic and spectrophotometric methods discussed above are not convenient.[92]

Electrochemical methods

It is necessary to transform nitrite and nitrate to nitrogen and ammonia in order to prevent these ions from entering ground waters. It is also necessary to establish conditions that maximise the current efficiency for the production of ammonia and/or nitrogen gas from the electrochemical reduction of nitrate and nitrite. Studies on the electrochemical reduction of these species in both the simulated and actual radioactive waste solutions have been conducted.[86,93] The products of electrochemical reduction of nitrate and nitrite depend on the conditions of the reduction such as electrode material, pH, coexisting ions and cell design. Products that have been observed for the electrochemical reduction of nitrite include ammonia, nitrogen, hydroxylamine and nitrous oxide.[86,93,95,97] With a proper choice of electrode material and applied potential, some selectivity in the products of the electrochemical reduction of nitrites may be achieved.

Catalytic polarography has been used to determine NO_2^- in water at the ppm level.[90] It was proposed that $[Fe(SCN)NO]^+$ is formed in a sample that contains ammonium ferrous sulphate, thiocyanate and nitrite in the presence of sodium perchlorate as a supporting electrolyte.[90] Single-sweep cathodic polarography was used in nitrite determination where a detection limit of 0.004×10^{-3} g of NO_2^- dm^{-3} was obtained.[90]

By a very simple technique, linear sweep voltammetry (LSV), vitreous carbon[94] or carbon fibre and gold ultramicroelectrodes[92] have been used successfully for electrochemical determinations of nitrite in pure and natural waters.[92] In these studies the peak for nitrite oxidation was observed at 0.85 V[92] or 1.0 V[94] vs. SCE where the detection limit was 2.60×10^{-6} mol dm^{-3},[92] and 5×10^{-5} mol dm^{-3},[94] respectively. It was observed that neither nitrate nor dissolved oxygen interfered in the nitrite determination using LSV making the technique one of the simplest possible.

Detection limits for nitrite analysis can be improved by the use of more sensitive electrochemical methods such as differential pulse techniques.[92]

NO_2^- reduction on Ag cathodes is accompanied by H_2 evolution. On Cu cathodes, NO_3^- and nitrite reduction occur at the same potential regions and show similar voltammetric profiles. The dominant product of nitrite reduction was NH_3. On the other hand nitrate may be reduced to nitrite at - 1.1 V vs. SCE and to ammonia with high yields at - 1.4 V vs. SCE.[95]

FIA coupled to electrochemical detection has been used to detect nitrite in residual water.[96] Determination of nitrite using this method was based on the reaction of nitrite with iodide in acidic media, the iodine formed being detected biamperometrically at two Pt electrodes polarised with a potential difference of 0.1 V.

Equations (1.37) to (1.39) below[97] show that nitrite can be reduced electrochemically to hydroxyl ions, nitrogen, ammonia and hydroxylamine. Specific reduction products obtained depend on electrode surface, media/pH and reduction potential. For example, in basic media, copper electrodes yield ammonia as the main product of nitrite reduction.

$$NO_2^- + 2H_2O + 3e^- \rightarrow \tfrac{1}{2}N_2 + 4OH^- \qquad 0.23V \text{ vs. } Ag|AgCl \quad (1.37)$$

$$NO_2^- + 5H_2O + 6e^- \rightarrow NH_3 + 7OH^- \qquad -0.36V \text{ vs. } Ag|AgCl \quad (1.38)$$

$$NO_2^- + 4H_2O + 4e^- \rightarrow NH_2OH + 5OH^- \qquad -0.65V \text{ vs. } Ag|AgCl \quad (1.39)$$

Of all the products of nitrite reduction, ammonia and hydrazine become useful as important industrial raw materials. Hydrazine is a strong reducing agent in alkaline media, being oxidised to nitrogen, hence the equation for hydrazine production is not given above.

1.4.3.3. Interaction of MPcs with nitrite

A study on the interaction between $[Co^{II}TSPc]^{4-}$ with nitrite in the presence of NO_3^- and ClO_4^- in water has been reported.[98] The rate of the forward reaction, k_f, was found to be 1.6×10^{-4} dm^3 mol^{-1} s^{-1} and the rate of the reverse reaction, k_r, was 2.9×10^{-6} s^{-1} in the presence of nitrate.[98] In the presence of ClO_4^-, the value of k_f was found to be equal to that in the presence of nitrate, with a k_r of 4.6×10^{-6} s^{-1} obtained.[98]

1.4.3.4. Electrocatalysis of nitrite using MPc

Nitrite-selective electrode based on electropolymerised cobalt(II) 4,4',4",4"'-tetraaminophthalocyanine has been reported.[99] Different polymerisation conditions and buffers were investigated in order to optimise the response of the electrode. The

electrodes were found to be most selective for nitrite. The detection limit was 1.7 x 10^{-4} mol dm^{-3}.[99]

A poly(vinyl chloride) membrane electrode based on 2,9,16,23-tetra-*tert*-butylphthalocyanine-cobalt has demonstrated excellent selectivity toward the nitrite ion.[100] The following selectivity sequence was observed on this electrode: nitrite > thiocyanate > iodide > perchlorate > bromide > nitrate > chloride.[100] Nitrite concentration was linear in the range 10^{-5} to 0.1 mol dm^{-3}.[100]

The electrochemical reduction of nitrite in alkaline solution has been studied on glassy carbon electrodes modified with Mn-, Fe-, Co-, Cu- and ZnPc.[97] The MPc complexes lowered the overpotential for the reduction of nitrite as follows: CuPc > FePc > NiPc > CoPc > MnPc > ZnPc > GCE. The main product of nitrite reduction was ammonia.[97]

Nitrite reduction by myoglobin in surfactant films has been discussed.[101] Catalytic nitrite peaks were observed at – 0.895 and – 1.205 V vs. SCE. The catalytic peaks shifted to more negative potentials and the currents decreased with increase in pH.[101]

An enzyme sensor has been developed for the detection of nitrite.[102] The enzyme, based on nitrite reductase, displayed a linear signal for nitrite detection in the concentration range 0.2 to 3 x 10^{-3} g dm^{-3}.[102] Electrocatalytic reduction of nitrite on iron porphyrin has been reported.[103,104] Electroreduction at - 0.9 V vs. SCE yielded ammonia as the main product and dinitrogen as a minor product.[103] Depending upon reaction conditions, ammonia, hydroxylamine and N_2O can be obtained as products in significant amounts.[104] Reduction of nitrite on hemin modified electrode (a metalloporphyrin) occurred at ~ - 0.7 V vs. SCE.[105]

Aims of the project

There is no literature on the kinetics and equilibria of the interactions of nitrite with porphyrazines. The thesis partly aims at studying the interactions between nitrite and $[CoTmtppa]^{4+}$ as a step towards the development of spectroscopic methods of NO_2^- detection. In this thesis MPcs and $[MTmtppa]^{4+}$ complexes, which are similar to porphyrins, are employed as catalysts for the analysis of nitrite and its reduction to ammonia.

1.4.4. Histidine and cysteine

1.4.4.1. General properties and applications

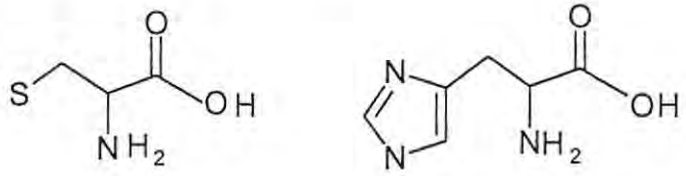

(a) cysteine (b) histidine

Histidine

L-histidine is an essential amino acid and must be incorporated in the daily food intake to be available to the body.[106] The food sources that contain histidine are dairy, meat, poultry, fish as well as rice, wheat and rye.

Histidine is a precursor of histamine,[107,108] a compound released by immune system cells during an allergic reaction. The body cannot maintain adequate histamine levels without adequate L-histidine stores. Histamine is well known for its role in stimulating the inflammatory response of skin[109] and mucous membranes such as those found in the nose - this action is essential in the protection of these barriers during infection. Histamine also stimulates the secretion of the digestive enzyme

gastrin.[106] Without adequate histamine production, healthy digestion can become impaired.

Metallothionein formation requires both L-cysteine[110] (usually derived from available glutathione stores) and L-histidine. Toxic metals such as mercury, lead, cadmium,[110] as well as excess amounts of the essential minerals zinc and copper stimulate the rapid formation of metallothionein inside cells of the brain, liver, and kidneys. Metallothionein is a molecule designed to store metals in such a way as to prevent uncontrolled oxidation reactions; protecting the normal functioning of the cell.

Histidinemia is an inborn error of the metabolism of histidine due to a deficiency of the enzyme histidase, where high levels of histidine are found in the blood and urine, manifesting in speech disorders and mental retardation.[111]

Histidine can be positively charged (at acidic pH)[110] or uncharged (under basic conditions)[110] depending on its local environment.[112] Histidine is often found in the active sites of enzymes, where its imidazole ring can readily switch between these states to catalyse the making and breaking of bonds.[110]

Cysteine

Cysteine is a sulphur-containing non-essential amino acid.[113] Cysteine is found in high protein foods such as poultry, wheat, broccoli, eggs as well as garlic, onions and red peppers. Cysteine is rarely used as a dietary supplement. N-acetyl cysteine, which contains cysteine, is more commonly used as a supplement.

Cysteine is only incorporated into proteins at the rate of 2.8 percent relative to the other amino acids, but the unique thiol side chain of this amino acid is often heavily involved in the three-dimensional structure of proteins and enzymes.[109] The

side chain is also often involved in the chemistry occurring at the active sites of many enzymes. Cysteine is also critical to the metabolism of a number of essential biochemicals including coenzyme A, heparin, biotin, lipoic acid, and glutathione.[107]

Cysteine is required in human skin; it assists in skin elasticity and texture. It is found in β-keratin (the main protein in nails), in skin as well as hair.[108] It is important in collagen production, and is required in the manufacture of the amino acid taurine. Cysteine is useful in detoxifying the body from harmful toxins and helps protect the brain and liver from damage by alcohol, drugs etc. It has been found that it may help in strengthening the protective lining of the stomach as well as intestines, which may help prevent damage caused by aspirin and similar drugs.[114]

Cysteine is occasionally converted into glucose and used as a source of energy. In addition, cysteine may play an important role in the communication between immune system cells.[115]

No direct effects of deficiencies of cysteine have been reported. However, according to several studies, blood levels of cysteine and glutathione are low in individuals infected with human immunodeficiency virus.[116]

1.4.4.2. Detection methods

Spectroscopic, chromatographic and chemical methods

Identification and quantification of amino acids in proteins have been achieved by reversed-phase high performance liquid chromatography.[117] The other methods employed in amino acid determinations are fluorimetry, ultraviolet absorption and infrared spectrophotometry.[117] The methods[117] of determination of proteins include: Biuret, Coomassie Brilliant (Bradford), silver bonding, turbidimetry methods and Kjeldahl analysis.

Amino acids are building blocks of proteins.[108] Several methods of protein analysis depend on the constituent amino acids.[106]

In Biuret method, cupric ions form a coordination complex with –NH groups present in peptide bonds giving an absorption maximum at 540 – 560 nm. Despite good reproducibility, the method lacks sensitivity and is not suitable for protein assay at concentrations less than 1 x 10^{-3} g dm^{-3}.

Coomassie Brilliant Blue is a dye that complexes with proteins to give an absorption maximum at 595 nm. Immediate signal response is obtained. The detection limit of 20 x 10^{-6} g dm^{-3} of protein can be obtained. The method is relative, as the amount of the dye binding to proteins appears to vary with the content of basic amino acid residues in the protein. This makes the choice of a standard difficult. Also, many proteins do not dissolve properly in the acidic reaction medium.

The turbidimetry method lies on the ability of strong or organic acids such as trichloroacetic and sulfosalicylic acid that cause proteins to precipitate.

The amount of the precipitate formed is measured by its light scattering intensity (turbidimetry).

The Kjeldahl analysis is a general chemical method for determining the nitrogen content of any compound. The method is reproducible and precise for the determination of nitrogen, but the determination of protein content is complicated by presence of nitrogen in the contaminants such as deoxyribonucleic acid.

Electrochemical methods

Histidine

In-situ Fourier transform infra-red (FTIR) studies of the electrochemical oxidation products of histidine in 0.1 mol dm^{-3} NaOH have been reported.[118] Histidine

was oxidised from + 1.1 V vs. Ag|AgCl. The major products of prolonged electrochemical oxidation of histidine were carbon dioxide, ammonia, formic acid and imidazole.

Cysteine

Boron-doped diamond (BDD) electrodes were used to examine L–cysteine oxidation in alkaline media.[119] Cyclic voltammogams of L-cysteine on BDD and glassy carbon electrodes exhibited a well-defined peak (~ 0.57 V vs. SCE).[119]

1.4.4.3. Interaction of MPcs and [MTmtppa]$^{4+}$ with cysteine or histidine

Kinetics of the interaction of $[Co^{II}TSPc]^{4-}$ with histidine in pH 7.2 buffer have been reported.[120] The rate was first order in both $[Co^{II}TSPc]^{4-}$ and the amino acid, with a rate constant of 0.16 dm^3 mol^{-1} s^{-1} obtained for histidine.[120]

Cobalt(II) porphyrins of the general formula $Co(P)L_2$, where P = TMPyP or tetrakis(4-carboxylatophenyl) porphine (TCPP) and L = amino acids have been studied in aqueous solution by ^1H NMR spectroscopy.[121] At pH above 7, predominant species are $Co(P)(L)_2$, whereas at lower pH values $Co(P)(L)(H_2O)$ species are also present. In the general case, two amino acid ligands were bound to cobalt atom through the NH_2 group. In the case of histidine, at pH 7, it was bound to cobalt exclusively through the imidazole group, while at higher pH (pH > 10), it was bound only through the NH_2 group.[121]

Kinetics of the interaction of $[Co^{II}TSPc]^{4-}$ with cysteine in pH 7.2 buffer have been reported.[120] The rates were first order in both $[Co^{II}TSPc]^{4-}$ and the amino acid, with a rate constant of 2.2 dm^3 mol^{-1} s^{-1} obtained.[120]

Addition of ascorbic acid to aqueous solutions of $[Co^{II}Tm\text{-}2,3\text{-}tppa]^{4+}$ resulted in a colour change from green to purple. ESR spectral results and the spectrophotometric titrations conclusively pointed out the Co^{I} complex (λ_{max} = 505 nm) to be the product of this reaction.[4] Addition of cysteine or ethylenediaminetetraacetate (EDTA) to $[ZnTm\text{-}2,3\text{-}tppa]^{4+}$, followed by irradiation, resulted in spectra typical of phthalocyamine dianion species.[5]

Addition of cysteine and histidine to $[PdTm\text{-}2,3\text{-}tppa]^{4+}$ or $[PtTm\text{-}2,3\text{-}tppa]^{4+}$ resulted in a decrease in the Q-band absorption spectrum, and formation of a new broad band near 525 nm. The colour of the solution changed from blue to purplish-blue.[12] These spectral changes were assigned to ring reductions and formation of monoanion species, $[MTmtppa(-3)]^{3+}$.

Interactions between $[Co^{II}Tm\text{-}3,4\text{-}tppa]^{4+}$ and the analytes nitrite, cysteine and histidine are studied in this thesis.

1.4.4.4. Electrocatalysis of histidine and cysteine using MPcs and $[MTmtppa]^{4+}$

To the author's knowledge, there are no reports on histidine electrocatalysis employing phthalocyanines, hence this thesis aims at histidine electrocatalytic detection employing $[CoTmtppa]^{4+}$ as a catalyst.

Oxidation of cysteine occurs at highly positive potentials on ordinary electrodes. Modification of electrodes with MPc lowers the oxidation potential of cysteine. The anodic currents of cysteine were observed at 0.82 V vs. Ag|AgCl in acidic media, on GCE modified with $[Co^{II}TSPc]^{4-}$ (denoted as $[Co^{II}TSPc]^{4-}$-GCE),[122] with the detection limit shown in Table 1.2. Catalytic activity for cysteine oxidation was also observed on electrodes modified with $Co^{II}Pc$, oxomolybdenum(V) phthalocyanine ($[OMo(V)(OH)Pc]^{4-}$) and the copper tetrasulfophthalocyanine, ($[Cu^{II}TSPc]^{4-}$).[123] Oxidation potentials and detection limits are shown in Table 1.2.

Table 1.2 E_p and detection limits for the MPc catalysed oxidation of cysteine.

MPc	Conditions	E_p/V (vs. Ag|AgCl)	Detection limit/mol dm^{-3}	Reference
$OMo^{V}(OH)Pc$	Carbon paste	0.26	$\sim 10^{-3}$	124
$[OMo^{V}TSPc]^{4-}$	Solution	0.28	$\sim 10^{-2}$	124
$[CoTSPc]^{4-}$	Glassy carbon	0.90	20*	123
CoPc	Carbon paste	0.77	$\sim 10^{-7}$	44
$[CoTSPc]^{4-}$	Solution	0.77	$\sim 10^{-7}$	44
$[CoTSPc]^{4-}$	Glassy carbon	0.82	1×10^{-8}	122
CoOBTPc	SAMs	~ 0.4	3.1×10^{-7}	125

* = Detection limit in $\mu g\ mL^{-1}$

$[OMo^{V}(OH)Pc]$ incorporated into graphite powder to form a chemically modified carbon paste electrode has been used in catalytic oxidation of cysteine. The detection limits for cysteine analysis are shown in Table 1.2, and the best detection limit was observed on $[Co^{II}TSPc]^{4-}$-GCE.[122] Solution catalysis using oxomolybdenum(V) tetrasulfophthalocyanine ($[OMo^{V}(OH)TSPc]^{4-}$), was also investigated. Cysteine oxidation occurred at 0.26 and 0.28 V vs. Ag|AgCl for catalysis by $OMo^{V}(OH)Pc$ and $[OMo^{V}(OH)TSPc]^{4-}$ respectively,[124] Table 1.2. There was thus a considerable lowering of the overpotential when molybdenum phthalocyanines were employed in comparison to when cobalt tetrasulfophthalocyanines was employed,[123] Table 1.2.

Detection of cysteine on SAM of octabutylthiophthalocyaninatocobalt(II) (CoOBTPc) has been reported,[125] with a detection limit shown in Table 1.2.

Electrocatalytic behaviour of differently substituted cobalt phthalocyanines towards cysteine oxidation has been investigated. The electrocatalytic oxidation was

related to Co^{III}/Co^{II} in acidic media and to Co^{II}/Co^{I} couple in basic media. Both the catalytic currents and the oxidation potential for cysteine were pH dependent.[126]

Aim of the thesis

There are no literature reports on the kinetics and equilibria of the interactions of histidine with cobalt porphyrazines. One of the aims of this thesis is to study the interactions of histidine with $[Co^{II}Tmtppa]^{4+}$. This will be an important step towards understanding the interactions of porphyrazines with biological systems. Positively charged $[M^{II}Tmtppa]^{4+}$ was employed to lower the potential and improve the sensitivity in histidine electrocatalytic detection.

One of the aims of this thesis is to study the interactions of cysteine with $[Co^{II}Tmtppa]^{4+}$. This will be an important step towards understanding the interactions of porphyrazines with biological systems. No cysteine electrocatalysis employing cobalt porphyrazines has been reported. One of the aims of this thesis is to study electrocatalytic detection of cysteine using cobalt porphyrazines.

1.5. SUMMARY OF AIMS OF THE PROJECT

The aims are to study:

(a) interactions between the pollutants (SO_2, NO_2^-, CN^-) and amino acids (cysteine and histidine) with metallophthalocyanines and metallotetramethyltetrapyridinoporphyrazines for use in spectroscopic determination of these analytes.

(b) catalytic behaviour of $M^{II}Pcs$ and $[M^{II}Tmtppa]^{4+}$ towards oxidation and reduction of these pollutants and amino acids.

CHAPTER 2

EXPERIMENTAL

2.1. Reagents

Distilled deionised Millipore water was employed for all studies in aqueous media. Dimethyl sulfoxide (DMSO) was dried on alumina and dimethylformamide (DMF) was freshly distilled. Tetraethylammonium perchlorate (TEAP) was recrystallized from ethanol before use as an electrolyte for the electrodeposition of cobalt(II) tetrasulfophthalocyanine $[Co^{II}TSPc]^{4-}$ onto a glassy carbon electrode (GCE) from DMF solutions. Dimethyl sulphate was distilled prior to use. 0.01 or 0.1 mol dm^{-3} (ionic strength = 0.5 mol dm^{-3} $NaClO_4$) tris(hydroxymethyl)aminomethane (Tris) buffer was employed for buffered solutions, pH 3.2 to 11. NaOH or HCl (0.1 mol dm^{-3}) was used to adjust pH. Phosphate (pH 4 and 7.4) and borate buffers (pH 10.8) were also employed. The buffer employed and pH has been stated in the relevant section of results.

Potassium hexacyanoferrate, $K_3[Fe(CN)_6]$ was purchased from Merck and used as received. KCN was purchased from Merck, sulphur dioxide was bought from Messer Grieshem, L-histidine and L-cysteine were purchased from Aldrich. Sodium nitrite was purchased from BDH. Sodium dithionite, sodium bisulphite and sodium sulphite were purchased from Aldrich. Cobalt(II) acetate, ammonium molybdate, ammoniun chloride, urea, 3,4-pyridinedicarboxylic acid, 2,3-pyridinedicarboxylic acid, nitrobenzene, sodium hydroxide, 4-sulfophthalic acid and silver nitrate were purchased from SAARCHEM. N_2 was purchased from MESSER Fedgas and dried with CaH_2. All reagents were of analytical grade.

2.2. Synthesis of metallophthalocyanine and metalloporphyrazine complexes

Cobalt phthalocyanine (CoPc) was purchased from Aldrich.

2.2.1. Synthesis of cobalt(II) tetrapyridinoporphyrazine complexes, Scheme 2.1.

Cobalt-3,4-tetrapyridinoporphyrazine (Co-3,4-tppa)

The complex was prepared according to the literature methods.[127] Urea (3.2 g), ammonium molybdate (0.126 g) and 3,4-pyridinedicarboxylic acid (1.0 g) were ground together until homogeneous. The mixture was stirred in 1,2,4-trichlorobenzene (40 cm^3) for 1 hour at 429 – 433 K. A ground mixture of cobalt(II) oxalate [$Co(C_2O_4).2H_2O$, 1.1 g] and urea (2.5 g) was slowly added under nitrogen. The temperature was maintained at 478 – 483 K for 3.5 hours. After this time, 1,2,4-trichlorobenzene was removed by distillation. The crude product was washed with benzene (0.1 dm^3), crushed and washed successively with ethanol, warm water, warm aqueous sodium hydroxide solution (5% w/v), warm water, warm dilute hydrochloric acid (2.5% v/v), warm water and dried at 80 °C over P_2O_5. Yield = 82%.

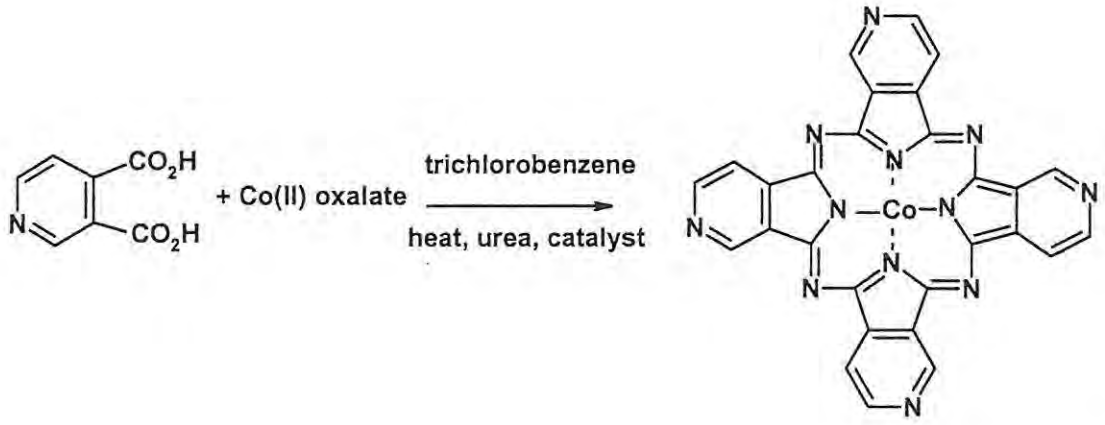

Scheme 2.1 Simplified synthetic route of Co-3,4-tppa.

Cobalt-2,3-tetrapyridinoporphyrazine (Co-2,3-tppa)

This complex was also prepared in a procedure similar to that described in the preparation of cobalt-3,4-tetrapyridinoporphyrazine, Scheme 2.1, except for substitution of 3,4- pyridinedicarboxylic acid by 2,3-pyridinedicarboxylic acid.[127] The same quantities of reagents were employed. Yield = 80%.

2.2.2. Synthesis of cobalt(II) tetramethyltetrapyridinoporphyrazine complexes

Cobalt-3,4-tetramethyltetrapyridinoporphyrazine ($[Co^{II}Tm\text{-}3,4\text{-}tppa)^{4+}$)

Quaternization of the (Co-3,4-tppa) from Scheme 2.1 to form cobalt-3,4-tetramethyltetrapyridinoporphyrazine ($[Co^{II}Tm\text{-}3,4\text{-}tppa)^{4+}$) was carried out following literature methods.[127] The cobalt-3,4-tetrapyridinoporphyrazine from Scheme 2.1 was refluxed in DMF at 393 K, Scheme 2.2. An excess of dimethyl sulphate was added dropwise. The mixture was heated with stirring for 30 min. At the end of the reaction, excess DMF was removed by distillation. The resultant slurry was poured into acetone and the product collected by centrifugation. It was washed with ethanol, followed by diethyl ether, and dried at 353 K over phosphorus pentoxide. IR spectra (KBr discs, cm^{-1}) 583w, 616m, 757s, 854m, 933m, 1001vs, 1057m, 1121vs, 1222vs, 1304w, 1443m, 1533m, 1643s, 2366w, 3069w, 3415s. UV/Vis in water (λ_{max}, nm (log ε)) 338 (5.1), 440 (4.6), 594 (4.7), 659 (5.0). Elemental analysis results calculated for $C_{32}H_{28}N_{12}O_{18}S_4Co.4H_2O$: C, 35.39; N, 17.00; H, 2.77. Found: C, 34.76; N, 16.09; H, 2.50%.

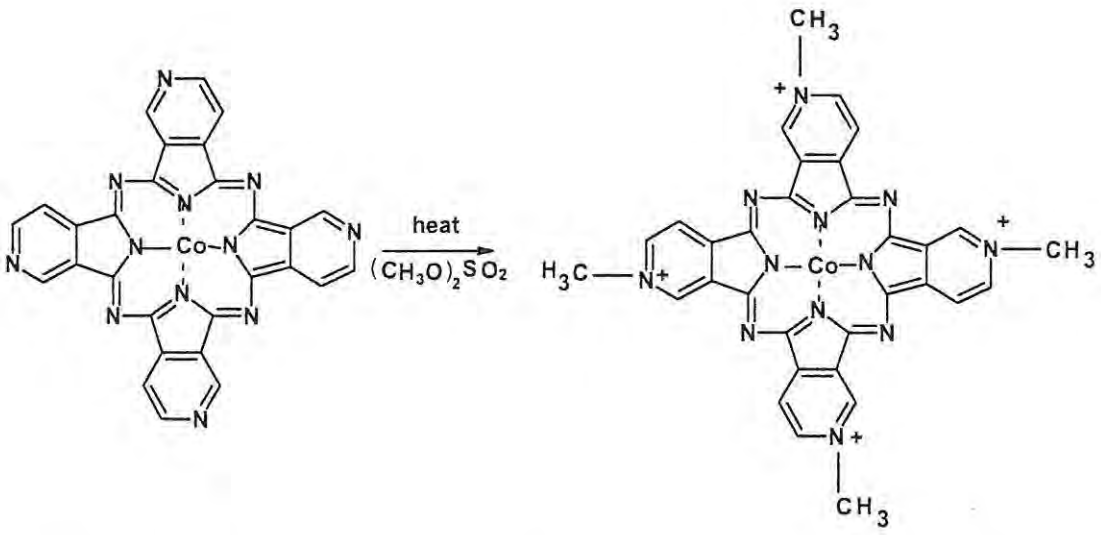

Scheme 2.2 Simplified synthetic route for quartenisation and formation of $[Co^{II}Tm\text{-}3,4\text{-}tppa]^{4+}$.

Cobalt-2,3-tetramethyltetrapyridinoporphyrazine ([CoTm-2,3-tppa]$^{4+}$)

The complex was prepared following the procedure outlined above for the preparation of [Co^{II}Tm-3,4-tppa)$^{4+}$, Scheme 2.2, except for substitution of Co-3,4-tppa by Co-2,3-tppa.[127] Same quantities of the reagents were employed. Yield = 60%. IR spectra (KBr discs, cm^{-1}) 443w, 628s, 748w, 981m, 1087vs, 1140m, 1438m, 1561m, 1655s, 2346w, 3390s. UV/Vis in water (λ_{max}, nm (log ε)) 341 (5.0), 428 (4.6), 561 (4.6), 616 (4.8). Elemental analysis results calculated for $C_{32}H_{28}N_{12}O_{18}S_4Co.2H_2O$: C, 36.59; N, 17.80; H, 2.50. Found: C, 36.08; N, 16.79; H, 3.90 %.

Synthesis of axially ligated [Co^{II}Tm-3,4-tppa)$^{4+}$ complexes

The solid [Co^{II}Tm-3,4-tppa)$^{4+}$ complex containing axially ligated nitrite was prepared by adding nitrite to aqueous solution of [Co^{II}Tm-3,4-tppa]$^{4+}$ until defined spectral changes were observed. Water was then removed by evaporation. IR spectra (KBr discs, cm^{-1}) 619w, 773w, 831m, 1002m, 1268vs, 1385m, 1630m (Co-nitrite), 2360w, 2553w, 3434s. UV/Vis in water (λ_{max}, nm (log ε)) 351 (4.5), 437 (3.8), 589 (4.2), 663 (4.5).

The solid [Co^{II}Tm-3,4-tppa]$^{4+}$ complex containing axially ligated cysteine was prepared by adding cysteine to aqueous solution of [Co^{II}Tm-3,4-tppa)$^{4+}$ until defined spectral changes were observed. Water was then removed by evaporation. IR spectra (KBr discs, cm^{-1}) 430w, 533m, 582m, 614s, 763vs, 847w, 1004vs, 1060m, 1216m, 1402sh, 1716s, 3207vs. UV/Vis in water (λ_{max}, nm (log ε)) 659 (1.5).

The solid [CoTm-3,4-tppa)$^{4+}$ complex containing axially ligated histidine was prepared by adding histidine to aqueous solution of [CoTm-3,4-tppa)$^{4+}$, until defined spectral changes were observed. Then water was evaporated off. IR spectra (KBr discs, cm^{-1}) 426vs, 538vs, 625vs, 651m, 685vs, 732w, 777s, 796s, 836w, 924vs,

967vs, 1064s, 1086m, 1112m,1172w, 1252vs, 1271s, 1416s, 1464s, 1568w, 1635vs, 2027m, 3012s. UV/Vis in water (λ_{max}, nm (log ε)) 659 (1.2).

2.2.3. Synthesis of cobalt(II) tetrasulfophthalocyanine ($[Co^{II}TSPc)^{4-}$), Scheme 2.3

$[Co^{II}TSPc]^{4-}$ was prepared and purified according to reported procedures,[3] Scheme 2.3. The monosodium salt of 4-sulfophthalic acid (4.32g), ammonium chloride (4.7g), urea (5.8g), ammonium molybdate (0.068g) and cobalt(II) sulphate (1.36g) were ground together to form a homogeneous mixture. 0.01 dm^3 nitrobenzene was added to a 0.15 dm^3 two-necked flask fitted with a condenser and a thermometer and heated to 453 K. The solid mixture was slowly added to the flask with stirring, while the temperature was kept between 433 and 463 K. The heterogeneous mixture was heated for 6 hours at 453 K. The crude product was ground and washed with methanol until the odor of nitrobenzene could no longer be detected. The remaining solid was added to 0.11 dm^3 of 1.0 mol dm^{-3} HCl saturated with sodium chloride. This step ensures removal of excess Co(II) from the product. The solution and accompaning undissolved material were briefly heated to boiling, cooled to room temperature and filtered. The resulting solid was dissolved in 0.07 dm^3 of 0.1 mol dm^{-3} NaOH. The solution was heated to 353 K and insoluble impurities were removed by filtration. NaCl (27g) was added to the solution. At this point some of the solid product precipitated. The slurry was heated and stirred at 353 K until ammonia evolution stopped. The product was obtained by filtration and the initial reprecipitation process was repeated twice. The solid was separated and washed with 80% aqueous ethanol until the filtrate was chloride free (using $AgNO_3$ test for Cl^-). The product was refluxed for 4 hours in 0.02 dm^3 of absolute ethanol, and the final blue product filtered and dried overnight. Yield = 80%. IR spectra (KBr discs, cm^{-1})

409m, 595s, 651s, 700s, 751s, 833m, 1031s, 1059m, 1112m, 1151w, 1189m, 1385s, 1438m, 1655m, 2347w. UV/Vis in water (λ_{max}, nm (log ε)) 320 (5.2), 625 (4.8), 660 (3.4). Elemental analysis results calculated for $Na_4C_{32}H_{16}N_8O_{13}S_4Co.4H_2O$: C, 35.72; N, 10.42; H, 1.86. Found: C, 35.07; N, 10.38; H, 1.68 %.

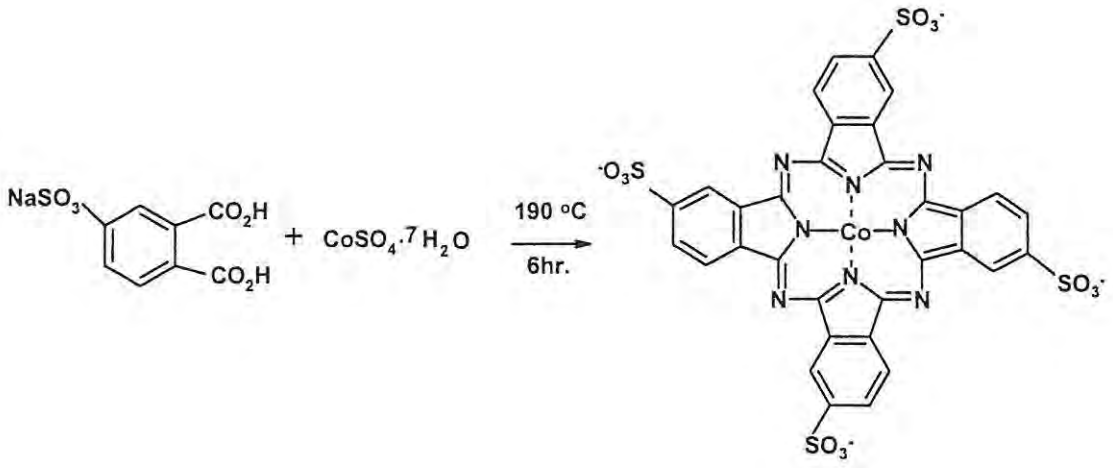

Scheme 2.3 Simplified synthetic route of $[Co^{II}TSPc]^{4-}$.

Synthesis of axially ligated $[Co^{II}TSPc)^{4-}$ complexes

The solid $[Co^{II}TSPc]^{4-}$ complex containing axially ligated cyanide was prepared by adding cyanide to aqueous solution of $[Co^{II}TSPc]^{4-}$ until defined spectral changes were observed. Water was then removed by evaporation. UV/Vis in pH 11 (λ_{max}, nm (log ε)) 329 (4.2), 449 (4.3), 428 (3.2), 610 (4.1), 676 (4.6). IR spectra (KBr discs, cm^{-1}) 571w, 596m, 651m, 699m, 750m, 833s, 934m, 1031vs, 1060m, 1150m, 1326m, 1652vs, 1993s, 2063w, 2130w (Co-CN), 2340w, 2364m, 3529vs.

The solid $[Co^{II}TSPc]^{4-}$ complex containing axially ligated SO_2 was prepared by bubbling SO_2 to aqueous solutions of $[Co^{II}TSPc]^{4-}$ until defined spectral changes were observed. Water was then removed by evaporation. UV/Vis in pH 11 (λ_{max}, nm (log ε)) 334 (3.8), 348 (3.8), 607 (3.5), 673 (4.1). IR spectra (KBr discs, cm^{-1}) 592s,

650sh, 700sh, 749w, 874s, 1035s, 1057s, 1112w, 1208vs (Co-SO_4^{2-}), 1403vs, 1652s, 2340m, 2358m, 3446vs.

2.2.4. Synthesis of iron(II) tetrasulfophthalocyanine ($[Fe^{II}TSPc]^{4-}$)

The procedure for the synthesis of $[Fe^{II}TSPc)^{4-}$ is similar to that employed for $[Co^{II}TSPc)^{4-}$, Scheme 2.3, with cobalt(II) sulphate replaced with iron(II) chloride tetrahydrate. Yield = 45%. IR spectra (KBr discs, cm^{-1}) 559sh, 594w, 631w, 698m, 741w, 832s, 930w, 1030vs, 1056w, 1110m, 1147w, 1191vs, 1368m, 1437w, 1561w, 1648w, 2839w, 2348w, 2839w, 3435vs. UV/Vis in water (λ_{max}, nm (log ε)) 327 (5.2), 631 (4.3), 663 (3.6).

2.2.5. Synthesis of $[Co^{II}TSPc]^{4-}.[Co^{II}Tm\text{-}3,4\text{-}tppa]^{4+}$ dimer

A mixture of $[Co^{II}Tmtppa]^{4+}$ and $[Co^{II}TSPc]^{4-}$ to form ($[Co^{II}Tmtppa]^{4+}.[CoTSPc]^{4-}$) species was prepared by mixing aqueous solutions (equimolar amounts) of the individual species, following the methods used for preparing 1:1 cationic/anionic porphyrin complexes.[13,16,128,129] A precipitate readily formed following mixing of the two solutions. The resulting precipitate was collected by evaporation in rotavapor and washed twice with methanol. IR spectra (KBr discs, cm^{-1}) 603sh, 637sh, 698s, 750m, 832sh, 933sh, 1029vs, 1060m, 1111sh, 1145m, 1190sh, 1217sh, 1328m, 1389sh. UV/Vis in water (λ_{max}, nm (log ε)) 320 (5.5), 490 (5.0), 620 (5.3), 660 (5.3). Elemental analysis results calculated for $Na_4C_{64}H_{44}N_{20}O_{31}S_8Co_2.8H_2O$: C, 34.04; N, 12.41; H, 2.66. Found: C, 33.60; N, 11.51; H, 3.35 %.

2.3. Methods

2.3.1. Electrochemical methods

2.3.1.1. Voltammetry

Cyclic voltammetry experiments were carried out in a one compartment, three-electrode cell. The working electrode was either an unmodified glassy carbon electrode (GCE) (area = 0.07 cm^2) or a GCE modified with MPcs and $[MTmtppa]^{4+}$. Silver|silver chloride (Ag|AgCl (3 mol dm^{-3} KCl)) reference was employed for all studies in aqueous media. A silver wire/silver ion electrode [(Ag/Ag^+ (0.1 mol dm^{-3})], containing a silver wire immersed in 0.1 mol dm^{-3} $AgNO_3$ and 0.1 mol dm^{-3} TEAP/DMSO was used as a non-aqueous reference electrode. Pt wire counter electrodes were employed. Solutions were deaerated with N_2 and a constant N_2 atmosphere was maintained throughout the voltammetry scans.

2.3.1.2. Electrode modification

Prior to modification, the GCE was polished with alumina (< 10 μm) on a Buehler felt pad, soaked in dilute nitric acid and rinsed in water. The GCE modification was performed by drop dry method or by electrodepositing from solutions of MPcs or $[MTmtppa]^{4+}$ in aqueous or organic media.

In the drop dry method, a drop of a saturated (~ 1 x 10^{-3} mol dm^{-3}) solution of MPc, MTppa or $[MTmtppa]^{4+}$ in pyridine or in water (for water soluble complexes) was placed on GCE and dried in air.

Electrodeposition was carried out at different pH (e.g. pH 4, 7.4 and 10.2) and in DMF containing TEAP. The choice of solvent and electrodeposition potential ranges was dependent on the stability of the resulting film. Following the report by Tse et.al.,[11] $[Co^{II}Tm\text{-}3,4\text{-}tppa]^{4+}$ was electrodeposited from pH 4 buffer (phosphate)

by repetitive scanning in the negative direction from 0 V to - 0.6 V vs. Ag|AgCl. $[CoTm\text{-}3,4\text{-}tppa]^{4+}$.$[Co^{II}TSPc]^{4-}$ was deposited in pH 4 buffer (phosphate) by scanning from - 0.2 to + 1.0 V. $[Co^{II}TSPc]^{4-}$ is known to readily form a film on the GCE when deposited from non-aqueous solvents in the positive potential range.[122] Hence, $[Co^{II}TSPc]^{4-}$ was deposited in this work from DMF containing TEAP in the potential range - 0.2 to + 1.0 V vs. Ag|AgCl. Purple films were observed in all cases after removal of the GCE from the respective solutions.

GCE modification was also performed by electrodepositing from a solution of $[Co^{II}TSPc]^{4-}$ in pH 10.2 Tris buffer. $[Fe^{II}TSPc]^{4-}$ was electrodeposited from pH 7.4 phosphate buffer. The deposition of $[Co^{II}TSPc]^{4-}$ or $[Fe^{II}TSPc]^{4-}$ was carried out by scanning (using cyclic voltammetry) at 0.1 V s^{-1} between - 0.9 to + 1.25 V vs. Ag|AgCl in pH 10.2 buffer or between - 1.5 to + 1.5 V vs. Ag|AgCl in pH 7.4 buffer.

The electrode was then placed in a cell containing the appropriate solvent, in the absence of catalyst, and scanned in the same potential range as for the deposition until the peak current was stable. The electrode was ready for analysis.

2.3.1.3. Osteryoung square wave voltammetry

Osteryoung square wave voltammetry (OSWV) was used to complement CV where good sensitivity was required. OSWV parameters were: amplitude = 25 mV, frequency = 15 Hz and step E = 4 mV.

2.3.1.4. Bulk electrolysis

For bulk electrolysis, platinum sheet auxiliary and Ag|AgCl (3 mol dm^{-3} KCl) reference electrodes were employed, the auxiliary electrode being separated from the compartment housing the reference and working electrodes by a fine glass frit. The

working electrode for bulk electrolysis was a carbon rod (area = 0.2 cm^2) coated with a known amount of the complexes using the drop dry method. The average concentration of the adsorbed complexes was then calculated from the amount deposited onto the electrode. The surface coverage was of the order of $\Gamma \sim 10^{-10}$ mol cm^{-2}, as estimated from the area under the reduction peak following cyclic voltammetry of the complexes in the blank solution (electrolyte or buffer only).

2.3.1.5. Spectroelectrochemical methods

Spectroelectrochemical studies (pH 7) were performed using an optically transparent thin layer electrochemical (OTTLE) cell described in the literature.[130] The OTTLE cell contains a platinum grit working and counter electrodes and a silver wire pseudo-reference electrode. The OTTLE cell was connected to the BioAnalytical Systems (BAS) CV 27 Voltammograph.

2.3.2. Analysis of products of bulk electrolysis of nitrite

2.3.2.1. Analysis of ammonia

The ammonia generated following bulk electrolysis of nitrite was determined using Nessler method.[132] The reagent was prepared according to the literature methods.[132] To 17.5 g potassium iodide dissolved in 0.05 dm^3 water, was added 4% mercury(II) chloride solution, with stirring, until a slight red precipitate remained. Next, a solution of 60 g sodium hydroxide in 0.125 dm^3 water was introduced with stirring and made up to 0.5 dm^3 with Millipore water. Small amounts of mercury(II) chloride solution was added until there was a permanent turbidity. The mixture was then allowed to stand for one day and then decanted from the sediment. The solution was kept stoppered in a dark-coloured bottle until use.

The standards of ammonium hydroxide were prepared. Equal amounts of Nessler's reagent added to each. The spectra of the yellow/brown product formed were recorded after 10 minutes equilibration time. A standard curve was obtained and used to determine the concentration of ammonia from the bulk electrolysis of nitrite. The Nessler's reagent ($K_2[HgI_4]$) reacts with ammonia according to equation 2.1.

$$\mathbf{2K_2[HgI_4] + 2NH_3 = NH_2Hg_2I_3 + 4KI + NH_4I} \qquad \mathbf{(2.1)}$$

($NH_2Hg_2I_3$ is the yellow/brown precipitate).

2.3.2.2. Analysis of hydroxylamine

Hydroxylamine was determined spectroscopically using established methods.[5] In this procedure, 0.0002 dm^3 of the electrolysis solution, 0.003 dm^3 of 0.3 mol dm^{-3} potassium hydrogen phthalate and 0.001 dm^3 of 0.01 mol dm^{-3} ferrozine were mixed and diluted to 0.008 dm^3 with Millipore water. After addition of 0.002 dm^3 of 0.01 mol dm^{-3} $FeCl_3$, the reaction was allowed to proceed for 7 min and the absorbance was then measured at 564 nm. From equation 2.2, 1 mole sodium nitrite gives 1 mole of hydroxylamine.

$$\mathbf{NO_2^- + 5H^+ + 4e^- \rightarrow NH_2OH + H_2O} \qquad \mathbf{(2.2)}$$

2.3.3. Kinetics and equilibria

Kinetic and equilibrium studies were run at precise temperatures between 20 and 21 °C and monitored with the spectrophotometer. The reactions were carried out in 0.1 or 0.01 mol dm^{-3} Tris buffer (ionic strength, μ = 0.5 mol dm^{-3} $NaClO_4$, pH 3.2 to 11). The appearance of the spectra due to the products formed following the addition of an analyte (cyanide, SO_2, nitrite or NO) to solutions of appropriate MPc or porphyrazine, was monitored. In some instances the disappearance in the spectra was employed (e.g. cysteine or histidine). Typically, a known volume of the solution of

$[Co^{II}TSPc]^{4-}$ or $[Co^{II}Tm\text{-}3,4\text{-}tppa]^{4+}$ was added to a 1 cm path length spectrophotometric cell. Then, a known volume of the aqueous solution of cyanide, SO_2, nitrite, NO, cysteine or histidine in an appropriate solvent was added to the cell and changes in absorbance monitored with time. The concentration of the $[Co^{II}TSPc]^{4-}$ complex in water was estimated from the published molar extinction coefficient of 5.8×10^4 dm^3 mol^{-1} cm^{-1} at 663 nm,[131] while that of $[CoTmtppa]^{4+}$ was estimated from the molar extinction coefficient of 9.2×10^4 dm^3 mol^{-1} cm^{-1} in water, at 659 nm, determined in this work. The concentrations of the analytes, MPc and $[MTmtppa]^{4+}$ are given in the relevant sections of the results and discussions and in Table 2.1. The concentrations of cyanide, SO_2, nitrite, NO, cysteine and histidine were at least tenfold larger than those of $[CoTSPc]^{4-}$ and $[CoTm\text{-}3,4\text{-}tppa]^{4+}$. Pseudo-first order conditions were assumed for kinetic studies.

Table 2.1 Concentrations of analytes, catalysts and pH employed in kinetics and equilibria studies

Analyte	**Catalyst**	**[Catalyst]/ mol dm^{-3}**	**pH**	**[Analyte]/mol dm^{-3} range**
CN^-	$[CoTSPc]^{4-}$	1.0×10^{-5}	11	$2.5.x\ 10^{-3}$ to 8.7×10^{-2}
SO_2	$[CoTSPc]^{4-}$	1.0×10^{-5}	7.4, 11	$2.0.x\ 10^{-3}$ to 1.6×10^{-2}
NO_2^-, NO	$[CoTm\text{-}3,4\text{-}tppa]^{4+}$	4.0×10^{-6}	4, 7	$1.5.x\ 10^{-5}$ to 2.4×10^{-2}
Cysteine, histidine	$[CoTm\text{-}3,4\text{-}tppa]^{4+}$	2.2×10^{-6}	3.2, 7	$2.2.x\ 10^{-5}$ to 2.0×10^{-4}

The concentration of cyanide in non-aqueous media was determined by titration with silver nitrate.[132]

SO_2 stock solutions were prepared by bubbling SO_2 gas into aqueous solutions. The flasks containing SO_2 were closed with a tight fitting stopper. SO_2

concentrations were determined by treatment with standard iodine, followed by titration with standard aqueous sodium thiosulphite.[132]

2.3.4. Preparation of NO

NO gas was prepared by adding saturated sodium nitrite drop-wise to a 0.2 mol dm^{-3} H_2SO_4 solution under nitrogen atmosphere. The NO produced was passed through a column containing solid potassium hydroxide to remove higher oxides of NO and then bubbled into nitrogen-saturated Millipore water. NO solutions were prepared freshly before use, kept in a glass flask fitted with a rubber septum and used for kinetic and equilibrium studies within six hours of preparation. NO concentration in water was calculated using the reported solubility of 2.2×10^{-3} mol dm^{-3} at 1 atm.[133]

2.4. Instrumentation

UV/Vis spectra were recorded with the Cary 500 UV/Vis/NIR Spectrophotometer. Infrared spectra (KBr discs) were recorded with the Perkin Elmer Spectrum 2000 FTIR spectrophotometer.

Cyclic voltammetry and OSWV were performed with a Bioanalytical system (BAS) model 100B/W electrochemical-workstation. ^{1}H-nuclear magnetic resonance (NMR, 400 MHz) spectra were obtained in D_2O using the Bruker EMX 400 NMR spectrometer.

RESULTS AND DISCUSSION

CHAPTER 3

CHARACTERISATION AND INTERACTIONS OF CATALYSTS WITH ANALYTES*

* Part of the work presented in this chapter has been published in the following journals: M. Thamae and T. Nyokong, (a) *J. Porphyrins Phthalocyanines,* **5** (2001) 839 and (b) *Polyhedron,* **21** (2002) 133.

3. CHARACTERISATION AND INTERACTIONS WITH ANALYTES.

3.1. Spectral characterisation

3.1.1. Metallotetrasulfophthalocyanine ($[M^{II}TSPc]^{4-}$)

Electronic absorption spectra of $[Co^{II}TSPc]^{4-}$ complexes have been described in terms of the monomer-dimer equilibrium.[131,134] The peak located at a higher-wavelength (~ 670 nm) has been attributed to a monomer peak and the lower-wavelength peak (~ 630 nm) to a dimer. This equilibrium is affected by conditions such as ionic strength, pH and temperature. In this work, for $[Co^{II}TSPc]^{4-}$, two peaks are observed at 625 and 660 nm in pH 4 buffer, Fig. 3.1(a). The B band was observed at 320 nm. The absorption bands and the molar absorptivities are shown in Table 3.1. The IR spectrum of $[Co^{II}TSPc]^{4-}$ is shown in Fig. 3.2 and the peak assignments in Table 3.2.

The nature of $[Fe^{II}TSPc]^{4-}$ complex has been investigated. Like all $[MTSPc]^{4-}$ complexes, the spectrum consists of monomer-dimer equilibrium in aqueous solutions. The monomer peak was observed at 663 nm and the dimer peak at 631 nm for $[FeTSPc]^{4-}$ species, Fig. 3.3. The B band was observed at 327 nm. The absorption bands and the molar absorptivities are shown in Table 3.1. The nature of $[FeTSPc]^{4-}$ species prepared by the method of Weber and Busch[3] has been found to vary from batch to batch. A wide range of iron phthalocyanine complexes have been found to be obtained with different preparation batches,[135] with some authors reporting on the formation of μ-oxo complexes, while some authors did not find any evidence for μ-oxo species. The spectrum shown in Fig. 3.3 is typical of dimeric $(FeTSPc)_2$ in equilibrim with the monomeric species.[136] The IR spectrum of $[Fe^{II}TSPc]^{4-}$ is typical

of MPc complexes, with peak assignments given in Table 3.2. There was no evidence of the oxo complex.

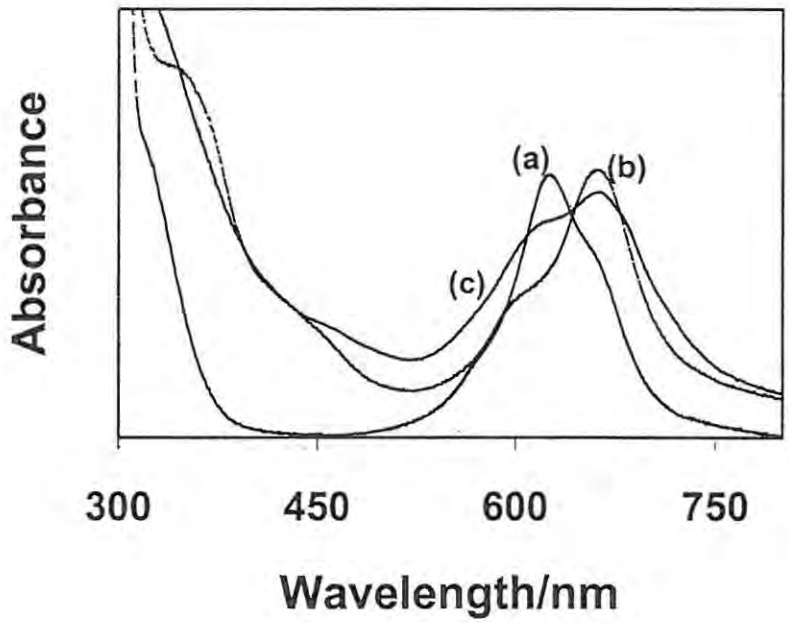

Fig. 3.1 Electronic absorption spectra in pH 4 buffer of (a) 9.0 x 10^{-6} mol dm^{-3} $[Co^{II}TSPc]^{4-}$, (b) 5.5 x 10^{-6} mol dm^{-3} $[Co^{II}Tm\text{-}3,4\text{-}tppa]^{4+}$ and (c) the mixture of complexes $[Co^{II}TSPc]^{4-}$ and $[Co^{II}Tm\text{-}3,4\text{-}tppa]^{4+}$, 2.2 x 10^{-6} mol dm^{-3}.

Table 3.1 Main absorption bands and molar absorptivities of $[M^{II}TSPc]^{4-}$ and $[Co^{II}Tmtppa]^{4+}$ complexes in water.

Complex	**Q band/nm (log ε)**	**B band/nm (log ε)**
[a]$[Co^{II}Tm\text{-}3,4\text{-}tppa]^{4+}$	659 (5.0)	330(5.1)
[b]$[Co^{II}Tm\text{-}2,3\text{-}tppa]^{4+}$	616 (4.8)	341 (5.0)
[a]$[Co^{II}TSPc]^{4-}$	625 (4.8) 660 (3.4)	320 (5.2)
[b]$[Fe^{II}TSPc]^{4-}$	631 (4.3) 663 (3.6)	327 (5.2)

[a] = pH 4 buffer, [b] = unbuffered

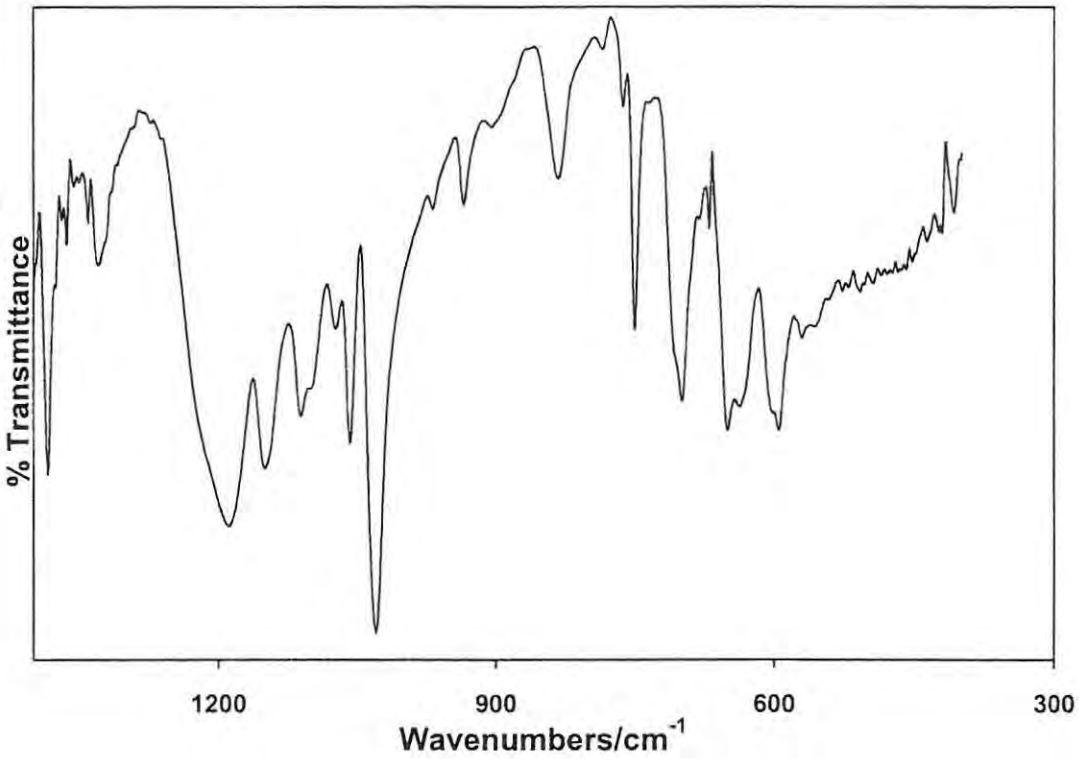

Fig. 3.2 The IR spectum of $[Co^{II}TSPc]^{4-}$. KBr discs.

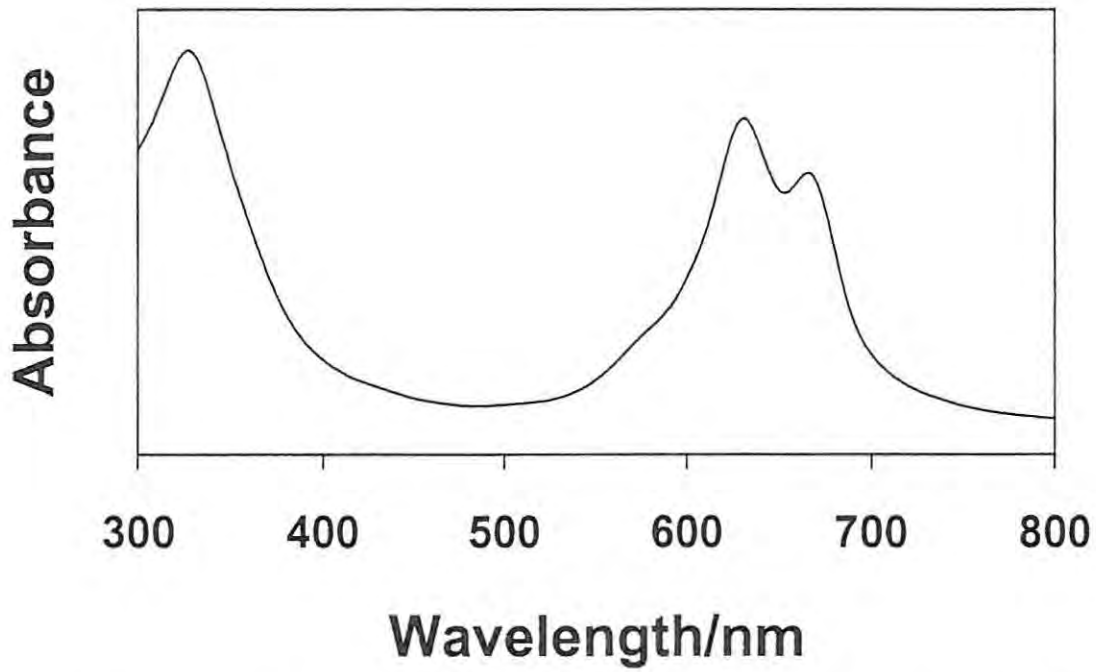

Fig. 3.3 Electronic absorption spectrum in water of 1.0×10^{-5} mol dm^{-3} $[Fe^{II}TSPc]^{4-}$.

Table 3.2 The IR data for $[M^{II}TSPc]^{4-}$ and $[M^{II}Tmtppa]^{4+}$ complexes. KBr discs.

$[Co\text{-}3,4\text{-}Tmtppa]^{4+}$	$[CoTm\text{-}2,3\text{-}tppa]^{4+}$	$[CoTSPc]^{4-}$	$[FeTSPc]^{4-}$	Assignments
	443w	409m	559w	
583w		595s	594w	
616m	628s	651s	631w	
		700s	698m	ν(S-O)
757s	748w	751s	741w	π(C-H)
854m		833m	832s	(C-H)
933m	981m		930w	
1001vs	1087vs	1031s	1030vs	δ(C-H)
1057m		1059m	1056w	(C-H)
1121vs	1140m	1112m	1110m	(C-C)
		1151w	1147w	
1222vs		1189m	1191vs	
1304w		1385s	1368m	
1443m	1438m	1438m	1437w	
1533m	1561m		1561w	ν(C-C)
1643s	1655s	1655m	1648w	(C-N)
2366w	2346w	2347w	2348w	ν(C-H)
3069w	3390s		2839w	
3415s	3512	3410s	3435s	

ν = stretching vibrations, δ = in-plane bending vibrations, π = out-of-plane bending vibrations, m = medium, s = strong, vs = very strong, w = weak.

3.1.2. Cobalt(II) tetramethyltetrapyridinoporphyrazine ($[Co^{II}Tmtppa]^{4+}$)

The spectra of the $[MTmtppa]^{4+}$ (M = Zn(II) and Cu(II)) complexes has been described in terms of DMF-insoluble (split Q band) and DMF-soluble (single Q band) fractions due to the presence of mixtures of isomers.[5] The DMF-soluble fraction contains at least three isomers, whereas the DMF-insoluble fraction contains at least two isomers. The electronic absorption spectrum showed a Q band at 659 nm, a shoulder at 595 nm and the B band at 330 nm for $[CoTm\text{-}3,4\text{-}tppa]^{4+}$ in pH 4 buffer, Fig. 3.1(b). The $[Co^{II}Tm\text{-}2,3\text{-}tppa]^{4+}$ complex in pH 4 buffer has a strong absorption at 616 nm and a broad shoulder at 561 nm. The B band was observed at 341 nm for $[Co^{II}Tm\text{-}2,3\text{-}tppa]^{4+}$. The absorption bands and the molar absorptivities are shown in Table 3.1. IR spectrum of $[Co^{II}Tm\text{-}3,4\text{-}tppa]^{4+}$ is shown in Fig. 3.4 and Table 3.2, gives peak assignments. The IR spectrum for $[CoTm\text{-}3,4\text{-}tppa]^{4+}$ is typical of metallophthalocyanine type molecules.

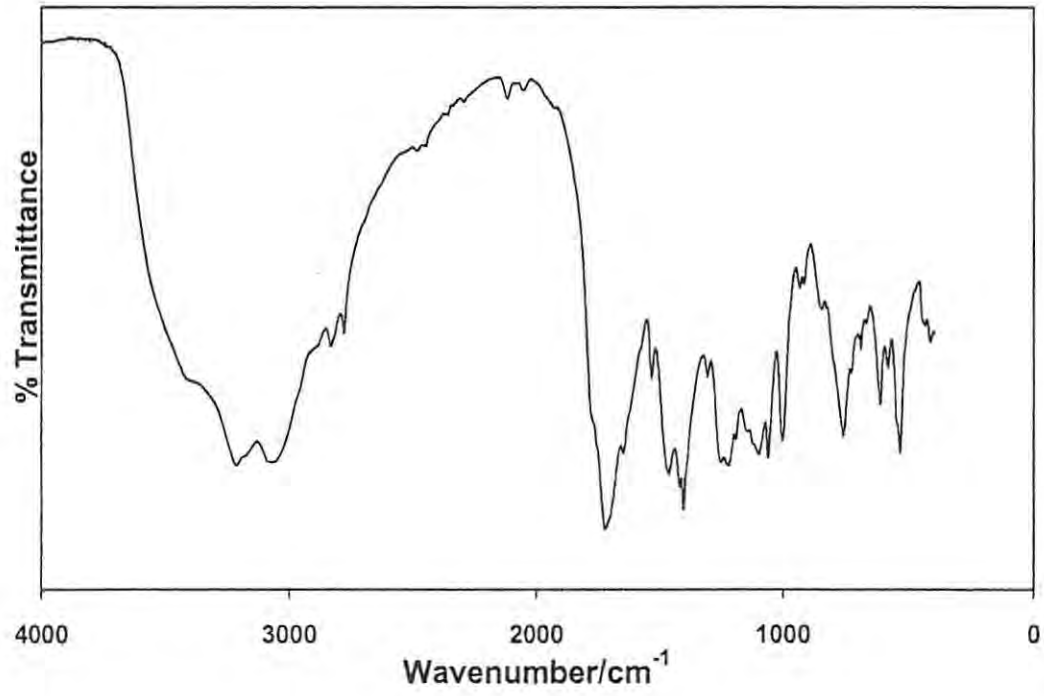

Fig. 3.4 IR spectrum of $[Co^{II}Tm\text{-}3,4\text{-}tppa]^{4+}$. KBr discs.

3.1.3. $[M^{II}Tmtppa]^{4+}.[M^{II}TSPc]^{4-}$ dimer

Fig. 3.1 compares the absorption spectrum, in pH 4 buffer, of the mixture of $[Co^{II}Tm\text{-}3,4\text{-}tppa]^{4+}$ and $[Co^{II}TSPc]^{4-}$ (hence, $[Co^{II}Tmtppa]^{4+}.[Co^{II}TSPc]^{4-}$ dimer) with that of the individual components. It is evident from Fig. 3.1(c) that the mixture is not simply the sum of the component monomer spectrum. The Q band of $[Co^{II}TSPc]^{4-}$ is observed at 625 nm (dimeric component) and at 659 nm for $[Co^{II}Tm\text{-}3,4\text{-}tppa]^{4+}$. The mixture of $[Co^{II}Tm\text{-}3,4\text{-}tppa]^{4+}$ and $[Co^{II}TSPc]^{4-}$ shows a split Q band with broad maxima at 660 nm and near 620 nm. There is a general broadening of the Q band for the dimer. The B band of the mixture of $[Co^{II}Tm\text{-}3,4\text{-}tppa]^{4+}$ and $[Co^{II}TSPc]^{4-}$ shows a broad envelope in the vicinity of 320 nm. The peak observed for $[Co^{II}Tm\text{-}3,4\text{-}tppa]^{4+}$ at 330 nm is not observed for the mixed complex. A broad feature is also observed near 490 nm for the complex formed by mixing the anionic $[Co^{II}TSPc]^{4-}$ with the cationic complex $[Co^{II}Tm\text{-}3,4\text{-}tppa]^{4+}$. This band was also observed for $[Co^{II}Tm\text{-}3,4\text{-}tppa]^{4+}$. Broadening and shifting in the Q band have been observed for the formation of cationic/anionic aggregates in porphyrins[16] as well as for the formation of aggregates between anionic and cationic porphyrin/phthalocyanine complexes.[15] Aggregation of oppositely charged porphyrin and phthalocyanine complexes is most conveniently studied by spectroscopic methods. Fig. 3.5(a) represents the spectral evolution observed on titration of $[Co^{II}TSPc]^{4-}$ with small aliquots of $[Co^{II}Tm\text{-}3,4\text{-}tppa]^{4+}$ complex. The formation of the aggregate between $[Co^{II}TSPc]^{4-}$ and $[Co^{II}Tm\text{-}3,4\text{-}tppa]^{4+}$ occurs with isosbestic points at 657 and 590 nm. The spectral changes consisted of the decrease in the dimeric peak of $[Co^{II}TSPc]^{4-}$, at 625 nm, and the increase and shifting in the monomeric peak of this complex from 660 to 668 nm. A new broad band appears near 490 nm on formation of the aggregated complex. At this stage, the spectrum is not similar to that observed

in Fig. 3.1(c), for the final product formed by the reaction of the cationic $[Co^{II}Tm\text{-}3,4\text{-}tppa]^{4+}$ and the anionic $[Co^{II}TSPc]^{4-}$. When the ratio of $[Co^{II}Tm\text{-}3,4\text{-}tppa]^{4+}$ with $[Co^{II}TSPc]^{4-}$ was approximately 1:1, a significant increase in the background was observed and spectral changes shown in Fig. 3.5(b) were obtained. These changes consisted of the shift of the two peaks in the Q band region from 625 and 668 nm to 620 and 660 nm, accompanied by the decrease in the absorption band at 620 nm and the increase in the intensity of the absorption band at 660 nm. A considerable broadening of the spectra was observed accompanying these spectral changes.

The spectral changes observed in Fig. 3.5 suggest that addition of small amounts of $[Co^{II}Tm\text{-}3,4\text{-}tppa]^{4+}$ to $[Co^{II}TSPc]^{4-}$ results in the shift of the monomer-dimer equilibrium in $[Co^{II}TSPc]^{4-}$ towards the monomeric side before the formation of the cationic/anionic aggregates.

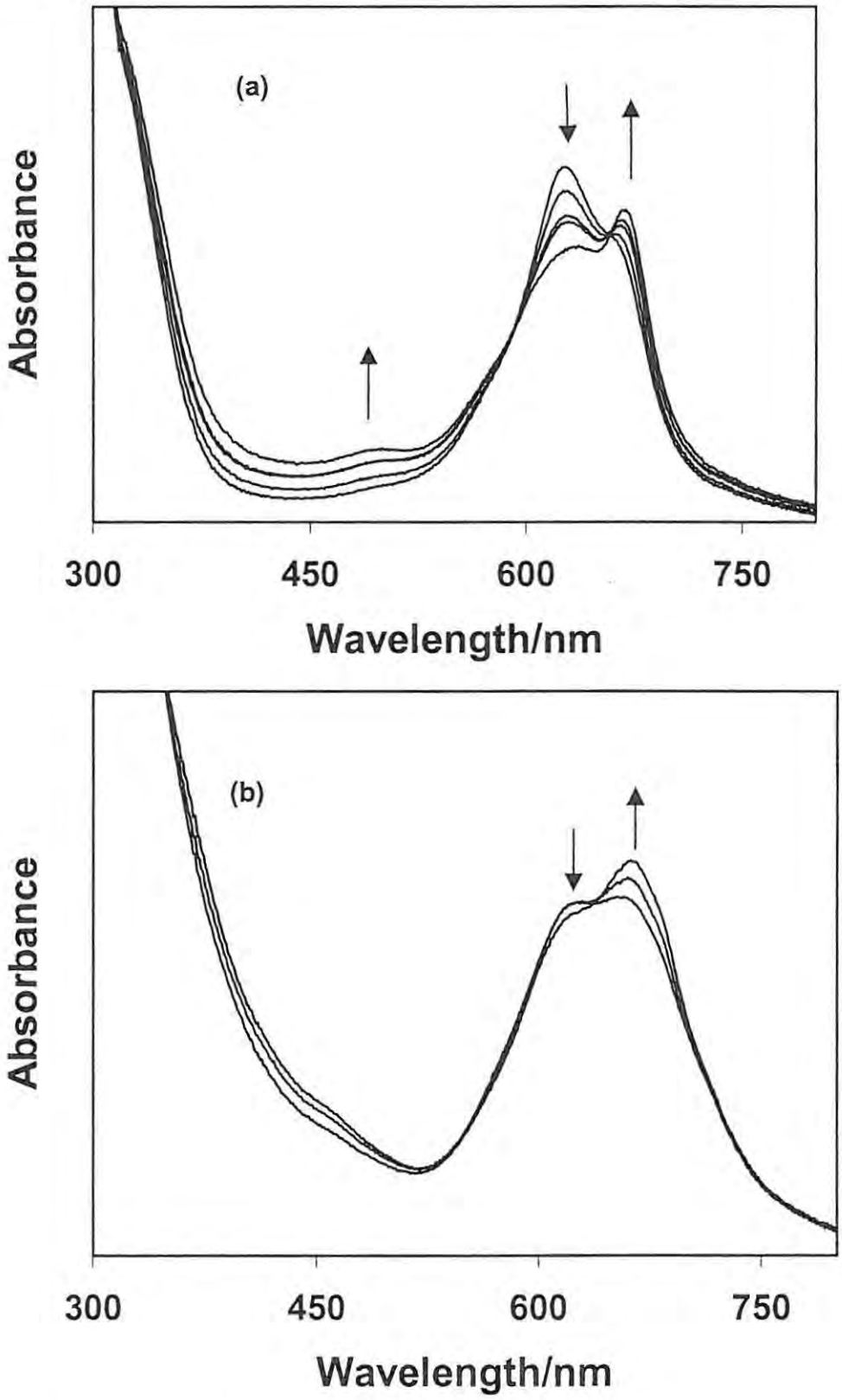

Fig. 3.5 Electronic absorption spectral changes observed on titration of $[Co^{II}TSPc]^{4-}$ with $[CoTm\text{-}3,4\text{-}tppa]^{4+}$ in pH 4 buffer. The initial concentration of $[Co^{II}TSPc]^{4-}$ = 8.75 x 10^{-6} mol dm^{-3}. Concentration of $[CoTm\text{-}3,4\text{-}tppa]^{4+}$ ranged from 4.4 x 10^{-7} to 1.75 x 10^{-5} mol dm^{-3}. Spectral changes before (a) and after (b) the attainment of 1:1 ratio of $[CoTm\text{-}3,4\text{-}tppa]^{4+}$ to $[CoTSPc]^{4-}$.

The stoichiometry of the mixed complex formed was deduced by Job's method.[14] In this method, the absorption, F(x), measured at a given wavelength for mixtures with various ratios of phthalocyanine (Pc) and porphyrazine (Pz) is calculated using the expression given by equation 3.1.

$$F(x) = d(x) - (\varepsilon_{Pc} - \varepsilon_{Pz})x - \varepsilon_{Pz} \qquad (3.1)$$

where $x = n_{Pc}/(n_{Pz} + n_{Pc})$ is the mole fraction of the Pc; ε_{Pc} and ε_{Pz} are the molar absorptivities of the Pc and of the Pz, respectively; d(x) is the actual optical density of the solution divided by the total concentration of chromophores. The Job diagram for the formation of the complex between $[Co^{II}Tm\text{-}3,4\text{-}tppa]^{4+}$ and $[Co^{II}TSPc]^{4-}$ is shown in Fig. 3.6. It consists of two straight lines intersecting at the mole fraction of $[Co^{II}Tm\text{-}3,4\text{-}tppa]^{4+}$ equal to 0.5, as is typical when a 1:1 complex is formed. This confirms the formation of the $[Co^{II}Tm\text{-}3,4\text{-}tppa]^{4+}.[Co^{II}TSPc]^{4-}$ dimer.

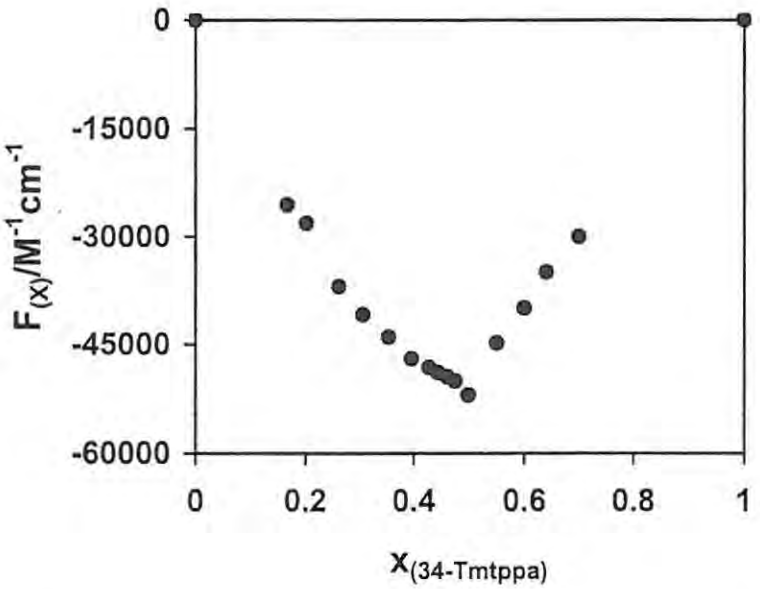

Fig. 3.6 Job plot of the electronic absorption spectral changes observed on addition of the cationic $[Co^{II}Tm\text{-}3,4\text{-}tppa]^{4+}$ to the anionic $[Co^{II}TSPc]^{4-}$, plotted against the mole ratio of $[Co^{II}Tm\text{-}3,4\text{-}tppa]^{4+}$. $\lambda = 659$ nm.

The reverse titration of $[Co^{II}Tm\text{-}3,4\text{-}tppa]^{4+}$ with $[Co^{II}TSPc]^{4-}$ was performed at pH 4 and pH 7, Fig. 3.7. Similar spectral changes were observed at both pH values. $[Co^{II}Tm\text{-}3,4\text{-}tppa]^{4+}$ is known to decompose in basic media, but are stable at acid or near neutral pH. Fig. 3.7 shows that there is considerable broadening of the Q band and shifting to longer wavelengths during the titration. The Q band shifts from 659 nm to a broad band near 610 nm. A broad feature is also formed near 470 nm. As observed in Fig. 3.5 for the titration of $[Co^{II}TSPc]^{4-}$ with $[CoTm\text{-}3,4\text{-}tppa]^{4+}$, when the ratio of the two components was 1:1, spectral changes different from those in Fig. 3.7(a) were observed as shown in Fig. 3.7(b). These changes consisted of the increase in the Q band and its resolution into two bands at 620 and 660 nm. These bands are similar to the maxima observed for the titration of $[Co^{II}TSPc]^{4-}$ with $[CoTm\text{-}3,4\text{-}tppa]^{4+}$, in Fig. 3.5(b). The relative intensities of the components of the Q band are however different in Fig. 3.7(b) when compared to Fig. 3.5(b). The possibility of the formation of aggregates higher than 1:1 ratio cannot be ruled out.

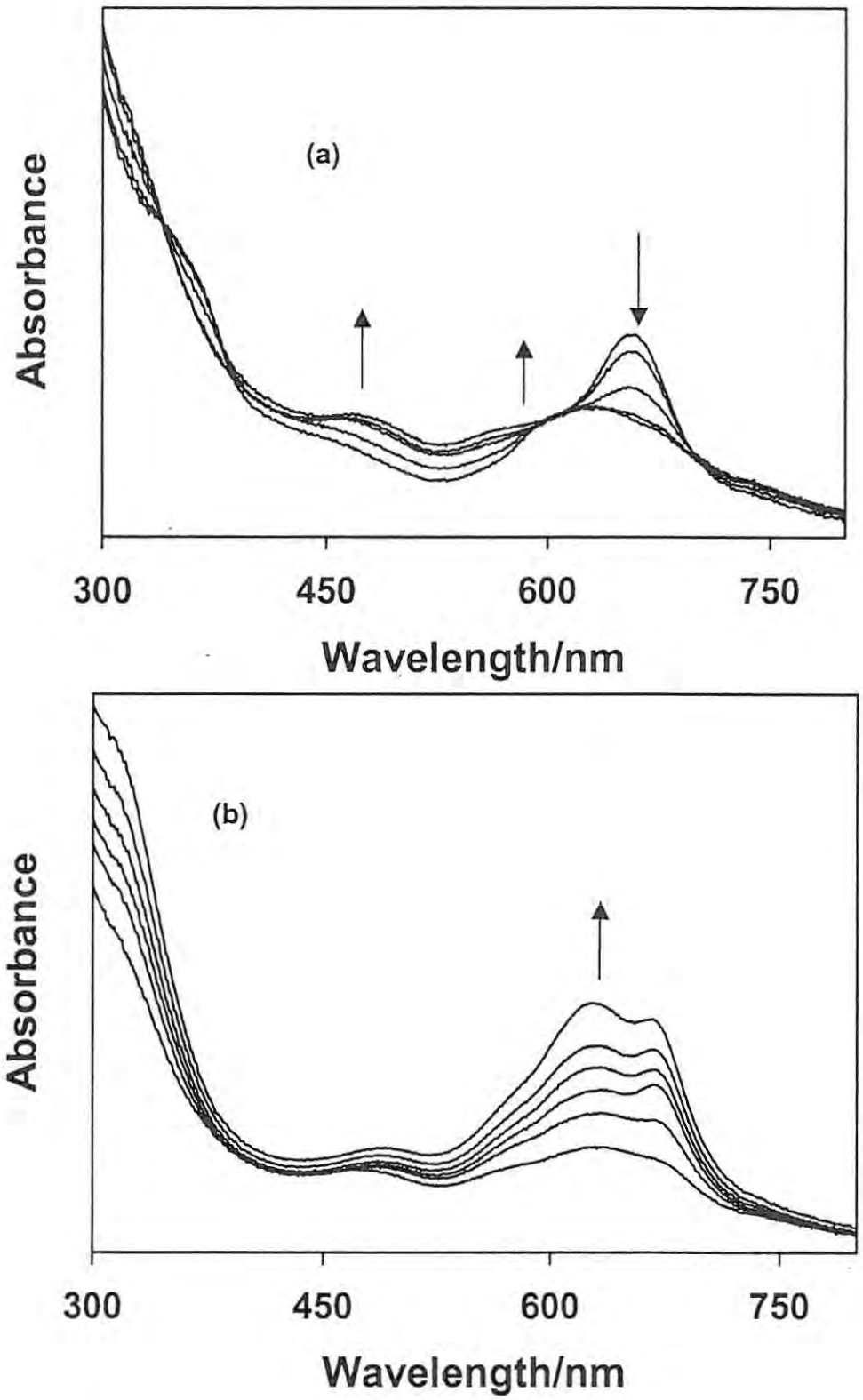

Fig. 3.7 Electronic absorption spectral changes observed on titration of $[CoTm\text{-}3,4\text{-}tppa]^{4+}$ with $[Co^{II}TSPc]^{4-}$ in pH 7 buffer. The initial concentration of $[CoTm\text{-}3,4\text{-}tppa]^{4+}$ = 2.68 x 10^{-6} mol dm^{-3}. Concentration of $[Co^{II}TSPc]^{4-}$ ranged from 8.72 x 10^{-7} to 8.72 x 10^{-6} mol dm^{-3}. Spectral changes before (a) and after (b) the attainment of 1:1 ratio of $[Co^{II}TSPc]^{4-}$ to $[Co^{II}Tm\text{-}3,4\text{-}tppa]^{4+}$.

3.2. Electrochemical characterisation

3.2.1 Cobalt(II) 3,4-tetramethyltetrapyridinoporphyrazine ($[Co^{II}Tm\text{-}3,4\text{-}tppa]^{4+}$)

Fig. 3.8 shows the cyclic voltammogram of $[Co^{II}Tm\text{-}3,4\text{-}tppa]^{4+}$ in pH 4 buffer. Two peaks are observed at $E_{½}$ = + 0.20 V and - 0.40 V vs. Ag|AgCl for couples I and II respectively, Fig. 3.8. Cyclic voltammetry of $[Co^{II}Tm\text{-}3,4\text{-}tppa]^{4+}$ has been described.[11,42] Two reduction couples were also observed before[11,42] in pH 4 buffer and on highly oriented pyrolytic graphite electrode; the first reduction was assigned to the Co^{II}/Co^{I} couple and the second couple to the ring based reduction. The reduction at + 0.20 V vs. Ag|AgCl is independent of pH. Couple I (+ 0.20 V) in Fig. 3.8 is assigned to first reduction of the metal ion in $[Co^{II}Tm\text{-}3,4\text{-}tppa(-2)]^{4+}$ and formation of $[Co^{I}Tm\text{-}3,4\text{-}tppa(-2)]^{3+}$, in comparison with the literature.[11,42] Couple II (- 0.40 V) in Fig. 3.8 corresponds to ring reduction in $[Co^{I}Tm\text{-}3,4\text{-}tppa(-2)]^{3+}$ and formation of $[Co^{I}Tm\text{-}3,4\text{-}tppa(-3)]^{2+}$. The Co^{II}/Co^{I} couple in $[Co^{II}Tm\text{-}3,4\text{-}tppa]^{4+}$ complexes occurs at a potential more positive than for any of the cobalt phthalocyanine derivatives.[11]

Couples I and II were observed at + 0.24 and – 0.55 V vs. Ag|AgCl for $[Co^{II}Tm\text{-}2,3\text{-}tppa]^{4+}$.

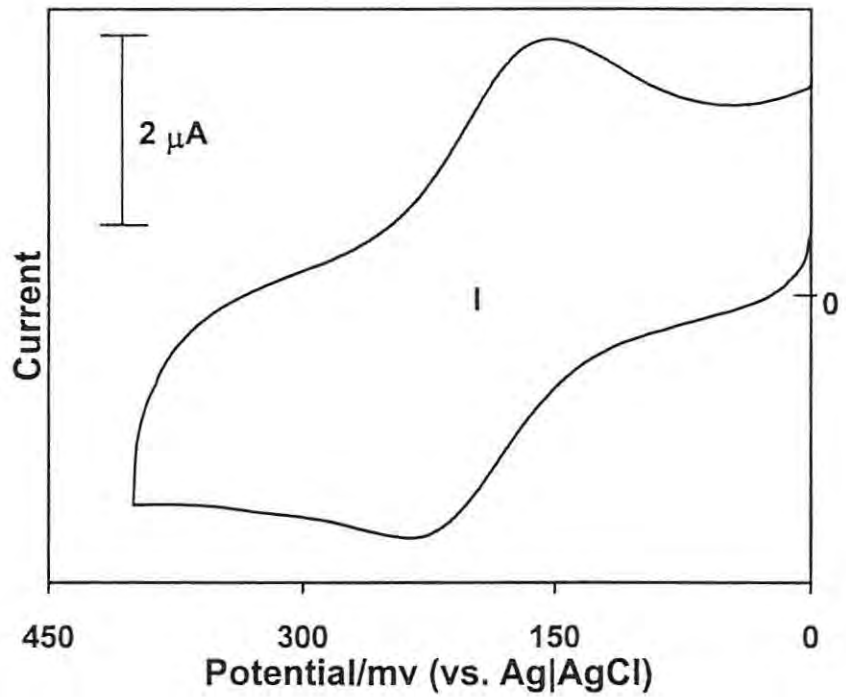

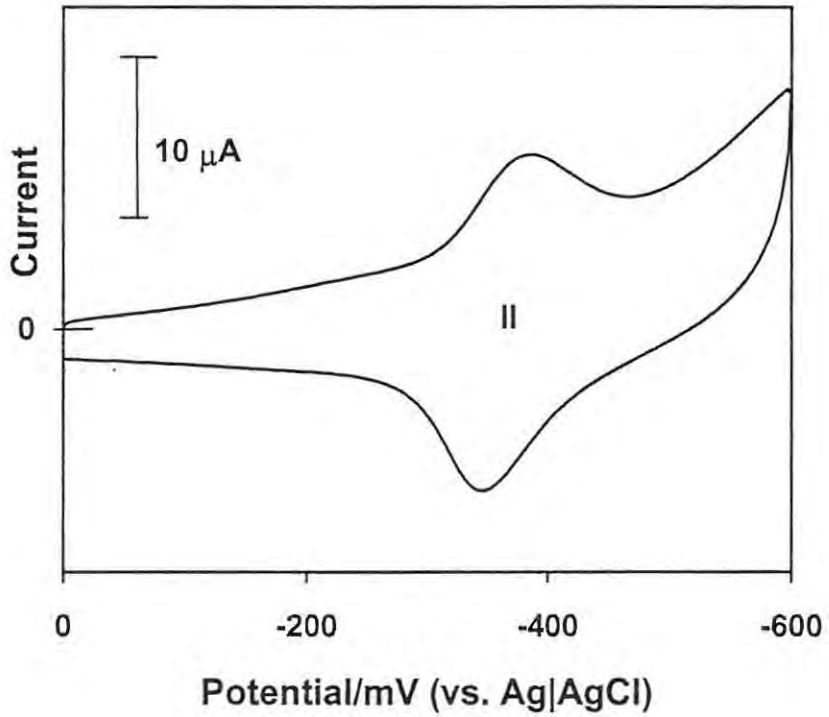

Fig. 3.8 Cyclic voltammogram of $[Co^{II}Tm\text{-}3,4\text{-}tppa]^{4+}$ in pH 4 buffer. Scan rate = 100 mV s^{-1}.

3.2.1.1. Spectroelectrochemical characterization of $[Co^{II}Tm\text{-}3,4\text{-}tppa]^{4+}$

In order to explain the behaviour of $[Co^{II}Tm\text{-}3,4\text{-}tppa]^{4+}$ complex on interaction with the nitrogen oxides species under discussion in this work, it was necessary to study the spectroelectrochemical behaviour of this complex. Cyclic voltammetry of this complex shows the first reduction at + 0.20 V vs. Ag|AgCl at pH 4 and 7. Electrolysis of the solution containing $[Co^{II}Tm\text{-}3,4\text{-}tppa]^{4+}$ in pH 7 buffer or water containing Na_2SO_4 at potentials of the first reduction, resulted in spectral changes shown in Fig. 3.9. These spectral changes consisted of the decrease in the Q-band at 659 nm and the simultaneous formation of new absorption bands, one near 470 nm and the other at 589 nm. A clear isosbestic point was observed at 543 nm and a diffuse one near 450 nm. From cyclic voltammetry studies above, the first reduction in $[Co^{II}Tmtppa]^{4+}$ occurs at the central metal with the formation of $[Co^{I}Tmtppa]^{3+}$ species. The formation of a violet coloured solution with a broad peak at 500 nm on addition of ascorbic acid to $[Co^{II}Tmtppa]^{4+}$ was also attributed to metal based reduction.[127] The $[Co^{I}Tmtppa]^{3+}$ species is insoluble and forms a purple precipitate. Spectral changes in Fig. 3.9 are similar to those reported[4] for the formation of the $[Co^{I}Tmtppa]^{3+}$ species. Absorption peaks in the 500 nm region are associated with ring reduction in $[M^{II}Tmtppa]^{4+}$ complexes containing non-transition metals (e.g. $[Zn^{II}Tmtppa]^{4+}$)[5] and are also typical of ring-based reductions in phthalocyanines.[9] However, $[Co^{I}Tmtppa]^{3+}$ shows an absorption in the 500 nm region and the Co^{I} oxidation state in $[Co^{I}Tmtppa]^{3+}$ species has been confirmed before by electron spin resonance spectroscopy (ESR).[4,5]

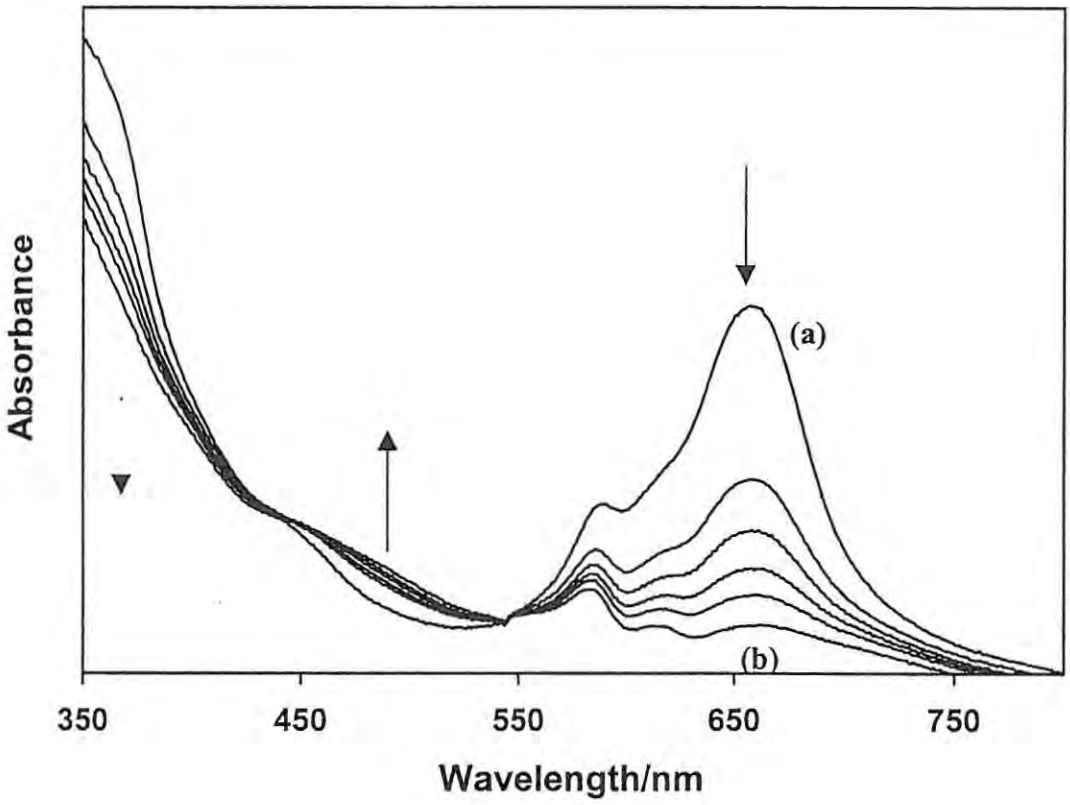

Fig. 3.9 Electronic absorption spectral changes observed on electrolysis (- 0.4 V) of $[Co^{II}Tm\text{-}3,4\text{-}tppa]^{4+}$, 2.2 x 10^{-6} mol dm^{-3} in water containing sodium sulphate (OTTLE cell). (a) spectrum before electrolysis, (b) spectrum at the end of electrolysis.

3.2.2. Metal(II) tetrasulfophthalocyanine ($[Co^{II}TSPc]^{4-}$)

Electrochemical properties of $[Co^{II}TSPc]^{4-}$ in aqueous[178] and non-aqueous[122] media have been described.

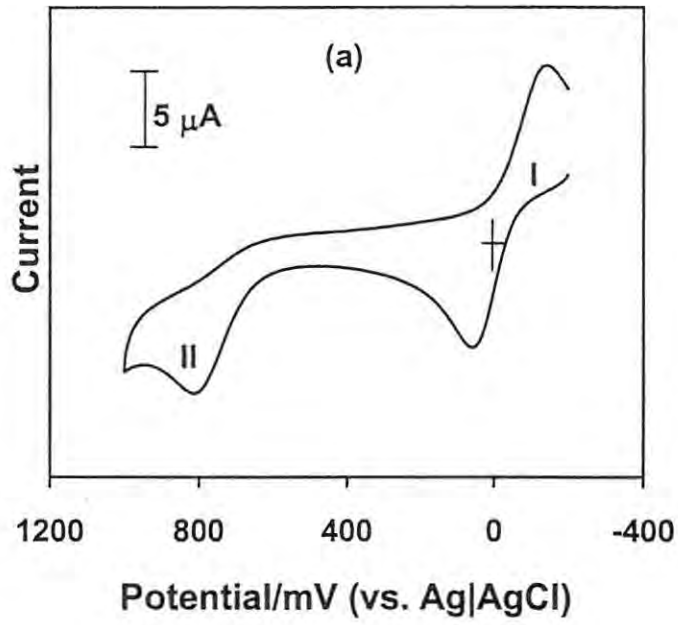

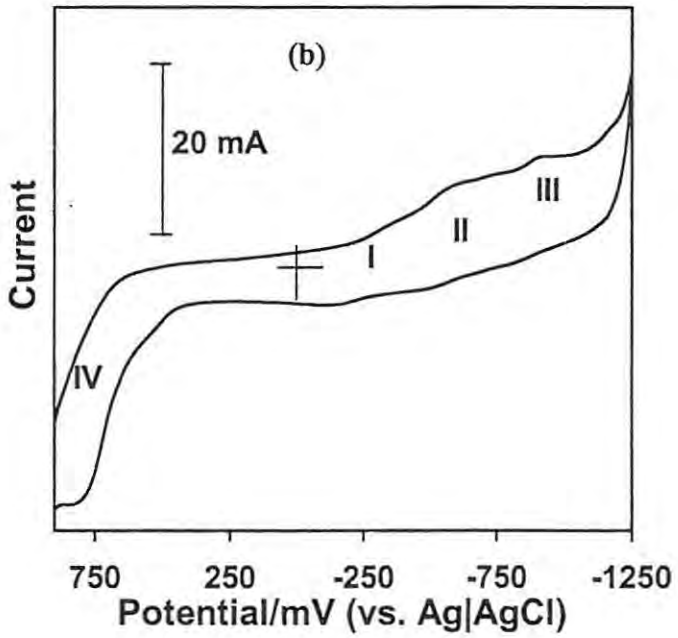

Fig. 3.10 Cyclic voltammogram of $[Co^{II}TSPc]^{4-}$ in (a) DMF containing 0.1 mol dm^{-3} TEAP and (b) in pH 10.2 buffer containing 0.1 mol dm^{-3} Na_2SO_4.

Fig. 3.10(a) shows the cyclic voltammogram for $[Co^{II}TSPc]^{4-}$ in DMF. The voltammogram consists of a couple at - 0.2 and a peak at + 0.8 V vs Ag|AgCl. According to the literature,[122] a quasi-reversible couple I may be assigned to reduction

of $[Co^{II}TSPc(2-)]^{4-}$ to $[Co^{I}TSPc(2-)]^{5-}$, since in donor solvents such as DMF, the first reduction in CoPc complexes occurs at the metal. Peak II in Fig. 3.10(a) is assigned to oxidation in $[Co^{II}TSPc]^{4-}$ and formation of $[Co^{III}TSPc]^{3-}$. As has been reported,[122] the first oxidation in $[Co^{II}TSPc]^{4-}$ is irreversible in DMF.

Cyclic voltammogram of $[Co^{II}TSPc]^{4-}$ in solution is known to exhibit broad ill-defined peaks,[178] hence the lack of clear resolution in Fig. 3.10 is not surprising. In Fig. 3.10(b), couples I to IV are observed at - 0.25, - 0.5, - 0.9 and + 0.8 V vs. Ag|AgCl and are assigned as follows, according to literature:[178] couple I is the reduction of metal ion in $[Co^{II}TSPc(-2)]^{4-}$ and formation of $[Co^{I}TSPc(-2)]^{5-}$, couple II corresponds to first ring reduction $[Co^{I}TSPc(-2)]^{5-}/[Co^{I}TSPc(-3)]^{6-}$, couple III corresponds to a second ring reduction $[Co^{I}TSPc(-3)]^{6-}/[Co^{I}TSPc(-4)]^{7-}$ and couple IV is the metal oxidation $[Co^{III}TSPc(-2)]^{3-}/[Co^{II}TSPc(-2)]^{4-}$.

Cyclic voltammogram of $[Fe^{II}TSPc]^{4-}$ shown in Fig. 3.11 is similar to that of $[Co^{II}TSPc(-2)]^{4-}$. Several authors have reported the difficulty in obtaining CV for $[Fe^{II}TSPc]^{4-}$, thus the observation of weak and irreversible peaks is not surprising. Despite extensive research on $[Fe^{II}TSPc]^{4-}$ as reported in literature, [3,137,138,139,140,141,178] no consensus has been found concerning the electrochemical behaviour of $[Fe^{II}TSPc]^{4-}$. Therefore, the paper by Zecevic et al.[178] was used to identify the observed peaks with respect to the wave potentials. However, their study showed that no peaks were observed during the first scan for $[Fe^{II}TSPc]^{4-}$, although broad peaks were observed for the first scan in this work. The peak (I) for first reduction in $[Fe^{II}TSPc]^{4-}$ was observed at - 0.5 V vs. Ag|AgCl and following literature assignments,[178] Peak I is assigned to metal reduction, Fe^{II}/Fe^{I}, in Fig. 3.11. Couple II, around 1.0 V vs. Ag|AgCl in Fig. 3.11, is attributed to Fe^{III}/Fe^{II} oxidation. A weak peak III near + 1.3 V vs. Ag|AgCl is attributed to ring oxidation in $[Fe^{III}TSPc(-2)]^{3-}$

giving $[Fe^{III}TSPc(-1)]^{2-}$. A relatively large irreversible reduction peak IV centered around 0.2 V vs. Ag|AgCl could be identified as the reduction of oxygen. Despite the fact that the experiments were carried out in solutions purged with nitrogen, oxygen was produced at the electrode surface at the most positive applied potentials. Scanning the potential to a value less positive (up to 1.25 V vs. Ag|AgCl) did not result in peak IV. It could therefore be concluded that this peak was due to oxygen reduction, and was not observed for $[Co^{II}TSPc]^{4-}$ (Fig. 3.10), since a less negative return potential was employed.

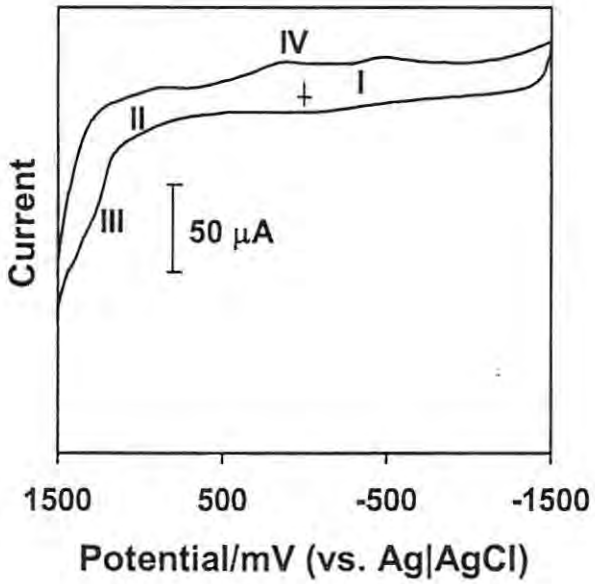

Fig. 3.11 Cyclic voltammogram of $[Fe^{II}TSPc]^{4-}$ in pH 7.4 buffer. Scan rate = 100 mV s^{-1}.

3.2.3. $[M^{II}Tm\text{-}3,4\text{-}tppa]^{4+}.[M^{II}TSPc]^{4-}$ dimer

3.2.3.1. Cyclic voltammetry

Cyclic voltammetry of the dimer, $[Co^{II}Tm\text{-}3,4\text{-}tppa]^{4+}.[Co^{II}TSPc]^{4-}$, in pH 4 buffer showed two reductions at $E_{½}$ = - 0.53 V and - 0.88 V vs. Ag|AgCl (Fig. 3.12(a)), couples I and II respectively, and one oxidation peak at + 0.78 V vs. Ag|AgCl (III). The first reduction was reversible with a cathodic to anodic (E_c - E_a)

peak separation of 60 mV and $i_p \alpha v^{1/2}$. For the second reduction, the cathodic currents were more enhanced when compared to the corresponding anodic currents. Both reduction peaks were located at potentials not associated with the reductions of the individual components of the mixture, implying that the cyclic voltammogram is not simply the sum of component voltammograms.

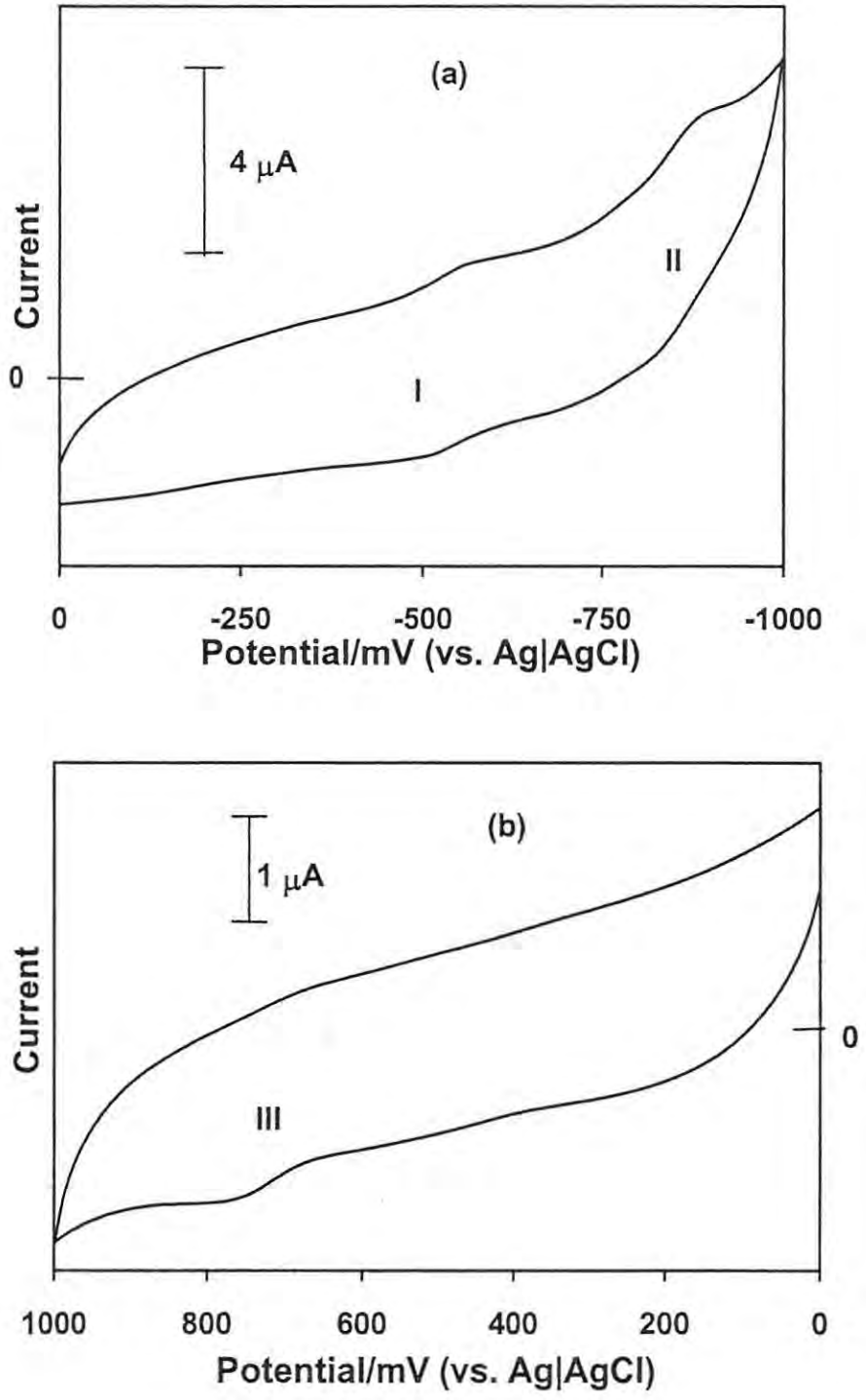

Fig. 3.12 Cyclic voltammetry of $[Co^{II}Tm\text{-}3,4\text{-}tppa]^{4+}.[Co^{II}TSPc]^{4-}$ aggregate in pH 4 buffer. Scan rate = 100 mV s^{-1}.

Under the same conditions used for CV of dimer (pH 4 buffer), the cyclic voltammogram of $[Co^{II}TSPc]^{4-}$ shows a peak at - 0.38 V vs. Ag|AgCl, Fig. 3.13, assigned to the reduction of the central metal from Co^{II} to Co^{I}. $[Co^{II}Tm\text{-}3,4\text{-}tppa]^{4+}$

shows reduction couples at + 0.20 V and - 0.40 V vs. Ag|AgCl, Fig 3.8, assigned above to metal (Co^{II}/Co^{I}) and ring reductions, respectively. Thus, the potential for the first reduction (I) of the aggregated $[Co^{II}Tm\text{-}3,4\text{-}tppa]^{4+}.[Co^{II}TSPc]^{4-}$ is closer to the potentials for the first reduction of the metal in $[Co^{II}TSPc]^{4-}$ or ring reduction in $[Co^{II}Tmtppa]^{4+}$. In Fig. 3.12(b), peak III is located in the potential region that corresponds to metal oxidation in $[Co^{II}TSPc]^{4-}$ species, at ~ 0.8 V.

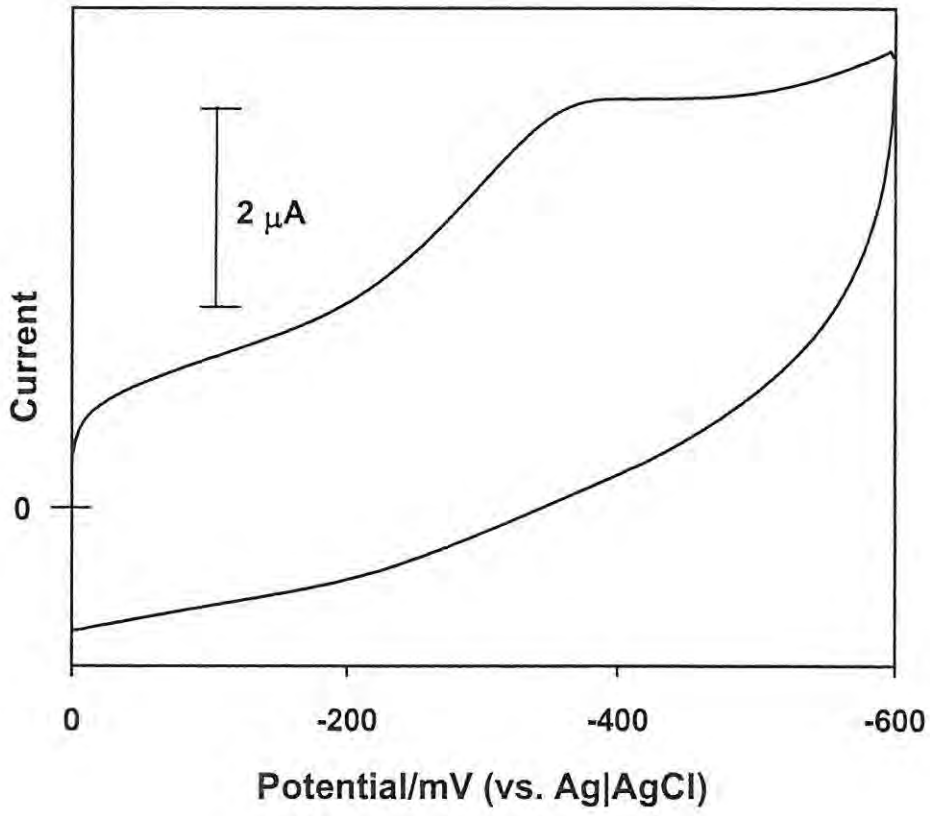

Fig. 3.13 Cyclic voltammogram of 1 x 10^{-3} mol dm^{-3} $[Co^{II}TSPc]^{4-}$ in pH 4 buffer.

3.2.3.2. Spectroelectrochemistry

In order to ascertain the site of redox activity in the cationic/anionic aggregates, reduction of the aggregated complex was performed using controlled potential electrolysis. Reduction at potentials slightly negative of the first reduction

couple (-0.6 V vs. Ag|AgCl) for $[Co^{II}Tm\text{-}3,4\text{-}tppa]^{4+}.[Co^{II}TSPc]^{4-}$ aggregate resulted in spectral changes shown in Fig. 3.14. These changes consisted of a decrease in the intensity of the Q band and the formation of a new broad band near 460 nm. The new spectrum is formed with a clear isosbestic point at 549 nm. The spectral changes shown in Fig. 3.14 are similar to those observed during metal reduction of $[Co^{II}TSPc]^{4-}$,[120] and the formation of $[Co^{I}TSPc]^{5-}$. This observation implies that the reduction of the aggregated $[Co^{II}Tm\text{-}3,4\text{-}tppa]^{4+}.[Co^{II}TSPc]^{4-}$ complex occurs on the phthalocyanine part of the aggregate. The reduction was reversible in that application of 0 V resulted in more than 90% regeneration of the spectra of the $[Co^{II}Tm\text{-}3,4\text{-}tppa]^{4+}.[Co^{II}TSPc]^{4-}$ aggregate.

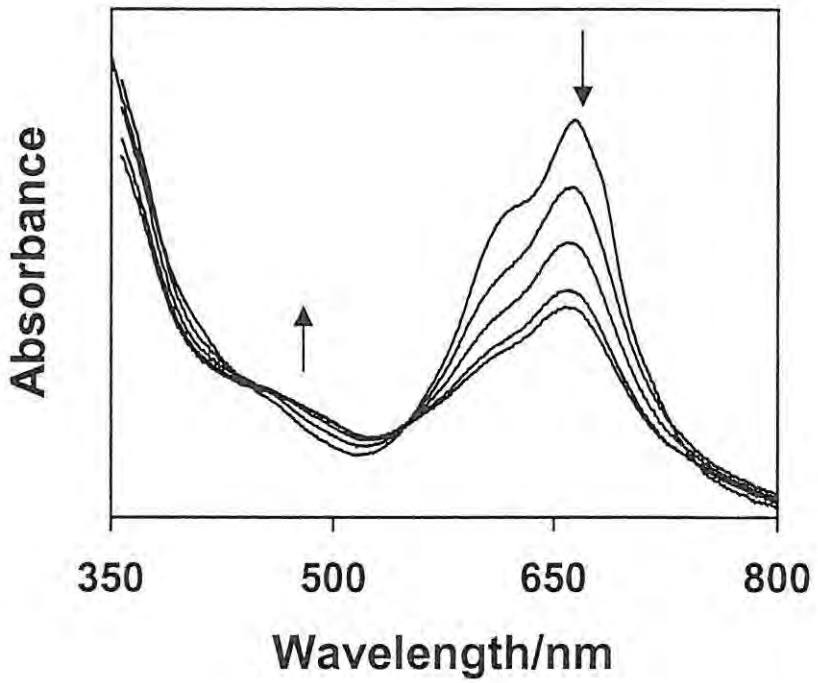

Fig. 3.14 Spectral changes observed during controlled potential electrolysis of the $[Co^{II}Tm\text{-}3,4\text{-}tppa]^{4+}.[Co^{II}TSPc]^{4-}$ aggregate in pH 4 buffer at potential of the first reduction couple (- 0.6 V vs. Ag|AgCl).

3.3. Spectral characterisation of interactions with analytes

The use of phthalocyanines as photosensitizers for photodynamic therapy (PDT) is of current interest.[142,143,144,145] Interaction of MPc complexes with proteins or amino acids is an important step towards understanding the mode of operation of these complexes as photosensitisers for PDT. Analysis of nitrite and cyanide are of importance due to their harmful effects. There is also a need to develop complexes that may scavenge nitric oxide.

3.3.1. Interaction of amino acids with $[Co^{II}Tm\text{-}3,4\text{-}tppa]^{4+}$

On addition of cysteine to the solutions of $[Co^{II}Tm\text{-}3,4\text{-}tppa]^{4+}$ under pH 3.2 or 7 conditions, spectral changes shown in Fig. 3.15 were observed. $[Co^{II}Tm\text{-}3,4\text{-}tppa]^{4+}$ decomposes at pH values higher than 7. Similar changes as shown in Fig. 3.15 were observed on addition of histidine to solutions of $[Co^{II}Tm\text{-}3,4\text{-}tppa]^{4+}$ species. These changes are similar to those shown in Fig. 3.9 for the electrochemical reduction of $[Co^{II}Tm\text{-}3,4\text{-}tppa]^{4+}$, thus confirming the formation of the same species in the presence of the amino acids and when electrochemical potential is applied to solutions of $[Co^{II}Tm\text{-}3,4\text{-}tppa]^{4+}$ species. Auto-reduction of $[Co^{II}Tm\text{-}3,4\text{-}tppa]^{4+}$ to $[Co^{I}Tm\text{-}3,4\text{-}tppa]^{3+}$ is thus observed in the presence of these amino acids.

For cysteine, the proposed mechanism for the auto-reduction may be represented by equation 3.1 and 3.2.

$$[Co^{II}Tmtppa(-2)]^{4+} + RSH \rightarrow [Co^{I}Tmtppa(-2)]^{3+} + RS^{\cdot} + H^{+} \quad (3.1)$$

$$2\,RS^{\cdot} \rightarrow RSSR \quad (3.2)$$

where RSH represents cysteine and RSSR represents its oxidation product, cystine. Equations similar to those shown in equation 3.1 and 3.2 may also be written for histidine, except the nature of the oxidation product of histidine has not yet been

determined. Coordination of the amino acids to the $[Co^{II}Tm\text{-}3,4\text{-}tppa]^{4+}$ species is expected to occur prior to electron transfer. The possibility of the formation of the cysteine-$[Co^{I}TSPc]^{5-}$ complex (instead of the formation of cystine) as reported by other researchers[146] cannot be ruled out. The coordination of amino acids to cobalt(III) porphyrins through the NH_2 of the amino acids has been observed[147] by using mainly ^1H NMR. In this work ^1H NMR spectra of the amino acids before and after addition of $[Co^{II}Tm\text{-}3,4\text{-}tppa]^{4+}$ were examined. The ^1H NMR spectra were not recorded at equilibrium. The ^1H NMR showed that the resonance for side chain ($-CH_2$) protons, labelled (1) in Fig. 3.16 for histidine showed a considerable broadening in the presence of $[Co^{II}Tm\text{-}3,4\text{-}tppa]^{4+}$ species, Fig. 3.16. This suggests that coordination occurs through the amino group on the side chain and not through ring nitrogen groups, even though the coordination bond may be weak. The ^1H NMR spectra of the ring protons of histidine were unaffected by coordination to $[Co^{II}Tm\text{-}3,4\text{-}tppa]^{4+}$ species. No new peaks were observed which could be attributed to the coupling reactions of histidine oxidation products. The CH_2 protons in cysteine were also broadened in the presence of $[Co^{II}Tm\text{-}3,4\text{-},tppa]^{4+}$ species.

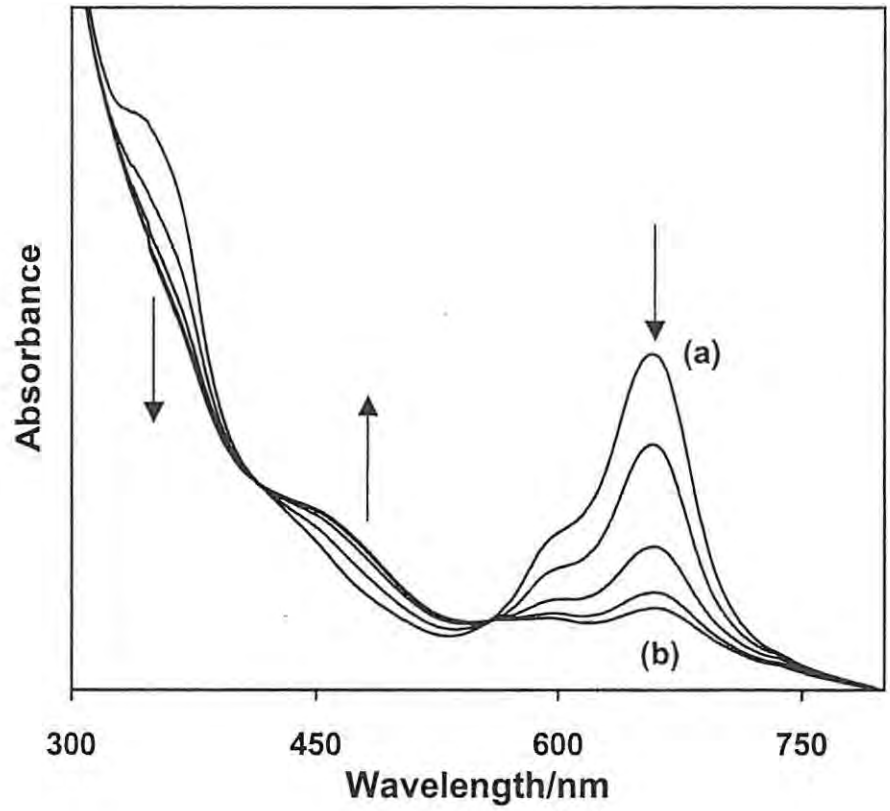

Fig. 3.15 Electronic absorption spectral changes observed on addition of 4.4 x 10^{-5} mol dm^{-3} cysteine to $[Co^{II}Tm\text{-}3,4\text{-}tppa]^{4+}$, 2.3 x 10^{-6} mol dm^{-3} solution at pH 3.2. (a) spectrum before addition of cysteine and (b) spectrum 2.5 minutes following addition of cysteine.

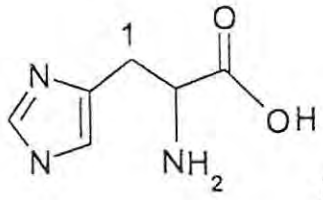

Histidine

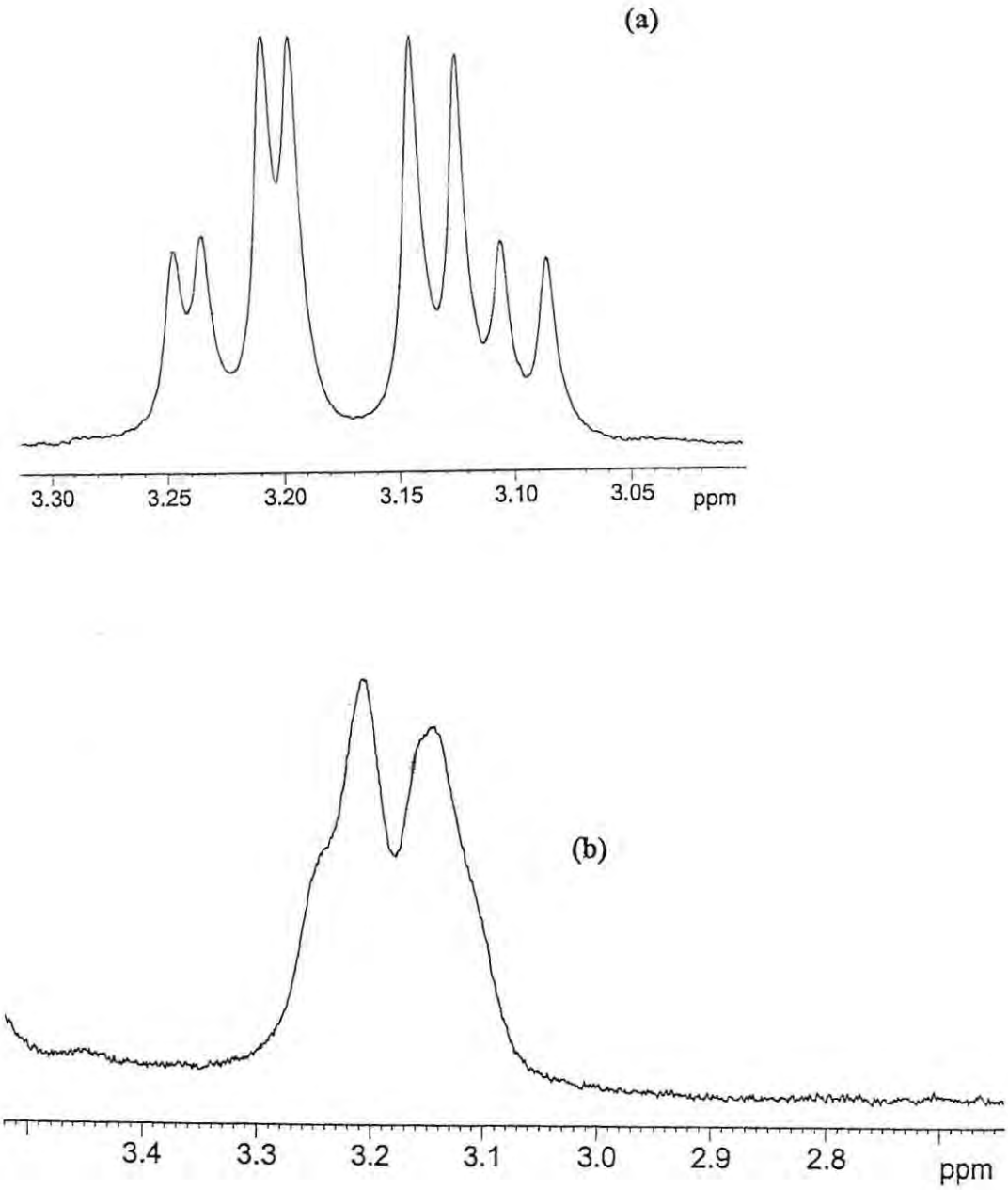

Fig. 3.16 The 400 MHz ^{1}H NMR spectra of histidine, 0.012 mol dm^{-3} (a) in the absence, and (b) in the presence of 0.008 mol dm^{-3} $[Co^{II}Tm\text{-}3,4\text{-}tppa]^{4+}$ under pH 7 conditions.

3.3.2. Interaction of NO and NO_2^- with $[Co^{II}Tm\text{-}3,4\text{-}tppa]^{4+}$

pH 4 studies

In pH 4 buffer, about 43% of nitrite disproportinates to NO.[148,149] The interaction of $[Co^{II}Tm\text{-}3,4\text{-}tppa]^{4+}$ with nitrite at pH 4 is attributed to NO. On addition of nitrite to $[Co^{II}Tm\text{-}3,4\text{-}tppa]^{4+}$ in pH 4 buffer, spectral changes shown in Fig. 3.17 were observed. As observed in Figs. 3.9 and 3.15, the UV/vis spectrum of $[Co^{II}Tm\text{-}3,4\text{-}tppa]^{4+}$ consists of a single Q band centred at 659 nm. The spectral changes shown in Fig. 3.17 consisted of the splitting of the Q band with the formation of bands at 666 and 678 nm. The Q band shifted to longer wavelengths and its intensity increased with time. Isosbestic points were observed at 384, 493 and 658 nm. There was an increase in the intensity of a broad feature near 410 nm. The B band decreased in intensity. These spectral changes are quite different from the ones reported above for the interactions of histidine and cysteine with the $[Co^{II}Tm\text{-}3,4\text{-}tppa]^{4+}$ complex, and hence are not due to the auto-reduction of the $[Co^{II}Tm\text{-}3,4\text{-}tppa]^{4+}$ species.

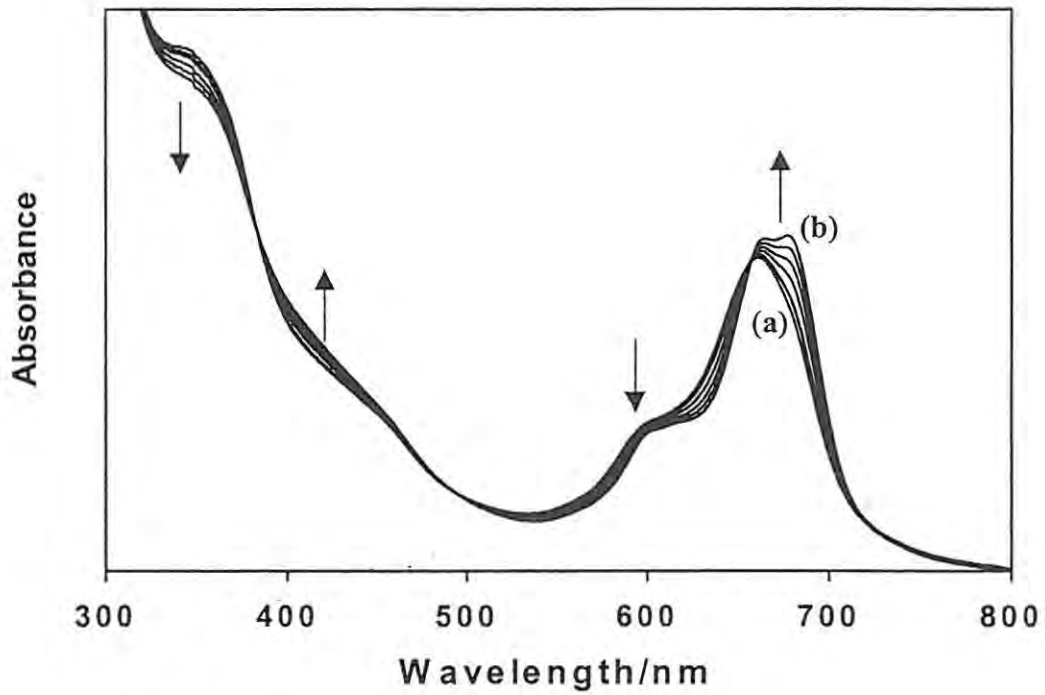

Fig. 3.17 Electronic absorption spectral changes observed on addition of NO (3.3×10^{-4} mol dm^{-3} NO_2^-) to $[CoTm\text{-}3,4\text{-}tppa]^{4+}$, 4.0×10^{-6} mol dm^{-3} solution at pH 4. (a) spectrum immediately following addition of NO and (b) final spectrum 20 minutes following addition of NO.

pH 7 studies

Under pH 7 buffer conditions, the disporpotionation of nitrite to NO is minimal, hence coordination of nitrite occurs under these conditions. On addition of nitrite to solutions of $[Co^{II}Tm\text{-}3,4\text{-}tppa]^{4+}$ in pH 7 buffer, spectral changes shown in Fig. 3.18 were observed. Spectral changes shown in Fig. 3.18 consisted of a shift of the Q band from 660 nm to 663 nm, accompanied by an increase in its intensity with isosbestic points at 422 and 575 nm. These spectral changes are associated with coordination of nitrite ion to $[Co^{II}Tm\text{-}3,4\text{-}tppa]^{4+}$ complex. Auto-reduction of $[Co^{II}Tm\text{-}3,4\text{-}tppa]^{4+}$ observed on addition of cysteine or histidine, was again not observed. There was no splitting of the Q band, which was observed in the presence of NO, Fig. 3.17, suggesting that a different complex is formed.

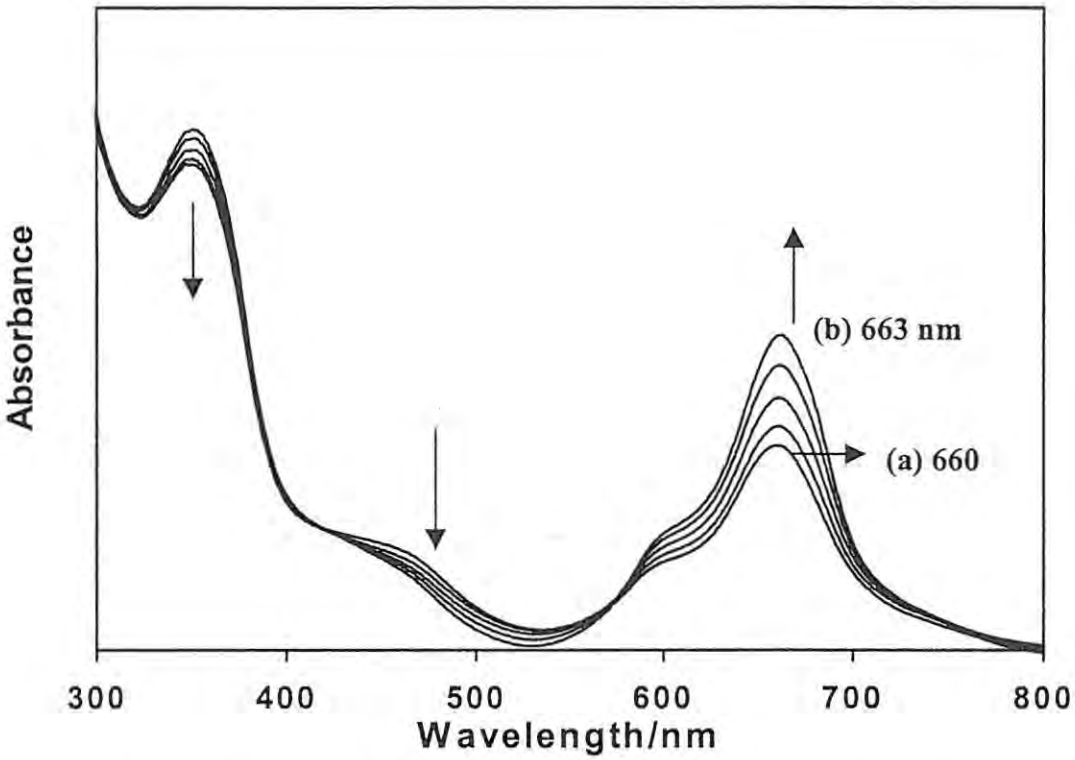

Fig. 3.18 Electronic absorption changes observed when nitrite (3.3×10^{-2} mol dm^{-3}) was added to solutions of $[Co^{II}Tm\text{-}3,4\text{-}tppa]^{4+}$, 4.0×10^{-6} mol dm^{-3} in pH 7 buffer. (a) spectrum immediately following addition of nitrite and (b) final spectrum 3 hours following addition of nitrite.

IR spectra of the solid product formed following evaporation of the solvent from a solution containing NO_2^- and $[Co^{II}Tm\text{-}3,4\text{-}tppa]^{4+}$ showed the formation of a new band at 1630 cm^{-1}. This value is in the range for vibrations of NO_2^- coordinated to Co(II) species in cobalamin.[150] Spectroscopic changes observed[100] on addition of nitrite to cobalt(II) 2,9,16.23-tetra(*tert*-butylphthalocyanine) (CoTTBPc) were attributed to the coordination of nitrite to CoTTBPc species. The selectivity of CoTTBPc for nitrite was attributed to this interaction. The coordination of the second nitrite ion to $[Co^{II}Tm\text{-}3,4\text{-}tppa]^{4+}$ species was not observed in this work. The earlier report on the interaction between nitrite and cobalt(II) tetrasulfophthalocyanine

showed that only one nitrite molecule coordinated to this species.[98] A 1:1 reaction between porphyrin derivatives and nitrite has also been reported.[151]

3.3.3. Interaction of cyanide with $[Co^{II}TSPc]^{4-}$

As already discussed above, electronic absorption spectra of $[Co^{II}TSPc]^{4-}$ complexes have been described in terms of the monomer-dimer equilibrium, and the position of the peaks is highly dependent on the medium (e.g. pH).[131,134] The monomer peak for $[Co^{II}TSPc]^{4-}$ species under pH 11 buffer conditions is observed as a broad shoulder near 666 nm, while the dimer peak is observed at 627 nm. On addition of cyanide to solutions of $[Co^{II}TSPc]^{4-}$ in pH 11 buffer, spectral changes shown in Fig. 3.19(a) were observed. pH 11 was deliberately chosen since at this pH it is expected that mainly the CN^- species exist in solution, hence avoiding complicating effects of HCN species. pKa for $[HCN]/([CN^-][H^+]$ is 9.14.[152] Spectral changes shown in Fig. 3.19(a) consisted of a decrease in the dimer peak at 627nm, as well as an increase accompanied by a shift in the monomer peak from 666 nm to 670 nm and finally to 676 nm. There were also new peaks at 610, 404 and 348 nm. The split in the B band with the shifting of one of the split peaks to wavelengths near 400 nm, is characteristic of cyanide coordination in MPc complexes.[6,65] Isosbestic points were observed at 652, 458 and 337 nm. The original spectrum before addition of cyanide did not pass precisely through the isosbestic point at 458 nm, suggesting that there are more than two species in solution. The shifting of the monomer peak from 666 nm to 670 and finally to 676 nm also shows that there are more than two species in solution. The solution changed from blue to green as the spectral changes shown in Fig. 3.19(a) progressed. No further spectral changes were observed following the formation of the species with a Q band at 676 nm.

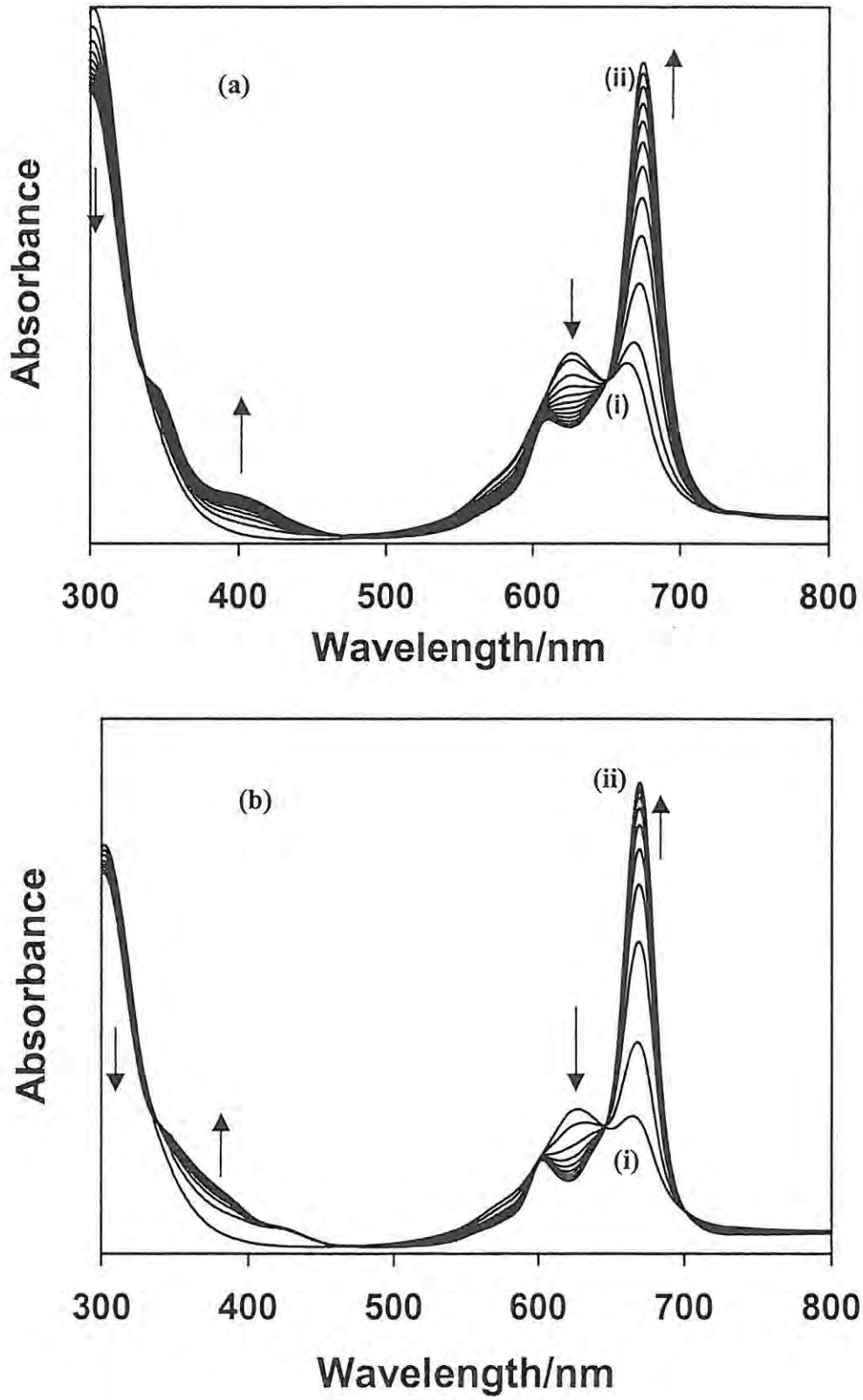

Fig. 3.19 Electronic absorption spectral changes observed on addition of (a) cyanide (1.8×10^{-4} mol dm^{-3}); (b) ferrocyanide (3.3×10^{-2} mol dm^{-3}) to solutions of $[Co^{II}TSPc]^{4-}$, 1.0×10^{-5} mol dm^{-3} in pH 11 buffer. (i) spectrum before addition of cyanide and (ii) final spectrum 2.5 min following addition of cyanide.

Weber and Busch[153] reported on the interaction of cyanide with $[Co^{II}TSPc]^{4-}$ and concluded that a cyanocobalt phthalocyanine did not form when solutions of cyanide were added to $[Co^{II}TSPc]^{4-}$, but that cyanocobalt(III) phthalocyanine complex was formed when ferricyanide was employed as a source of cyanide. Fig. 3.19(b) shows spectral changes obtained on addition of ferricyanide to solutions of $[Co^{II}TSPc]^{4-}$ under pH 11 buffer conditions. Spectral changes similar to those shown in Fig. 3.19(a) were obtained, except that the monomer peak shifted only from 666 nm to 670 nm, with no further shift to 676 nm, which was observed in Fig. 3.19(a). There was evidence of coordination of cyanide since there was a split in the B band with a formation of a broad band near 400, nm as was observed in Fig. 3.19(a). Thus, these results show that cyanide coordination is observed when either cyanide or ferricyanide are added to the solutions of $[Co^{II}TSPc]^{4-}$ in basic media. Stable cyanocobalt(III) phthalocyanine complexes have been reported from addition of cyanide to other CoPc[6,65] complexes in non-aqueous media. Literature reports have thus shown that coordination of cyanide to $Co^{II}Pc$ complexes results in the oxidation of the central metal with the formation of $Co^{III}Pc$ complexes.[6,65,154] Autooxidation of $[Co^{II}TSPc]^{4-}$ is known to depend on the nature of the axial ligands.[153,155]

The fact that the final Q band maxima in Figs. 3.19(a) and 3.19(b) are different (yet in both cases coordination of cyanide occurs, as evidenced by split in the B band), suggests that different levels of axial ligand coordination occurs in the two situations. Since the final Q band maxima on addition of ferricyanide to $[Co^{II}TSPc]^{4-}$ is at the same wavelength as the Q band observed when cyanide is first added to $[Co^{II}TSPc]^{4-}$ species, it can be proposed that on addition of ferricyanide, only one cyanide ligand is coordinated, since further spectral changes to 676 nm were not observed. In the case where cyanide (instead of ferricyanide) was added to the

$[Co^{II}TSPc]^{4-}$ solutions, Fig. 3.19(a), the first spectral changes with a Q band located at 670 nm are due to the coordination of the first cyanide in a similar manner (and with a similar Q band maxima) to when ferricyanide is added. The further shifting of the spectra to 676 nm in the case of addition of cyanide is due to the coordination of the second cyanide and the formation of $[(CN^-)_2Co^{III}TSPc]^{5-}$ species. Coordination of cyanide to CoPc complexes is known to result in dicyano complexes.[6,65] Coordination of the first cyanide to other MPc complexes (e.g. $(L)_2FePc$) is known to occur much faster than the coordination of the second cyanide.[66] In general, coordination of the first axial ligands in MPc complexes occurs much faster than the coordination of the second ligands.[66,67,156,161] The fact that gradual spectral changes were not observed for the formation of the monocyano species with a Q band maxima at 670 nm on addition of cyanide, under aqueous conditions, even though gradual changes were observed when ferricyanide was employed as a source of cyanide, may be a result of the extent of cyanide availability in the latter. Gradual evolution of the 670 nm band was not observed even on addition of very small amounts of cyanide. Instantaneous formation of the species with a Q band centered at 670 nm was observed under all circumstances.

In order to confirm the step-wise coordination of cyanide to $[Co^{II}TSPc]^{4-}$ species, spectral changes for this complex in the presence of cyanide using DMSO as a solvent were monitored. Spectral changes observed in Fig. 3.20 clearly showed the stepwise coordination of cyanide to the $[Co^{II}TSPc]^{4-}$ species. In DMSO the $[Co^{II}TSPc]^{4-}$ species is in the monomeric form only. The spectral changes shown in Fig. 3.20(a) consisted of a decrease in the Q-band (located at 663 nm) accompanied by an isosbestic shift to 670 nm. When the solution that resulted in spectral changes of Fig. 3.20(a) is left for longer periods, or when larger cyanide concentrations (0.03

mol dm^{-3}) were added to $[Co^{II}TSPc]^{4-}$ solutions, spectral changes shown in Fig. 3.20(b) were observed, consisting of a shift of the Q band from 670 nm to 680 nm. Thus, in organic media, stepwise spectral changes were observed corresponding to the stepwise coordination of cyanide. Fig. 3.20(a) corresponds to the coordination of the first cyanide and Fig. 3.20(b) to the coordination of the second cyanide. The fact that these stepwise coordinations are observed in organic media and not in aqueous solutions is a result of the slower kinetics in the former.

It is suggested that coordination of cyanide to $[Co^{II}TSPc]^{4-}$ species occurs simultaneously with the oxidation of Co^{II} to Co^{III} and hence the formation of the $[(CN^-)_2Co^{III}TSPc]^{5-}$ species in aqueous solutions. As mentioned above, oxidation of Co^{II} to Co^{III} occurs on addition of cyanide to CoPc complexes.[6,65] Addition of bromine to aqueous solutions of $[Co^{II}TSPc]^{4-}$ resulted in the formation of the Q band at 670 nm (due to the formation of $[Co^{III}TSPc]^{3-}$ species) and the disappearance of the dimer band. Central metal oxidation in $[Co^{II}TSPc]^{4-}$ complex results in the disappearance of the dimer peak and the shifting of the Q band to longer wavelengths.[98,120,162] Addition of a reducing agent (e.g. sodium borohydride) at the end of the reaction between cyanide and $[Co^{II}TSPc]^{4-}$ and the formation of species with a Q band located at 676 nm, resulted in regeneration of the original spectrum in Fig. 3.19(a), confirming that oxidation accompanies the coordination of cyanide to $[Co^{II}TSPc]^{4-}$ species and that cyanide binds reversibly to $[Co^{II}TSPc]^{4-}$.

The slight deviation from the isosbestic point at 458 nm of the spectrum before addition of cyanide in Fig. 3.19(a) may be attributed to the presence of more than two species in solution, these being the dimer, monomer, monocyano and dicyano species.

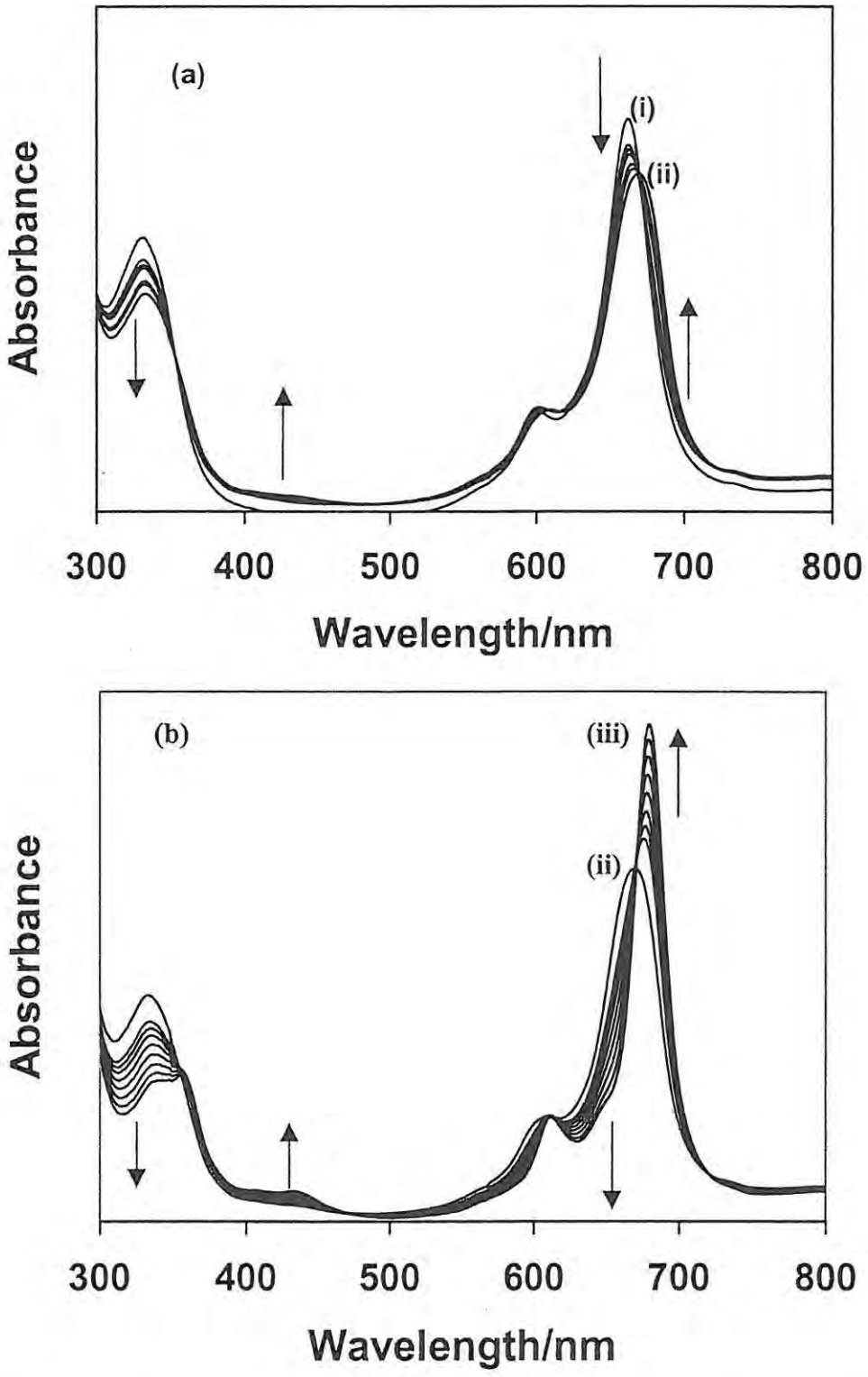

Fig. 3.20 Electronic absorption spectral changes observed on addition of cyanide (6.7×10^{-3} mol dm^{-3}) to solutions of $[Co^{II}TSPc]^{4-}$, 1.0×10^{-5} mol dm^{-3} in DMSO. (i) spectrum before addition of cyanide, (ii) final spectrum 2.5 min following addition of cyanide and (iii) spectrum 6 hours after addition of cyanide. (a) and (b) represent the spectral changes for the coordination of the first and second cyanides, respectively.

The ligation of cyanide to $[Co^{II}TSPc]^{4-}$ was evidenced by IR spectra of the solid complex produced when cyanide was added to solutions of $[Co^{II}TSPc]^{4-}$ and then evaporating off the solvent. υ_{CN^-} was observed at 2130 cm^{-1}. This value is larger than that reported by Weber and Busch for the formation of cyanocobalt(III) phthalocyanine complex using ferricyanide as a source of cyanide,[153] but is in the range reported for υ_{CN^-} (2120 cm^{-1}) in dicyanoiron phthalocyanine.[66]

Earlier studies[162] have shown that bubbling oxygen through a solution of $[Co^{II}TSPc]^{4-}$ resulted in an increase in the monomer peak of the spectrum of this complex, followed by a further shift to longer wavelengths. These spectral changes were attributed to formation of an adduct between oxygen and $[Co^{II}TSPc]^{4-}$. No spectral changes for $[Co^{II}TSPc]^{4-}$ in the absence of cyanide were observed, showing that residual oxygen present in water is not enough to oxidize $[Co^{II}TSPc]^{4-}$ in the absence of cyanide under pH 11 conditions. It has been reported before[157] that the adduct between $[Co^{II}TSPc]^{4-}$ and oxygen is only formed at pH values greater than 12.

The relatively strong ligands, cyanide[153] and imidazoles,[120,153] are known to facilitate central metal oxidation in $[Co^{II}TSPc]^{4-}$ by atmospheric oxygen. The spectral changes observed when oxygen was deliberately bubbled into the solution containing $[Co^{II}TSPc]^{4-}$ and cyanide are similar to those observed in the presence of residual oxygen, and as will be shown in the next section, the rate of formation of products is much faster when oxygen is bubbled, clearly showing that oxygen is involved in the oxidation of $[Co^{II}TSPc]^{4-}$ on coordination of cyanide.

Assuming that two molecules of water are initially ligated to the $[Co^{II}TSPc]^{4-}$ forming $[(H_2O)_2Co^{II}TSPc]^{4-}$ as has been suggested before,[134] the mechanism for the coordination of cyanide to $[Co^{II}TSPc]^{4-}$ is proposed as follows, equations 3.3 and 3.4.

$$[(H_2O)_2Co^{II}TSPc]^{4-} + CN^- \xrightarrow{O_2} [(H_2O)(CN^-)Co^{III}TSPc]^{4-} + H_2O + O_2^- \qquad (3.3)$$

$$[(H_2O)(CN^-)Co^{III}TSPc]^{4-} + CN^- \rightarrow [(CN^-)_2Co^{III}TSPc]^{5-} + H_2O \qquad (3.4)$$

Equation 3.3 is a result of the fast coordination of the first cyanide ligand with a Q band maxima centered at 670 nm in Fig. 3.19(a). Equation 3.4 is proposed for the coordination of the second cyanide with gradual spectral changes in Fig. 3.19(a) and the final formation of a Q band at 676 nm.

3.3.4. Interaction of SO_2 with $[Co^{II}TSPc]^{4-}$

Fig. 3.21 shows spectral changes observed when sulphur dioxide solutions were added to solutions of $[Co^{II}TSPc]^{4-}$ under pH 11 buffer conditions in the presence of residual oxygen (no oxygen bubbled). Basic solutions were chosen for this study in order to allow for comparison with the studies for cyanide coordination discussed above. The spectral changes shown in Fig. 3.21 are similar to those observed in Fig. 3.19(a) for the addition of cyanide to $[Co^{II}TSPc]^{4-}$ species, except that the final spectrum showed a Q band at 673 nm, and not 676 nm, observed for cyanide coordination. The monomer peak shifted from 666 nm to 670 nm and finally to 673 nm, with clear isosbestic points at 710, 649, 502 and 341 nm. Similar spectral changes were observed in pH 7.4 buffer. The similarities between spectral changes on addition of SO_2 to $[Co^{II}TSPc]^{4-}$ to the changes observed on coordination of cyanide above, suggests that similar processes are taking place in both cases. Thus, coordination of SO_2 to $[Co^{II}TSPc]^{4-}$ is proposed for changes observed in Fig. 3.21 in a similar manner to coordination of cyanide, with coordination of the first SO_2 occurring fast, resulting in the Q band shift to 670 nm. The final spectral changes leading to the observation of the Q band at 673 nm is due to the coordination of the second SO_2 molecule. This coordination results in the formation of a disulphite complex, since SO_3^{2-} is the prominent form of SO_2 in basic media. The exact nature of the complex formed has

not yet been determined. However, the step-wise coordination of SO_2 to the $[Co^{II}TSPc]^{4-}$ species was confirmed by the observation of spectral changes (in DMSO) similar to those shown in Fig. 3.20 for the coordination of cyanide.

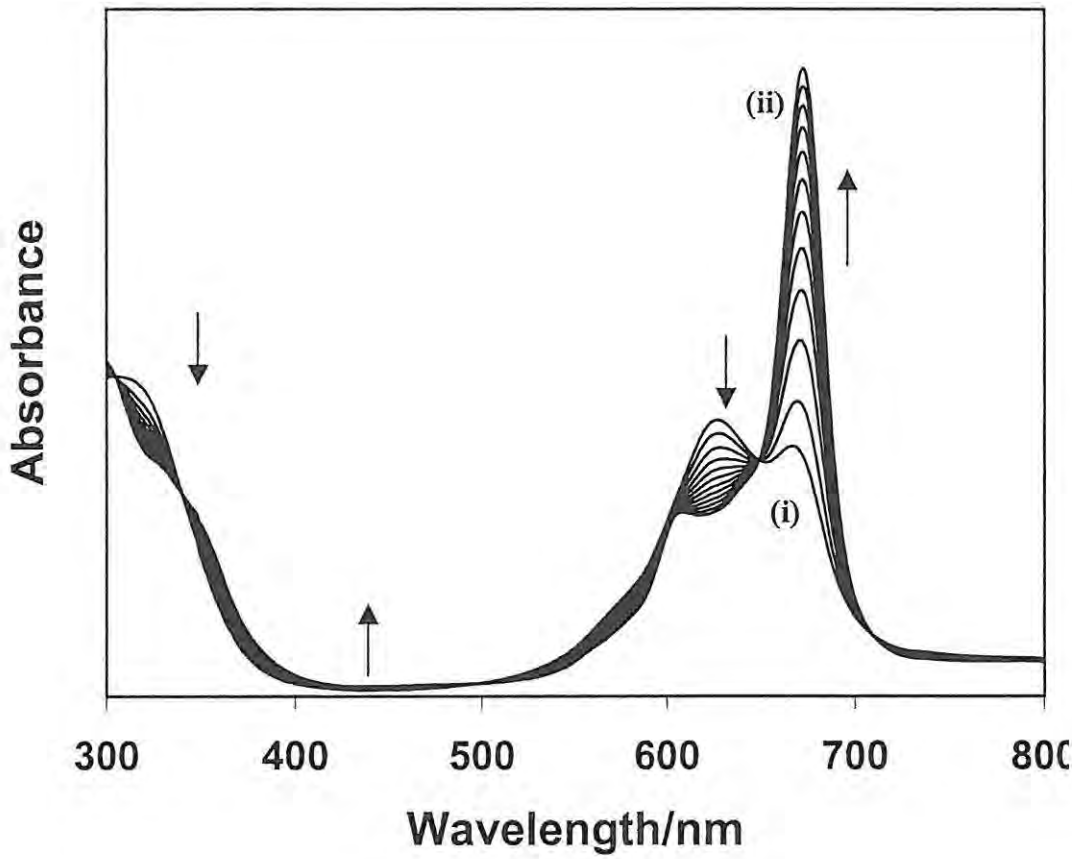

Fig. 3.21 Electronic absorption changes observed on addition of SO_2 (2.1×10^{-3} mol dm^{-3}) to solutions of $[Co^{II}TSPc]^{4-}$, 1.0×10^{-5} mol dm^{-3} in pH 11 buffer (i) spectrum before addition of sulphur dioxide and (ii) final spectrum, 2.5 min following addition of SO_2.

In comparison with cyanide, it is likely that the coordination of SO_2 is also accompanied by electron transfer and oxidation of $[Co^{II}TSPc]^{4-}$ to $[Co^{III}TSPc]^{3-}$ species. Earlier studies[77] showed that photochemical reduction of tin(IV) phthalocyanine complexes, $(OH)_2SnPc$ or $(Cl)_2SnPc$ in the presence of SO_2 resulted in

the ring reduction of these SnPc complexes, whereas oxidation of Pc(-2)Sn(IV)Pc(-2) to the Pc(-1)Sn(IV)Pc(-2) species was observed on addition of sulphur dioxide.[79] The fact that the final spectrum peak is observed at different wavelengths for cyanide ($\lambda_{Q\ band}$ = 676 nm) and SO_2 ($\lambda_{Q\ band}$ = 673 nm) coordination to $[Co^{II}TSPc]^{4-}$ confirms that different complexes are formed due to axial ligation. Despite the fact that solutions of SO_2 and sulphites are commonly used as reducing agents,[182] the spectral changes observed on addition of SO_2 to $[Co^{II}TSPc]^{4-}$ solutions are similar to those observed in the presence of bromine. As a result, oxidation, and not reduction is implicated.

Metalloporphyrin complexes are known to react with SO_2 to form porphyrin sulphate complexes,[158,159] with the IR spectrum of monocoordinated sulphate groups being observed at 1147, 1098 and 464 cm^{-1}.[160] IR spectra of the solid product formed following evaporation of the solvent from a solution containing SO_2 and $[Co^{II}TSPc]^{4-}$ results in formation of a sulphate-ligated $[Co^{II}TSPc]^{4-}$ complex (SO_2 is oxidized by oxygen to SO_4^{2-}), with IR band at 1208 cm^{-1}. However, the IR spectra were complicated by the presence of vibrations from the SO_3^- groups attached to the phthalocyanine ring in the $[Co^{II}TSPc]^{4-}$ complex. The peaks are observed at 1112 and 1151 cm^{-1} in $[Co^{II}TSPc]^{4-}$. In the SO_4^{2-}-ligated complex, the 1112 cm^{-1} peak persisted while the 1151 cm^{-1} peak shifted to higher wavenumbers, and is observed as a strong peak at 1208 cm^{-1}, assigned to the metal coordinated S = O bond.

3.4. Kinetics and equilibria studies

The equilibrium data was analysed by standard spectrophotomeric methods using equation 3.5.

$$\log[(A_{eq} - A_o)/(A_\infty - A_{eq})] = \log K + n\log[L] \qquad (3.5)$$

where A_{eq} is the equilibrium absorbance, A_o is the absorbance before addition of analyte. A_∞ can be determined from the final absorbance following complete formation of a complex under investigation. L is the coordinating ligand.

Reactions catalysed by MPc complexes are often mediated by axial ligation of the species to be catalysed. Axial ligand substitution reactions in metallophthalocyanine and metalloporphyrin complexes are dissociative with the formation of a highly reactive five-coordinate intermediate.[161,162,163] The coordination of axial ligands to metallophthalocyanine complexes occurs in two steps, with the coordination of the first ligand occurring faster than that of the second.

It is assumed that $[Co^{II}Tm\text{-}3,4\text{-}tppa]^{4+}$ and $[Co^{II}TSPc]^{4-}$ exist in aqueous solution with two molecules of water axially ligated to the metal centre, $[(H_2O)_2Co^{II}Tm\text{-}3,4\text{-}tppa]^{4+}$ or $[(H_2O)_2Co^{II}TSPc]^{4-}$. The five coordinate reactive intermediate, $[(H_2O)Co^{II}Tmtppa]^{4+}$ or $[(H_2O)Co^{II}TSPc]^{4-}$ forms prior to ligand (L) exchange, equations 3.6 and 3.7.

$$[(H_2O)_2MPc] \underset{k_{-1}}{\overset{k_1}{\rightleftharpoons}} [(H_2O)MPc] + H_2O \qquad (3.6)$$

$$[(H_2O)MPc] + L \underset{k_{-2}}{\overset{k_2}{\rightleftharpoons}} [(H_2O)(L)MPc] \qquad (3.7)$$

where MPc = $[Co^{II}Tm\text{-}3,4\text{-}tppa]^{4+}$ or $[Co^{II}TSPc]^{4-}$. The rate law of the reaction (equations 3.6 and 3.7) can then be described by equations similar to equations 3.8 to 3.11.[164]

$$k_{obs} = \frac{k_1k_2[L] + (k_{-1}k_{-2}[H_2O]}{k_{-1}[H_2O] + k_2[L]} \qquad (3.8)$$

Since the solvent is in excess, it may be assumed that $k_{-1}[H_2O] \gg k_2[L]$, then equation 3.8 becomes 3.9.

$$k_{obs} = \frac{k_1 k_2[L] + (k_{-1}k_{-2}[H_2O]}{k_{-1}[H_2O]} \quad (3.9)$$

Equation 3.9 can be simplified to equation 3.10.

$$k_{obs} = \frac{k_1 k_2[L]}{k_{-1}[H_2O]} + k_{-2} \quad (3.10)$$

if $\frac{k_1 k_2}{k_{-1}[H_2O]} = k_f$, and $k_{-2} = k_r$, equation 3.10 may be written as equation 3.11.

$$k_{obs} = k_f [L] + k_r \quad (3.11)$$

Where k_f is the rate for the forward reaction and k_r is the rate for the reverse reaction.

3.4.1. Interactions of amino acids with $[Co^{II}Tm\text{-}3,4\text{-}tppa]^{4+}$

For these studies the concentration of $[Co^{II}Tm\text{-}3,4\text{-}tppa]^{4+}$ was kept constant at 2.2×10^{-6} mol dm^{-3}, while the concentration of cysteine and histidine were varied between 2.2×10^{-5} and 2.0×10^{-4} mol dm^{-3}. Since the concentrations of cysteine and histidine were much larger than that of $[Co^{II}Tm\text{-}3,4\text{-}tppa]^{4+}$, pseudo-first order conditions were assumed for kinetic studies.

The disappearance in Q-band at 659 nm with time following addition of either cysteine or histidine to the $[Co^{II}Tm\text{-}3,4\text{-}tppa]^{4+}$ species, Fig. 3.15, was followed in pH 3.2 or 7 buffer systems. The plots of the logarithm of absorbance at 659 nm versus time were linear, Fig. 3.22, confirming the assumption of a first order reaction with respect to the $[Co^{II}Tm\text{-}3,4\text{-}tppa]^{4+}$ species. The observed rate constants, k_{obs}, were obtained from the slopes of these plots and are plotted vs. [L] in Fig. 3.23. A linear plot (Fig. 3.23) was observed for both cysteine and histidine, showing that the reaction was first order in both of these amino acids, and suggesting that the rate law of equation 3.11 is obeyed for the reduction of $[Co^{II}Tm\text{-}3,4\text{-}tppa]^{4+}$ by histidine and cysteine, where L represents histidine or cysteine, k_f is the rate constant for the

formation of the product and k_r is the rate constant for the reverse reaction (i.e. the re-generation of the starting complex).

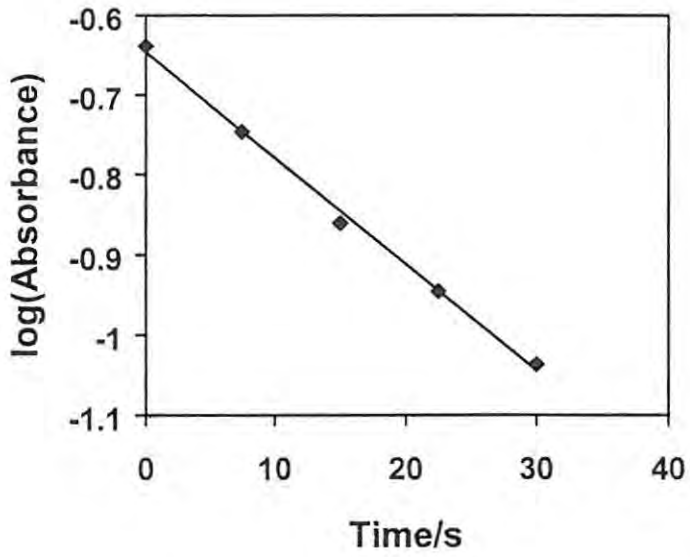

Fig. 3.22 Log absorbance vs. time for the reaction of cysteine (2.3×10^{-3} mol dm^{-3}) with $[Co^{II}Tm\text{-}3,4\text{-}tppa]^{4+}$ (2.0×10^{-6} mol dm^{-3}) in pH 3.2 buffer.

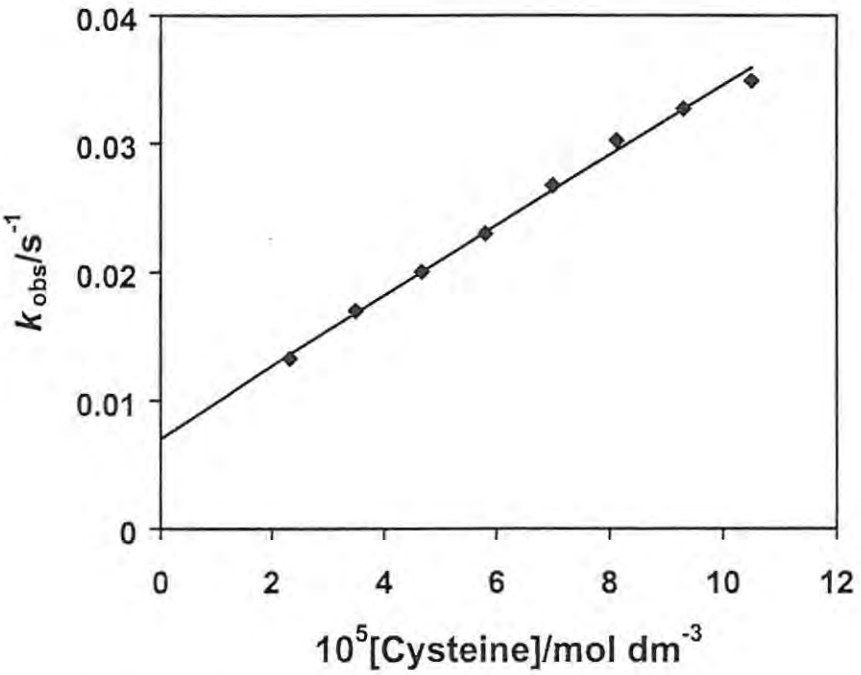

Fig. 3.23 k_{obs} versus concentration for the interaction of cysteine with $[Co^{II}Tm\text{-}3,4\text{-}tppa]^{4+}$ in pH 3.2 buffer.

Least square analysis of the data represented in Fig. 3.23 gave k_f value from the slope and k_r value from the intercept. For the auto-reduction of $[Co^{II}Tm3,4\text{-tppa}]^{4+}$ in the presence of cysteine in pH 3.2 buffer, the values of k_f and k_r were determined to be $2.7 \pm 0.3 \times 10^2$ dm^3 mol^{-1} s^{-1} and $7.3 \pm 0.5 \times 10^{-3}$ s^{-1}, respectively. Using these values, the equilibrium constant was estimated from $K = k_f/k_r$ to be $K = 3.7 \times 10^4$ dm^3 mol^{-1} for auto-reduction of $[Co^{II}Tm\text{-}3,4\text{-tppa}]^{4+}$ complex in the presence of cysteine in pH 3.2 buffer. The values of the constants are listed in Table 3.3.

Table 3.3. Equilibrium and rate constants for the interactions of 3,4-pyridinoporphyrazines or phthalocyanines with nitrogen oxides and amino acids. pH 7 conditions unless stated otherwise.

Complex	Molecule	[a]K (dm^3 mol^{-1})	k_f (dm^3 mol^{-1} s^{-1})	k_r (s^{-1})	[b]Ref
$[Pt^{II}Tmtppa]^{4+}$	Cysteine		$8.8 \pm 0.1 \times 10^{-2}$		12
$[Pt^{II}Tmtppa]^{4+}$	Histidine		$1.9 \pm 0.1 \times 10^{-3}$		12
$[Co^{II}Tmtppa]^{4+}$	Cysteine	7.5×10^{2}	$2.1 \pm 0.3 \times 10^{1}$	$2.8 \pm 0.5 \times 10^{-2}$	tw
$[Co^{II}Tmtppa]^{4+}$	Cysteine[c]	3.7×10^{4}	$2.7 \pm 0.3 \times 10^{2}$	$7.3 \pm 0.5 \times 10^{-3}$	tw
$[Co^{II}Tmtppa]^{4+}$	Histidine	1.3×10^{4}	2.8 ± 0.6	$2.1 \pm 0.5 \times 10^{-4}$	tw
$[CoTmtppa]^{4+}$	NO[d]	$2.2 \pm 0.1 \times 10^{2}$	$2.1 \pm 0.1 \times 10^{-1}$	1.0×10^{-3}	tw
$[CoTmtppa]^{4+}$	NO[e]	$2.3 \pm 0.1 \times 10^{4}$	7.5 ± 0.1	$2.9 \pm 0.2 \times 10^{-4}$	tw
$[CoTmtppa]^{4+}$	NO_2^-	2.0×10^{2}	$4.0 \pm 0.1 \times 10^{-3}$	$2.4 \pm 0.9 \times 10^{-5}$	tw
$[CoTSPc]^{4-}$	NO_2^-	4.7	1.6×10^{-4}	2.9×10^{-6}	98

[a] K values for histidine and cysteine interactions estimated from k_f/k_r.
[b] tw = this work.
[c] cysteine = studies in pH 3.2 buffer.
[d] NO = NO from disproportionation of nitrite. pH 4. [NO] = 0.43 [NO_2^-] used in determining constants
[e] NO = NO prepared by reaction between sulphuric acid and nitrite, as explained in Section 2.3.4. pH = 4

The spectral changes for addition of cysteine to $[Co^{II}Tm\text{-}3,4\text{-}tppa]^{4+}$ obtained at pH 7 were similar to those shown in Fig. 3.15. For the auto-reduction of $[Co^{II}Tm\text{-}3,4\text{-}tppa]^{4+}$ in the presence of cysteine, at pH 7, k_f and k_r values were determined to be $2.1 \pm 0.3 \times 10^{1}$ dm^3 mol^{-1} s^{-1} and $2.8 \pm 0.5 \times 10^{-2}$ s^{-1}, respectively. For auto-reduction of $[Co^{II}Tm\text{-}3,4\text{-}tppa]^{4+}$ in the presence of histidine at pH 7, k_f and k_r were =

2.8 ± 0.6 dm^3 mol^{-1} s^{-1} and $2.1 \pm 0.5 \times 10^{-4}$ s^{-1}, respectively. Using these values, the equilibrium constants were estimated from $K = k_f/k_r$ to be $K = 7.5 \times 10^2$ dm^3 mol^{-1} and 1.3×10^4 dm^3 mol^{-1} for auto-reduction of $[Co^{II}Tm\text{-}3,4\text{-}tppa]^{4+}$ complex at pH 7 and in the presence of cysteine and histidine, respectively, Table 3.3. No spectral changes were observed for histidine at low pH values. The equilibrium constants could not be determined directly from the UV/Vis data since as discussed above, there is slow precipitation following the auto-reduction reactions. The k_f values reported here are much higher than the values reported[12] for the auto-reduction of the Pd- and Pt-$[Tmtppa]^{4+}$ complexes in the presence of cysteine or histidine, Table 3.3, showing that the cobalt complex is more readily auto-reduced in the presence of cysteine than the Pt and Pd complexes. However, the site of reduction in $[Pt^{II}Tmtppa]^{4+}$ and $[Pd^{II}Tmtppa]^{4+}$ is different from that in $[Co^{II}Tmtppa]^{4+}$, in that reduction occurs at the ring and not at the metal in Pt and Pd complexes. The rate constants are close to the values reported for the coordination of thiolates to $[Co^{II}TSPc]^{4-}$.[165,166]

The values of rate constants for the auto-reduction of $[Co^{II}Tm\text{-}3,4\text{-}tppa]^{4+}$ in the presence of cysteine depended on pH. k_f is 10 times larger at pH 3.2 than at pH 7. Under acid conditions, cysteine is protonated, pKa = 8.36, equation 3.12, and is still expected to be protonated in neutral media (pH 7). At this pH, both species I and III exist, equation 3.12. Since high k_f values are observed at low pH, the protonated form is more reactive in the reaction.

$$\underset{\text{II}}{H_2NCHRCOO^-} \underset{OH^+}{\overset{H^+}{\rightleftharpoons}} \underset{\text{I}}{{}^+H_3NCHRCOO^-} \underset{OH^+}{\overset{H^+}{\rightleftharpoons}} \underset{\text{III}}{{}^+H_3NCHRCOOH} \qquad (3.12)$$

where $R = HSCH_2$ (for cysteine)

3.4.2. Interaction of NO_2^- and NO with $[Co^{II}Tm\text{-}3,4\text{-}tppa]^{4+}$

The concentration of $[Co^{II}Tm\text{-}3,4\text{-}tppa]^{4+}$ was kept constant at 4.0×10^{-6} mol dm^{-3}, while nitrite and nitric oxide concentrations were varied from 1.5×10^{-5} to 2.4×10^{-2} mol dm^{-3}. Since the concentrations of nitrite and nitric oxide were much larger than that of $[Co^{II}Tm\text{-}3,4\text{-}tppa]^{4+}$, pseudo-first order conditions were assumed for kinetic studies.

pH 4 studies

As discussed in Section 3.3.2, the spectral changes shown in Fig. 3.17 (at pH 4) are associated with the coordination of NO to the $[Co^{II}Tm\text{-}3,4\text{-}tppa]^{4+}$ species and the formation of $[(NO)CoTm\text{-}3,4\text{-}tppa]^{4+}$. Equilibrium data for the formation of the complex between NO and the $[CoTm\text{-}3,4\text{-}tppa]^{4+}$ species were determined by monitoring changes in the Q band and using equation 3.5, with L representing NO. In this section A_{eq} is the equilibrium absorbance at 678 nm, A_o is the absorbance at 678 nm before addition of NO as nitrite, from Fig. 3.17. A_∞, the absorbance after complete formation of the complex was determined from the final absorbance at 678 nm. From the plot of $\log[(A_{eq} - A_o)/(A_\infty - A_{eq})]$ versus $\log [NO_2^-]$, Fig. 3.24, an equilibrium constant of $K = 2.2 \pm 0.1 \times 10^2$ dm^3 mol^{-1} was determined for the formation of $[(NO)CoTm\text{-}3,4\text{-}tppa]^{4+}$, and the value of n was found to be near unity ($n = 0.9 \pm 0.1$) showing that one molecule of NO coordinates to the $[Co^{II}Tm\text{-}3,4\text{-}tppa]^{4+}$ species forming $[(NO)CoTm\text{-}3,4\text{-}tppa]^{4+}$ species. In an alternative method, equilibrium constant may be determined by a double reciprocal plot (1/Δabsorbance vs. 1/[ligand]).[166]

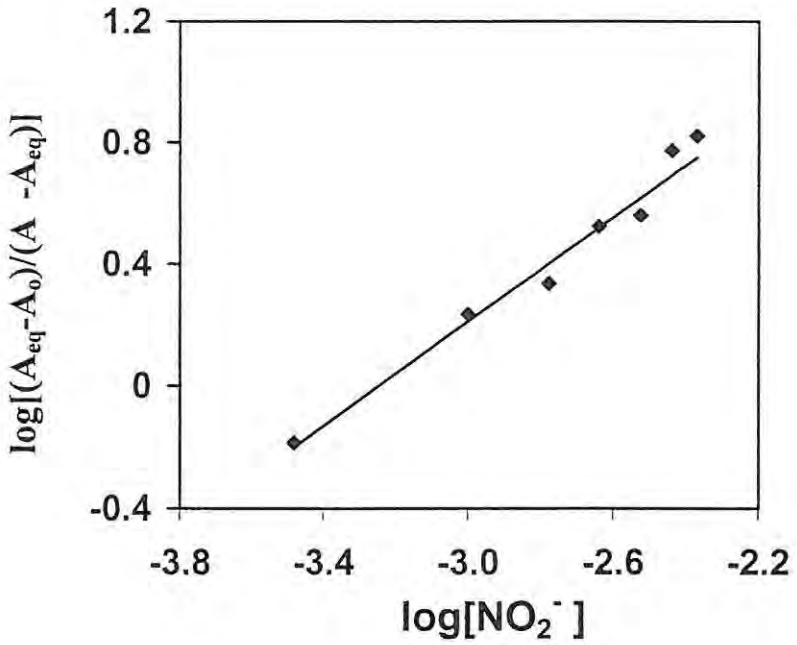

Fig. 3.24 Plot of $\log[(A_{eq} - A_o)/(A_\infty - A_{eq})]$ versus $\log [NO_2^-]$ in pH 4 buffer for coordination of NO with $[Co^{II}Tm\text{-}3,4\text{-}tppa]^{4+}$.

For the formation of $[(NO)CoTm\text{-}3,4\text{-}tppa]^{4+}$species, plots of $\ln(A_\infty - A_t)$ against time (where A_∞, and A_t are defined above) were linear, Fig. 3.25.

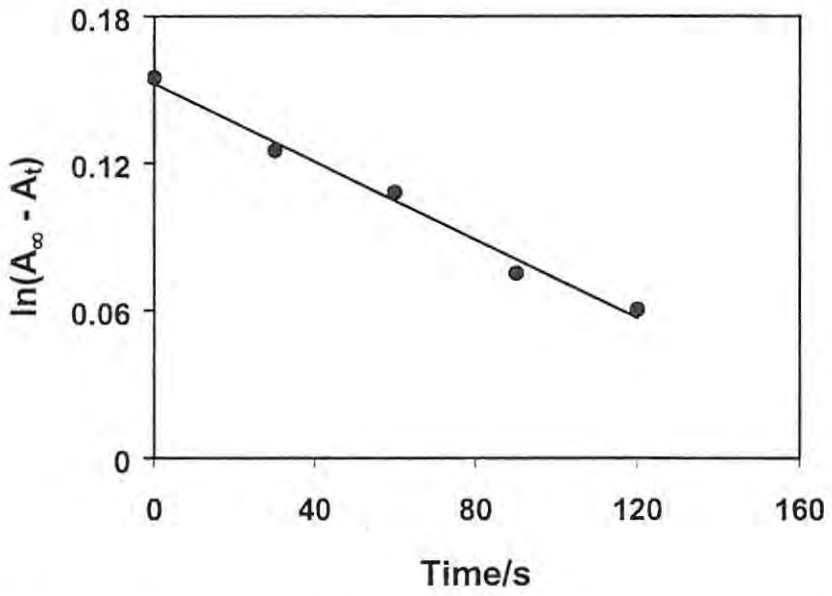

Fig. 3.25 Plot of $\ln(A_\infty - A_t)$ vs. time, for the reaction of 1.67 x 10^{-3} mol dm^{-3} NO_2^- with $[Co^{II}Tm\text{-}3,4\text{-}tppa]^{4+}$ (4.0 x 10^{-6} mol dm^{-3}). pH 4 buffer.

The plot of the observed rate constant (k_{obs}) versus nitrite concentration as NO was linear (Fig. 3.26) for the data shown in Fig. 3.17, showing that the coordination is first order in NO and obeys the rate law of equation 3.11, which is typical of coordination of axial ligands to MPc complexes. k_f is the rate constant for the formation of $[(NO)CoTm\text{-}3,4\text{-}tppa]^{4+}$ and k_r is the dissociation of the complex. The rate constants were as follows, $k_f = 2.1 \pm 0.1 \times 10^{-1}$ dm^3 mol^{-1} s^{-1} and $k_r = 1.0 \times 10^{-3}$ s^{-1}. Using these values, the equilibrium constant was estimated to be $K \sim 2.1 \times 10^2$ dm^3 mol^{-1} in agreement with the value determined from equilibrium data.

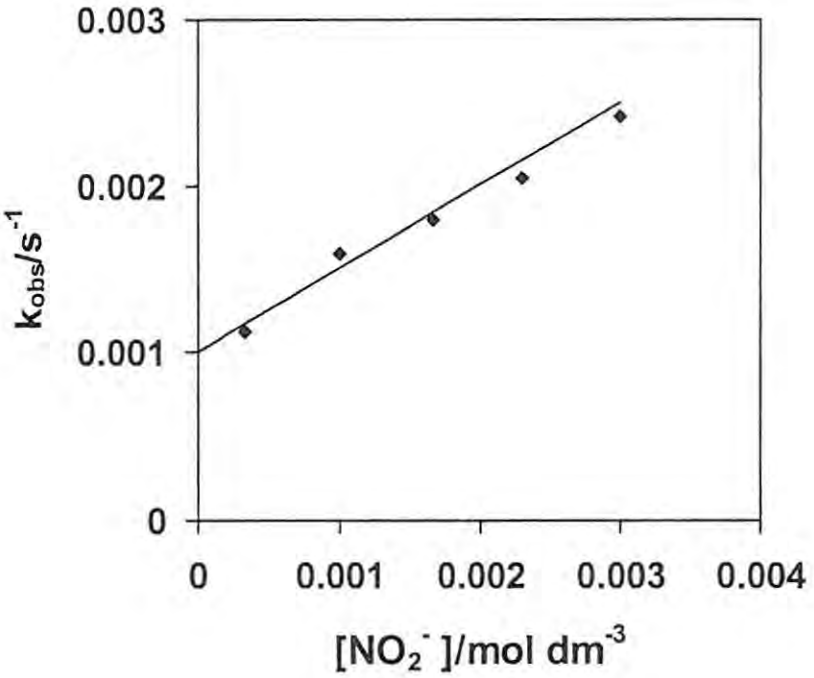

Fig. 3.26 Plot of k_{obs} (s^{-1}) versus [NO_2^-] in pH 4 buffer for coordination of NO with [Co^{II}Tm-3,4-tppa]$^{4+}$.

NO formed on disproportionation of nitrite at low pH is in equilibrium with nitrite and nitrate, which may influence the interactions between NO and [Co^{II}Tm-3,4-tppa]$^{4+}$ complex. For comparison purposes, kinetic and equilibria studies were also conducted using dissolved NO gas prepared from H_2SO_4 and nitrite as explained in Section 2.3.4. Oxygen was excluded from solutions containing NO in order to avoid the formation of nitrite. When NO (synthesized from H_2SO_4 and nitrite) solution in pH 4 buffer was added to solutions of [Co^{II}Tm-3,4-tppa]$^{4+}$ in pH 4 buffer, spectral changes observed were similar to those observed in Fig. 3.17 for the addition of NO (as nitrite) to the [CoTm-3,4-tppa]$^{4+}$ species, with a split Q band at 666 and 678 nm. The fact that the Q band was observed at similar wavelengths for coordination of NO (added as nitrite) and NO prepared from nitrite and H_2SO_4 confirms that the same complex is formed due to axial ligation of NO to [Co^{II}Tm-3,4-tppa]$^{4+}$ species. The equilibrium and kinetic data for the interaction of [Co^{II}Tm-3,4-

tppa]$^{4+}$ species with NO from the different sources are listed in Table 3.1. Larger equilibrium and rate constants were observed when NO gas, prepared as outlined in Section 2.3.4, was employed. It is likely that when nitrite is employed as a source of NO, a six-coordinate complex containing both NO and NO_2^-, [(NO)(NO_2^-)CoTm-3,4-tppa]$^{4+}$, is formed. A mixed complex of this nature has been reported for porphyrin complexes,[167] whereas a complex containing only NO, [(NO)CoTm-3,4-tppa]$^{4+}$, is formed when pure NO is employed. This would then result in the observed differences in the constants.

pH 7 studies

Under pH 7 buffer conditions, the disporpotionation of nitrite to NO is minimal, hence coordination of nitrite occurs under these conditions. Kinetics and equilibria for the formation of the new species were followed by monitoring the appearance of the peak due to product formation (at 663 nm, Fig. 3.18) with time. The equilibrium data were analysed by standard spectrophotomeric methods using equation 3.5, where A_{eq} is the equilibrium absorbance at 663 nm, A_o is the absorbance at 663 nm before addition of nitrite. A_∞ was determined from the final absorbance at 663 nm in Fig. 3.18 following complete shifting of the Q band to 663 nm. From the plot of $\log[(A_{eq} - A_o)/(A_\infty - A_{eq})]$ versus $\log [NO_2^-]$ (Fig. 3.27), an equilibrium constant, $K = 2.0 \times 10^2$ dm^3 mol^{-1} was determined for the coordination of nitrite to [CoTmtppa]$^{4+}$. The value of $n = 1.1 \pm 0.1$ was obtained from the slope showing that one molecule of nitrite has coordinated to [Co^{II}Tm-3,4-tppa]$^{4+}$ complex, forming [(NO_2^-)CoTm-3,4-tppa]$^{3+}$ species.

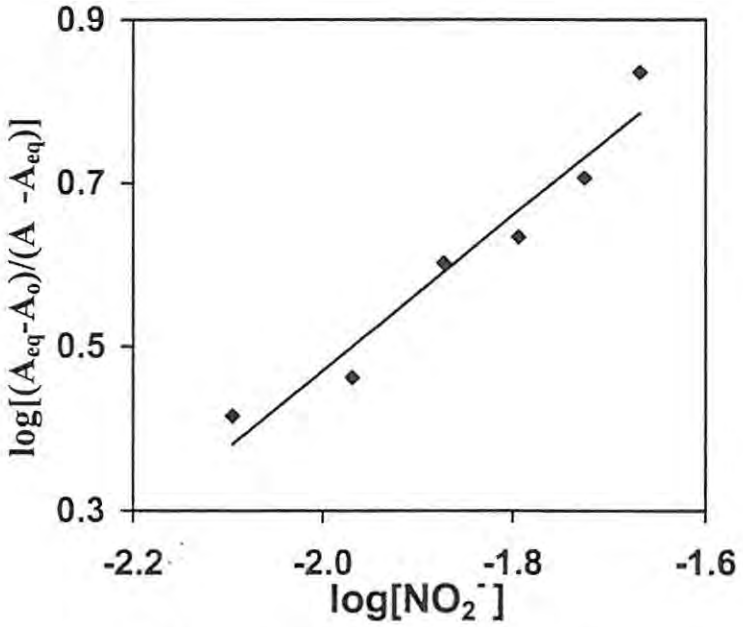

Fig. 3.27 Plot of $\log[(A_{eq} - A_o)/(A_\infty - A_{eq})]$ versus log $[NO_2^-]$ in pH 7 buffer for coordination of NO_2^- with $[Co^{II}Tm\text{-}3,4\text{-}tppa]^{4+}$.

For the formation of $[(NO_2^-)CoTm\text{-}3,4\text{-}tppa]^{3+}$ species, plots of $\ln(A_\infty - A_t)$ against time (where A_∞, and A_t are defined above) were linear, Fig. 3.28.

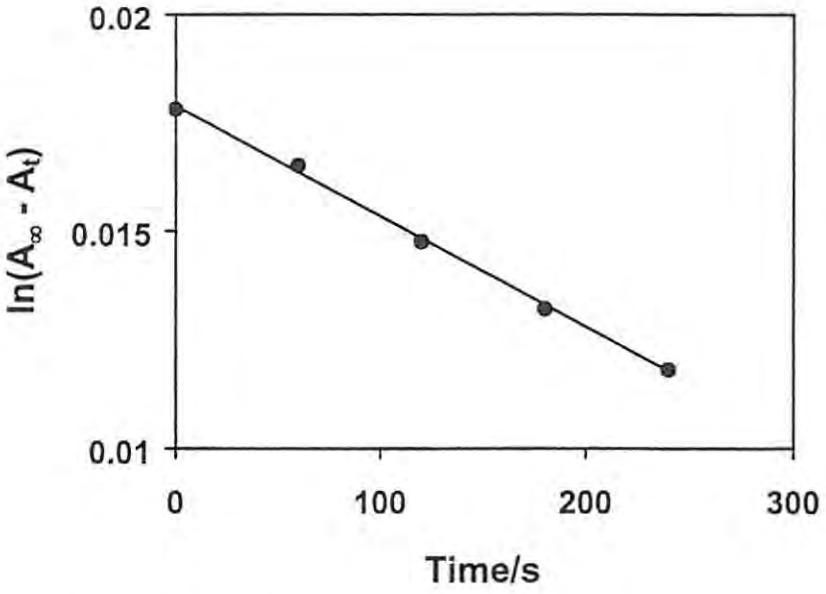

Fig. 3.28 Plot of $\ln(A_\infty - A_t)$ vs. time, for the reaction of NO_2^- (1.34×10^{-2} mol dm^{-3}) with $[Co^{II}Tm\text{-}3,4\text{-}tppa]^{4+}$ (4.0×10^{-6} mol dm^{-3}). pH 7 buffer.

The plot of the observed rate constant (k_{obs}) versus nitrite concentration was linear (Fig. 3.29) for the data shown in Fig. 3.18, showing that the coordination is first order in nitrite and obeys the rate law of equation 3.11, with L representing NO_2^-. Least-square analysis of the data gave $k_f = 4.0 \pm 0.1 \times 10^{-3}$ dm^3 mol^{-1} s^{-1} from the slope and $k_r = 2.4 \pm 0.9 \times 10^{-5}$ s^{-1} from the intercept. Using these values, the equilibrium constant was estimated to be $K \sim 1.7 \times 10^2$ dm^3 mol^{-1}, in good agreement with the value determined from equilibrium data. The value of the equilibrium constant is about 42 times higher than that obtained for coordination of nitrite to the negatively charged $[Co^{II}TSPc]^{4-}$ complex,[98] Table 3.3, whereas the rate constant for the forward reaction was approximately 25 times larger.

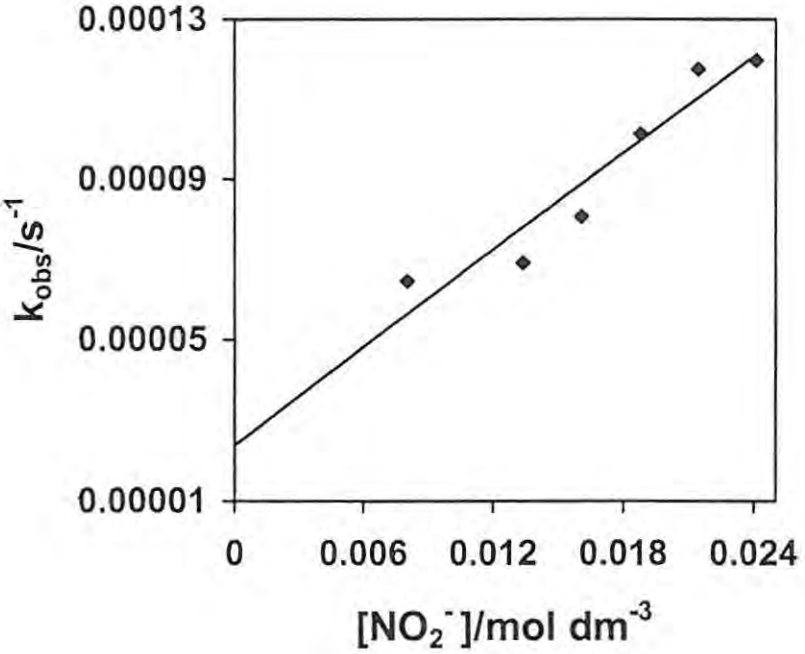

Fig. 3.29 Plot of k_{obs} (s^{-1}) versus $[NO_2^-]$ in pH 7 buffer for coordination of NO_2^- with $[Co^{II}Tm\text{-}3,4\text{-}tppa]^{4+}$.

3.4.3. General discussion on the interaction of analytes with $[Co^{II}Tm\text{-}3,4\text{-}tppa]^{4+}$

The rate constants for the auto-reduction of $[Co^{II}Tmtppa]^{4+}$ by cysteine were found to be higher than those for histidine as was also reported for $[Pt^{II}Tmtppa]^{4+}$ and $[Pd^{II}Tmtppa]^{4+}$ complexes.[12] The differences in the rate constants for the auto-reduction of $[M^{II}Tmtppa]^{4+}$ complexes in the presence of histidine and cysteine may be due to differences in abilities of the protonated and deprotonated forms of these amino acids in effecting the auto-reduction process. Spectral changes shown in Fig. 3.17 were observed for histidine only at pH values greater than 6, thus showing that the extent of deprotonation of histidine is important for the auto-reduction process. For cysteine, auto-reduction was observed from pH values less than 3 to physiological pH values (~7). Thus, the protonated forms of cysteine are involved in the auto-reduction of the $[Co^{II}Tmtppa]^{4+}$ species. $[M^{II}(Tmtppa)]^{4+}$ complexes are unstable in highly basic media, hence studies at pH values larger than 7 were not undertaken.

Reduction of $[Co^{II}TSPc]^{4-}$ and $[M^{II}(Tmtppa)]^{4+}$ complexes in the presence of cysteine is well documented.[5,12,120,168] Histidine has been shown[12] to reduce $[M^{II}(Tmtppa)]^{4+}$ (where M = Pd or Pt) at the ring, but to oxidize $[Co^{II}TSPc]^{4-}$ to Co^{III} species[12,169] in the presence of oxygen. There was no evidence of the oxidation of $[Co^{II}Tmtppa]^{4+}$ complex in the presence of histidine even when oxygen was not excluded from the solution.

Auto-reduction of $[Co^{II}TSPc]^{4-}$ in the presence of cysteine is known to be pH dependent in that it occurs at pH values greater than 4, but at pH values between 9.5 and 12, $[Co^{I}TSPc]^{5-}$ catalyses the reduction of cystine to cysteine.[168] However, it was observed in this work that cysteine auto-reduces $[Co^{II}Tm\text{-}3,4\text{-}tppa]^{4+}$ species at pH values less than 4, reflecting the ease of reduction of this positively charged complex, compared to $[Co^{II}TSPc]^{4-}$. As explained above, the interactions in highly basic media could not be undertaken since $[Co^{II}Tm\text{-}3,4\text{-}tppa]^{4+}$ complex decomposes under these conditions.

Interactions of $[Co^{II}Tm\text{-}3,4\text{-}tppa]^{4+}$ with NO and NO_2^- resulted in different spectroscopic behaviour than observed for histidine and cysteine. Interaction between NO or NO_2^- with $[Co^{II}TSPc]^{4-}$ has been studied.[36,98] Auto-oxidation of $[Co^{II}TSPc]^{4-}$ to $[Co^{III}TSPc]^{3-}$ has been implicated on interaction of this species with NO or nitrite. Oxidation of the $[Co^{II}Tm\text{-}3,4\text{-}tppa]^{4+}$ species is expected to occur with difficulty due to the presence of positive charges, when compared to oxidation of $[Co^{II}TSPc]^{4-}$. There was no evidence of the oxidation of $[Co^{II}Tm\text{-}3,4\text{-}tppa]^{4+}$ species on interaction with NO or nitrite.

Therefore, it has been shown in this work that autoreduction of $[Co^{II}Tm\text{-}3,4\text{-}tppa]^{4+}$ occurs in the presence of either histidine or cysteine, with the formation of metal reduced species, $[Co^{I}Tmtppa(-2)]^{3+}$. NO and nitrite coordinate to $[Co^{II}Tm\text{-}3,4\text{-}$

tppa]$^{4+}$ species, without auto-reduction of this species, observed for cysteine or histidine. There was also no spectroscopic evidence for the coordination of two nitrite or NO ligands to [Co^{II}Tm-3,4-tppa]$^{4+}$ species. Ring modifications from negatively charged [Co^{II}TSPc]$^{4-}$ to positively charged [Co^{II}Tm-3,4-tppa]$^{4+}$ resulted in an improved rate in the interaction of these species with nitrite.

3.4.4. Interaction of cyanide with cobalt tetrasulfophthalocyanine

Kinetic and equilibrium data for the formation of new species following addition of cyanide to [Co^{II}TSPc]$^{4-}$ was determined by monitoring the spectrum due to the product, [(CN$^-$)$_2$Co^{III}TSPc]$^{5-}$, with a Q band at 676 nm, Fig. 3.19(a). The concentration of [Co^{II}TSPc]$^{4-}$ was kept constant at 1.0×10^{-5} mol dm^{-3}, while cyanide concentrations were varied from 2.5×10^{-3} to 8.7×10^{-2} mol dm^{-3}. Since the concentrations of cyanide were much larger than that of [Co^{II}TSPc]$^{4-}$, pseudo-first order conditions were assumed for kinetic studies. A pH of 11 was employed.

The equilibrium data were analysed by standard spectrophotomeric methods using equation 3.5. Where A_{eq} is the equilibrium absorbance at 676 nm, A_o is the absorbance at 676 nm before addition of cyanide. A_∞ was determined from the final absorbance at 676 nm in Fig. 3.19(a), following complete formation of [(CN$^-$)$_2$Co^{III}TSPc]$^{5-}$ complex. From the plot of $\log[(A_{eq} - A_o)/(A_\infty - A_{eq})]$ versus log [CN$^-$], Fig. 3.30, an equilibrium constant of $K = 2.1 \pm 0.1 \times 10^1$ dm^3 mol^{-1} was determined for the formation of [(CN$^-$)$_2$Co^{III}TSPc]$^{5-}$ when oxygen was deliberately bubbled through the solution. A lower value of the equilibrium constant of $K = 6.0 \pm 0.1$ dm^3 mol^{-1} (Table 3.4) was observed when no oxygen was bubbled into solution (i.e. in the presence of residual oxygen in water). The number of moles of electrons transferred of near unity ($n = 0.9 \pm 0.1$) was obtained from the slope of the plot shown

in Fig. 3.30, showing coordination of one molecule of cyanide at this stage. As has been discussed above, the coordination of the second cyanide is responsible for the formation of species with Q band at 676 nm, hence the determined equilibrium constant is for the formation of $[(CN^-)_2Co^{III}TSPc]^{5-}$ species by equation 3.4. The value of the equilibrium constant could be slightly affected by the initial formation of the monocyano species.

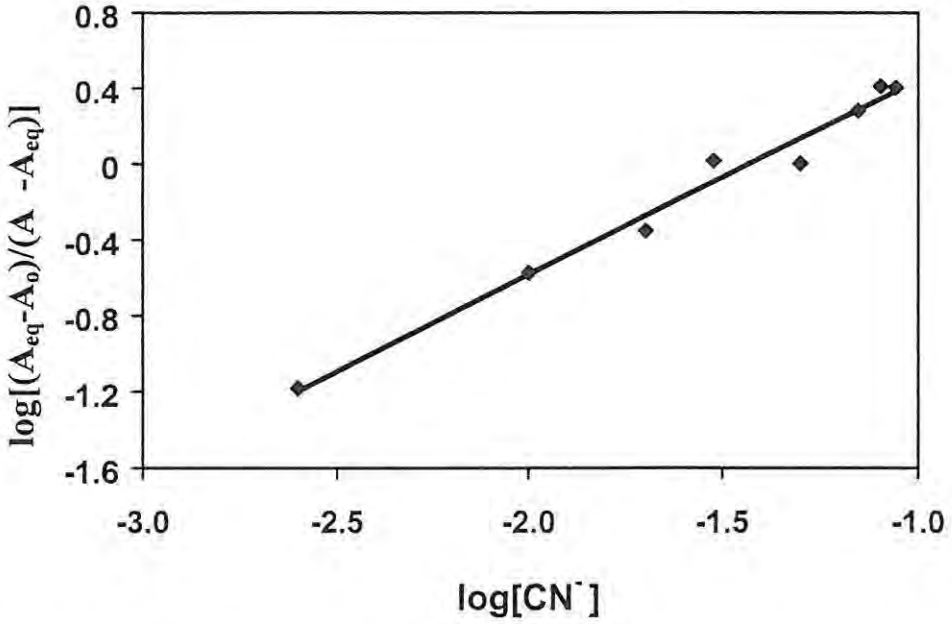

Fig. 3.30 Plots of $\log[(A_{eq} - A_o)/(A_\infty - A_{eq})]$ vs. $\log [CN^-]$ for coordination of CN^- to $[Co^{II}TSPc]^{4-}$

For the formation of $[(CN^-)_2Co^{III}TSPc]^{5-}$ species, plots of $\ln(A_\infty - A_t)$ against time, (where A_∞, and A_t are defined above) were linear, Fig. 3.31.

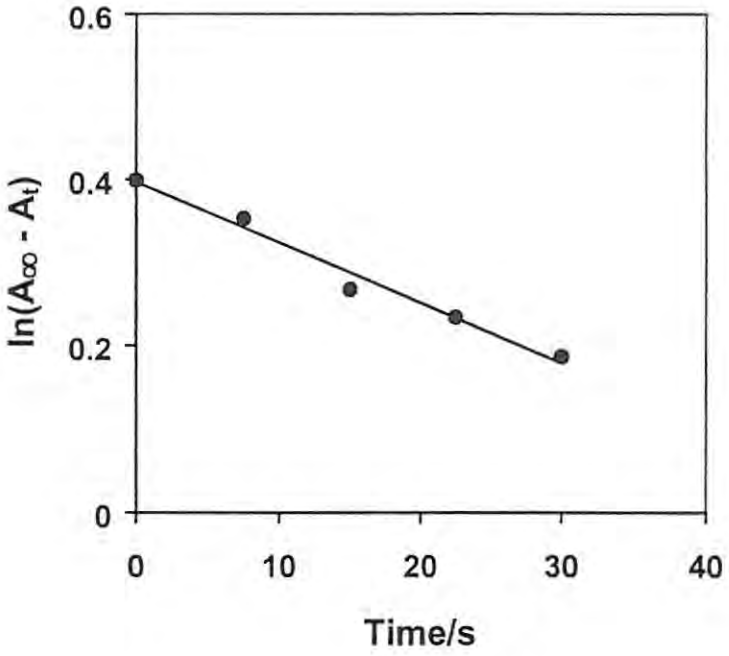

Fig. 3.31 Plot of $\ln(A_\infty - A_t)$ vs. time, for the reaction of cyanide (8.76 x 10^{-2} mol dm^{-3}) with $[Co^{II}TSPc]^{4-}$ (1.0 x 10^{-5} mol dm^{-3}).

The observed rate constant (k_{obs}) is given by the slope of the plot of $\ln(A_\infty - A_t)$ against time. The observed rate constant was obtained for several cyanide concentrations. The plot of the observed rate constant (k_{obs}) versus cyanide concentration was linear (Fig. 3.32) for the data represented in Fig. 3.19(a), showing that the coordination is first order in cyanide and obeys the rate law of equation 3.11, which is typical of coordination of axial ligands to MPc complexes. k_f is the rate constant for the formation of $[(CN^-)_2Co^{III}TSPc]^{5-}$ and is given by $k_1k_2/k_{-1}[CN^-]$. k_r is the rate constant for the dissociation of the complex. Least-square analysis of the data gave $k_f = 0.12 \pm 0.03$ dm^3 mol^{-1} s^{-1} from the slope and $k_r = 5.7 \pm 0.2$ x 10^{-3} s^{-1} from the intercept for the case when oxygen was bubbled through the solution, and $k_f = 0.10 \pm 0.03$ dm^3 mol^{-1} s^{-1} and $k_r = 1.6 \pm 0.02$ x 10^{-2} s^{-1}, in the presence of residual oxygen (i.e. no oxygen bubbled through the solution). Using k_f and k_r values, the equilibrium

constants were estimated to be K ~ 2.1 x 10^1 and 6.0 dm^3 mol^{-1}, respectively, for situations when oxygen was bubbled or in the presence of residual oxygen. These values are in good agreement with the values determined from equilibrium data. Oxidation of thiols with $[Co^{II}TSPc]^{4-}$ and the subsequent reduction of the latter to $[Co^{I}TSPc]^{5-}$ has been reported.[170,171]

Rates and equilibrium constants are higher when oxygen was bubbled through the solution, hence showing that the formation of oxidised $[(CN^-)_2Co^{III}TSPc]^{5-}$ species is dependent on oxygen. Also a larger equilibrium constant in the presence of oxygen indicates formation of a more stable complex. As has been mentioned above, it has been reported in the literature that cyanide facilitates central metal oxidation in $[Co^{II}TSPc]^{4-}$ by atmospheric oxygen.[153] Kinetic studies were not affected by varying the concentration of Tris buffer employed.

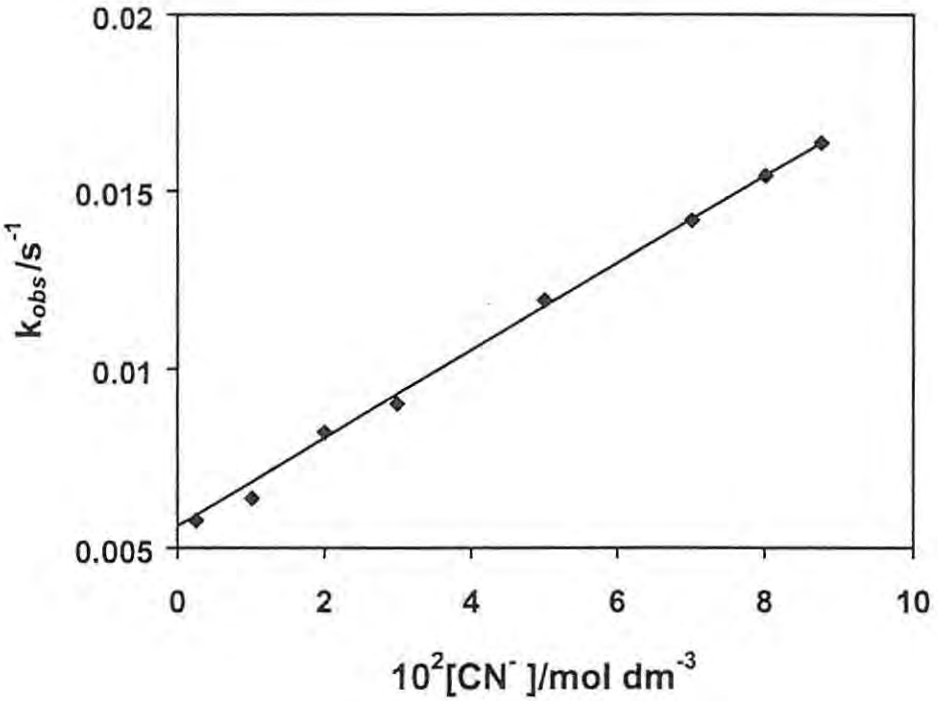

Fig. 3.32 Plot of k_{obs} (s^{-1}) versus concentration for the coordination cyanide to $[Co^{II}TSPc]^{4-}$, 1.0 x 10^{-5} mol dm^{-3} species. pH 11 buffer.

Table 3.4 compares the equilibrium and rate constants for the coordination of cyanide to $[Co^{II}TSPc]^{4-}$ complex, to the constants reported for the coordination of cyanide to FePc complexes. Table 3.4 shows that the rate constants for the coordination of cyanide to $[Co^{II}TSPc]^{4-}$ complex in aqueous solutions is in the range with those reported for the coordination of cyanide to FePc complexes in DMSO. Coordination of axial ligands (e.g. pyridine) to FePc was found[172] to occur faster than its coordination to CoPc complexes in DMSO solutions, suggesting faster axial ligand exchange reactions in FePc complexes compared to CoPc complexes. As has been mentioned above, in the presence of DMSO, coordination of cyanide to $[Co^{II}TSPc]^{4-}$ was slower (hence the observation of a stepwise cyanide coordination in DMSO) than in water, thus the nature of the solvent plays an important role. The rate constants for the coordination of cyanide to CoPc in non-aqueous solutions have not been

reported. The rate constant reported for the coordination of cyanide to the $[Co^{II}TSPc]^{4-}$ species is much lower than the rate constant of 3×10^4 dm^3 mol^{-1} s^{-1} reported for the coordination of cyanide to cobalt tetraphenyl porphyrin.[173]

Table 3.4 Equilibrium and rate constants for the coordination of cyanide and SO_2 to MPc complexes. The data is for the coordination of second cyanide or sulphur dioxide ligands.

Complex	Ligand	Conditions	K (dm^3 mol^{-1})	k_f (dm^3 mol^{-1} s^{-1})	k_r (s^{-1})	Ref.[a]
[b][CoTSPc]$^{4-}$	CN^-	pH 11	$2.1 \pm 0.1 \times 10^1$	0.12 ± 0.03	$5.7 \pm 0.2 \times 10^{-3}$	tw
[c][CoTSPc]$^{4-}$	CN^-	pH 11	6.0 ± 0.1	0.10 ± 0.03	$1.6 \pm 0.2 \times 10^{-2}$	tw
FePc	CN^-	DMSO	5.7×10^2	0.2	3.5×10^{-4}	161
$FePc(Cl)_{16}$	CN^-	DMSO	1.6×10^3	4.2×10^{-3}	2.3×10^{-6}	66
$[CoTSPc]^{4-}$	SO_2	pH 11	$8.7 \pm 0.2 \times 10^1$	3.5 ± 0.3	$3.8 \pm 0.3 \times 10^{-2}$	tw
$[CoTSPc]^{4-}$	SO_2	pH 7.4	$1.3 \pm 0.2 \times 10^2$	4.0 ± 0.2	$3.2 \pm 0.3 \times 10^{-2}$	tw

[a] tw = this work. [b] = Oxygen bubbled. [c] = Residual oxygen (no oxygen bubbled)

3.4.5. Interaction of SO_2 with $[Co^{II}TSPc]^{4-}$

Equilibrium data for the formation of the SO_2 complex was determined as explained above using equation 3.5, with L replaced by SO_2. The concentration of $Co^{II}TSPc]^{4-}$ was kept constant at 1.0×10^{-5} mol dm^{-3}, while SO_2 concentrations were varied from 2.0×10^{-3} to 1.6×10^{-2} mol dm^{-3}. Since the concentrations of SO_2 were much larger than that of $[Co^{II}TSPc]^{4-}$, pseudo-first order conditions were assumed for kinetic studies. pH 11 and 7.4 conditions were employed.

The increase in the monomer peak in Fig. 3.21 was monitored. In equation 3.5, A_{eq} is the equilibrium absorbance at 673 nm; A_o is the absorbance at 673 nm before addition of SO_2. A_∞ is the absorbance after complete formation of the complex,

determined from the final absorbance at 673 nm. From the plot of log $[(A_{eq} - A_o)/(A_\infty - A_{eq})]$ versus log $[SO_2]$, Fig. 3.33, an equilibrium constant of $K = 8.7 \pm 0.3 \times 10^1$ dm^3 mol^{-1} was determined for the formation of the proposed $[(SO_3^{2-})_2CoTSPc]^{5-}$ complex. The value of n was found to be near unity ($n = 1.1 \pm 0.1$) showing that the coordination of one molecule of SO_2 results in the observed spectral evolution with a Q band centred at 673 nm in Fig. 3.21.

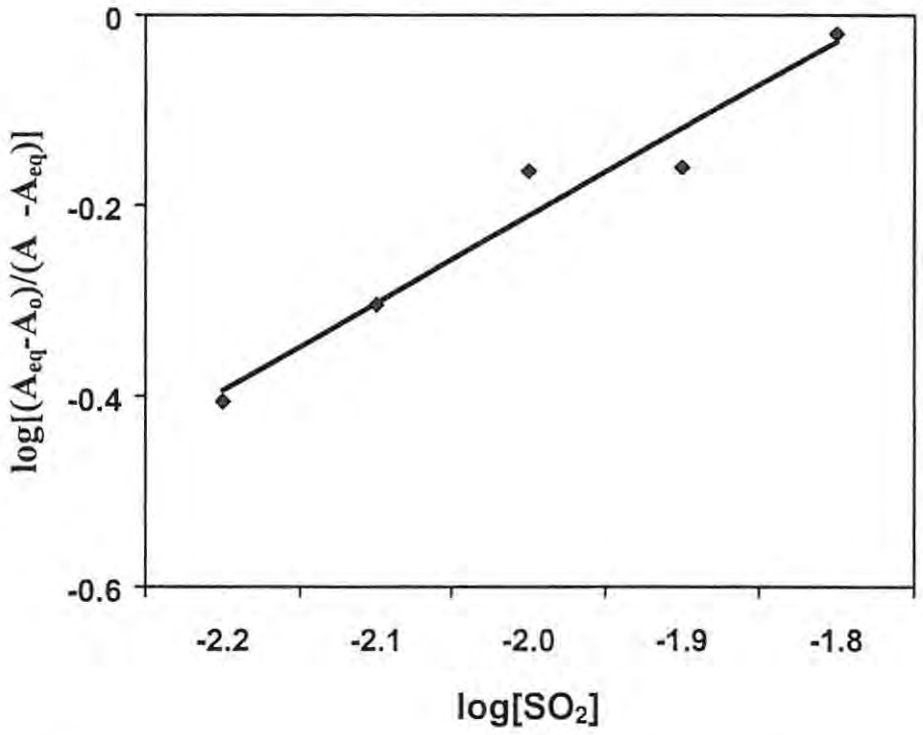

Fig. 3.33 Plots of $\log[(A_{eq} - A_o)/(A_\infty - A_{eq})]$ versus $\log [SO_2]$ in pH 11 buffer for coordination of SO_2 to $[CoTSPc]^{4-}$.

For the formation of $[(SO_3^{2-})_2CoTSPc]^{6-}$ species, plots of $\ln(A_\infty - A_t)$ against time (where A_∞, and A_t are defined above) were linear, Fig. 3.34.

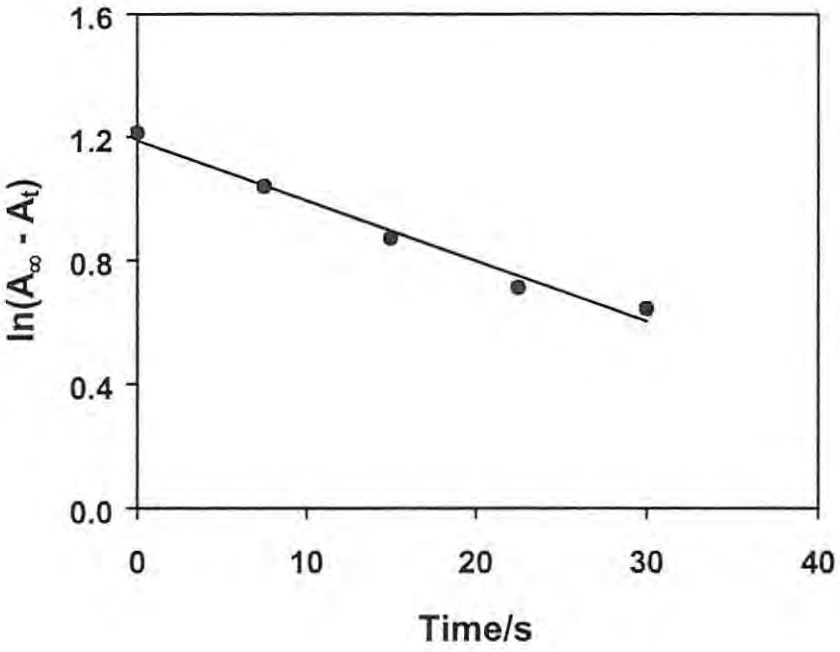

Fig. 3.34 Plot of $\ln(A_\infty - A_t)$ vs. time, for the reaction of SO_2 (2.06×10^{-3} mol dm^{-3}) with $[Co^{II}TSPc]^{4-}$ (1.0×10^{-5} mol dm^{-3}). pH 11.

The plot of k_{obs} versus $[SO_2]$ for the data shown in Fig. 3.21 was linear, Fig. 3.35, with $k_f = 3.5 \pm 0.3$ dm^3 mol^{-1} s^{-1} and $k_r = 3.8 \pm 0.3 \times 10^{-2}$ s^{-1}, under pH 11 conditions. Using these values the equilibrium constant was estimated to be $K \sim 9.0 \times 10^1$ dm^3 mol^{-1} in agreement with the value determined from equilibrium data. The plot in Fig. 3.34 confirms that a rate law similar to that shown by equation 3.11 is obeyed for the coordination of SO_2 to $[Co^{II}TSPc]^{4-}$ species and that the coordination is first order in SO_2. Equilibrium and rate constants for the reaction between SO_2 and $[Co^{II}TSPc]^{4-}$ at pH 11 are shown in Table 3.4, and are compared with those obtained at pH 7.4. Similar rate constants are obtained at these two pH values. The equilibrium constant at pH 7.4 was slightly higher than that obtained at pH 11, but the difference was not significant. As discussed above, in basic media, it is expected that the predominant species for SO_2 are SO_3^{2-} species. Thus, at both pH 7.4 and pH 11, the same species (SO_3^{2-}) is expected to coordinate to $[Co^{II}TSPc]^{4-}$ complex; pKa = 1.81

and 6.9 for H_2SO_3. Dissolved $SO_2.H_2O$ may form HSO_3^- by equation 1.13, which in turn may form $S_2O_5^{2-}$ in basic media according to equation 3.13.[182]

$$2HSO_3^- \rightleftharpoons S_2O_5^{2-} + H_2O \qquad (3.13)$$

Thus HSO_3^- and $S_2O_5^{2-}$ may compete with SO_3^{2-} for binding to the phthalocyanine species. However, $S_2O_5^{2-}$ readily converted to SO_3^{2-} according to equation 1.34.

The effect of this reaction was not observed using this technique.

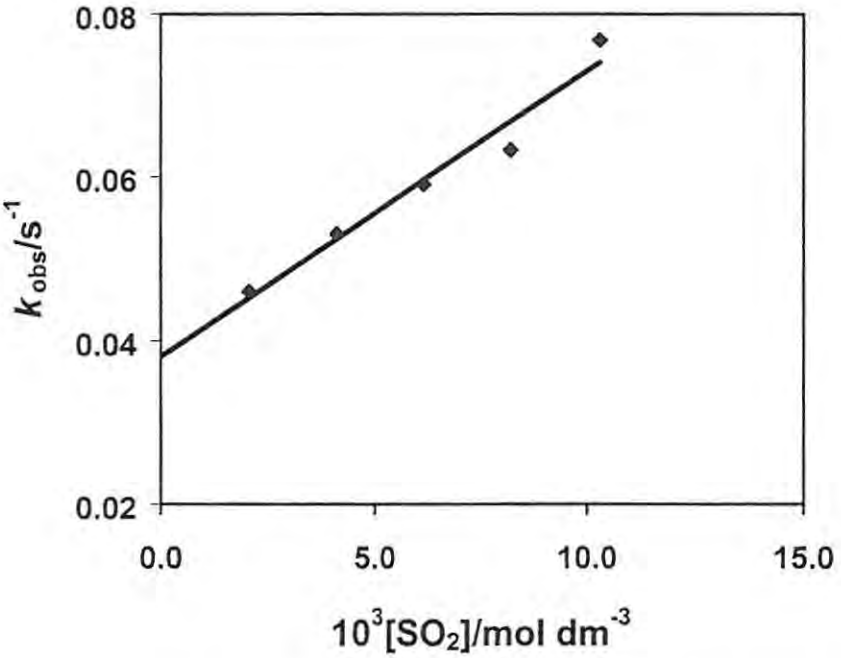

Fig. 3.35 Plots of k_{obs} (s^{-1}) versus concentration for the coordination of sulphur dioxide to $[Co^{II}TSPc]^{4-}$, 1.0 x 10^{-5} mol dm^{-3} species. pH 11 buffer.

3.4.6. Discussion on the interaction of analytes with $[Co^{II}TSPc]^{4-}$

It has been shown in this work that cyanide and SO_2 coordinate to $[Co^{II}TSPc]^{4-}$ species. The coordination is accompanied by oxidation of the central Co(II) metal forming Co(III) species. The rate constants reported here for cyanide coordination to the $[Co^{II}TSPc]^{4-}$ complex are in the range for those reported for the coordination of cyanide to FePc and RuPc complexes in non-aqueous media.

CHAPTER 4

ELECTROCATALYTIC STUDIES

4. ELECTROCATALYTIC STUDIES*

4.1. Electrodeposition

The choice of the solvent for electrodeposition depended on the stability of the modified electrode towards the detection of the species. Different methods were thus employed for different analytes, as outlined below.

4.1.1. Electrodeposition of $[Co^{II}Tm\text{-}3,4\text{-}tppa]^{4+}$

The glassy carbon electrode modified with $[Co^{II}Tm\text{-}3,4\text{-}tppa]^{4+}$, represented as $[CoTm\text{-}3,4\text{-}tppa]^{4+}$-GCE was employed for catalysis of nitrite, cyanide and amino acids. The electrode modification was obtained by cathodic electrodeposition from a 1 x 10^{-3} mol dm^{-3} solution of $[Co^{II}Tm\text{-}3,4\text{-}tppa]^{4+}$ in pH 4 phosphate buffer, as explained in the experimental section (Section 2.3.1.2). The deposition was carried out by repetitively scanning between 0 and - 0.6 V vs. Ag|AgCl, Fig. 4.1. The reduced species readily formed an electrically conducting film on the carbon electrode.[11,42] After deposition, the electrode was rinsed with water, followed by pH 4 buffer, and then a CV scan recorded in the blank (pH 4 buffer), in the potential range 0 to - 0.6 V yielding a well-developed couple I, which corresponds to the first ring reduction, as has been reported before and as discussed in Section 3.2.[11,42]

* Part of the work in this chapter has resulted in the following publications: M. Thamae and T. Nyokong, *J. Electroanal. Chem.*, **470** (1999) 126, M. Thamae, P. Westbroek and T. Nyokong, *Mikrochimica Acta*, in press.

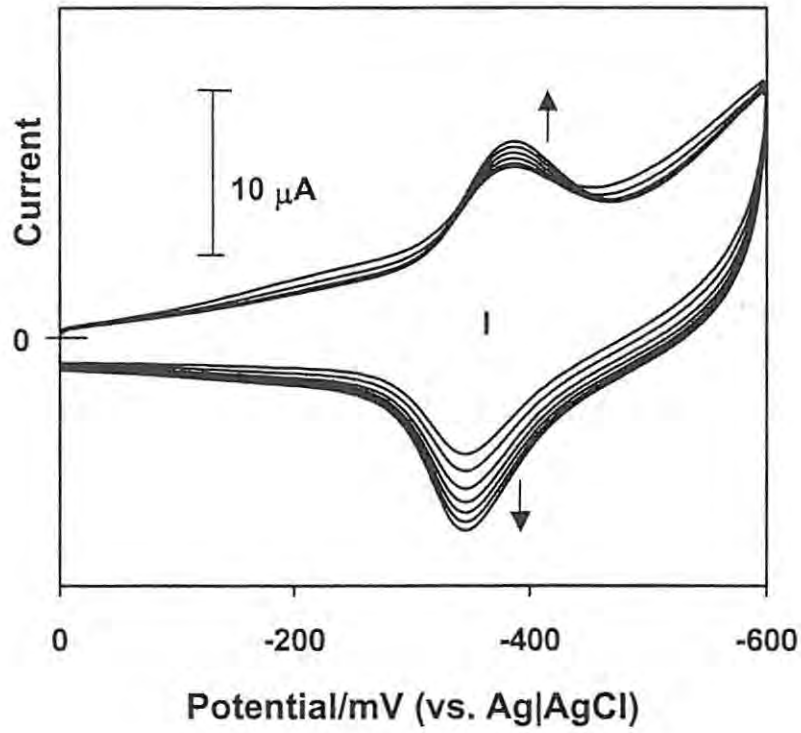

Fig. 4.1 Repetitive cyclic voltammograms of $[Co^{II}Tm\text{-}3,4\text{-}tppa]^{4+}$, (1 x 10^{-3} mol dm^{-3}) for electrodeposition in pH 4 phosphate buffer. Scan rate = 100 mV s^{-1}.

To check the stability of $[Co^{II}Tm\text{-}3,4\text{-}tppa]^{4+}$-GCE, repetitive scanning was performed in the potential range 0 to - 0.6 V vs. Ag|AgCl in a blank (pH 4 buffer), until no further decrease in the peak current was observed. The electrode was then ready for use.

4.1.2. Electrodeposition of $[Co^{II}TSPc]^{4-}$

The GCE electrode modified with $[Co^{II}TSPc]^{4-}$ represented as $[Co^{II}TSPc]^{4-}$-GCE was employed in nitrite electrocatalysis in addition to $[Co^{II}Tm\text{-}3,4\text{-}tppa]^{4+}$-GCE. The deposition was carried out as explained in the experimental section (Section 2.3.1.2) by repetitively scanning at 100 mV s^{-1} between + 1.0 and - 0.2 V vs. Ag|AgCl

(non-aqueous), Fig. 4.2 from a 1 x 10^{-3} mol dm^{-3} solution of $[Co^{II}TSPc]^{4-}$ in DMF containing 0.1 mol dm^{-3} TEAP as an electrolyte.

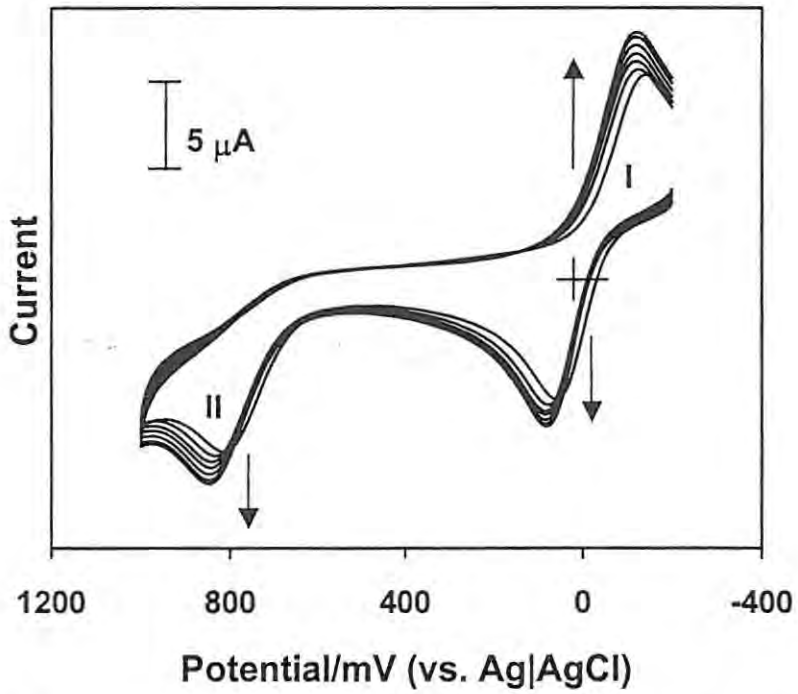

Fig. 4.2 $[Co^{II}TSPc]^{4-}$ cyclic voltammogram in DMF and TEAP as an electrolyte showing repetitive scanning for electrodeposition onto a GCE. Scan rate = 100 mV s^{-1}.

The redox processes labelled I and II are assigned to metal reduction and oxidation in $[Co^{II}TSPc]^{4-}$ with the formation of $[Co^{I}TSPc]^{5-}$ and $[Co^{III}TSPc]^{3-}$, respectively. See also Fig. 3.10(a) in Section 3.2.2.

$[Co^{II}TSPc]^{4-}$ is water soluble and it is known to be irreversibly bound to the glassy carbon electrode upon electrochemical deposition.[122] The $[Co^{II}TSPc]^{4-}$ complex was also adsorbed onto the GCE using repetitive cyclic voltammetry scanning from - 0.9 to + 1.25 V vs. Ag|AgCl, Fig. 4.3 (in pH 10. 2 buffer), and was employed for SO_2 detection. Similar electrocatalysis results were observed when $[Co^{II}TSPc]^{4-}$-GCE was electrodeposited from DMF and from pH 10.2 buffer as

explained above. No SO_2 catalysis was observed when electrodepositing from pH 7.4 buffer.

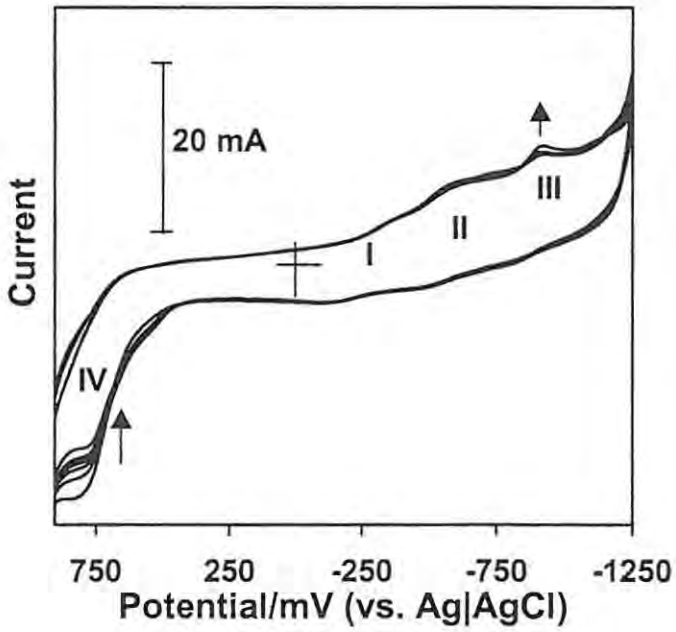

Fig. 4.3 Cyclic voltammogram of $[Co^{II}TSPc]^{4-}$ in pH 10.2 buffer, showing repetitive scanning for electrodeposition onto a GCE. Scan rate = 100 mV s^{-1}.

An increase in peak III was observed with repetitive cycling under pH 10.2 buffer conditions, but a decrease was observed for peak IV, Fig 4.3, (see Section 3.2.2 for peak assignments). At the end of electrodeposition, a purple layer was observed on the elecrode surface indicating the presence of a catalyst on the electrode surface.

4.1.3. Electrodeposition of $[Fe^{II}TSPc]^{4-}$

In Fig. 4.4 the electrodeposition of $[Fe^{II}TSPc]^{4-}$ is shown as a function of scan number and was carried out in a 10^{-3} mol dm^{-3} solution of $[Fe^{II}TSPc]^{4-}$. Five peaks could be observed during this experiment, all of them increasing with scan number. This means that $[Fe^{II}TSPc]^{4-}$ is indeed depositing onto the surface of the electrode. Assignments of peaks were discussed in Section 3.2.2 above.

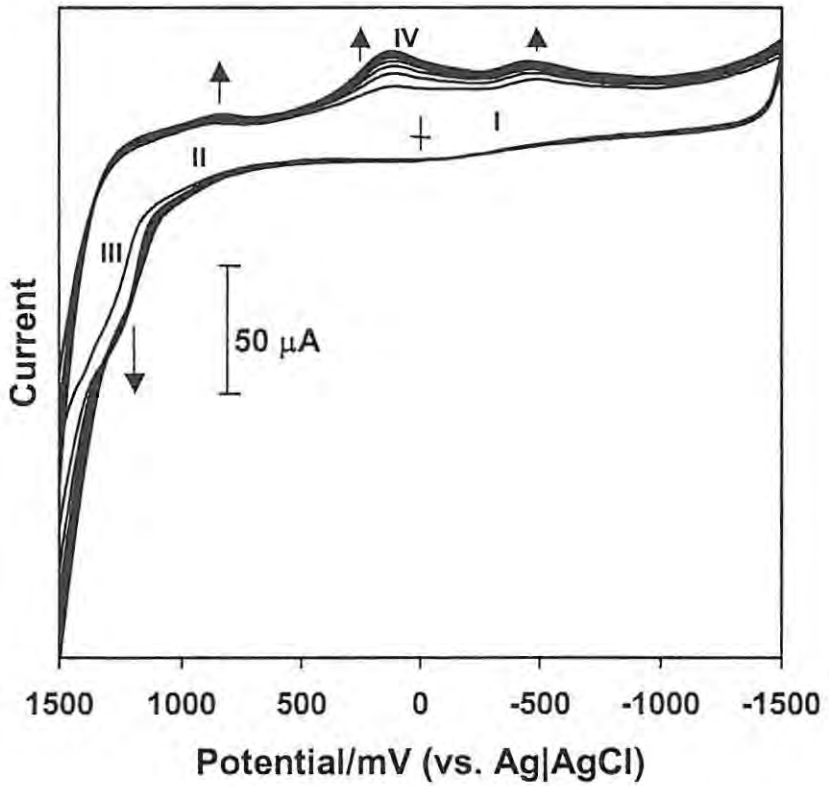

Fig. 4.4 Voltammetric curves of the electrodeposition of $[Fe^{II}TSPc]^{4-}$ at a glassy carbon electrode in pH = 7.4 buffer containing 10^{-3} mol dm^{-3} $[Fe^{II}TSPc]^{4-}$. Scan rate = 100 mV s^{-1}.

4.1.4. Electrodeposition of $[Co^{II}Tmtppa]^{4+}.[CoTSPc]^{4-}$

Studies on porphyrin complexes have shown that mixing cationic metal(II) tetrakis(N-methylpyridyl) porphyrinato with the anionic metal(II) tetrakis (4-sulfonatophenyl) porphyrinato in polar solvents leads to the formation of a stable 1:1 dimeric complex,[13,16,128,129,174] which readily adsorbs electrochemically onto a glassy carbon electrode and shows high catalytic efficiency towards four electron reduction of oxygen.[174] In this work the catalytic activities of the anionic, $[Co^{II}TSPc]^{4-}$, and the cationic, $[Co^{II}Tm\text{-}3,4\text{-}tppa]^{4+}$, complexes towards nitrite reduction are compared with the activity of the mixture of these complexes, represented as $[Co^{II}Tmtppa]^{4+}.[Co^{II}TSPc]^{4-}$.

The GCE electrode modified with $[Co^{II}Tm\text{-}3,4\text{-}tppa]^{4+}.[Co^{II}TSPc]^{4-}$ is represented as $[Co^{II}Tm\text{-}3,4\text{-}tppa]^{4+}.[Co^{II}TSPc]^{4-}$-GCE. The deposition of GCE was performed as explained in the experimental section (Section 2.3.1.2).[122] In this method the deposition was carried out by repetitively scanning at 100 mV s^{-1} between + 1.0 and - 0.2 V vs. Ag|AgCl in pH 4 buffer, Fig. 4.5, from a 1 x 10^{-3} mol dm^{-3} solution of $[Co^{II}Tm\text{-}3,4\text{-}tppa]^{4+}.[Co^{II}TSPc]^{4-}$ in pH 4 buffer.

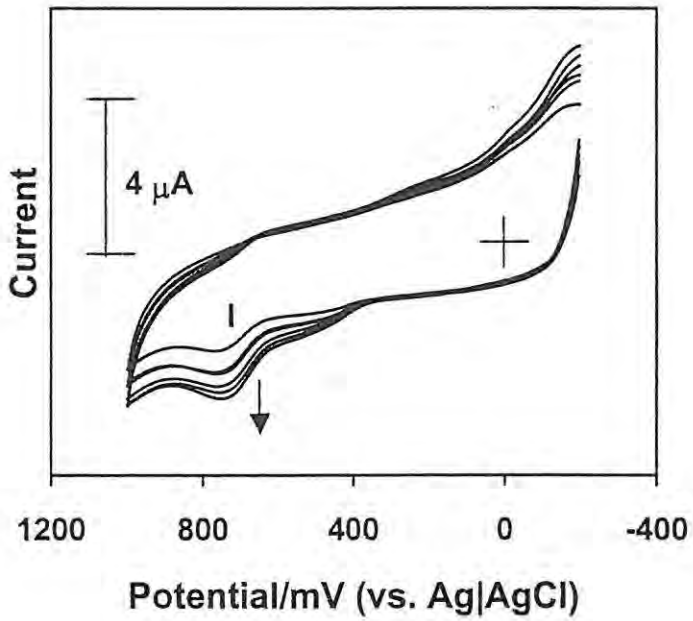

Fig. 4.5 $[Co^{II}Tm\text{-}3,4\text{-}tppa]^{4+}.[Co^{II}TSPc]^{4-}$ cyclic voltammogram in pH 4 buffer showing repetitive scanning for electrodeposition onto a GCE. Scan rate = 100 mV s^{-1}.

Peak I in Fig. 4.5 corresponds to metal oxidation of the $[Co^{II}TSPc]^{4-}$ component of $[Co^{II}Tm\text{-}3,4\text{-}tppa]^{4+}.[Co^{II}TSPc]^{4-}$ complex.

4.2. Electrocatalytic studies of nitrite and nitric oxide

Catalytic activity of MPc complexes is known to depend on the central metal ion. MPc complexes with an electroactive central metal ion, e.g. CoPc and FePc have

been shown to exhibit better catalytic activity than those MPc complexes with ring based redox processes.[22] Studies have shown that $Co^{II}Pc$ complexes exhibit good selectivity toward nitrite ion determination.[100] In this section, the porphyrazine and phthalocyanine complexes: cobalt(II) tetra-2,3-pyridinoporphyrazine (Co^{II}tppa), cobalt(II) N,N,N ,N -tetramethyltetra-2,3-pyridinoporphyrazine ([Co^{II}Tm-2-3-tppa]$^{4+}$), cobalt(II) N,N,N ,N -tetramethyltetra-3,4-pyridinoporphyrazine ([Co^{II}Tm-3,4-tppa]$^{4+}$), cobalt(II) tetrasulfophthalocyanine ([Co^{II}TSPc]$^{4-}$) and the mixture of [Co^{II}TSPc]$^{4-}$ and [Co^{II}Tm-3,4-tppa]$^{4+}$ are studied with respect to their catalytic activity towards nitrite reduction, and compared to $Co^{II}Pc$.

4.2.1. Reduction of NO under homogeneous conditions

In an attempt to identify the porphyrazine redox species that may be responsible for the catalytic reduction of nitrite, homogeneous catalysis of nitrite using [Co^{II}Tm-3,4-tppa]$^{4+}$was studied. When NO_2^- was added to [Co^{II}Tm-3,4-tppa]$^{4+}$ in pH 4 buffer, the cyclic voltammogram shown in Fig. 4.6(a) was obtained. This voltammogram is compared with a voltammogram in the absence of NO_2^-, Fig. 4.6(b). A large enhancement of the cathodic currents was observed at potentials assigned to the reduction of the porphyrazine ring in [Co^{II}Tm-3,4-tppa]$^{4+}$. Metal reductions to Co^{II} species occur at positive potentials as discussed in Section 3.2.1. The large increase in the cathodic currents is typical behaviour for catalytic reduction. No cathodic catalytic currents were observed within the potential range reported in Fig. 4.6, in the absence of [Co^{II}Tm-3,4-tppa]$^{4+}$. At near neutral pH conditions, there is only a small disporpotionation of nitrite to NO while under acid conditions the disproportionation of nitrite to NO is significant and the catalytic reduction corresponds to the reduction of NO under these conditions.[175,176] Thus the catalytic

reduction currents observed in Fig. 4.6 are due to the reduction of NO. A broad peak near - 0.6 V vs. Ag|AgCl is observed for the reduction of NO in the presence of $[Co^{II}Tm\text{-}3,4\text{-}tppa]^{4+}$, Fig. 4.6. Similar results were observed when $[Co^{II}Tm\text{-}2,3\text{-}tppa]^{4+}$ was employed, with the reduction peak at - 0.6 V vs. Ag|AgCl. A rise in catalytic currents was also observed at about - 0.6 V vs. Ag|AgCl for reduction of NO on electrodes modified with the cobalt(II) tetrakis(*N*-methyl-2-pyridyl)porphine complex.[176] For this porphine complex, the catalytic currents were observed at potentials associated with Co^{III}/Co^{II} couple. The observation of the catalytic currents for NO reduction in Fig. 4.6, at potentials associated with the reduction of the porphyrazine ring, suggests that ring-based reductions may be involved in catalysing the reduction. The catalytic activities of phthalocyanine complexes are generally achieved through the conventional regenerative catalytic mechanism.[177] Electrocatalytic reductions using cobalt(II) phthalocyanine are known to involve only the metal-based reductions.[22] This work suggests a possibility of the involvement of ring-based reductions in the catalytic processes, equations 4.1 to 4.3.

$$\mathbf{[(NO)Co^{II}Tmtppa(-2)]^{4+} + e^- \rightarrow [(NO)Co^{I}Tmtppa(-2)]^{3+}} \qquad \mathbf{(4.1)}$$

$$\mathbf{[(NO)Co^{I}Tmtppa(-2)]^{3+} + e^- \rightarrow [(NO)Co^{I}Tmtppa(-3)]^{2+}} \qquad \mathbf{(4.2)}$$

$$\mathbf{[(NO)Co^{I}Tmtppa(-3)]^{2+} + ne^- \rightarrow NH_3 + NH_2OH + \text{other products}} \qquad \mathbf{(4.3)}$$

The possible coordination of NO to the $[Co^{II}Tm\text{-}3,4\text{-}tppa(-2)]^{4+}$ species is based on the spectroscopic studies, as discussed in chapter 3. The absorption spectrum of $[Co^{II}Tmtppa(-2)]^{4+}$ showed a single Q band at 659 nm in pH 4 buffer, and after addition of nitrite a splitting of the Q band was observed, Fig 3.17. Coordination was confirmed by equilibrium studies. Equation 4.1 is based on the fact that reduction occurs at the metal first before ring reduction. It is expected that the catalyst is regenerated by equation 4.3. NH_3 and NH_2OH are some of the likely products for the

reduction of NO in acid media. The formation of these products in basic media are confirmed below, Section 4.2.2.2 by bulk electrolysis.

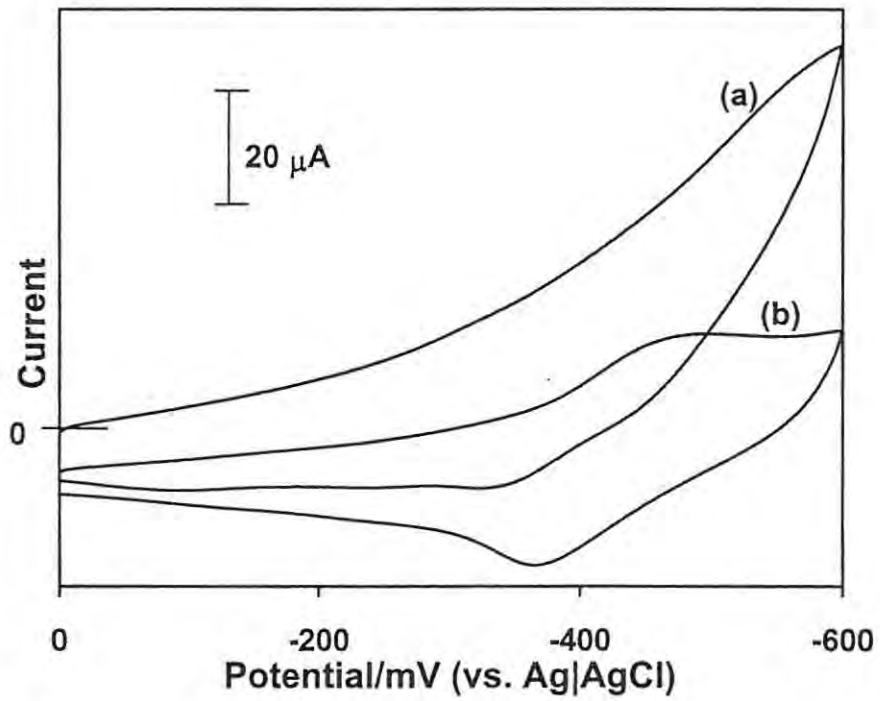

Fig. 4.6 Cyclic voltammograms for NO reduction, on an unmodified glassy carbon electrode and in pH 4 buffer for $[Co^{II}Tm\text{-}3,4\text{-}tppa(-2)]^{4+}$ (a) in the presence of NO_2^- (0.02 mol dm^{-3}) and (b) in the absence of nitrite. Scan rate = 100 mV s^{-1}.

4.2.2. Reduction and oxidation of nitrite under heterogeneous conditions

4.2.2.1. Electrocatalytic reduction of nitrite in neutral pH

Experiments were performed to study the catalytic behaviour of the porphyrazine complex, $[Co^{II}Tm\text{-}3,4\text{-}tppa]^{4+}$ employing low concentrations (< 10^{-9} mol dm^{-3}) of nitrite and near neutral conditions. The electrolyte used for these studies was water containing 0.01 mol dm^{-3} Na_2SO_4 (pH ~ 7, unbuffered) or pH 7 buffer solutions. Electrodes in this section were modified by electrodeposition as described above.

The catalytic behaviour of $[Co^{II}Tm\text{-}3,4\text{-}tppa]^{4+}$ towards nitrite reduction was compared with the behaviour of the adsorbed $[Co^{II}TSPc]^{4-}$ and of the adsorbed mixture $[Co^{II}Tmtppa]^{4+}.[Co^{II}TSPc]^{4-}$. Linear sweep voltammetry was employed for $[Co^{II}Tm\text{-}3,4\text{-}tppa]^{4+}$-GCE and $[Co^{II}Tm\text{-}3,4\text{-}tppa]^{4+}.[Co^{II}TSPc]^{4-}$-GCE. For $[Co^{II}TSPc]^{4-}$-GCE, the current response using linear sweep voltammetry was too weak, hence Osteryoung square wave voltammetry was employed. Catalytic currents were observed in the presence of nitrite in all cases.

The adsorbed $[Co^{II}Tm\text{-}3,4\text{-}tppa]^{4+}.[Co^{II}TSPc]^{4-}$ complex showed a peak at - 0.45 V in the absence of nitrite. On addition of nitrite, there was a considerable enhancement in the reduction currents with a shift of the peak to near - 0.6 V vs. Ag|AgCl, Fig. 4.7. These reduction currents increased with increase in nitrite concentration, Fig. 4.8.

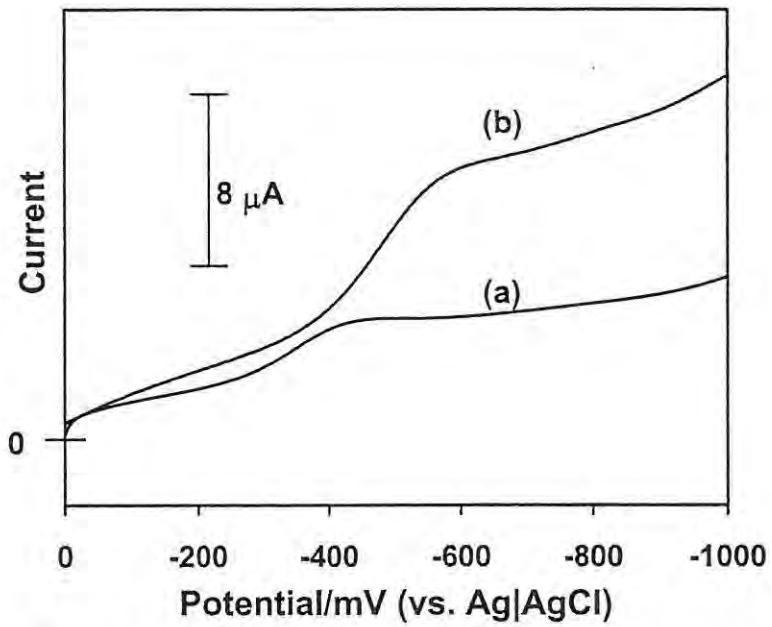

Fig. 4.7 OSW voltammogram (a) in the absence of nitrite and (b) in the presence of 2 x 10^{-10} mol dm^{-3} nitrite on $[Co^{II}Tm\text{-}3,4\text{-}tppa]^{4+}$. $[Co^{II}TSPc]^{4-}$-GCE in water containing 0.01 mol dm^{-3} Na_2SO_4. Scan rate = 100 mV s^{-1}.

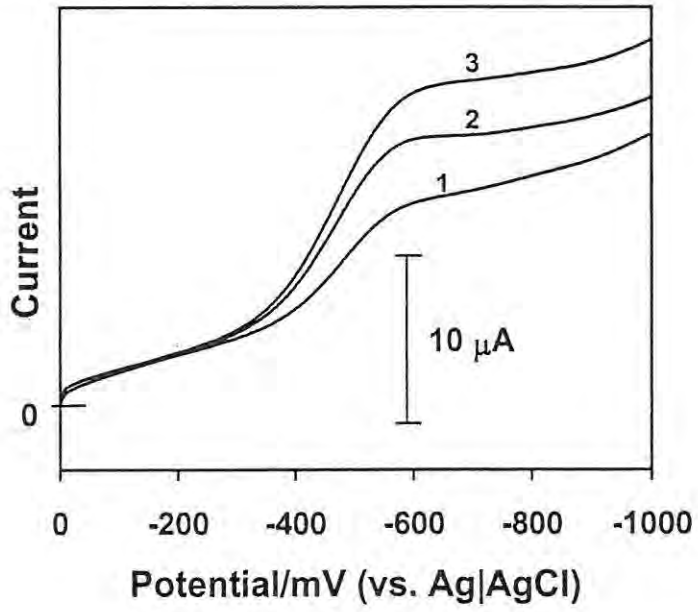

Fig. 4.8 OSW voltammogram of nitrite on $[Co^{II}Tm\text{-}3,4\text{-}tppa]^{4+}$.$[Co^{II}TSPc]^{4-}$-GCE in water containing 0.01 mol dm^{-3} Na_2SO_4. $[NO_2^-]$ = (1) 2 x 10^{-10} (2) 8 x 10^{-10} and (3) 4 x 10^{-9} mol dm^{-3}. Scan rate = 100 mV s^{-1}.

The voltammograms of adsorbed $[Co^{II}TSPc]^{4-}$ were featureless, but on addition of nitrite, catalytic currents were observed at - 0.37 V vs. Ag|AgCl, Fig. 4.9.

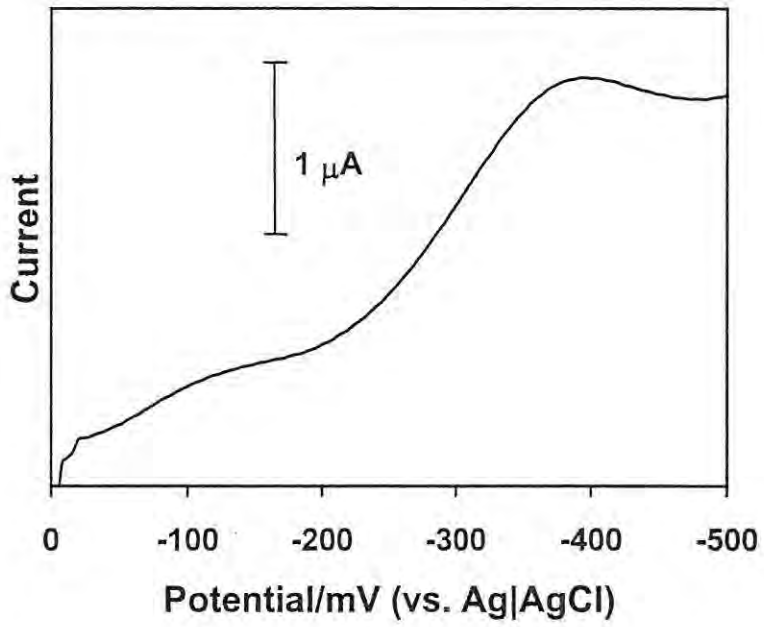

Fig. 4.9 OSW voltammogram of nitrite (2 x 10^{-10} mol dm^{-3}) on $[Co^{II}TSPc]^{4-}$-GCE in water containing 0.01 mol dm^{-3} Na_2SO_4. Scan rate = 100 mV s^{-1}.

On $[CoTm\text{-}3,4\text{-}tppa]^{4+}$-GCE, the catalytic currents for nitrite reduction were observed at - 0.50 V vs. Ag|AgCl.

The stability of the electrodes: $[Co^{II}Tm\text{-}3,4\text{-}tppa]^{4+}$-GCE, $[Co^{II}TSPc]^{4-}$-GCE and $[Co^{II}Tmtppa]^{4+}$.$[Co^{II}TSPc]^{4-}$-GCE towards the detection of nitrite was illustrated by a study of the variation of current response with the scan number, Fig. 4.10. All of the electrodes were reletively stable towards nitrite reduction under the present conditions since no further decrease in current with scan number was observed after 8 scans in each case. In addition, considering the similar concentrations of nitrite, higher currents were observed on $[Co^{II}Tm\text{-}3,4\text{-}tppa]^{4+}$-GCE than for the other electrodes, even after a hundred scans, showing that this electrode is comparatively more selective than the other two. However, loss of sensitivity is observed in all cases since the current signals are smaller when compared with first scans.

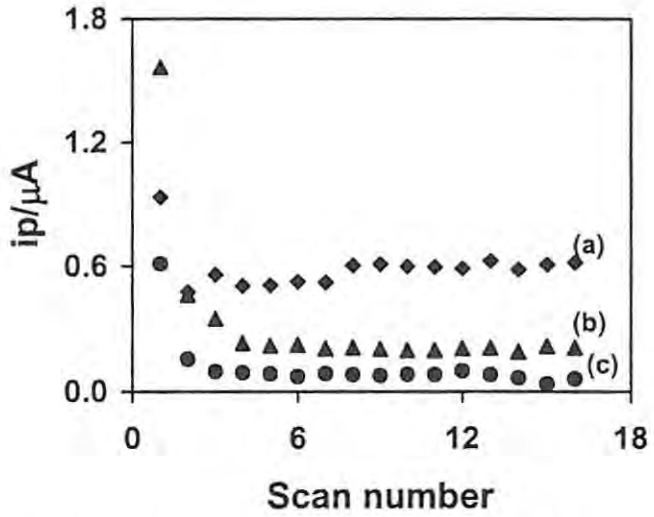

Fig. 4.10 The variation of peak currents with scan number for the voltammetric response of 1.0 x 10^{-10} mol dm^{-3} NO_2^- on (a) GCE-$[Co^{II}Tm\text{-}3,4\text{-}tppa]^{4+}$, (b) GCE-$[Co^{II}Tm\text{-}3,4\text{-}tppa]^{4+}.[Co^{II}TSPc]^{4-}$ and (c) GCE-$[Co^{II}TSPc]^{4-}$. Scan rate = 100 mV s^{-1}. Electrolyte = water containing 0.01 mol dm^{-3} Na_2SO_4.

Linear dependence of the catalytic currents on the concentration of nitrite (in the concentration range 1 x 10^{-10} to 7 x 10^{-9} mol dm^{-3}) was observed for electrodes modified with $[Co^{II}Tm\text{-}3,4\text{-}tppa]^{4+}$, $[Co^{II}TSPc]^{4-}$ and $[Co^{II}Tm\text{-}3,4\text{-}tppa]^{4+}.[Co^{II}TSPc]^{4-}$ dimer, Fig. 4.11. The highest currents were obtained with the mixture, followed by $Co^{II}Tm\text{-}3,4\text{-}tppa]^{4+}$ while $[Co^{II}TSPc]^{4-}$ gave the lowest current response. Using the slopes of the plots in Fig. 4.11 as a measure of the relative catalytic activities, the mixed complex showed the highest catalytic activity when compared to the catalytic activity of individual complexes towards the reduction of nitrite.

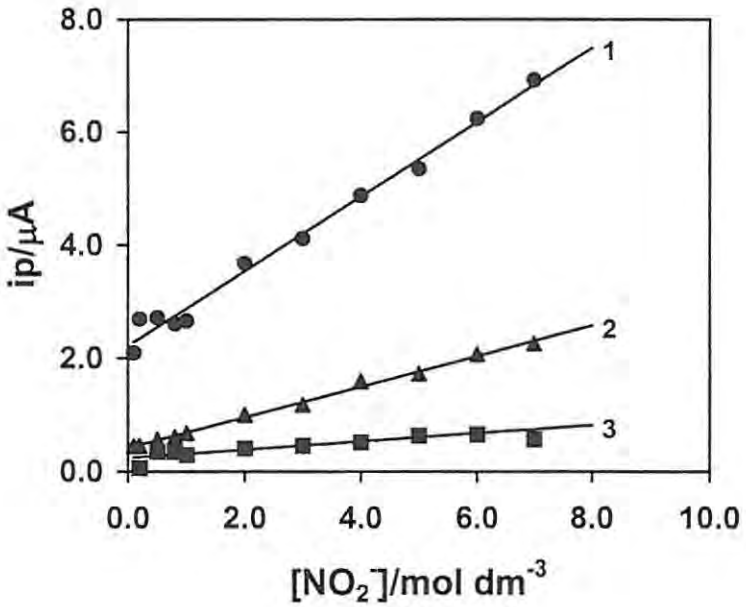

Fig. 4.11 Variation of cathodic currents (1st scans) with NO_2^- concentration for the reduction on (1) GCE-[Co^{II}Tm-3,4-tppa]$^{4+}$.[Co^{II}TSPc]$^{4-}$, (2) GCE-[Co^{II}Tm-3,4-tppa]$^{4+}$, (3) GCE-[Co^{II}TSPc]$^{4-}$. Electrolyte = water containing 0.01 mol dm^{-3} Na_2SO_4. Scan rate = 100 mV s^{-1}. Linear sweep voltammetry was used for (1) and (2), and Osteryoung square wave voltammetry was employed for (3).

4.2.2.2. Electrocatalytic reduction of nitrite in basic media

Nitrite, nitrate and hydroxide ions are the main components of low-level radioactive waste solutions. Electrochemical reduction of nitrite and nitrate in basic media is thus of environmental importance. In this work, carbon electrodes modified with Co^{II}Tppa, [Co^{II}Tm-2-3-tppa]$^{4+}$ and [Co^{II}Tm-3,4-tppa]$^{4+}$ were used for the heterogeneous catalytic reduction of nitrite.

Studies on the catalytic behaviour of these complexes towards the reduction of nitrite in basic media (0.5 mol dm^{-3} NaOH), were performed by adsorbing the complexes onto a glassy carbon electrode. Glassy carbon electrodes were modified with Co^{II}tppa (Cotppa-GCE), [Co^{II}Tm-2-3-tppa]$^{4+}$ ([CoTm-2-3-tppa]$^{4+}$-GCE) and [Co^{II}Tm-3,4-tppa]$^{4+}$ ([CoTm-3,4-tppa]$^{4+}$-GCE) by drop dry method as described in

the experimental (Section 2.3.1.2). Under these highly basic conditions, the catalytic currents observed are due to the reduction of nitrite since the concentration of NO formed by disproprtionation of nitrite is insignificant and can be ignored. Catalytic reduction currents were observed on Cotppa-GCE, $[CoTm\text{-}2\text{-}3\text{-}tppa]^{4+}$-GCE and $[CoTm\text{-}3,4\text{-}tppa]^{4+}$-GCE, in the presence of nitrite, showing that $Co^{II}tppa$, $[Co^{II}Tm\text{-}2\text{-}3\text{-}tppa]^{4+}$ and $[Co^{II}Tm\text{-}3,4\text{-}tppa]^{4+}$ catalyse the reduction of nitrite. Also, $[Tmtppa]^{4+}$ is unstable in basic media when in solution, but seem to be stable in basic media when adsorbed, hence catalytic activity is observed for the adsorbed species.

For $[CoTm\text{-}3,4\text{-}tppa]^{4+}$, two reduction peaks of the adsorbed species were observed at - 1.09 V and - 1.33 V vs. Ag|AgCl, Fig. 4.12(a) in electrolyte alone. In the presence of nitrite, a catalytic peak was observed at - 1.40 V vs. Ag|AgCl, Fig. 4.12(b). The currents for the reduction of nitrite increased with increase in nitrite concentration as shown in Fig. 4.13.

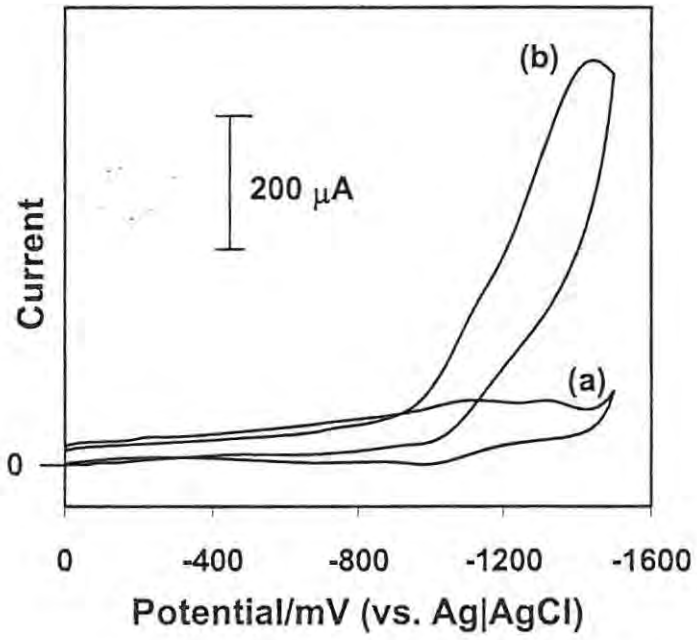

Fig. 4.12 Cyclic voltammograms for $[Co^{II}Tm\text{-}3,4\text{-}tppa]^{4+}$-GCE in the absence (a) and presence (b) of 0.14 mol dm^{-3} nitrite. Electrolyte = 0.5 mol dm^{-3} NaOH. Scan rate = 100 mV s^{-1}.

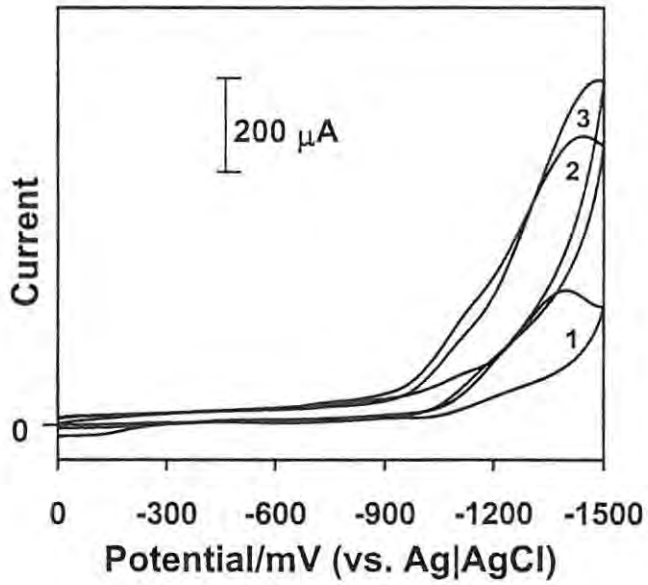

Fig. 4.13 Cyclic voltammograms for $[Co^{II}Tm\text{-}3,4\text{-}tppa]^{4+}$-GCE in the presence of increasing concentrations of nitrite: (1) 0.02, (2) 0.14 and (3) 0.20 mol dm^{-3}. Electrolyte = 0.5 mol dm^{-3} NaOH. Scan rate = 100 mV s^{-1}.

For $[Co^{II}Tm\text{-}2\text{-}3\text{-}tppa]^{4+}$, a reduction peak for the adsorbed species was observed at - 1.40 V vs. Ag|AgCl, Fig. 4.14(a), in the absence of nitrite. The reduction peak for $[Co^{II}Tm\text{-}2\text{-}3\text{-}tppa]^{4+}$ was observed at potentials more negative than observed for this complex in solution, although solution catalysis was performed in pH 4 buffer, Section 4.2.1. Because of the interaction between the adsorbed phthalocyanine complexes and the electrode surface, redox potentials differing from those in homogeneous solution are generally observed for the adsorbed species.[178] For $[Co^{II}Tm\text{-}2\text{-}3\text{-}tppa]^{4+}$ nitrite reduction peak was observed at - 1.44 V vs. Ag|AgCl, Fig. 4.14(b). The currents for the reduction of nitrite increased with increase in nitrite concentration, Fig. 4.15.

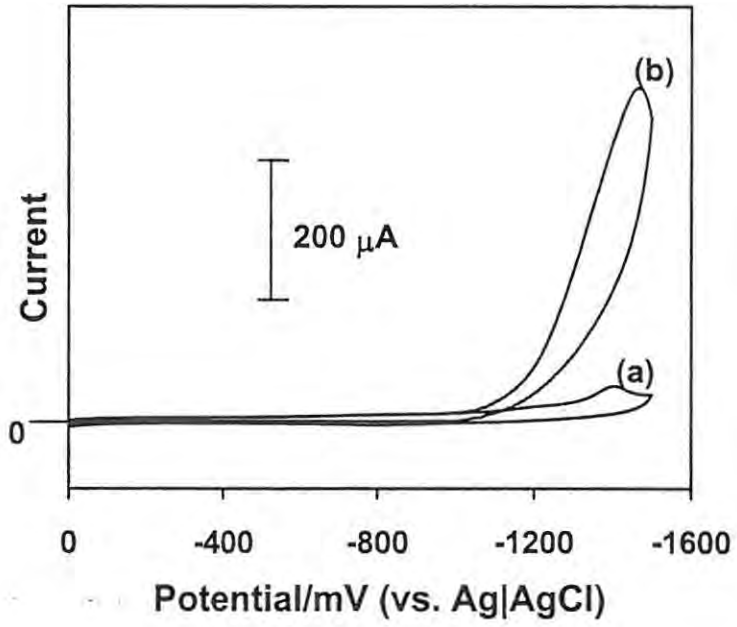

Fig. 4.14 Cyclic voltammograms for $[Co^{II}Tm\text{-}2,3\text{-}tppa]^{4+}$-GCE in the absence (a) and presence (b) of 0.14 mol dm^{-3} nitrite. Electrolyte = 0.5 mol dm^{-3} NaOH. Scan rate = 100 mV s^{-1}.

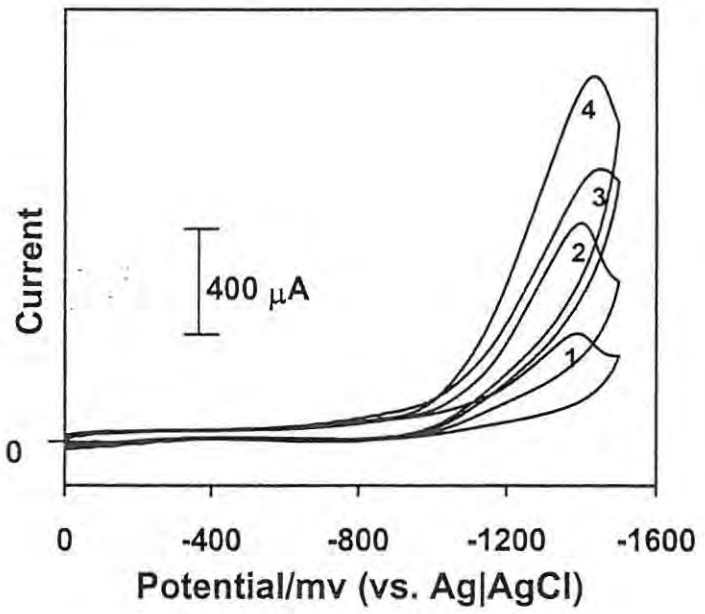

Fig. 4.15 Cyclic voltammograms for $[Co^{II}Tm\text{-}2,3\text{-}tppa]^{4+}$-GCE in the presence of increasing concentrations of nitrite: (1) 0.04, (2) 0.20 (3) 0.32 and (4) 0.44 mol dm^{-3}. Electrolyte = 0.5 mol dm^{-3} NaOH. Scan rate = 100 mV s^{-1}.

For Co^{II}2,3-tppa, the adsorbed species showed a weak reduction peak near -1.4 V vs. Ag|AgCl, Fig. 4.16(a), in the absence of nitrite. For the GCE modified with Co-2,3-tppa, a broad peak was observed near -1.4 V for nitrite reduction, Fig. 4.16(b).

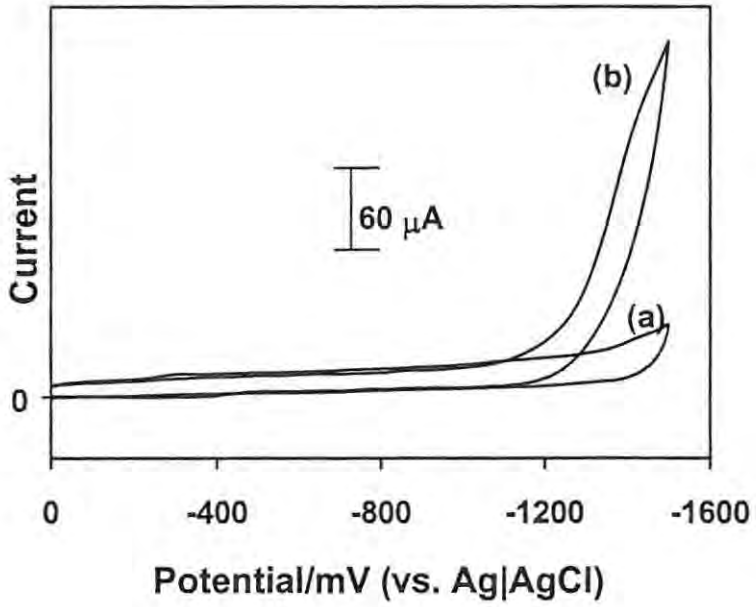

Fig. 4.16 Cyclic voltammograms for Co-2,3-tppa-GCE in the absence (a) and presence (b) of 0.14 mol dm^{-3} nitrite. Electrolyte = 0.5 mol dm^{-3} NaOH. Scan rate = 100 mV s^{-1}.

Ealier studies reported[179] that the cyclic voltammogram of adsorbed Co^{II}Pc show a pair of reduction peaks near - 0.15 V, which has been assigned to Co^{III}/Co^{II} and Co^{II}/Co^{I} species, in the absence of nitrite.[179] It has been shown before[97] that catalytic currents were observed for reduction of NO_2^- on Co^{II}Pc-GCE, but with no defined peak.

The presence of pyridinium rings (in porphyrazine complexes) instead of benzene rings (in Co^{II}Pc) results in the lowering of the potential for the reduction of nitrite. Hence, a peak for the reduction of nitrite was observed for $[Co^{II}Tm\text{-}2,3\text{-}tppa]^{4+}$ and $[Co^{II}Tm\text{-}3,4\text{-}tppa]^{4+}$ and not observed for Co^{II}Pc.

The currents for the reduction of nitrite increased linearly with increase in NO_2^- concentration, Fig. 4.17. For CoPc-GCE, the currents used in Fig. 4.17 correspond to the currents observed at average potential for the reduction of nitrite on Cotppa-GCE, $[CoTm\text{-}2\text{-}3\text{-}tppa]^{4+}$-GCE and $[CoTm\text{-}3,4\text{-}tppa]^{4+}$-GCE, since no nitrite peaks were observed on CoPc-GCE. The slopes of the plots in Fig. 4.17 give a reasonable measure of the relative catalytic activities of $Co^{II}Pc$, $Co^{II}2,3\text{-}tppa$, $[Co^{II}Tm\text{-}2\text{-}3\text{-}tppa]^{4+}$ and $[Co^{II}Tm\text{-}3,4\text{-}tppa]^{4+}$. It is clear from Fig. 4.17 that the highest catalytic activity was observed for $[Co^{II}Tm\text{-}2\text{-}3\text{-}tppa]^{4+}$ and that CoPc showed the lowest catalytic activity. The currents for the reduction of nitrite on unmodified GCE were lower than observed on CoPc-GCE as has been observed before.[97] Some earlier reports [97] showed that a peak for nitrite reduction was observed on GCE modified with CuPc (CuPc-GCE), but no peak was observed on CoPc-GCE. Peak potentials for the reduction of nitrite on Cotppa-GCE, $[CoTm\text{-}2\text{-}3\text{-}tppa]^{4+}$-GCE and $[CoTm\text{-}3,4\text{-}tppa]^{4+}$-GCE were compared with the potential reported earlier for reduction of nitrite on CuPc-GCE.[97] The main reduction peak for nitrite on CuPc-GCE was observed at -1.7 V vs. Ag|AgCl during the first scan, whereas when $Co^{II}tppa$, $[Co^{II}Tm\text{-}2\text{-}3\text{-}tppa]^{4+}$ and $[Co^{II}Tm\text{-}3,4\text{-}tppa]^{4+}$ are employed as catalysts, the peak potential for nitrite reduction is observed at ~ -1.4, -1.44 and -1.40 V, respectively. Thus, the Co porphyrazine complexes lower the potential for NO_2^- reduction to a larger extent than CuPc. It is however important to note, that CuPc-GCE exhibited autocatalytic behaviour towards reduction of nitrite in that the peak currents increased with repetitive scanning.[97]

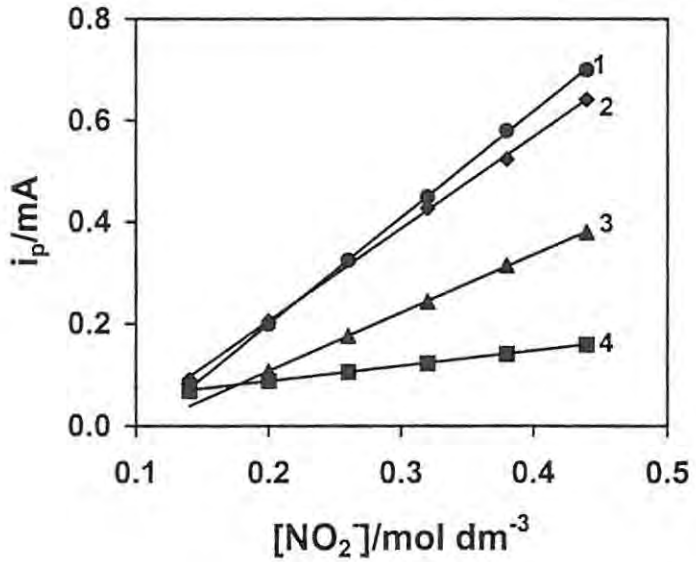

Fig. 4.17 Plot of nitrite concentration vs. reduction catalytic currents on various porphyrazine and MPc complexes: (1) [CoTm-2,3-tppa]$^{4+}$-GCE, (2) [CoTm-3,4-tppa]$^{4+}$-GCE, (3) [Co-2,3-tppa]$^{4+}$-GCE and (4) CoPc-GCE. Electrolyte = 0.5 mol dm^{-3} NaOH.

Analysis of the reduction products

Controlled potential electrolysis of NO_2^- at - 1.6 V vs. Ag|AgCl on carbon rod electrodes (represented as CE) modified with Co^{II}tppa, [Co^{II}Tm-2-3-tppa]$^{4+}$ and [Co^{II}Tm-3,4-tppa]$^{4+}$ (Cotppa-CE, [CoTm-2-3-tppa]$^{4+}$-CE or [CoTm-3,4-tppa]$^{4+}$-CE, respectively), produced ammonia and hydroxylamine as some of the products. Hydroxylamine has been reported before as one of the products of the reduction of nitrite.[176] The results of the constant potential electrolysis of nitrite on Cotppa-CE, [CoTm-2-3-tppa]$^{4+}$-CE and [CoTm-3,4-tppa]$^{4+}$-CE are listed in Table 4.1 and compared with results of reduction of nitrite on CoPc modified carbon electrodes. Ammonia was the prominent product of the reduction. Coulometric studies showed that an overall 6-electron transfer was involved during the catalytic reduction of nitrite. Ammonia production is highly dependent on the pH of the solution,[176,179] with higher ammonia yields being produced at low pH. The relatively low yields of

ammonia production observed in Table 4.1 are a result of the high pH employed for the electrolysis. The amount of hydroxylamine produced was less than the amount of ammonia formed under the same conditions and on the same electrode, Table 4.1. More ammonia was formed on electrodes modified with $[Co^{II}Tm\text{-}2\text{-}3\text{-}tppa]^{4+}$, and $[Co^{II}Tm\text{-}3,4\text{-}tppa]^{4+}$, than for $Co^{II}tppa$ or $Co^{II}Pc$, showing that the presence of electron withdrawing methyl groups in $[Co^{II}Tm\text{-}2\text{-}3\text{-}tppa]^{4+}$ and $[Co^{II}Tm\text{-}3,4\text{-}tppa]^{4+}$ enhances the catalytic activity of these complexes. As Table 4.1 shows, relatively high current efficiencies for ammonia production were obtained for the reduction of NO_2^- on carbon electrodes modified with $[Co^{II}Tm\text{-}2\text{-}3\text{-}tppa]^{4+}$, than with $Co^{II}Tppa$ or $[Co^{II}Tm\text{-}3,4\text{-}tppa]^{4+}$, or with $Co^{II}Pc$, showing that the position of the methylpyridinium group plays an important part in the catalytic activities of the complexes.

Table 4.1 Results of controlled potential electrolysis (after 17 minutes) of 10 ml NO_2^- (2.8 mM) on carbon electrodes (CE) modified with $Co^{II}2,3\text{-}tppa$, $[Co^{II}Tm\text{-}2\text{-}3\text{-}tppa]^{4+}$, $[Co^{II}Tm\text{-}3,4\text{-}tppa]^{4+}$ and $Co^{II}Pc$. (Applied potential, E_{app} = - 1.6 V vs. Ag|AgCl; electrolyte = 0.5 mol dm^{-3} NaOH).

Electrode	**η/%[a] NH_3**	**$[NH_3]$/mM**	**$[NH_2OH]$/mM**
CE-CoPc	63	0.11	0.013
CE-Cotppa	70	0.12	0.011
CE-$[CoTm\text{-}2,3\text{-}tppa]^{4+}$	97	0.21	0.012
CE-$[CoTm\text{-}3,4\text{-}tppa]^{4+}$	72	0.21	0.013

[a] η = current efficiency: charge used to generate product over total charge.

The nature of the macrocycle is known to affect the catalytic activity of the phthalocyanine and porphyrin complexes towards the reduction of nitrite.[100] It has also been shown that the close proximity of the *N*-methylpyridinium group to the

porphyrin ring in metal(II) tetrakis(*N*-methyl-2-pyridyl)porphine complex has strong effects on the properties of the metalloporphyrin complexes.[180] It is thus expected that the position of the methylpyridinium groups in $[Co^{II}Tm\text{-}2\text{-}3\text{-}tppa]^{4+}$ and $[Co^{II}Tm\text{-}3,4\text{-}tppa]^{4+}$ will affect the catalytic behaviour of these complexes. $[Co^{II}Tm\text{-}2\text{-}3\text{-}tppa]^{4+}$ shows a larger current efficiency for NH_3 production from nitrite than $Co^{II}2,3\text{-}tppa$ or $[Co^{II}Tm\text{-}3,4\text{-}tppa]^{4+}$. Higher yields of ammonia production are also observed for $[Co^{II}Tm\text{-}2\text{-}3\text{-}tppa]^{4+}$ and $[Co^{II}Tm\text{-}3,4\text{-}tppa]^{4+}$, which have methyl groups, than for $Co^{II}Pc$ and $Co^{II}2,3\text{-}tppa$.

4.2.2.3. Electrocatalytic oxidation of nitrite in neutral media

Nitrites find use mostly as preservatives and colour-enhancing agents in the food industry. The maximum allowable level of nitrite in potable water is 4.0×10^{-6} mol dm^{-3}.[49] Some of the meat products often treated with sodium nitrite are frankfurters, bologna, spiced ham and vienna sausage.[84,85] Regulations allow as much as 200 ppm of nitrite in meat.[85]

Nitrite is readily oxidised, most likely to NO_3^- and NO_2 on electrodes such as carbon, platinum and gold.[94,181] Nitrate is the most common interfering ion in the analysis of nitrite, but has been found not to interfere with nitrite determination when electrochemical oxidation, rather than reduction, of nitrite is employed for its analysis.[94,181] Oxidation of nitrite is thus used in this work for its analysis. Even though the oxidation peak of nitrite is well defined, the use of electrocatalysts in modifying electrodes for detection of nitrite is essential for the analysis of low concentrations. Such modified electrodes may also show improved stability towards analysis of nitrite. pH 7 buffer was employed for the oxidation of nitrite. At this pH value, disproportion of nitrite to nitric oxide is negligible.

The use of a glassy carbon electrode modified with $[Co^{II}TSPc]^{4-}$ for nitrite analysis, based on its catalytic oxidation is reported. Despide the poor performance of $[Co^{II}TSPc]^{4-}$ when used as a catalyst in reduction reactions discussed above, $[Co^{II}TSPc]^{4-}$ is a good catalyst when its oxidation is employed. Osteryoung square wave (OSW) voltammetry was employed for electrocatalytic oxidation.

Electrodeposition of $[Co^{II}TSPc]^{4-}$ was performed in DMF,[122] as described in Section 4.1.2. As already described, the first oxidation in $[Co^{II}TSPc]^{4-}$ occurs at the central metal with the formation of the $[Co^{III}TSPc]^{3-}$ species. It is the later species which oxidise the species to be catalysed such as NO_2^-. On unmodified GCE, no peak for nitrite oxidation was observed, for 1 x 10^{-6} mol dm^{-3} nitrite solution. Large background currents were observed on unmodified GCE in the presence of nitrite. Fig. 4.18(a) shows the cyclic voltammogram of $[Co^{II}TSPc]^{4-}$ adsorbed onto GCE, in the blank (pH 7 buffer) solution. A broad anodic peak corresponding to the $[Co^{III}TSPc]^{3-}/[Co^{II}TSPc]^{4-}$ couple was observed near 1 V vs. Ag|AgCl, as has been reported before.[123] On addition of nitrite (1 x 10^{-6} mol dm^{-3}) an enhancement of currents of oxidation peak at 0.93 V vs. Ag|AgCl was observed, Fig. 4.18(b). The enhancement in the oxidation currents indicate catalytic activity of the GCE when modified with $[Co^{II}TSPc]^{4-}$. Further studies may be to detect nitrite in real environmental samples such as some meat products, water and many more.

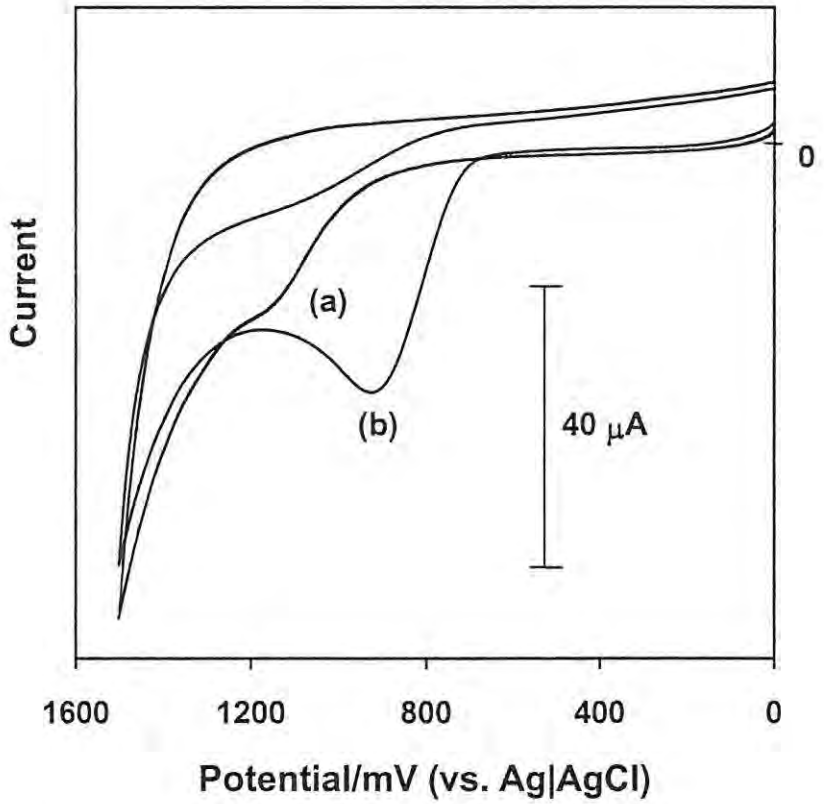

Fig. 4.18 Voltammogram of $[Co^{II}TSPc]^{4-}$ modified GCE in the absence (a) and presence (b) of 1 x 10^{-6} mol dm^{-3} NO_2^- on $[Co^{II}TSPc]^{4-}$-GCE in pH 7 buffer. Scan rate = 100 mV s^{-1}.

Electrocatalytic oxidation reactions involving CoPc complexes have been described as a two-step process involving the oxidation of $Co^{II}Pc$ to $Co^{III}Pc$,[44] followed by electron transfer from the species to be catalysed to $Co^{III}Pc$ species. Thus, the proposed mechanism for electrocatalytic oxidation of nitrite on GCE modified with $[Co^{II}TSPc]^{4-}$ is shown by equations 4.4 and 4.5.

$$[Co^{II}TSPc]^{4-} \rightarrow [Co^{III}TSPc]^{3-} + e^- \qquad (4.4)$$

$$[Co^{III}TSPc]^{3-} + NO_2^- \rightarrow [Co^{II}TSPc]^{4-} + \text{Oxidation products (e.g. } NO_3^- + NO_2) \qquad (4.5)$$

The enhancement in the anodic currents for the oxidation of nitrite in the presence of $[Co^{II}TSPc]^{4-}$ is a consequence of electron transfer reactions through

equations 4.4 and 4.5. The enhancement in currents show that electrode kinetics is improved when $[Co^{II}TSPc]^{4-}$ is used as a catalyst adsorbed on a GCE.

The catalytic currents for the oxidation of nitrite on GCE modified with $[Co^{II}TSPc]^{4-}$ increased linearly with nitrite concentrations as shown in Fig. 4.19. A correlation coefficient of 0.993 was obtained. Modification of the electrode improved the detection limit of nitrite by an order of magnitude to 2×10^{-7} mol dm^{-3}. Addition of nitrate had no significant effect on Fig. 4.19, showing that nitrate does not interfere with the determination of nitrite on GCE modified with $[Co^{II}TSPc]^{4-}$ employing oxidation. Plots of the square root of scan rate vs. peak current were linear indicating a diffusion-controlled process. Fig. 4.20 shows that the electrodes modified with $[Co^{II}TSPc]^{4-}$ had more sensitivity for NO_2^- oxidation than the unmodified GCE, in that repetitive scanning of the solution containing NO_2^- did not result in a fast loss in current response observed on unmodified GCE. Higher peak currents were observed on $[Co^{II}TSPc]^{4-}$ modified GCE for all scan numbers. The currents were 5 μA after 10 scans on $[Co^{II}TSPc]^{4-}$ modified GCE when compared to < 0.8 μA for the same concentration of NO_2^- (1×10^{-6} mol dm^{-3}) on unmodified GCE. For catalytic studies a newly coated GCE surface was employed as a way of obtaining reproducible results. It will be important to do studies on nitrite detection on environmental samples (e.g. meat products and water) in the future.

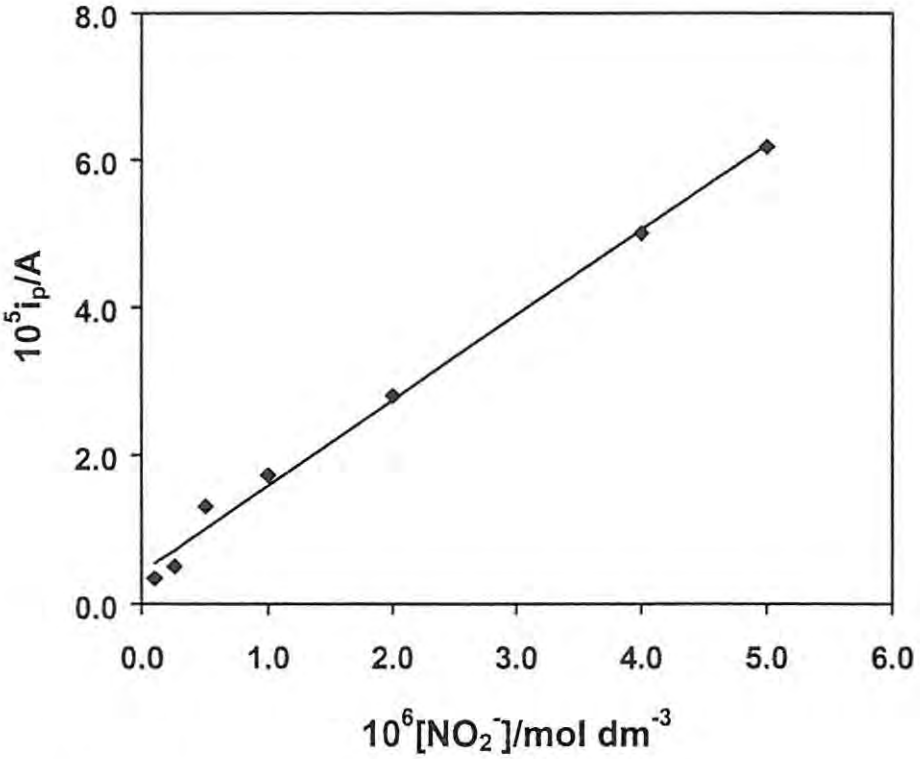

Fig. 4.19 Variation of peak currents with NO_2^- concentration for NO_2^- oxidation on $[CoTSPc]^{4-}$-GCE. Electrolyte = pH 7 buffer. Scan rate = 100 mV s^{-1}.

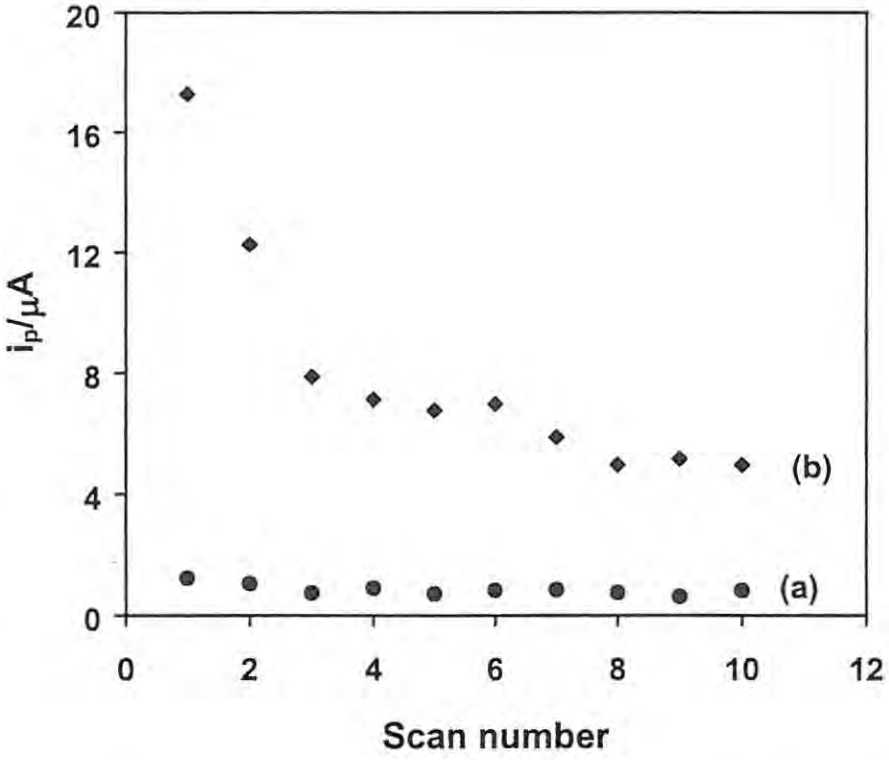

Fig. 4.20 Variation of oxidation peak currents with scan number on (a) unmodified GCE and (b) $[Co^{II}TSPc]^{4-}$-GCE. $[NO_2^-] = 4 \times 10^{-5}$ mol dm^{-3}. Electrolyte = pH 7 buffer. Scan rate = 100 mV s^{-1}.

In summary, it has been shown in this work that the nature of the ring plays an important role in the catalytic reduction of nitrite. Nitrite concentrations as low as 1 x 10^{-10} mol dm^{-3} could be determined in water containing Na_2SO_4, using electrodes modified with $[Co^{II}Tm\text{-}3,4\text{-}tppa]^{4+}.[Co^{II}TSPc]^{4-}$, $[Co^{II}Tm\text{-}3,4\text{-}tppa]^{4+}$ and $[Co^{II}TSPc]^{4-}$. However, the anionic complex, $[Co^{II}TSPc]^{4-}$, showed lower catalytic activity than both the cationic species, $[Co^{II}Tm\text{-}3,4\text{-}tppa]^{4+}$ and the mixture of the cationic and anionic species.

It has also been shown in this work that the use of $[Co^{II}TSPc]^{4-}$ to modify the GCE results in the enhancement of the oxidation currents for NO_2^-. Addition of NO_3^-, a common interferent for NO_2^- determination had no effect on the cyclic

voltammogram of nitrite when oxidation is employed. $[Co^{II}TSPc]^{4-}$ improved the sensitivity of the GCE towards the detection of nitrite when compared to unmodified GCE. The detection limit of 2×10^{-7} mol dm^{-3} was obtained for nitrite analysis on GCE modified with $[Co^{II}TSPc]^{4-}$.

4.3. Electrocatalytic studies of sulphur dioxide and sulphite

SO_2 is a major atmospheric pollutant in industrial areas. SO_2 is a component of acid rain, which has a serious impact on buildings and vegetation. Monitoring of SO_2 is of importance in relation to environmental pollution, occupational health and control of industrial emission.

Dependent on the pH of the solution, sulphur dioxide transforms into bisulphite and/or sulphite according to equations 4.6 and 4.7.[182]

$$SO_2.xH_2O \underset{k_{-1}}{\overset{k_1}{\rightleftharpoons}} HSO_3^- + H^+ + (x-1)H_2O \qquad (4.6)$$

$$HSO_3^- \underset{k_{-2}}{\overset{k_2}{\rightleftharpoons}} SO_3^{2-} + H^+ \qquad (4.7)$$

with k_1, k_2, k_{-1} and k_{-2}, the rate constants and $K_1 = 1.54 \times 10^{-2}$ mol dm^{-3} and $K_2 = 1.02 \times 10^{-7}$ mol dm^{-3}, the equilibrium constants.[183]

Despite many electrochemical methods that describe the detection of sulphur dioxide, there remains a problem of instability of this compound in the presence of other sulphur containing compounds which are present in SO_2 solutions.[184,185] At some electrode materials the kinetics of sulphur dioxide oxidation and/or reduction are slow.[186,187,188] This fact limits the amount of suitable electrode materials.

The use of a glassy carbon electrode modified with (a) $[Fe^{II}TSPc]^{4-}$ for the determination of sulphur dioxide in acidic to basic media, based on its catalytic

oxidation and reduction and (b) $[Co^{II}TSPc]^{4-}$ for the determination of sulphur dioxide in basic media, based on its catalytic oxidation is reported in this section.

4.3.1. $[Fe^{II}TSPc]^{4-}$ as a catalyst

In this work the detection of sulphur dioxide is studied as a function of pH at a glassy carbon electrode modified using iron(II) tetrasulfophthalocyanine as a catalyst. The electrode was modified by electrodeposition.

4.3.1.1. Studies in 1.0 mol dm^{-3} H_2SO_4

Fig. 4.21 shows current-potential curves recorded at a glassy carbon electrode modified with $[Fe^{II}TSPc]^{4-}$, with increasing concentrations of sulphur dioxide in a 1.0 mol dm^{-3} H_2SO_4 solution. Similar curves were obtained for sodium sulphite, which means that in strongly acidic solutions, sulphite is almost completely transformed to $SO_2.xH_2O$ (Table 4.2). This also means that k_{-1} and k_{-2} in equations 4.6 and 4.7 are high. Indeed, the typical smell of SO_2 was detected by dissolving sodium sulphite in 1.0 mol dm^{-3} H_2SO_4. However, if a bare glassy carbon electrode is used, ill-defined and poorly visible waves were obtained, hence the need for electrode modification. This is a first indication that $[Fe^{II}TSPc]^{4-}$ electrocatalyses the observed reactions.

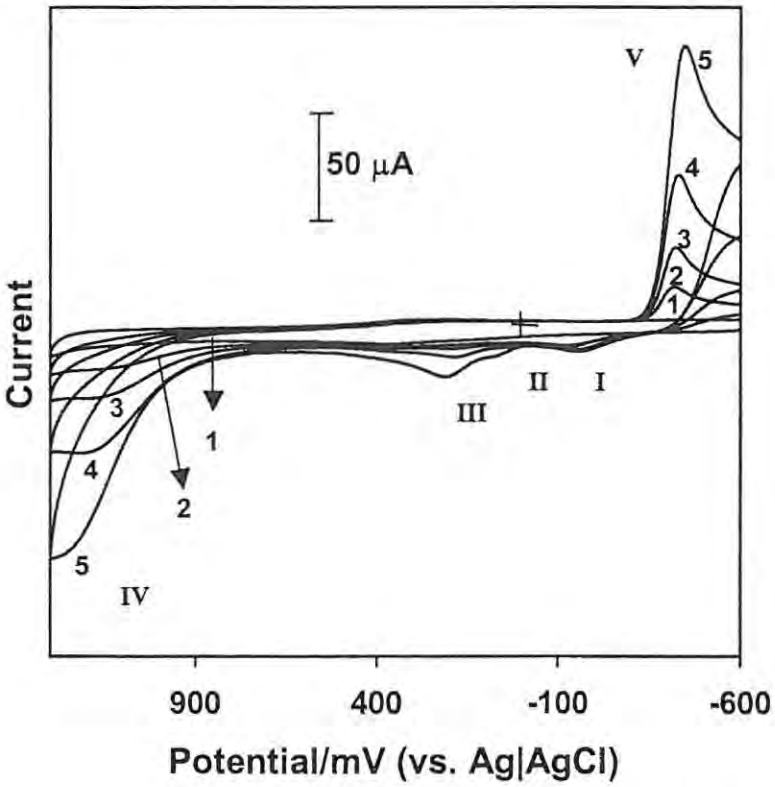

Fig. 4.21 Current-potential curves recorded in 1.0 mol dm^{-3} H_2SO_4 solution for increasing SO_2 concentrations at a glassy carbon electrode modified with $[Fe^{II}TSPc]^{4-}$. SO_2 concentrations are (1) 0, (2) 3.37 x 10^{-4}, (3) 6.42 x 10^{-4}, (4) 1.21 x 10^{-3} and (5) 2.20 x 10^{-3} mol dm^{-3}. Scan rate = 100 mV s^{-1}.

Two main waves IV and V can be observed, attributed respectively to oxidation (equation 4.8) and reduction of sulphur dioxide. The latter reaction will be discussed further below.

$$SO_2 + 2H_2O \rightleftharpoons SO_4^{2-} + 4H^+ + 2e^- \qquad (4.8)$$

Besides these main waves, three other waves are observed. Wave I and II are attributed to oxidation of reaction products formed in wave V. This was proved by cycling the potential between - 0.3 and 0.6 V vs. Ag|AgCl, where waves II and I were absent, and by addition of sodium dithionite to the solution (in the same potential range), waves I and II again appeared. This indicates that the reaction product formed in wave V is dithionite. Waves II and I were also observed at a bare glassy carbon electrode after addition of sodium dithionite. Therefore it is not clear if these reactions

are electrocatalysed by $[Fe^{II}TSPc]^{4-}$. However, when cycling between – 0.3 and 0.6 V vs. Ag|AgCl wave III still occurred under these conditions, indicating that this wave is attributed to a species in solution.

Table 4.2 Actual fraction* of SO_2, HSO_3^- and SO_3^{2-} in solution as a function of pH

K_1	K_2	C_H^+ (mol dm^{-3})	pH	Fraction SO_2	Fraction HSO_3^-	Fraction SO_3^{2-}
$1.54x10^{-2}$	$1.02x10^{-7}$	1	0	$9.85x10^{-1}$	$1.52x10^{-2}$	$1.55x10^{-9}$
$1.54x10^{-2}$	$1.02x10^{-7}$	10^{-1}	1	$8.67x10^{-1}$	$1.33x10^{-1}$	$1.36x10^{-7}$
$1.54x10^{-2}$	$1.02x10^{-7}$	10^{-2}	2	$3.94x10^{-1}$	$6.06x10^{-1}$	$6.18x10^{-6}$
$1.54x10^{-2}$	$1.02x10^{-7}$	10^{-3}	3	$6.10x10^{-2}$	$9.39x10^{-1}$	$9.58x10^{-5}$
$1.54x10^{-2}$	$1.02x10^{-7}$	10^{-4}	4	$6.45x10^{-3}$	$9.93x10^{-1}$	$1.01x10^{-3}$
$1.54x10^{-2}$	$1.02x10^{-7}$	10^{-5}	5	$6.42x10^{-4}$	$9.89x10^{-1}$	$1.01x10^{-2}$
$1.54x10^{-2}$	$1.02x10^{-7}$	10^{-6}	6	$5.89x10^{-5}$	$9.07x10^{-1}$	$9.26x10^{-2}$
$1.54x10^{-2}$	$1.02x10^{-7}$	10^{-7}	7	$3.21x10^{-6}$	$4.95x10^{-1}$	$5.05x10^{-1}$
$1.54x10^{-2}$	$1.02x10^{-7}$	10^{-8}	8	$5.80x10^{-8}$	$8.93x10^{-2}$	$9.11x10^{-1}$
$1.54x10^{-2}$	$1.02x10^{-7}$	10^{-9}	9	$6.30x10^{-10}$	$9.71x10^{-3}$	$9.90x10^{-1}$
$1.54x10^{-2}$	$1.02x10^{-7}$	10^{-10}	10	$6.36x10^{-12}$	$9.79x10^{-4}$	$9.99x10^{-1}$

* These values were determined using known $[SO_2]$ and equations 4.6 and 4.7.

Both, waves IV and V in Fig. 4.21, correspond to diffusion-controlled reactions, because a linear relationship is obtained between the peak current and the square root of the scan rate. Also, waves IV and V do not overlap with water oxidation and reduction of dissolved oxygen, respectively, since two peaks were not observed in either case, even at the lowest concentrations of SO_2. However, the slope of the relationship between the peak current and $SO_2.xH_2O$ concentration is slightly higher for the reduction than for the oxidation (Fig. 4.22, curves 1 and 2, respectively). A different number of electrons exchanged in both reactions cannot explain the small peak current differences of these waves. As described above, wave III corresponding to curve 3 in Fig. 4.22 was attributed to a species present in solution. Moreover, it can be seen that the sum of the peak currents of waves III

(curve 3) and IV (curve 2) is equal to the peak current of wave V (curve 1 in Fig. 4.22). Therefore, it is supposed that wave III corresponds to the oxidation of bisulphite (equation 4.9), which is present at about 1.5 % of the analytical sulphur dioxide concentration (Table 4.2). This wave is observed at similar potentials as those for the oxidation of the Fe-metal ion in $[Fe^{II}TSPc]^{4-}$. Therefore, it is supposed that the bisulphite oxidation is electrocatalysed by the central metal ion of $[Fe^{II}TSPc]^{4-}$. Wave III was not observed on bare GCE.

$$HSO_3^- + H_2O \rightleftharpoons SO_4^{2-} + 3H^+ + 2e^- \qquad (4.9)$$

However, an additional condition, that k_1 in equation 4.6 is relatively small, needs to be fulfilled. This is indeed the case and is confirmed by two additional experiments. In the first experiment the pH was varied from 0 to 2 in 5 steps. The peak height of wave III in Fig. 4.21 increased while that of wave IV decreased with increasing pH value, due to formation of HSO_3^- with increasing pH. In a second experiment a preconditioning of the electrode at a potential of + 0.6 V vs. Ag|AgCl was applied prior to cycling from + 0.6 V to + 1.3 V vs. Ag|AgCl. With increasing preconditioning time, the peak height of wave IV decreased, indicating that during the preconditioning $SO_2.xH_2O$ is transformed (however slowly) to HSO_3^-, which is in turn oxidised at the preconditioning potential. Despite the fact that k_1 in equation 4.6 is relatively small, the reaction of $SO_2.xH_2O$ to HSO_3^- still occurs. Indeed, a much higher ratio of $i_{p,III}/i_{p,IV}$ is obtained than was found for the actual concentration ratio of $[HSO_3^-]/[SO_2.xH_2O]$ in solution (Table 4.2). This shows that during the oxidation of HSO_3^-, fresh HSO_3^- is produced by reaction 4.6. This result also suggests that the peak current of waves III and IV in Fig. 4.21 cannot be attributed to the actual concentrations of bisulphite and sulphur dioxide in solution. However, the sum of

these peak currents is proportional to the analytical concentration of sulphur dioxide and can therefore be used for analytical purposes.

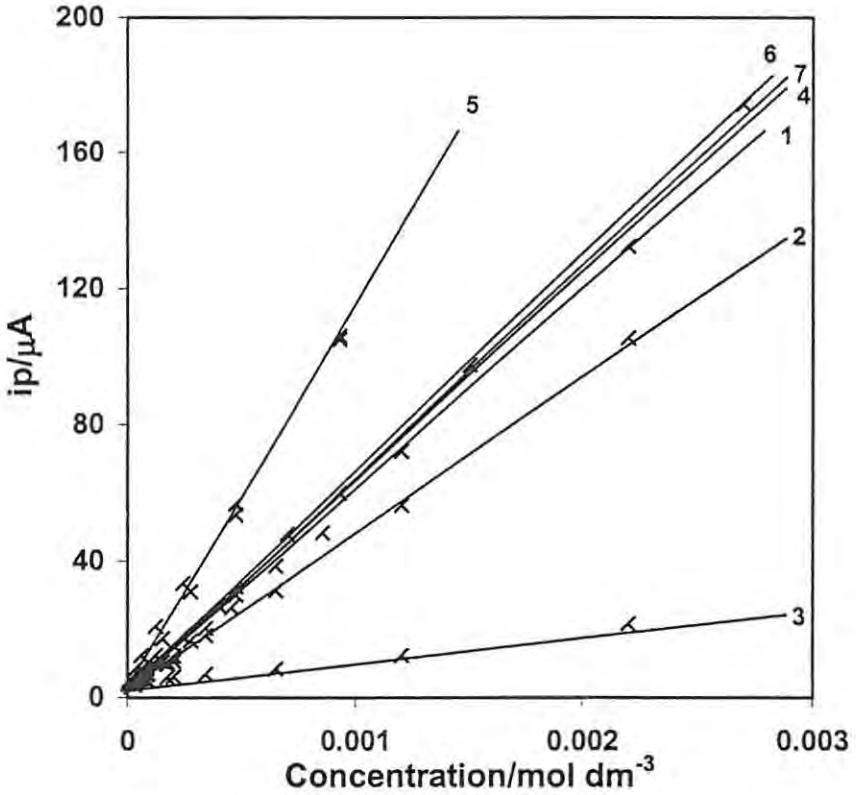

Fig. 4.22 Calibration plots of the oxidation and reduction of SO_2 and its related compounds at a glassy carbon electrode modified with $[Fe^{II}TSPc]^{4-}$. (1) SO_2 reduction in 1.0 mol dm^{-3} H_2SO_4, (2) SO_2 oxidation in 1.0 mol dm^{-3} H_2SO_4, (3) HSO_3^- oxidation in 1.0 mol dm^{-3} H_2SO_4, (4) HSO_3^- oxidation in pH 4 buffer, (5) HSO_3^- reduction in pH 4 buffer (6) SO_3^{2-} oxidation in pH 8 buffer and (7) SO_3^{2-} oxidation in pH 10 buffer.

Another possibility is making use of the reduction wave V. No reduction prewave of HSO_3^- was observed and since k_{-1} in reaction 4.6 is high, it can be concluded that HSO_3^- is transformed fast into $SO_2.xH_2O$, during sulphur dioxide reduction. As was pointed out earlier, dithionite is supposed to be the reaction product, therefore wave V is attributed to equation 4.10.

$$2SO_2 + 2e^- \rightleftharpoons S_2O_4^{2-} \qquad (4.10)$$

Based on the reduction of $SO_2.xH_2O$ a detection limit of $8.5 \pm 0.1 \times 10^{-5}$ mol dm^{-3} is obtained, which is lower than that obtained by using waves III and IV ($1.2 \pm 0.1 \times 10^{-4}$ mol dm^{-3}). The determination of the detection limit was based on the criterion that the detection limit corresponds to an electrode signal of twice the background current. However, an advantage of using the oxidation for detection limit is that sulphate is formed as a reaction product instead of dithionite. The latter species itself is electroactive and relatively unstable. Decomposition occurs easily into sulphite and related products. Therefore dithionite can become an influencing species in continuous measurement or for measurements in small volume cells.

4.3.1.2. Studies in pH 4 buffer

Fig. 4.23 shows current-potential curves for different sulphur dioxide concentrations, recorded in pH 4 buffer at a $[Fe^{II}TSPc]^{4-}$ modified glassy carbon electrode. Two waves can be detected: an oxidation wave centered around 0.05 V vs. Ag|AgCl (a) and a reduction wave with a peak potential of - 0.65 V vs. Ag|AgCl (b). Based on the results obtained above in 1.0 mol dm^{-3} H_2SO_4, the oxidation wave corresponds to electrocatalytic oxidation of HSO_3^- catalysed by $[Fe^{II}TSPc]^{4-}$, which is oxidised to $[Fe^{II}TSPc]^{4-}$ at the same potentials. No wave for $SO_2.xH_2O$ is observed because SO_2 is transformed almost totally into HSO_3^- (Table 4.2) at this pH. A similar voltammogram to that shown in Fig. 4.23 was obtained using sodium sulphite as a starting species. The oxidation wave corresponds to reaction 4.9 with exchange of two electrons and is proportional to the analytical concentration of sulphur dioxide and sulphite (Fig. 4.22, curve 4).

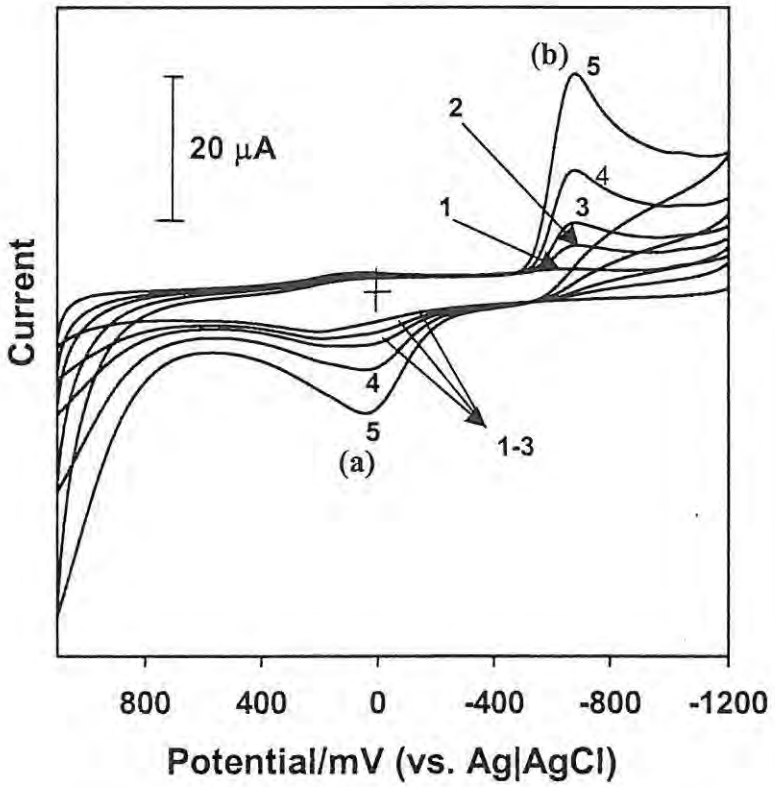

Fig. 4.23 Current-potential curves recorded in pH 4 buffer solution for increasing SO_2 concentrations at a glassy carbon electrode modified with $[Fe^{II}TSPc]^{4-}$. SO_2 concentrations are (1) 0, (2) 8.79×10^{-5}, (3) 1.51×10^{-4}, (4) 2.71×10^{-4} and (5) 4.71×10^{-4} mol dm^{-3}. Scan rate = 100 mV s^{-1}.

The reduction wave cannot be attributed to reduction of $SO_2.xH_2O$ or HSO_3^- with exchange of two electrons. Its slope is twice as high as that for the oxidation (Fig. 4.22, curve 5). Therefore this wave is assumed to be the reduction of HSO_3^- (because this is the only compound in solution) to $S_2O_3^{2-}$ (equation 4.11) with exchange of four electrons, because $S_2O_3^{2-}$ does not show electroactive properties over the entire potential region and is a relatively stable species.

$$2HSO_3^- + 4H^+ + 4e^- \rightleftharpoons S_2O_3^{2-} + 3H_2O \qquad (4.11)$$

Because of the higher slope obtained for the reduction, a lower detection limit can be obtained. Detection limits of $3.8 \pm 0.1 \times 10^{-5}$ and $7.4 \pm 0.1 \times 10^{-5}$ mol dm^{-3} were obtained respectively for the reduction and oxidation of $SO_2.xH_2O$, with HSO_3^- as electroactive species.

4.3.1.3. Studies at pH 8 and pH 10 buffer

In pH 8 buffer completely different results were obtained for sulphur dioxide and sodium sulphite as starting species. Starting from sulphite, only one oxidation wave was obtained around 0.7 V vs. Ag|AgCl. From Table 4.2 it can be seen that sulphite itself is the main compound in solution, therefore this wave can be attributed to equation 4.12. Its slope (Fig. 4.22, curve 6), obtained by plotting the peak current vs. concentration, is situated in the range that allows exchange of 2 electrons.

$$SO_3^{2-} + H_2O \rightleftharpoons SO_4^{2-} + 2H^+ + 2e^- \qquad (4.12)$$

Starting from sulphur dioxide, only one wave around 0.7 V vs. Ag|AgCl was observed at small concentrations, Fig. 4.24. At higher concentrations this wave disappears and two new waves with E_p = - 0.2 and - 1.1 V vs. Ag|AgCl are observed, Fig. 4.25. It is well known that SO_3^{2-} reacts to form $HS_2O_5^-$ in an excess of SO_2.[182] This excess is temporarily present during dissolution of SO_2. It is expected that this indeed occurs, but $HS_2O_5^-$ itself decomposes further. However, the new waves occurring are not proportional to the SO_2 concentration. Similar results were obtained in buffer solutions from pH 7.5 – 9.0. Therefore, it is clear that SO_2 cannot be detected in the pH range from 7.5 – 9.0 due to the instability of $SO_2.xH_2O$ or its related compounds HSO_3^- and SO_3^{2-}. However, sulphite can be detected in the absence of SO_2 in pH 8 buffer.

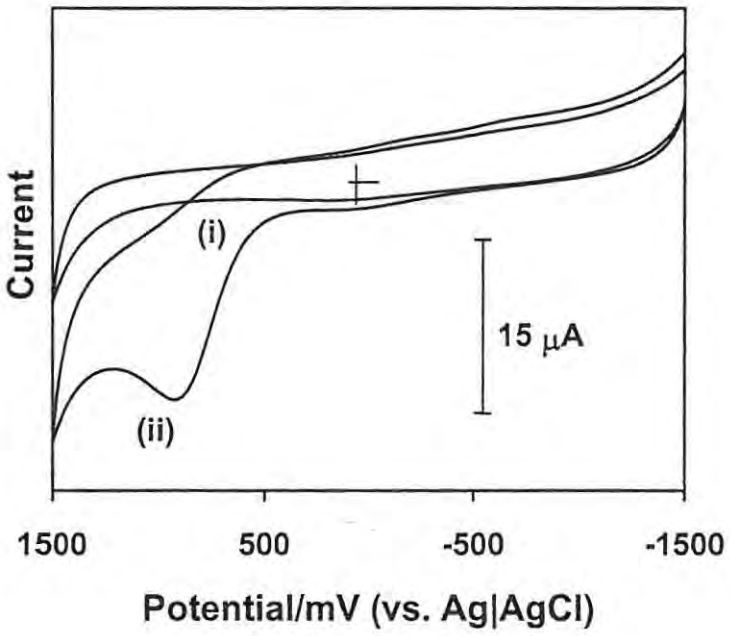

Fig. 4.24 Current-potential curves recorded in pH 8 buffer solution in the absence (i) and presence (ii) of 1.45 x 10^{-4} mol dm^{-3} SO_2 at a glassy carbon electrode modified with $[Fe^{II}TSPc]^{4-}$. Scan rate = 100 mV s^{-1}.

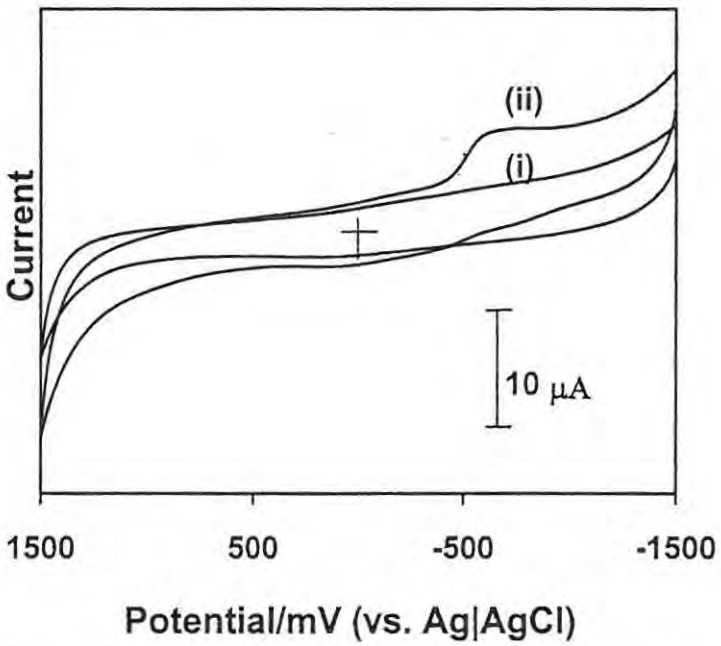

Fig. 4.25 Current-potential curves recorded in pH 8 buffer solution in the absence (i) and presence (ii) of 4.8 x 10^{-4} mol dm^{-3}. SO_2 at a glassy carbon electrode modified with $[Fe^{II}TSPc]^{4-}$. Scan rate = 100 mV s^{-1}.

Fig. 4.26 shows current-potential curves of increasing SO_2 concentrations, recorded in pH 10 buffer at a glassy carbon electrode modified with $[Fe^{II}TSPc]^{4-}$. It can be seen that in this highly alkaline solution only one wave is obtained at 0.75 V vs. Ag|AgCl, which is identical to the one obtained for sodium sulphite. Therefore, it can be proposed that SO_3^{2-} is the main (Table 4.2) electroactive compound in solution, at pH 10. As expected, the slope of peak current vs. SO_2 or Na_2SO_3 concentrations corresponds to exchange of 2 electrons (Fig. 4.22, curve 7) and a detection limit of 7.3 $\pm$ 0.1 x 10^{-5} mol dm^{-3} was obtained.

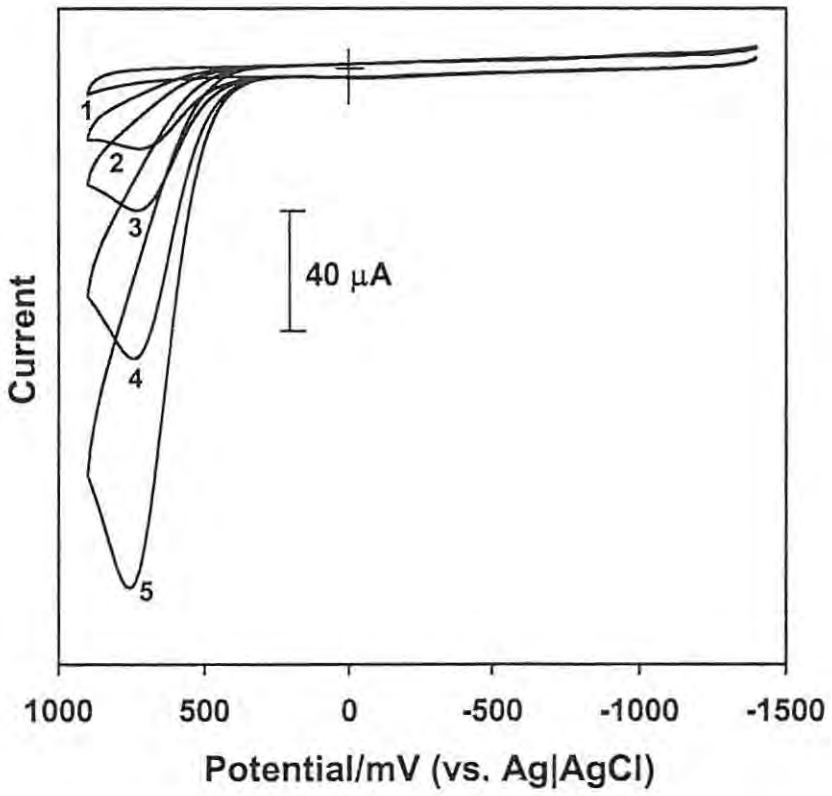

Fig. 4.26 Current-potential curves recorded in pH 10 buffer solution for increasing SO_2 concentrations at a glassy carbon electrode modified with $[Fe^{II}TSPc]^{4-}$. SO_2 concentrations are (1) 0, (2) 3.92 x 10^{-4}, (3) 6.95 x 10^{-4}, (4) 1.51 x 10^{-3} and (5) 2.70 x 10^{-3} mol dm^{-3}. Scan rate = 100 mV s^{-1}.

It has thus been shown in this work that the electrocatalytic detection of SO_2 is not simple and is strongly dependent on pH. From this study it can also be concluded

that strongly acidic or alkaline solutions should be used as electrolyte in SO_2-gas sensing applications. For an optimal detection limit a buffer of pH 4 should be used in combination with the reduction reaction of HSO_3^-, the main compound in solution related to SO_2. In acidic or basic pH, the oxidation of SO_2 (and related compounds) to sulphate should be explored for analysis, since reduction of SO_2 causes formation of possible interfering and poisoning products. Except for the pH range from 7.5 – 9, a detection limit of about $4.0 \pm 0.1 \times 10^{-5}$ mol dm^{-3} in pH 4 buffer (reduction) and $7.5 \pm 0.1 \times 10^{-5}$ mol dm^{-3} for other pH values are possible for SO_2 and its related compounds, HSO_3^- and SO_3^{2-}.

4.3.2. $[Co^{II}TSPc]^{4-}$ as a catalyst

SO_2 studies in the pH range 7.4 to 10.8 were also investigated on $[Co^{II}TSPc]^{4-}$. Only the results for pH 10.8 are discussed and compared when $[Fe^{II}TSPc]^{4-}$ is used as a catalyst. The GCE was modified by electrodeposition from pH 10.2 buffer as described in Section 4.1.2.[122]

Voltammograms for SO_2 oxidation are similar to those observed on $[Fe^{II}TSPc]^{4-}$-GCE in pH 10 buffer. Under these conditions SO_2 exists as SO_3^{2-} as explained above. Cyclic voltammogram of $[Co^{II}TSPc]^{4-}$ adsorbed onto GCE, in the blank (pH 10.8 buffer) did not show the broad anodic peak corresponding to $[Co^{III}TSPc]^{3-}/[Co^{II}TSPc]^{4-}$ couple near 0.9 V vs. Ag|AgCl, Fig 4.27(a), as observed in this work in organic media, or as observed in pH 9 buffer. On addition of SO_2 a strong catalytic peak was observed at 0.85 V vs. Ag|AgCl, Fig. 4.27(b). The large enhancement of the SO_2 oxidation peak is observed on GCE modified with $[Co^{II}TSPc]^{4-}$. The enhancement in the oxidation currents indicate improved catalytic

activity of the GCE when modified with $[Co^{II}TSPc]^{4-}$. On unmodified GCE, no peak for SO_2 oxidation was observed for the same concentration of SO_2 solution.

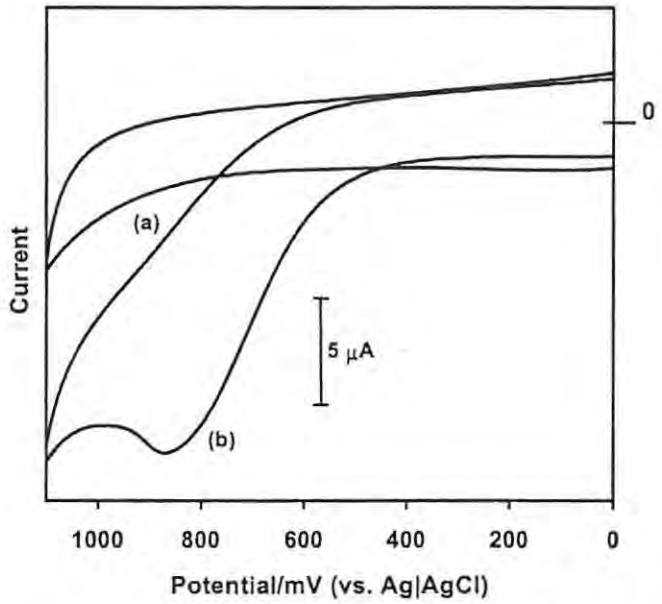

Fig. 4.27 Current-potential curves recorded in pH 10.8 buffer solution for SO_2 at a glassy carbon electrode modified with $[Co^{II}TSPc]^{4-}$ in the absence (a) and presence (b) of 1.300×10^{-4} mol dm^{-3} SO_2. Scan rate = 100 mV s^{-1}.

As discussed above, Section 4.2.2.3, electrocatalytic oxidation reactions involving CoPc complexes have been described as a two-step process involving first the oxidation of $Co^{II}Pc$ to $Co^{III}Pc$, followed by electron transfer from the species to be catalysed to the $Co^{III}Pc$ species. Thus, the proposed mechanism for electrocatalytic oxidation of SO_2 on GCE modified with $[Co^{II}TSPc]^{4-}$ is shown by equations 4.13 to 4.15.

$$[Co^{II}TSPc]^{4-} \rightarrow [Co^{III}TSPc]^{3-} + e^- \quad (4.13)$$

$$[Co^{III}TSPc]^{3-} + SO_3^{2-} \rightarrow [Co^{III}(SO_3^{2-})TSPc]^{5-} \quad (4.14)$$

$$[Co^{III}(SO_3^{2-})TSPc]^{5-} + H_2O \rightarrow [Co^{II}TSPc]^{4-} + SO_4^{2-} + 2H^+ + e^- \quad (4.15)$$

A similar mechanism may be proposed for $[Fe^{II}TSPc]^{4-}$.

The enhancement in the anodic currents for the oxidation of SO_2 in the presence of $[Co^{II}TSPc]^{4-}$ are a consequence of electron transfer reactions through equations 4.13 to 4.15. The enhancement in currents show that electrode kinetics is improved when $[Co^{II}TSPc]^{4-}$ is used as a catalyst adsorbed on a GCE compared to unmodified GCE. Equation 4.14 is proposed based on the fact that electron transfer reactions are generally mediated by axial ligation of the analyte.

The possible coordination of SO_3^{2-} to $[Co^{II}TSPc]^{4-}$ prior to electron transfer was examined using electron absorption spectroscopy in Section 3.3.3.

The catalytic currents for the oxidation of SO_2 (as SO_3^{2-}) on GCE modified with $[Co^{II}TSPc]^{4-}$ increased linearly with SO_2 concentrations in pH 10.8 buffer, Fig. 4.28. Plots of square root of scan rate vs. peak current were linear indicating a diffusion-controlled process. The detection limit of SO_2 was found to be 1.2×10^{-5} mol dm^{-3} (or 0.76 ppm). In determining the detection limit it is assumed that the detection limit corresponds to twice the background current. The detection limits of 500 ppb[82] and 1ppb[81] SO_2 have been reported. The detection limit of 1.2×10^{-5} mol dm^{-3} is an improvement over that obtained on $[Fe^{II}TSPc]^{4-}$-GCE (7.3×10^{-5} mol dm^{-3}) above. Despite the fact that the detection limits of SO_2 reported in this work are higher than literature reports, this work is an improvement economically, since the cheaper glassy carbon electrode (modified with cheaper and easy to synthesise MPcs) is employed as opposed to more expensive platinum and gold electrodes.

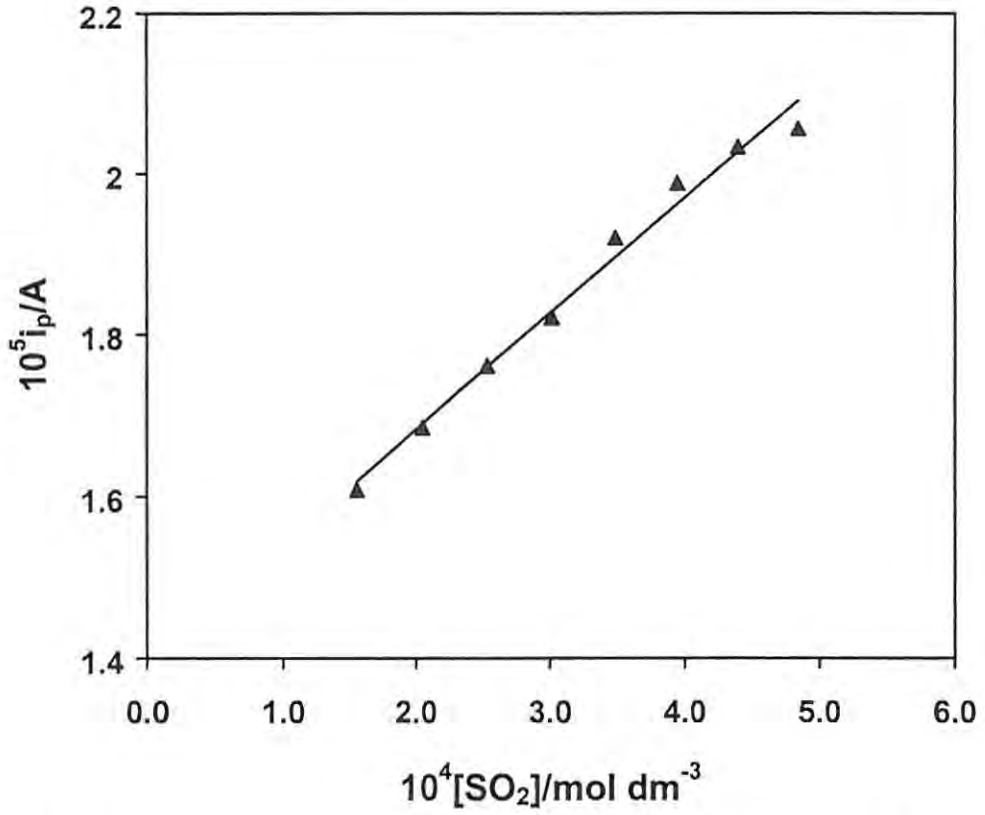

Fig. 4. 28 Plot of $[SO_2]$ vs. current on $[Co^{II}TSPc]^{4-}$-GCE in pH 10.8 buffer.

In summary, it has been shown in this work that the use of $[Co^{II}TSPc]^{4-}$ to modify the GCE results in the enhancement of the oxidation currents for SO_2. Concentration of SO_2 of the order of 10^{-5} mol dm^{-3} could be determined using the $[Co^{II}TSPc]^{4-}$ modified GCE in pH 10.8 buffer.

4.4. Electrocatalytic studies of cyanide

Cyanide detection is of importance due to its great toxicity. Electrode modification was performed by electrodeposition from $[Co^{II}Tm\text{-}3,4\text{-}tppa]^{4+}$,[11] as described before in Section 4.1.1. Fig 4.29 (curve 1) shows the cyclic voltammogram of $[Co^{II}Tm\text{-}3,4\text{-}tppa]^{4+}$-GCE in the buffer (pH 10.8) alone. In Fig. 4.29, (curve 1) two broad peaks are observed, one peak near + 0.20 V and a broader feature near + 1.2 V

vs. Ag|AgCl. The peak near + 0.20 V vs. Ag|AgCl is assigned to metal reduction, $[Co^{II}Tm\text{-}3,4\text{-}tppa]^{4+}/[Co^{I}Tm\text{-}3,4\text{-}tppa]^{3+}$,[11] see also Section 3.2.1. The broad feature near 1.2 V vs. Ag|AgCl may be due to Co^{III}/Co^{II}. It is very difficult to oxidise these positively charged molecules, but the first oxidation is expected to occur at the central metal. On addition of cyanide, the peak near + 0.20 V vs. Ag|AgCl disappeared, and an enhanced more-defined peak, which can be attributed to cyanide catalysis was observed at + 1.27 V vs. Ag|AgCl, Fig. 4.29 (curve 2). The peak increased with an increase in cyanide concentration, Fig. 4.29 (curves 2 to 4).

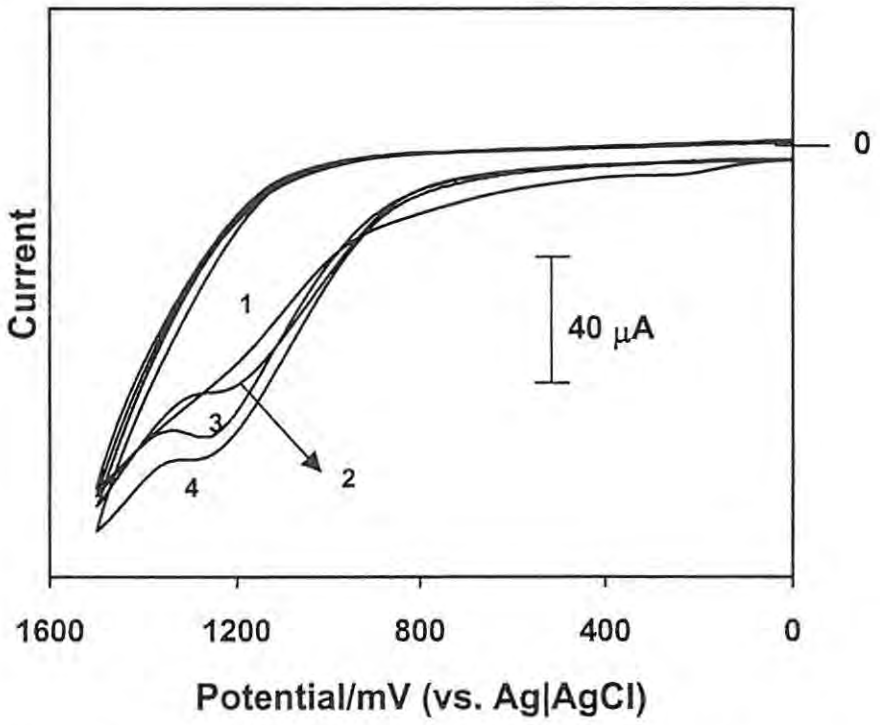

Fig. 4.29 Current-potential curves recorded in pH 10.8 borate buffer solution for increasing concentrations of cyanide on $[CoTm\text{-}3,4\text{-}tppa]^{4+}$-GCE. Cyanide concentrations are (1) 0, (2) 1.69×10^{-11}, (3) 1.07×10^{-10}, and (4) 1.67×10^{-10} mol dm^{-3}.

A negligible peak for cyanide oxidation was observed on unmodified glassy carbon electrode (for the same concentration range employed in Fig. 4.29), Fig. 4.30. Fig 4.31 shows a linear plot of cyanide concentration vs. peak current. The lowest

cyanide concentration that could be determined was 1 x 10^{-11} mol dm^{-3}. A plot of cyanide concentration vs. scan rate was linear indicating a diffusion-controlled process. Interestingly, a new peak at + 1.4 V vs. Ag|AgCl appeared as the oxidation in cyanide progressed. Similar behaviour has been observed before,[61] and it has been explained as follows: the first oxidation corresponds to cyanide oxidation, but as oxidation progresses the anodic potential rises to the characteristic value of the onset of oxidation of oxygen. Sodium cyanide oxidation has been observed at + 0.58 V vs. standard hydrogen electrode on titanium/cobalt oxide anodes.[61] The product of cyanide oxidation has been reported to be cyanate,[55,56] equation 4.16.[61]

$$CN^- + 2OH^- \rightarrow OCN^- + H_2O + 2e^- \qquad (4.16)$$

A similar mechanism is proposed in this work, that is, cyanide is oxidised to cyanate on $[Co^{II}Tm\text{-}3,4\text{-}tppa]^{4+}$-GCE in pH 10.8 buffer.

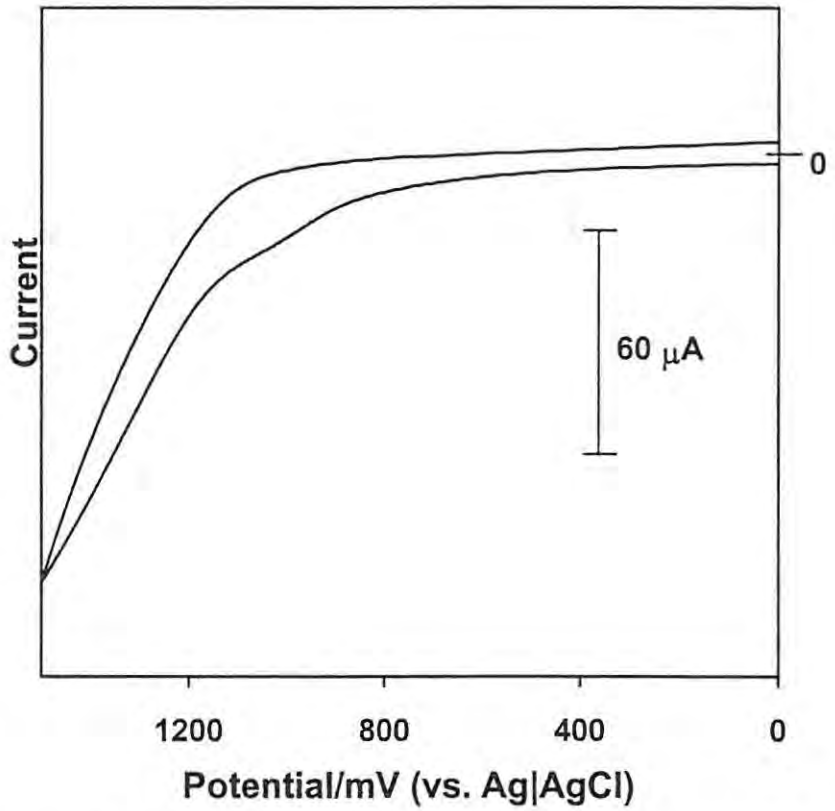

Fig. 4.30 Current-potential curve recorded in pH 10.8 borate buffer solution for 1.67 x 10^{-10} mol dm^{-3}cyanide on unmodified GCE.

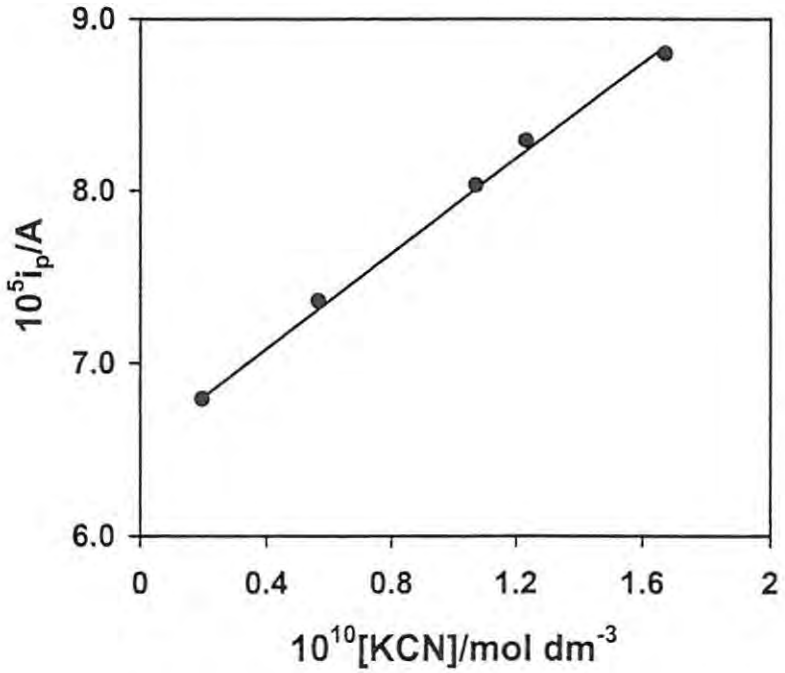

Fig. 4.31 A plot of variation of catalytic currents against cyanide concentration for cyanide oxidation on $[Co^{II}Tm\text{-}3,4\text{-}tppa]^{4+}$-GCE in pH 10.8 buffer. Scan rate = 100 mV s^{-1}.

Table 4.3 compares detection limits for cyanide available in the literature with that obtained in this work. Lowest detection limits are observed in this work, although the oxidation potential is a highly positive value. This calls for future research, which will involve investigation of catalysts that will give both very low detection limits and less positive cyanide oxidation potential.

Table 4.3 E_p and detection limits for cyanide oxidation

E_p (vs. Ag|AgCl)	Method	Detection limit (mol dm^{-3})	Reference
+ 0.226 V	Normal pulse voltammetry	1.2×10^{-7}	67
- 0.26 V*	Polarography	1.25×10^{-3}**	68
+ 1.27 V	Cyclic voltammetry	1×10^{-11}	This work

* = Reference electrode is SCE, ** = Detection limit in g dm^{-3}

To determine the mechanism of the reaction, spectroelectrochemistry experiments could be undertaken in aqueous solution of $[Co^{II}Tm\text{-}3,4\text{-}tppa]^{4+}$ in the presence of cyanide, under experimental conditions (e.g. temperature and environment) similar to those used for electrocatalysis and in pH 10.8 buffer. As has already been discussed,[4] $[Co^{II}Tm\text{-}3,4\text{-}tppa]^{4+}$ is stable in acid solutions, but readily decomposes in alkaline media. It was not therefore possible to perform homogenous electrocatalytic oxidation of cyanide using $[Co^{II}Tm\text{-}3,4\text{-}tppa]^{4+}$. While brown solutions of $[Co^{II}Tm\text{-}3,4\text{-}tppa]^{4+}$were obtained in basic media, the adsorbed $[Co^{II}Tm\text{-}3,4\text{-}tppa]^{4+}$ complex is stable for the catalytic studies in basic media discussed above. Cyanide oxidation on ion-selective electrodes based on polyacrylamide modified with cobalt phthalocyanine has been reported.[189] Two peaks were observed at + 0.6 and +

1.55 V (vs. Ag|0.01 mol dm^{-3} Ag^{+}, using 0.1 mol dm^{-3} tetraethylammonium perchlorate in acetonitrile) in non-aqueous media, which were assigned to oxidation of cyanide trapped (merely retained) in polyacrylamide matrix and cyanide chemically bonded to CoPc.[189] The bond was confirmed by visible spectroscopy and the mechanism, based on ESR spectroscopy was proposed to be a one-electron oxidation from $2CN^{-}$ to $(CN)_2$.

Homogeneous catalysis of cyanide could not be performed at low pH values, as under these conditions cyanide exits mainly as HCN.[55] In pH 7 buffer, cyanide exists as 100% HCN while at pH 10.2 more than 90% of total cyanide is free cyanide. HCN has a relatively high vapour pressure, volatilising under ambient conditions, resulting in loss of cyanide from the solution.

It has been shown in this work that cyanide can be detected down to 1×10^{-11} mol dm^{-3} using $[Co^{II}Tm\text{-}3,4\text{-}tppa]^{4+}$-GCE in pH 10.8 buffer. It is suggested that the $[Co^{III}Tm\text{-}3,4\text{-}tppa]^{5+}$ species are involved in the catalytic process.

4.5. Electrocatalytic studies of histidine and cysteine

Histidine and cysteine detection is of importance since the molecules are components of biological systems. Electrode modification was performed by electrodeposition of $[Co^{II}Tm\text{-}3,4\text{-}tppa]^{4+}$,[11] as described in Section 4.1.1 above. Fig. 4.32 (curve 1) shows the cyclic voltammogram of $[Co^{II}Tm\text{-}3,4\text{-}tppa]^{4+}$-GCE in the buffer (pH 10.8) alone. Basic pH was chosen since histidine showed no electrocatalytic peaks in acidic to neutral pH values. At a pH of 10.8, the unprotonated form of histidine is determined. In Fig. 4.32, (curve 1) a broad peak observed near + 0.20 V Ag|AgCl, is assigned to metal reduction, $[Co^{II}Tm\text{-}3,4\text{-}tppa]^{4+}/[Co^{I}Tm\text{-}3,4\text{-}tppa]^{3+}$, see Section 4.4.[11] On addition of histidine, a new peak at

0.37 V vs. Ag|AgCl was formed, which decreased with histidine concentration, while an enhanced well-defined peak, which can be attributed to histidine electrocatalytic oxidation was observed at + 0.88 V vs. Ag|AgCl, Fig. 4.32 (curve 2). The peak increased with an increase in histidine concentration, Fig. 4.32 (curves 2 to 4).

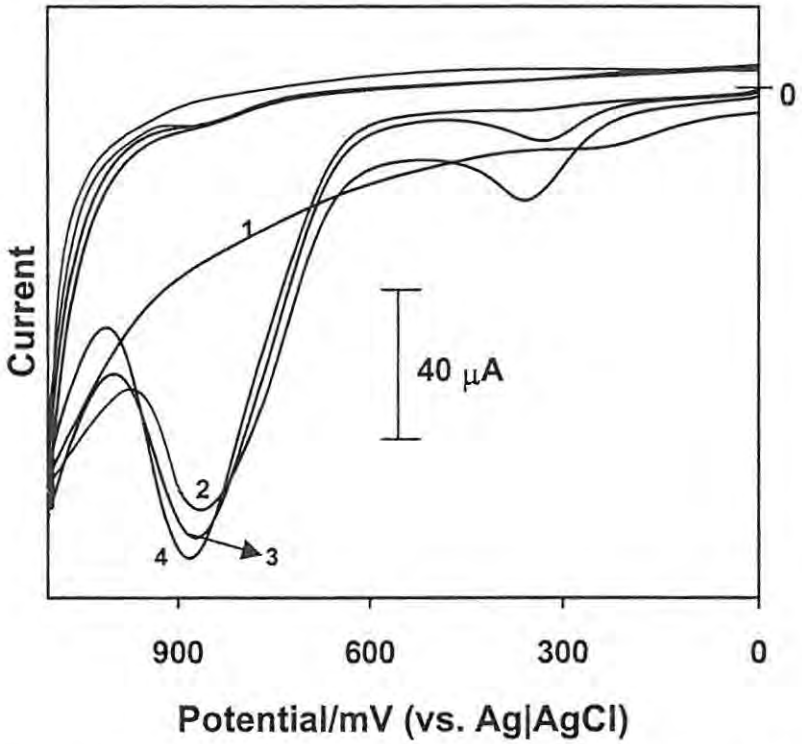

Fig. 4.32 Current-potential curves recorded in pH 10.8 Tris buffer solution for increasing concentrations of histidine on $[Co^{II}Tm\text{-}3,4\text{-}tppa]^{4+}$-GCE. Histidine concentrations are (1) 0, (2) 2.91 x 10^{-7}, (3) 3.85 x 10^{-7} and (4) 4.76 x 10^{-7} mol dm^{-3}.

Fig. 4.32 may be explained by spectroscopic studies or by literature reports.[118] In neutral media, addition of histidine to $[Co^{II}Tm\text{-}3,4\text{-}tppa]^{4+}$ resulted in spectral changes that indicated formation of $[Co^{I}Tm\text{-}3,4\text{-}tppa]^{3+}$ species, as discussed in Section 3.3.2. The interaction of histidine with $[Co^{II}Tm\text{-}3,4\text{-}tppa]^{4+}$ under neutral pH results in the reduction of this complex to $[Co^{I}Tm\text{-}3,4\text{-}tppa]^{3+}$ in solution, thus in the presence of histidine, $[Co^{I}Tm\text{-}3,4\text{-}tppa]^{3+}$ is present, and the observed peak at 0.37 V vs. Ag|AgCl is due to oxidation of these species to $[Co^{II}Tm\text{-}3,4\text{-}tppa]^{4+}$. However, the peak at 0.37 V vs. Ag|AgCl corresponding to Co^{II}/Co^{I} species decreased with increase

in histidine concentration. Reports have shown that the oxidation of histidine on Pt disc consisted of a peak at + 0.6 V vs. Ag|AgCl which was attributed to the secondary amine group in histidine.[118] The decrease of the peak at 0.37 V vs. Ag|AgCl with histidine concentration may suggest that the oxidation of the secondary amine group of histidine is producing a poisoning effect on the electrode. The poisoning effect could also be a result of the negligible amounts of cyanide (from byproducts of histidine oxidation) present in solution. Very small amounts of cyanide have been detected[118] from histidine oxidation. Also, the poisoning effect of cyanide to the Co^{II}/Co^{I} species is clearly demonstrated in Section 4.4 above, where the Co^{II}/Co^{I} peak completely disappears on addition of cyanide, Fig. 4.29.

The peak due to histidine oxidation, at + 0.88 V vs. Ag|AgCl may be assigned to oxidative decomposition of histidine to CO_2. A similar peak has been observed before,[118] on Pt discs at 1.1 V vs. Ag|AgCl.

No peak for histidine oxidation was observed on an unmodified glassy carbon electrode. Fig. 4.33 shows a linear plot of histidine concentration vs. peak current. The lowest histidine concentration that could be determined was 2.24×10^{-7} mol dm^{-3}. A plot of histidine concentration vs. scan rate was linear indicating a diffusion-controlled process.

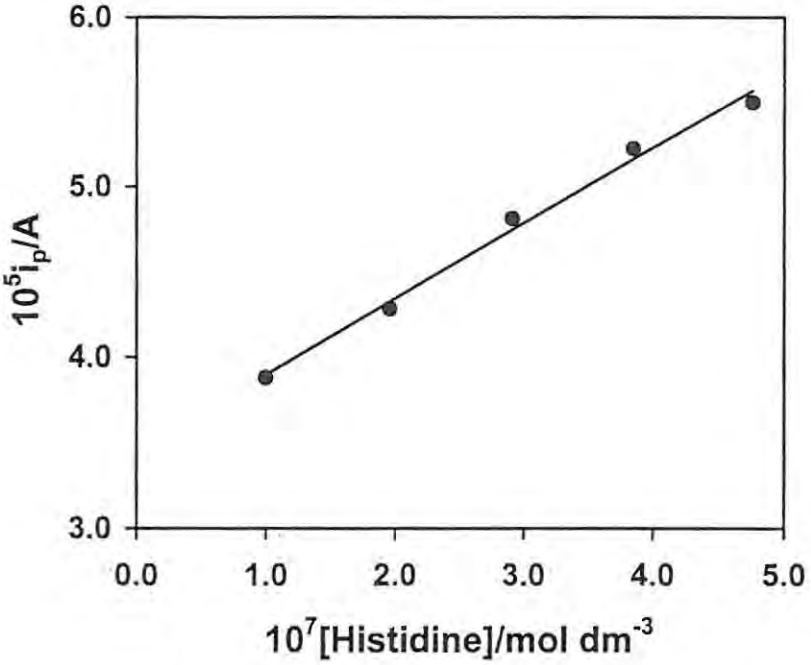

Fig. 4.33 A plot of variation of catalytic currents against histidine concentration for histidine oxidation on $[Co^{II}Tm\text{-}3,4\text{-}tppa]^{4+}$-GCE in pH 10. 8 buffer. Scan rate = 100 mV s^{-1}.

It is tentatively proposed that Co^{III} in $[CoTm\text{-}3,4\text{-}tppa]^{4+}$ catalyses histidine oxidation, as is typical for CoPc catalysed oxidation: some of the products of histidine oxidation are CO_2 and NH_3.[118] It has thus been shown in this work that histidine determination, using its oxidation, can be performed on $[Co^{II}Tm\text{-}3,4\text{-}tppa]^{4+}$-GCE in pH 10.8 buffer, with a detection limit of 2.24 x 10^{-7} mol dm^{-3}.

A peak for cysteine oxidation occurs at highly positive potentials on an unmodified glassy carbon electrode. Metallophthalocyanines lower the oxidation potential of cysteine when adsorbed on carbon electrodes.[44,45,123] Fig. 4.34 shows that in the presence of cysteine, the peak near 0.20 V vs. Ag|AgCl, which has been assigned to metal oxidation, $[Co^{II}Tm\text{-}3,4\text{-}tppa]^{4+}/[Co^{I}Tm\text{-}3,4\text{-}tppa]^{3+}$ increased. This peak also shifted to 0.22 V vs. Ag|AgCl. The increase in currents in the presence of cysteine indicates a catalytic process. The peak due to cysteine oxidation increased

with an increase in cysteine concentration, Fig. 4.35 (curves 1 to 3). The dip in the peak upon the return scan is typical[44] of catalytic oxidation of cysteine. The observation of the catalytic peak in the region of Co^{II}/Co^{I} thus confirms that this couple catalyses cysteine oxidation in neutral media. See mechanism later.

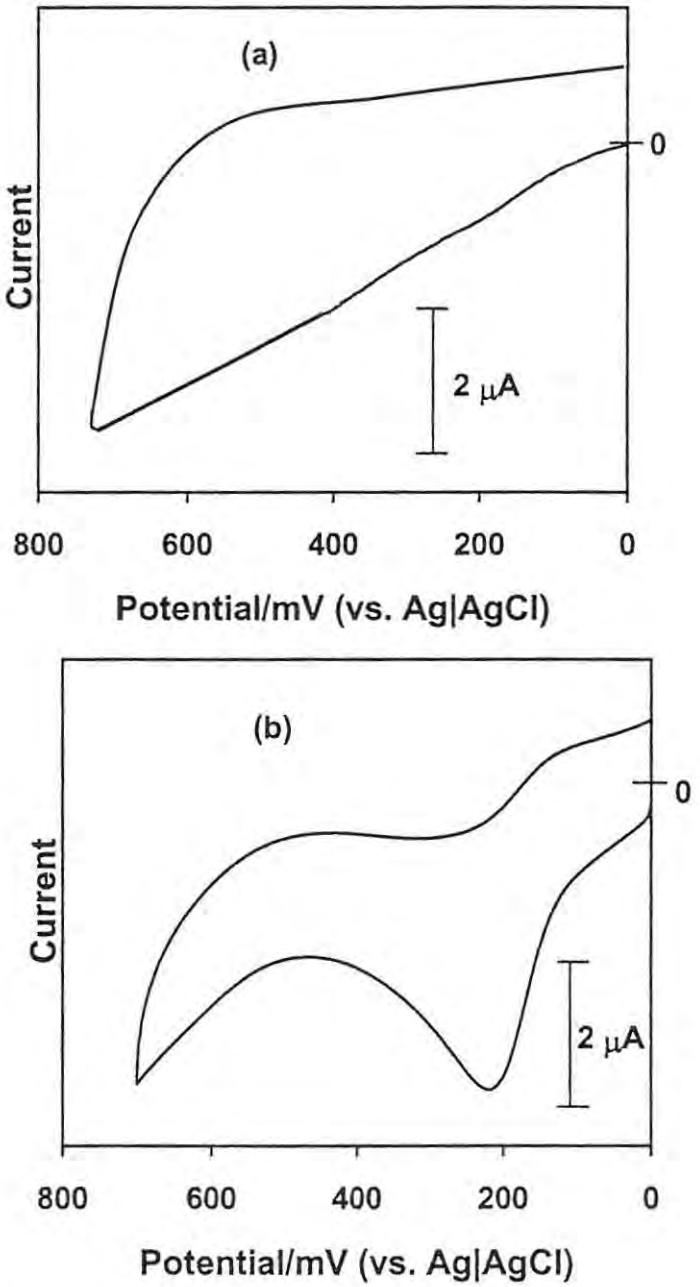

Fig. 4.34 Current-potential curves recorded in pH 7 Tris buffer solution for $[Co^{II}Tm\text{-}3,4\text{-}tppa]^{4+}$-GCE in the (a) absence and presence (b) of 1.0×10^{-4} and mol dm^{-3} cysteine.

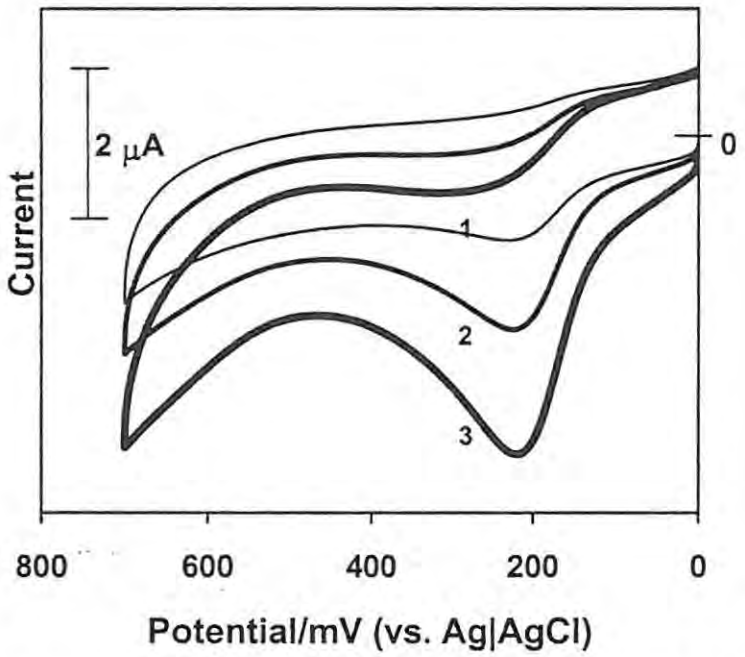

Fig. 4.35 Current-potential curves recorded in pH 7 Tris buffer solution for increasing concentrations of cysteine on $[Co^{II}Tm\text{-}3,4\text{-}tppa]^{4+}$-GCE. Cysteine concentrations are (1) 1.67×10^{-5}, (2) 8.35×10^{-5} and (3) 1.00×10^{-4} mol dm^{-3}.

Fig. 4.36 shows a linear plot of cysteine concentration vs. peak current. The lowest cysteine concentration that could be determined was 1.0×10^{-5} mol dm^{-3}. This result is listed in Table 4.4 and compared with previous studies. A plot of cysteine concentration vs. square root of scan rate was linear indicating a diffusion-controlled process, Fig. 4.37. The linearity was observed at lower scan rates only (up to 250 mV s^{-1}). At higher scan rates, deviation from linearity was observed and could be explained by the fact that the overall reaction is no longer diffusion-controlled, if the saturation current is exceeded. Similar results have been observed before.[125]

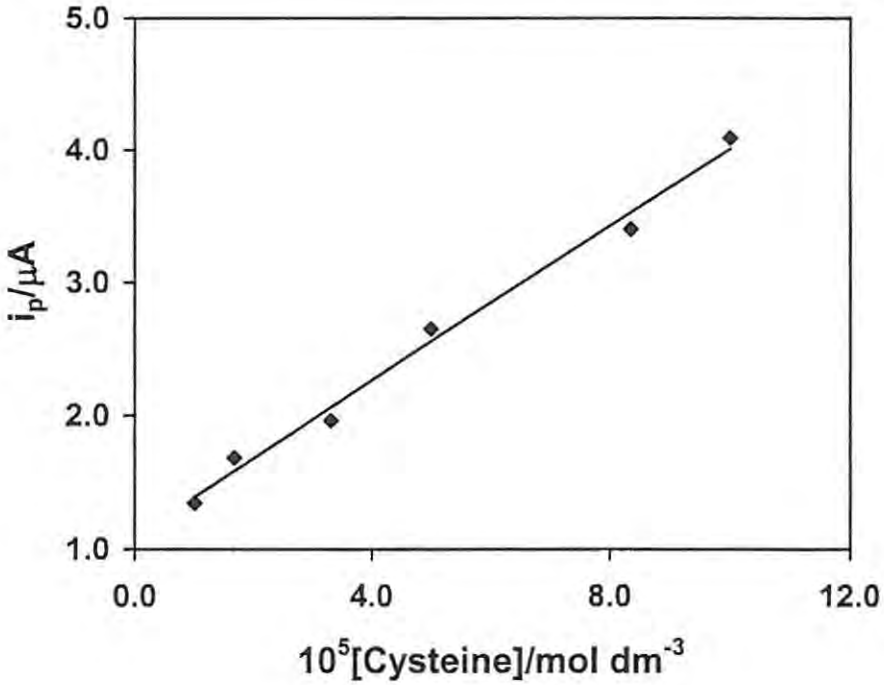

Fig. 4.36 A plot of variation of catalytic currents against cysteine concentration for cysteine oxidation on $[CoTm\text{-}3,4\text{-}tppa]^{4+}$-GCE in pH 7 buffer. Scan rate = 100 mV s^{-1}.

Table 4.4 shows that the catalytic peak for cysteine oxidation was observed at a lower potential of 0.22 V Vs. Ag|AgCl on $[Co^{II}Tm\text{-}3,4\text{-}tppa]^{4+}$-GCE in pH 7 buffer, compared to other catalysts. However, the detection limit of 1 x 10^{-5} mol dm^{-3} is not low enough when compared with 1 x 10^{-8} mol dm^{-3} reported on $[CoTSPc]^{4-}$-GCE, Table 4.4.[122] In general, Table 4.4 shows that the phthalocyanines that greatly lower the potential for cysteine oxidation, do not generally show a low detection limit. For example, a detection limit of ~ 10^{-3} mol dm^{-3} was observed on $OMo^{V}(OH)Pc$, with a peak potential at 0.26 V vs. Ag|AgCl[190] while a detection limit of ~ 10^{-7} mol dm^{-3} was observed on CoPc with a peak potential at 0.77 V vs. Ag|AgCl.[44] Therefore, more research is needed to develop a catalyst that could show both low detection limit and low oxidation potential for cysteine.

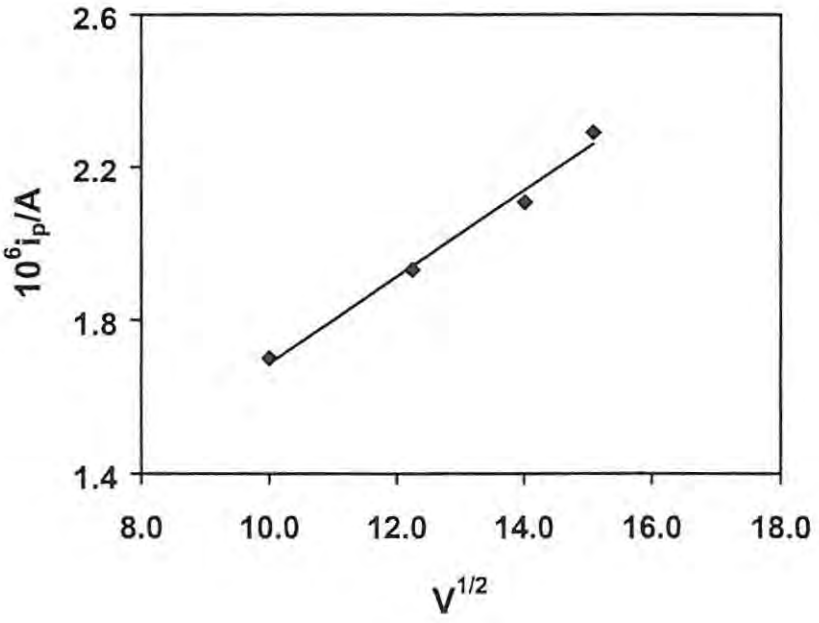

Fig. 4.37 A plot of square root of scan rate vs. peak current for 1.8×10^{-3} mol dm^{-3} cysteine on $[Co^{II}Tm\text{-}3,4\text{-}tppa]^{4+}$-GCE in pH 7 buffer. Scan rate = 100 mV s^{-1}.

Table 4.4 E_p and detection limits for the MPc catalysed oxidation of cysteine.

MPc	Conditions	E_p/V (vs. Ag|AgCl)	Detection limit/mol dm^{-3}	Reference
$OMo^{V}(OH)Pc$	Carbon paste	0.26	$\sim 10^{-3}$	190
$[OMo^{V}TSPc]^{4-}$	Solution	0.28	$\sim 10^{-2}$	124
$[Co^{II}TSPc]^{4-}$	Glassy carbon	0.90	20*	123
$Co^{II}Pc$	Carbon paste	0.77	$\sim 10^{-7}$	44
$[Co^{II}TSPc]^{4-}$	Solution	0.77	$\sim 10^{-7}$	44
$[Co^{II}TSPc]^{4-}$	Glassy carbon	0.82	1×10^{-8}	122
CoOBTPc	SAM	~ 0.4	3.1×10^{-7}	191
$[Co^{II}Tmtppa]^{4+}$	Glassy carbon	0.22	1.0×10^{-5}	This work

* = Detection limit in $\mu g\ mL^{-1}$

To determine the number of electrons involved in the reaction, pH studies were performed. Fig. 4.38 shows a plot of potential as a function of pH. The plot is linear with a slope of 50.8 mV per pH, implying n = 1 (n = number of electrons) at pH 7, in agreement with the literature.[122,125] Peak current decreased with scan number, Fig. 4.39. This can be attributed to poisoning of the electrode by cysteine oxidation product, cystine. Similar observations have been evidenced before,[126] on cysteine oxidation. It has been shown before[123] that the poisoning is not observed in acidic pH, since cystine dissolves and does not poison the electrode through adsorption.

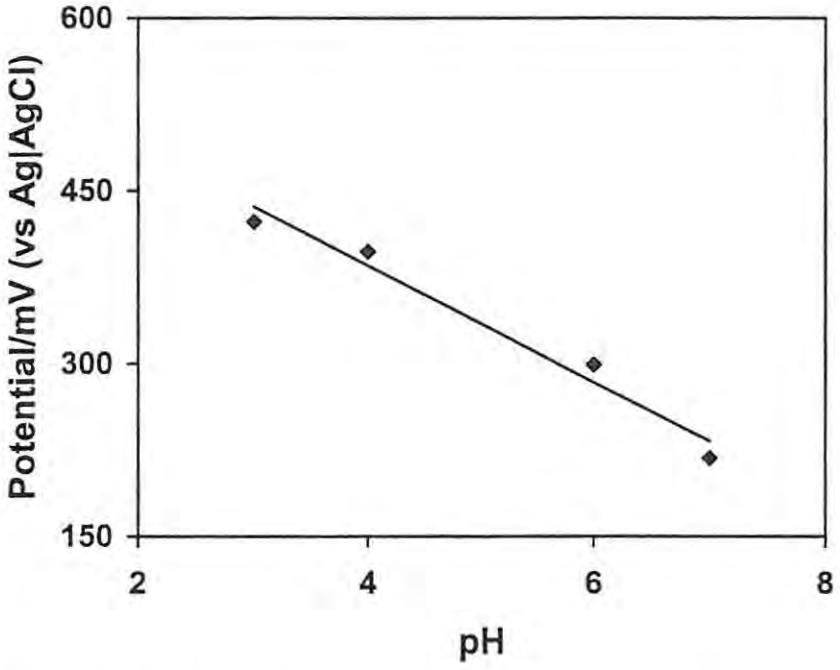

Fig. 4.38 A plot of peak potential against pH values in the presence of 1.8×10^{-3} mol dm^{-3} cysteine on $[Co^{II}Tm\text{-}3,4\text{-}tppa]^{4+}$-GCE. Scan rate = 100 mV s^{-1}.

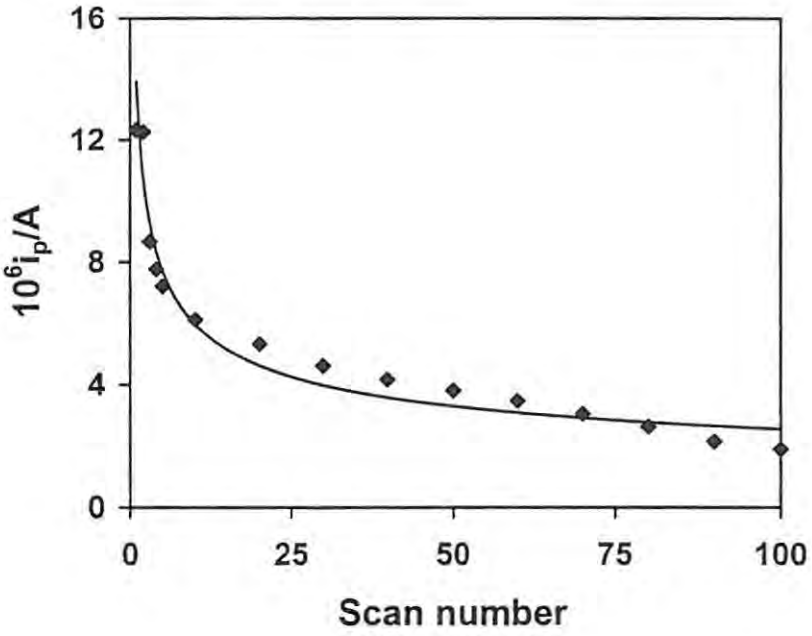

Fig. 4.39 Plot of peak current as a function of scan number in the presence of 1.8 x 10^{-3} mol dm^{-3} cysteine on $[Co^{II}Tm\text{-}3,4\text{-}tppa]^{4+}$-GCE in pH 7 buffer. Scan rate = 100 mV s^{-1}.

Ligation of cysteine to metallophthalocyanine prior to electron transfer has been proposed above, Section 3.3.1. Following this evidence, the mechanism proposed for this catalytic oxidation of cysteine at pH 7 may be represented by equations 4.17 to 4.20,

$$RSH + OH^- \rightarrow RS^- + H_2O \qquad (4.17)$$

$$[Co^{II}Tm\text{-}3,4\text{-}tppa]^{4+} + RS^- \rightarrow [Co^{I}Tm\text{-}3,4\text{-}tppa]^{3+} + RS^{\cdot} \qquad (4.18)$$

$$[Co^{I}Tm\text{-}3,4\text{-}tppa]^{3+} \rightarrow [Co^{II}Tm\text{-}3,4\text{-}tppa]^{4+} + e^- \qquad (4.19)$$

$$RS^{\cdot} + RS^{\cdot} \rightarrow RSSR \qquad (4.20)$$

where RSH represents cysteine and RSSR is the cystine. The enhancement of the anodic currents observed in Fig. 4.34(a) is a consequence of electron transfer by

equations 4.18 and 4.19. Co^{II}/Co^{I} couple for $[Co^{II}Tm\text{-}3,4\text{-}tppa]^{4+}$ has been employed in electrocatalysis of a variety of molecules.[41,42]

Homogeneous catalysis was also performed in pH 7 buffer. The peak potential was observed at 0.42 V vs. Ag|AgCl.

Experiments were also performed in pH 4 buffer under homogeneous conditions. Fig. 4.40(a) and (b) shows $[Co^{II}Tm\text{-}3,4\text{-}tppa]^{4+}$ in pH 4 buffer in the absence and presence of cysteine, respectively. The anodic peak for cysteine oxidation was observed at 0.52 V vs. Ag|AgCl and is assumed to be catalysed by Co^{II}/Co^{I} species in $[Co^{II}Tm\text{-}3,4\text{-}tppa]^{4+}$ at this pH. The potential shifts positively with decrease in pH as in Fig. 4.38.

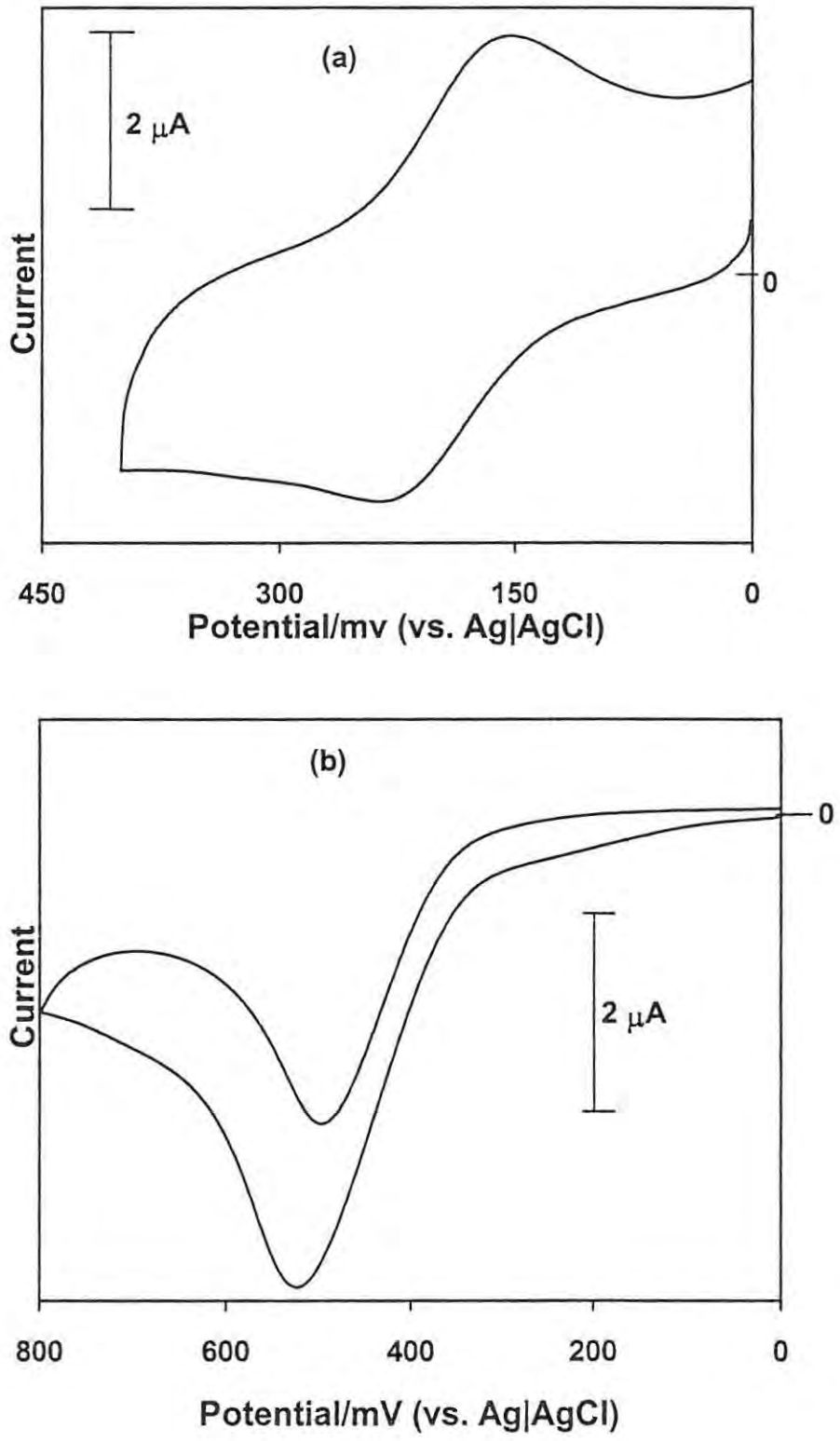

Fig. 4.40 Current-potential curves recorded in pH 4 Tris buffer solution for $[Co^{II}Tm\text{-}3,4\text{-}tppa]^{+4}$ in the absence (a) and presence (b) of 7.2×10^{-4} mol dm^{-3} cysteine.

Therefore, it has been shown in this work that cysteine determination through its oxidation can be performed on $[Co^{II}Tm\text{-}3,4\text{-}tppa]^{4+}$-GCE in pH 7 (biological pH) Tris buffer. The detection limit of 1.0×10^{-5} mol dm^{-3} can be obtained.

CHAPTER 5

CONCLUSION

It has been shown in this work that the nature of the ring affects the catalytic activity of phthalocyanine complexes towards the reduction of nitrite. The presence of pyridinium rings (in porphyrazine complexes) instead of benzene rings (in CoPc) results in the lowering of the potential for the reduction of nitrite. Hence, a peak for the reduction of nitrite was observed for [Co^{II}tppa], [Co^{II}Tm-2,3-tppa]$^{4+}$ and [Co^{II}Tm-3,4-tppa]$^{4+}$ and was not observed for Co^{II}Pc. The position of the methyl groups on the pyridinium ring also plays an important role in the catalytic reduction of nitrite. [Co^{II}Tm-2,3-tppa]$^{4+}$ shows a larger current efficiency for NH_3 production from nitrite than [Co^{II}2,3-tppa] or [Co^{II}Tm-3,4-tppa]$^{4+}$. Higher yields of ammonia production are also observed for [Co^{II}Tm-2,3-tppa]$^{4+}$ and [Co^{II}Tm-3,4-tppa]$^{4+}$, which have methyl groups, than for CoPc and [Cotppa]. Nitrite concentrations as low as 1×10^{-10} mol dm^{-3} could be determined in water containing Na_2SO_4, using electrodes modified with [Co^{II}Tm-3,4-Tppa]$^{4+}$, [Co^{II}TSPc]$^{4-}$ and a mixture of [Co^{II}TSPc]$^{4-}$and [Co^{II}Tm-3,4-tppa]$^{4+}$. The anionic complex, [Co^{II}TSPc]$^{4-}$, however showed lower catalytic activity than both the cationic species, Co^{II}Tm-3,4-tppa]$^{4+}$ and the mixture of the cationic and anionic species. The nitrite reduction process was found to be ring-based.

In this work the use of [Co^{II}TSPc]$^{4-}$ to modify GCE resulted in the enhancement of the oxidation currents for NO_2^-. Addition of NO_3^-, a common interferent for NO_2^- determination had no effect on the cyclic voltammogram of nitrite. [Co^{II}TSPc]$^{4-}$ improved the stability of the GCE towards the detection of nitrite when compared to unmodified GCE. Concentrations of nitrite of the order of 2×10^{-7} mol dm^{-3} could be detected using the [Co^{II}TSPc]$^{4-}$ modified GCE. This is a lower detection limit than reported in the literature for nitrite determination using its oxidation, on modified and unmodified electrodes.

It has been shown that the electrocatalytic detection of SO_2 is pH dependent. Except for the pH range from 7.5 – 9, SO_2 or its related compounds HSO_3^- and SO_3^{2-}, can be detected on $[Fe^{II}TSPc]^{4-}$-GCE with a detection limit of the order of 10^{-5} mol dm^{-3}.

It has also been shown in this work that cysteine and histidine determinations may be performed on $[Co^{II}Tm\text{-}3,4\text{-}tppa]^{4+}$-GCE in pH 7 and 10.8 Tris buffer, respectively. The detection limits are 1.0×10^{-5} and 2.24×10^{-7} mol dm^{-3} for cysteine and histidine, respectively.

Cyanide can be detected down to 1×10^{-11} mol dm^{-3} using $[Co^{II}Tm\text{-}3,4\text{-}tppa]^{4+}$-GCE in pH 10.8 buffer.

Interaction of $[Co^{II}TSPc]^{4-}$ with cyanide is accompanied by oxidation of $[Co^{II}TSPc]^{4-}$ to $[Co^{III}TSPc]^{3-}$ by oxygen. The $[Co^{III}TSPc]^{3-}$ species are also formed on interaction of $[Co^{II}TSPc]^{4-}$ with SO_2.

Interactions between cysteine and histidine with $[Co^{II}Tm\text{-}3,4\text{-}tppa]]^{4+}$ results in the formation of $[Co^{I}Tm\text{-}3,4\text{-}tppa]^{3+}$. Interactions of amino acids with porphyrazines are an important step towards modelling of biological systems, due to the similarity between porphyrazines and porphyrins.

References

1 N.B. Mckeown, *Chemistry and Industry*, (1999) 92.

2 C.C. Leznoff in Phthalocyanine: Properties and Applications, Vol. 1, (A.B.P. Lever and C.C. Leznoff, eds) VCH, New York, (1989).

3 J.H. Weber and D.H. Bush, *Inorg. Chem.*, **4** (1965) 469.

4 T.D. Smith, J. Livorness, H. Taylor, J.R. Pilbrow and G.R. Sinclair, *J. Chem., Soc. Dalton Trans.*, (1983) 1391.

5 D. Wöhrle, J. Gitzel, I. Okura and S. Aono, *J. Chem. Soc. Perkin Trans. II* (1985) 1171.

6 M.J. Stillman and T. Nyokong in Phthalocyanine: Properties and applications, Vol. 1, (A.B.P. Lever and C.C. Leznoff, eds) VCH, New York, (1989).

7 A.B.P. Lever and J.P. Wilshire, *Inorg. Chem.*, **17** (1978) 1145.

8 A.B.P. Lever and J.P. Wilshire, *Can. J. Chem.*, **54** (1976) 2514.

9 M.J. Stillman in Phthalocyanine: Properties and Applications, Vol. 3, (A.B.P. Lever and C.C. Leznoff eds) VCH, New York, (1993).

10 A.B.P. Lever, E.R. Milaeva and G. Spencer in Phthalocyanine: Properties and Applications, Vol. 3, (A.B.P. Lever and C.C. Leznoff eds) VCH, New York, (1993).

11 Y.-H. Tse, P. Janda and A.B.P. Lever, *Anal. Chem.*, **66** (1994) 384.

12 M. Sekota and T. Nyokong, *J. Porphyrins Phthalocyanines*, **3** (1999) 477.

13 L. Ruhlmann, A. Nakamura, J.G. Vos and J.-H. Fuhrhop, *Inorg. Chem.*, **37** (1998) 6052.

14 J.F. Lipskier and T.H. Tran-Thi, *Inorg. Chem.*, **32** (1993) 722.

15 D.K. Geiger and C.A. Kelly, *Inorg. Chim. Acta*, **154** (1988) 137.

16 E. Ojadi, R. Selzer and H. Linschitz, *J. Am. Chem. Soc.*, **107** (1985) 7783.

17 T. Saji in Phthalocyanines: Properties and Applications, Vol. 2, (A.B.P. Lever and C.C. Leznoff eds) VCH, New York, (1993).

18 B. Simic-Glavaski in Phthalocyanine: Properties and Applications, Vol. 3, (A.B.P. Lever and C.C. Leznoff, eds) VCH, New York, (1993).

19 H.S. Nalwa and J.S. Shirk in Phthalocyanines: Properties and Applications, Vol. 4, (A.B.P. Lever and C.C. Leznoff eds) VCH, New York, (1996).

20 K. Hanabusa and H. Shirai in Phthalocyanine: Properties and Applications, Vol. 2, (A.B.P. Lever and C.C. Leznoff eds) VCH, New York, (1993).

21 I. Rosenthal and E. Ben-Hur in Phthalocyanine: Properties and Applications, Vol. 1, (A.B.P. Lever and C.C. Leznoff, eds) VCH, New York, (1989).

22 J.H. Zagal, *Coord. Chem. Rev.*, **119** (1992) 89.

23 C.M.A. Brett and A.M.O. Brett in Electrochemistry; Principles, Methods and Applications, Oxford University Press Inc. Publishers, USA, (1993).

24 W.R. Heineman and P.T. Kissinger in Laboratory Techniques in Electroanalytical Chemistry, (P.T. Kissinger and W.R. Heineman, eds) (2nd ed.), Marcel Dekker, New York, (1996).

25 A.J. Bard and L.R. Faulkner in Electrochemical Methods; Fundamentals and Applications, John Wiley & Sons, Inc., USA, (1980).

26 J. Wang in Analytical Electrochemistry, 1st edn., VCH publishers, New York, (1994).

27 W.E. Van Der Linden, J. Dicher, *Anal. Chim. Acta,* **119** (1980) 1.

28 J. Koryta, J. Dvořák and V. Boháčková in Electrochemistry, Methuen and Co publishers, Great Britain (1970).

29 M.N. Golovin, P. Seymour, K. Jayaraj, Y. Fu and A.B.P. Lever, *Inorg. Chem.*, **29** (1990) 1719.

30 C.M. Lieber and N.S. Lewis, *J. Am. Chem. Soc.*, **106** (1984) 5033.

31 Z. Sun and H. Tachikawa, *Anal. Chem.*, **64** (1992) 1112.

32 Y.-H. Tse, P. Janda, H. Lam and A.B.P. Lever, *Anal. Chem.*, **67** (1995) 981.

33 G. Favaro and M. Fiorani, *Anal. Chim. Acta,* **332** (1996) 249.

34 J.P. Hart and A.K. Abass, *Anal. Chim. Acta,* **342** (1997) 199.

35 N. Kobayashi, P. Janda and A.B.P. Lever, *Inorg. Chem.*, **31** (1992) 5172.

36 S. L. Vilakazi and T. Nyokong, *Polyhedron,* **17** (1998) 4415.

37 J. Oni and T. Nyokong, *Anal. Chim. Acta,* **434** (2001) 9.

38 N. Grootboom and T. Nyokong, *Anal. Chim. Acta,* **432** (2001) 49.

39 S. Vilakazi and T. Nyokong, *Polyhedron,* **19** (2000) 229.

40 T. Mafatle and T. Nyokong, *Anal. Chim. Acta,* **354** (1997) 307.

41 Z. Jiujun, T. Yu-Hong, W.J. Pietro and A.B.P. Lever, *J. Eletroanal. Chem.*, **406** (1996) 203.

42 P. Janda, J. Weber, L. Dunsch and A.B.P. Lever, *Anal. Chem.*, **68** (1996) 960.

43 Z. Jiujun, W.J. Pietro and A.B.P. Lever, *J. Electroanal. Chem.*, **403** (1996) 93.

44 M.K. Halbert and R.P. Baldwin, *Anal. Chem.*, **57** (1985) 591.

45 M. Sekota and T. Nyokong, *Electroanalysis,* **9** (1997) 1257.

46 IUPAC recommendations (1997), *Pure and Applied Chemistry,* **69** (1997) 1318.

47 C.R. Martin and C.A. Foss, Jr. in Laboratory Techniques in Electroanalytical Chemistry, (P.T. Kissinger and W.R. Heineman, eds) (2nd ed.), Marcel Dekker, New York, (1996).

48 Z. Li and M. Lieberman in Fundamental and Applied Aspects of Chemically Modified Surfaces, (J.P.Blitz and C.B. Little, eds) Royal Soc. of Chem., (1999).

49 R.J. Davenport and D.C. Johnson, *Anal. Chem.*, **46** (1971) 1974.

50 E.R. Homan in Clinical and Experimental Toxicoloy of Cyanides, (B. Ballantyne and T.C. Marrs, eds) Wright Publishers, Bristol, (1987).

51 B. Ballantyne and T.C. Marrs in Clinical and Experimental Toxicoloy of yanides, (B. Ballantyne and T.C. Marrs, eds) Wright Publishers, Bristol, (1987), chapter 9.

52 B. Ballantyne and T.C. Marrs in Clinical and Experimental Toxicoloy of Cyanides, (B. Ballantyne and T.C. Marrs, eds) Wright Publishers, Bristol, (1987) chapter 23.

53 J.C. Linnell in Clinical and Experimental Toxicoloy of Cyanides, (B. Ballantyne and T.C. Marrs, eds) Wright Publishers, Bristol, (1987).

54 G.E. Isom and J.D. Johnson in Clinical and Experimental Toxicoloy of Cyanides, (B. Ballantyne and T.C. Marrs, eds) Wright Publishers, Bristol, (1987).

55 J. Marsden and I. House in The Chemistry of Gold Extraction, Ellis Horwood, Chichester, England (1992).

56 C.A. Young, S.P. Cashin and F.E. Diebold in Separation Processes Heavy Metals, Ions and Minerals, (M. Misra ed.) TMS publication, Warrendale, (1995).

57 V. Augugliaro, J. Blanco Gálvez, J. Cáceres Vázquez, E. García López, V. Loddo, M.J. López Muñoz, S. Malato Rodríguez, G. Marcí, L. Palmisano, M. Schiavello and J. Soria Ruiz, *Catal. Today,* **54** (1999) 245.

58 J. Epstein, *Anal. Chem.*, **19** (1947) 272.

59 S. Nagashima, *Anal. Chem.*, **56** (1984) 1944.

60 N.B.H. Anh and M. Sharp, *Anal. Chim. Acta,* **405** (2000) 145.

61 A. Stavart and A.V. Lierde, *J. App. Electrochem.*, **31** (2001) 469.

62 E. Kirowa-Eisner, D. Talmor and J. Osteryoung, *Anal. Chem.*, **53** (1981) 581.

63 J.H. Karchmer and M.T. Walker, *Anal. Chem.*, **27** (1955) 37.

64 D.R. Canterford, *Anal. Chem.*, **47** (1975) 88.

65 M.J. Stillman and A.J. Thomson, *J. Chem. Soc, Faraday Trans II*, **70** (1974) 790.

66 T. Nyokong, *Polyhedron,* **14** (1995) 643.

67 T. Nyokong and J. Guthrie-Strachan, *Inorg. Chim. Acta,* **208** (1993) 239.

68 P. Hambright, *Inorg. Chim. Acta*, **137** (1987) 209.

69 B.W. Ng, R. Lenigk, Y.L. Wong, X. Wu, N.T. Yu and R. Renneberg, *J. Electrochem. Soc.*, **147** (2000) 2350.

70 M. Radojevi□ and V.N. Bashkin in Practical Environmental Analysis, Royal Society of Chemistry, Cambridge, U.K. (1999).

71 Y. Yang, X-X. Zhang, T. Korenaga and K. Higuchi, *Talanta*, **45** (1997) 445.

72 A.P. Altshuller in Analytical Chemistry: Key to Progress on National Problems. National Bureau of Standards, U.S. (1972).

73 B. Chachulski, *Analyst*, **123** (1998) 1141.

74 D.T. Sawyer, R.S. George and R.C. Rhodes, *Anal. Chem.*, **31** (1959) 2.

75 R.W. Garber, and C.E. Wilsons, *Anal. Chem.*, **44** (1972) 1357.

76 A.W.E. Hodgson, P. Jacquinop and P.C. Hauser, *Anal. Chem.*, **71** (1999) 2831.

77 T. Nyokong, *J. Chem. Soc., Chem. Comm.*, (1994) 1983.

78 P.C. Minor, M. Gouterman and A.B.P. Lever, *Inorg. Chem.*, **24** (1985) 1894.

79 N. Nensala, A. Nzimande and T. Nyokong, *J. Photochem. Photobiol., A: Chem.*, **98** (1996) 129.

80 W.R. Scheidt, Y. Ja Lee and M. G. Fennegan, *Inorg. Chem.*, **27** (1988) 4725.

81 I. Nikolov, K. Petrov and T. Vitanov, *J. App. Electrochem.*, **26** (1996) 703.

82 I. Nikolov, I. Vitanova, V. Najdenov, T. Milusheva and T. Vitanov, *J. Appl. Electrochem.*, **27** (1997) 77.

83 M.A. Kline, M.H. Barley and T.J. Meyer, *Inorg. Chem.*, **26** (1987) 2196.

84 J.F. Van Staden, and T.A Van der Merwe, *S. Afr. J. Chem.*, **51** (1998) 109.

85 I.T. Glover and F.T. Johnson, *J. Chem. Ed.*, **50** (1973) 426.

86 J.D. Genders, D. Hartsough and D.T. Hobbs, *J. Applied. Electrochem.*, **26** (1996) 1.

87 D.S. Hage, A. Chattopadhyay, C.A.C. Wolf, J. Grundman and P.B. Kelter, *J.Chem. Ed.*, **75** (1998) 1588.

88 A. A. Ensafi and G.B. Dehaghei, *Fresenius J. Anal. Chem.*, **363** (1999) 131.

89 T. Hamano, Y. Mitsuhashi, N. Aoki, M. Semma, Y. Ito and Y. Oji, *Analyst,* **123** (1998) 1127.

90 P. MacCarthy, R.W. Klusman and S.W. Cowling, *Anal. Chem.*, **63** (1991) 301R.

91 G.F. Wang, M. Satake and K. Horita, T*alanta,* **46** (1998) 671.

92 S.M. Silva, C.R. Alves, S.A.A. Machado, L.H. Mazo and L.A. Avaca, *Electroanalysis,* **8** (1996) 1055.

93 J.O.M. Bockris and J. Kim, *J. Appl. Electrochem.*, **27** (1997) 623.

94 R.B. Almeida, S.S.S. Borges and G. Gomes, *Analytical Letters,* **32** (1999) 1203.

95 S. Cattarin, *J. App. Electrochem.*, **22** (1992) 1077.

96 A.F. Danet and V. David, *Analytical letters,* **31** (1998) 751.

97 N. Chebotareva and T. Nyokong, *J. App. Electrochem.*, **27** (1997) 975.

98 N. Chebotareva and T. Nyokong, *J. Coord. Chem.*, **46** (1999) 433.

99 R. Allen, A. Florido, S.D. Young, S. Daunert and L.G. Bachas, *Electroanalysis,* **7** (1995) 710.

100 J.-Z. Li, X. Pang and R-Q. Yu, *Anal. Chim. Acta*, **297** (1994) 437.

101 R. Lin, M. Bayachou, J. Greaves and P.J. Farmer, *J. Am. Chem. Soc., Chem. Commun.*, **119** (1997) 12689.

102 B. Strehlitz, B. Gründig, K.-D. Vorlop, P. Bartholmes, H. Kotte and V. Stottmeister, *Fresenius J. Anal. Chem.*, **349** (1994) 676.

103 M.H. Barley, K.J. Takeuchi, W.R. Murphy, Jr. and T.J. Meyer, *J. Chem. Soc. Chem. Commun.*, (1985) 507.

104 M.H. Barley, K.J. Takeuchi and T.J. Meyer, *J. Am. Chem. Soc.*, **108** (1986) 5876.

105 F. Bedioui, S. Trevin, V. Albin, M.G.G. Villegas and J. Devynck, *Anal. Chim. Acta,* 341 (1997) 177.

106 G.I. Sackheim and R.M. Schultz in Chemistry of the Health Sciences, (2nd ed.), Macmillan Company, New York, (1973).

107 L. Stryer in Biochemistry, (3rd ed.), W.H. Freeman and company, New York, (1988).

108 S. Miller in Biology, (N.A. Campbell, ed) (2nd ed.), Benjamin/Cummings publishing company, USA, (1990).

109 R.A. Wallace, G.P. Sanders and R.J. Ferl in Biology The Science of Life, HapperCollins, USA, (1991).

110 L. Stryer in Biochemistry, (3rd ed.), W.H. Freeman and Company, New York, (1988).

111 H.E. Umbarger and G. Zubay in Biochemistry, (G.Zubay, ed.) (3rd ed.), Wm. C. Brown, USA, (1993).

112 L.A. Fothergill-Gilmore in Protein Biochemistry Isolation, Characterisation and Stabilisation, (F. Franks ed.), Humana Press, New Jersey, (1993).

113 W. Bartley, L.M. Birt and P. Banks in The Biochemistry of the Tissues, John Wiley & Sons Ltd, London, New York, (1968).

114 A.S. Salim, *Can. J. Surgery,* **36** (1993) 53.

115 W. Dröge, H.P. Eck, H. Gmünder and S. Mihm, *Am. J. Med,* **91** (1991) 3C:140S.

116 W. Dröge, H-P. Eck and S. Mihn, *Immunol. Today,* **13** (1992) 211.

117 K. Wilson in Practical Biochemistry Principles and Techniques, (K. Wilson and J. Walker, eds) (4th ed.), Cambidge University Press, Great Britain, (1994).

118 K. Ogura, M. Kobayashi, M. Nakayama and Y. Miho, *J. Electroanal. Chem.*, **463** (1999) 218.

119 N. Spătaru, B.V. Sarada, E. Popa, D.A. Tryk and A. Fujishima, *Anal. Chem.*, **73**

(2001) 514.

120 M. Sekota and T. Nyokong, *Polyhedron,* **16** (1996) 3279.

121 E. Mikros, F. Gaudemer and A. Gaudemer, *Inorg. Chem.,* **30** (1991) 1806.

122 J. Limson and T. Nyokong, *Electroanalysis,* **9** (1997) 255.

123 J. Limson and T. Nyokong, *Electroanalysis*, **10** (1998) 988.

124 T.J. Mafatle and T. Nyokong, *J. Electroanal. Chem.,* **408** (1996) 213.

125 K. Ozoemena, P. Westbroek and T. Nyokong, *Electrochem. Commun.,* **3** (2001) 529.

126 S. Maree and T. Nyokong, *J. Electroanal. Chem.,* **492** (2000) 120.

127 T.D. Smith, J. Livorness, H. Taylor, J.R. Pilbrow and G.R. Sinclair, *J. Chem. Soc. Dalton Trans.,* (1983) 1391.

128 R. Purrello, L. M'Scolaro, E. Bellacchio, S. Gurrieri and A Romeo, *Inorg. Chem.,* **37** (1998) 3646.

129 A. Berg, M. Rachamin, T. Galili and H. Levanon, *J. Phys. Chem.,* **100** (1996) 8791.

130 Krejčik M, Dan k M. F Hartl. *J. Electroanal. Chem.,* **317** (1991) 179.

131 L.C. Gruen, R.J. Blagrove, *Aust. J. Chem.,* **26** (1973) 319.

132 A.I. Vogel in A textbook of quantitative inorganic analysis including elementary instrumental analysis, 3rd edn., (London) 1968.

133 P. Ascenzi, R. Fruttero, C.I. Ercolan and F. Monacelli, *Analusis* **24** (1996) 316.

134 A.B.P. Lever, M.R. Hempstead, C.C. Leznoff, W. Liu, M. Melnik, N.A. Nevin and P. Seymour, *Pure and Appl. Chem.,* **58** (1986) 1467.

135 A. Hadasch, A. Sorokin, A. Rabion, L. Fraisse and B. Meunier, *New J. Chem.,* (1998) 45.

136 J. Oni and T. Nyokong, *J. Porphyrins Phthalocyanines,* (2002) in press.

137 J. Zagal, R.K. Sen and E. Yeager, *J. Electroanal. Chem.*, **83** (1977) 207.

138 J. Zagal, P. Bindra and E. Yeager, *J. Electrochem. Soc.*, **127** (1980) 1506.

139 B. Simic-Glavaski, S. Zecevic and E. Yeager, *J. Electroanal. Chem.,* **150** (1983) 469.

140 G. Mc Lendon and A.E. Martell, *Inorg Chem.*, **16** (1977) 1812.

141 D. Vonderschmitt, K. Bernauer and S. Fallab, *Helv Chim Acta*, **48** (1965) 951.

142 E.A. Lukyanets, *J. Porphyrins Phthalocyanines,* **3** (1999) 424.

143 D. Phillips, *Pure & Appl. Chem.*, **67** (1995) 117.

144 S. Dhami and D. Phillips, *J. Photochem Photobiol. A: Chem.*, **100** (1996) 77.

145 R. Bonnet, *Chem. Soc. Rev.*, **24** (1995) 19.

146 J. Dolanský, D.M. Wagnerová and J. Vepřek-Šiška, *Collection Czechoslov. Chem. Commun.*, **41** (1976) 2327.

147 N.N. Kundo and N.P. Keier, *Russ. J. Phys. Chem.*, **4** (1968) 707.

148 S.-H. Cheng and Y.O. Su, *Inorg. Chem.* **33** (1994) 5847.

149 C.-H. Yu and Y.O.Su, *J. Electroanal. Chem.*, **368** (1994) 323.

150 H. Kruszyna, J.S. Magyar, L.G. Rochelle, M.A. Russell, R.P. Smith and D.E. Wilcox, *J. Pharmacology and Experimental Therapeutics,* **285** (1998) 665.

151 T. Kawakani and S. Igarashi, *Anal. Chim. Acta,* **354** (1997) 159.

152 P. Hampbright, *Inorg. Chim. Acta,* **157** (1989) 95.

153 J.H. Weber and D.H. Busch, *Inorg. Chem.*, **4** (1965) 472.

154 P. Day, P.A. O'Hill and M.G. Price, *J. Chem. Soc. A,* (1968) 90.

155 R.J. Sundberg and R.B. Martin, *Chem. Rev.*, **74** (1974) 496.

156 A. Boffi, E. Ercolani, F. Monacelli, P. Ascenzi, *Inorg. Chim. Acta,* **267** (1998) 109.

157 D.M. Wagnerova, E. Schwertnerova and J. Veprek-Siska, *Collection Czechoslov. Chem. Commun.*, **39** (1974) 1980.

158 W.R. Scheidt, Y.J. Lee and M.G. Finngan, *Inorg. Chem.*, **27** (1988) 4725.

159 K. Shin and H.M. Goff, *J. Chem. Soc., Chem Commun.*, (1990) 461.

160 A.R. Miksztal and J.S. Valentine, *Inorg. Chem.*, **23** (1984) 3548.

161 T. Nyokong, *J. Chem. Soc. Dalton Trans.*, (1993) 3601.

162 G. Pennesi, E. Ercolani, P. Ascenzi, M. Brunori and F. Monacelli, *J. Chem. Soc. Dalton Trans.*, (1985) 1107.

163 D.A. Sweigart, *J. Chem. Soc. Dalton Trans.*, (1976) 1476.

164 M. Hoshino, L. Laverman and P.C. Ford, *Coord. Chem. Rev.*, **187** (1999) 75.

165 E.M. Tyapochkin and E.I. Kozliak, *J. Porphyrins Phthalocyanines*, **5** (2001) 405.

166 A. Navid, E.M. Tyapochkin, C.J. Archer and E.I Kozliak, *J. Porphyrins Phthalocyanines*, **3** (1999) 654.

167 R. Lin, P.J. Farmer, *J. Am. Chem. Soc.*, **123** (2001) 1143.

168 D.J. Cookson, T.D. Smith, J.F. Boas, P.R. Hicks and J.R. Pilbrow, *J. Chem. Soc., Dalton Trans.*, (1977) 109.

169 R.F. Pasternack, *Inorg. Chem.*, **15** (1976) 643.

170 P.-S.K. Leung, E.A. Betterton and M.R. Hoffmann, *J. Phys. Chem*, **93** (1989) 430.

171 P.-S.K Leung, M.R. Hoffmann, *J. Phys. Chem*, **93** (1989) 434.

172 T. Nyokong, *Polyhedron*, **14** (1995) 2325.

173 P. Hambright and R. Langley, *J. Inorg. Biochem.*, **32** (1988) 197.

174 F. D' Souza, Y.-Y. Hsich and G.R. Deviprasad, *Chem. Commun.*, (1998) 1027.

175 C.-H. Yu and Y.O. Su, *J. Electroanal. Chem.*, **368** (1994) 323.

176 S.-H. Cheng and Y.O. Su, *Inorg. Chem.*, **33** (1994) 5847.

177 S.-I. Mho, B. Ortiz, N. Doddapaneni and S.-M. Park, *J. Electrochem Soc.*, **142** (1995) 1047.

178 S. Zecevic, B. Simic-Glavaski, E. Yeager, A.B.P. Lever and P.C. Minor, *J. Electroanal. Chem.*, **196** (1985) 339.

179 A.B.P. Lever, M.R. Hempstead, C.C. Leznoff, W. Liu, M. Melnik, W.A. Nevin and P. Seymour, *Pure & Appl. Chem.*, **58** (1986) 1467.

180 R.J.H. Chan, Y.O. Su and T. Kuwana, *Inorg. Chem.*, **24** (1985) 3777.

181 N. G. Carpenter, and D. Pletcher, *Anal. Chem.*, **317** (1995) 287.

182 F.A. Cotton, G. Wilkinson and P.L. Gaus in Basic Inorganic Chemistry, John Wiley and Sons, New York, (1987).

183 R.C. Weast in CRC Handbook of Chemistry and Physics, 64th edition, CRC Press, Boca Raton, Canada (1983).

184 T.J. Cardwell and M.J. Christophersen, *Anal. Chim. Acta*, **416** (2000) 105.

185 L.M. de Carvalho and G. Schwedt, *Anal. Chim. Acta*, **436** (2001) 293.

186 E. Gasana, P. Westbroek, E. Temmerman and H.P. Thun, *Anal. Commun.*, **36** (1999) 387.

187 E. Gasana, P. Westbroek, E. Temmerman, H.P. Thun and F. Twagiramungu, *Electrochem. Commun.*, **2** (2000) 727.

188 P. Westbroek, K. Van Uytvangh, J. De Strycker and E. Temmerman, *J. Electroanal. Chem.*, in press.

189 H. Tatsuta, T. Nakamura and T. Hinoue, *Anal. Sci.*, **17** (2001) 991.

190 T.J. Mafatle and T. Nyokong, *J. Electroanal. Chem.*, **408** (1996) 213.

191 K. Ozoemena, P. Westbroek and T. Nyokong, *Electrochem. Commun.*, **3** (2001) 529.